# Synthesis of organogels and characterization by X-ray techniques

Danilo Rosa Nunes

université PARIS-SACLAY

# Synthesis of organogels and characterization by X-ray techniques

**Thèse de doctorat de l'université Paris-Saclay**

École doctorale n° 564, : physique de l'Ile-de-France (PIF)
Spécialité de doctorat: physique
Unité de recherche : Université Paris-Saclay, CNRS, Laboratoire de Physique des Solides, 91405, Orsay, France
Référent : Faculté des sciences

**Thèse présentée et soutenue à Orsay, le 16 Janvier 2020, par**

**Danilo ROSA NUNES**

## Composition du Jury

| | |
|---|---|
| **Philippe Roger**<br>Professeur, Université Paris-Saclay | Président |
| **Franck Artzner**<br>Directeur de recherche, Université e Rennes | Rapporteur |
| **David Canevet**<br>Maîtres de conférences, Université de Angers | Rapporteur |
| **Nathalie Guillou**<br>Chargé de recherche, Université Paris-Saclay | Examinatrice |
| **Amparo Ruiz-Carretero**<br>Chargé de recherche, Université de Strasbourg | Examinatrice |
| **Pierre-Antoine Albouy**<br>Directeur de recherche, Université Paris-Saclay | Directeur de thèse |
| **Laurent Bouteiller**<br>Directeur de recherche, Sorbonne Université | Invité |
| **Pascale Foury-Leylekian**<br>Professeur, Université Paris-Saclay | Invitée |

Thèse de doctorat

NNT : 2020UPASS006


Université Paris - Saclay
Ecole Doctorale Physique en Île-de-France

# Synthesis of organogels and characterization by X-ray techniques

Thèse de doctorat en physique

Danilo Rosa Nunes

# 1. Résume

Les gels sont des matériaux semi-solides, formés par un réseau qui est présent dans tout le volume d'un fluide. La transition de l'état liquide à l'état solide de ces matériaux s'appelle gélification et est provoquée par la formation d'un réseau interne, qui représente normalement moins de 5% de l'ensemble du système. À l'état de gel, les gels peuvent supporter une contrainte de cisaillement et peuvent aller de matériaux mous à durs ou de matériaux fragiles à étirables. Ces matériaux hétérogènes se situent à la frontière entre un solide et un fluide et en raison de leurs propriétés particulières sont présents dans de nombreuses d'applications courantes. L'industrie alimentaire continue d'être l'un des plus grands utilisateurs de ces matières, produisant de grandes quantités de gélatine et de gelée. Dans le domaine des produits cosmétiques, les gels servent généralement de base au transport des ingrédients actifs vers la peau et peuvent également être observés dans des produits tels que les dentifrices et les gels capillaires. Avec une approche plus médicinale, l'industrie pharmaceutique utilise des gels spéciaux conçus comme agents d'administration du médicament en raison de la grande modulabilité de la transition sol-gel ou comme dispositifs médicaux en raison de leur aptitude à être facilement mouillable tout en restant solide (c.-à-d. lentilles de contact). L'industrie des matériaux utilise également des gels dans la formulation de peintures et de matériaux adhésifs. Les applications de ces matériaux sont innombrables et avec la découverte de nouveaux moyens de mieux ajuster les propriétés sol-gel et d'introduire de nouvelles fonctions dans ces matériaux, les applications ne feront que croître.

Les organogels sont un type particulier de gels formés dans des liquides organiques avec un réseau polymère supramoléculaire. Ces matériaux diffèrent principalement des autres classes de gels en raison de la nature de leur réseau. Les gélifiants de faible poids moléculaire (LMWG) ont tendance à s'auto-agréger dans une seule direction préférentielle. Cela conduit à la formation de structures allongées, principalement des fibres, qui, par une évolution continue du processus d'assemblage, forment un réseau fibrillaire auto-assemblé enchevêtré (SAFIN). Ce mécanisme d'auto-assemblage est dirigé par des interactions non covalentes telles que la liaison hydrogène, l'empilement $\pi - \pi$, les interactions donneur – accepteur, la coordination des métaux et les interactions de van der Waals. La formation d'un réseau basé uniquement sur des interactions faibles affecte considérablement l'intégrité structurelle, rendant les organogels métastables et thermoréversibles.

Il existe une grande variété structurelle entre différents organogélateurs, ce qui en fait un type de matériau aussi intéressant, permettant un large éventail de propriétés et d'applications. Le principal

défi des organogels est de prédire quelles molécules organiques sont capables de gélifier quels liquides. Bien que sachant qu'une molécule organique commune a normalement besoin de groupes fonctionnels fournissant une interaction non covalente forte entre les molécules, cela n'est pas suffisant pour prédire la gélification. En raison de l'absence de méthodologie prédictive, la découverte de nouveaux organogélateurs est principalement livrée au hasard et leurs capacités de gélification sont généralement vérifiées par des processus exhaustifs d'essais et d'erreurs. Ainsi, il devient nécessaire de développer une méthodologie capable de réduire le temps et les dépenses lors de la recherche de nouveaux organogélateurs ou du réglage de leurs propriétés.

Cette thèse se divise principalement en deux parties. Nous abordons d'abord les outils permettant d'étudier l'auto-assemblage des gélateurs et d'améliorer une méthode pour rationaliser l'organogélation. La seconde partie consiste en l'application de telles méthodes dans des systèmes d'organogélateurs. Nous étudions l'effet qu'une altération structurelle (dans ce cas, la longueur des chaînes alkyles) peut avoir en organogélation.

Nous avons étudié l'empilement moléculaire dans les fibres de gel dans l'espoir de mieux comprendre certains phénomènes d'organogélation. En utilisant des méthodologies basées sur les techniques de diffraction des rayons X et à l'aide de techniques de modélisation moléculaire, nous avons pu obtenir un modèle illustrant la conformation et la position relative que les molécules gélatrices adoptent après auto-assemblage. La méthodologie adoptée pour étudier la structure moléculaire des fibres de gel dépend du type de diagramme de poudre mesuré par rayons X à partir des fibres de gel séchés (xérogels). Si les gélifiants s'assemblent de manière très organisée avec des périodicités bien définies, le diagramme de poudre de rayons X présente un nombre considérable de pics de diffraction fins. Il est donc possible d'extraire des données précises et d'effectuer une modélisation structurale (en particulier). Ce cas est appelé méthode de l'espace direct. Si le gélifiant s'assemble de manière moins organisée, le diagramme de rayons X résultant présente un nombre réduit de pics de diffraction larges. Lorsque c'est le cas, l'extraction d'informations à partir du diagramme de rayons X devient compliquée et l'utilisation de la fonction de distribution de paires (PDF) devient la seule alternative pour extraire des informations sur l'empilement moléculaire. Avec le PDF, l'accent est mis davantage sur la structure locale (conformation et molécules voisines) que sur la périodicité et les groupes de symétrie. Grâce à ces techniques, nous avons pu fournir des modèles explicatifs de la structure moléculaire pour la plupart des familles de gélifiants étudiées. Ce modèle a permis de mieux comprendre les mécanismes de l'auto-assemblage menant à la gélification.

La découverte de nouveaux LMWG est encore principalement le résultat du hasard et leurs capacités de gélification sont généralement vérifiées par des processus exhaustifs d'essais et d'erreurs. Dans le but à long terme d'éviter ce travail laborieux, nous avons proposé une méthodologie de rationalisation de l'organogel basée sur les paramètres de solubilité de Hansen (HSP). Les HSP résultent d'une

approche thermodynamique et permettent de prédire, notamment, la solubilité des polymères. Selon cette approche, chaque molécule possède un ensemble de trois densités d'énergie cohésives différentes dues aux interactions dispersives ($\delta_D$), aux interactions polaires ($\delta_P$) et aux liaisons hydrogène ($\delta_H$), qui peuvent ensuite être utilisées comme coordonnées pour tracer un diagramme 3D (l'espace de Hansen). En testant la solubilité d'un composé donné dans un ensemble de liquides de HSP connus, une sphère peut être calculée dans l'espace de Hansen, de sorte que cette sphère contienne la plupart des liquides qui dissolvent le composé testé. Si un liquide non testé possède des valeurs de HSP placées à l'intérieur de la sphère de solubilité, il est prévu que ce liquide dissolve le composé. Cette méthodologie peut-être appliquée aux organogels: il est possible de calculer un nouveau domaine avec tous les liquides gélifiés. Semblable au domaine de solubilité, si un liquide non testé est situé à l'intérieur du domaine de gélification, il est prédit que ce liquide sera gélifié par le composé. Lors de cette thèse, la méthodologie originelle de calcul du domaine de gélification a été améliorée afin d'obtenir une méthode générale de détermination du domaine de gélification des LMWG compatible avec toutes les données publiées. Cette nouvelle méthodologie est nommée "AO" pour "allowed overlap". Elle consiste à déterminer la plus petite sphère possible qui inclut tous les liquides gélifiés (G) et exclut les liquides (P) qui précipitent le gélifiant, sans tenir compte des liquides (S) qui solubilisent le gélifiant. L'exclusion des points S de la détermination de la sphère de gélification permet (mais ne force pas) les sphères de gélification et de solubilité de partager un volume commun, chose qui n'était pas possible avec la méthodologie précédente et qui s'est avéré être un facteur clé dans le développement d'une méthodologie générale.

Après avoir compilé une méthodologie complète pour étudier l'empilement moléculaire à partir de méthodes de diffraction X et affiné la méthode de rationalisation de l'organogélation en utilisant les paramètres de solubilité de Hansen, nous avons sélectionné cinq groupes différents d'organogélateurs possédant une ou plusieurs chaînes alkyles dont la longueur a été variée. Il a été observé que l'augmentation de la longueur d'une chaîne alkyle conduit à trois comportements différents lorsqu'on étudie la gélification à l'aide de l'espace de Hansen. Deux des cinq groupes de gélifiants étudiés présentent un déplacement du centre de la sphère de gélification vers une zone de moindre polarité avec l'augmentation de la longueur des chaînes alkyles. Ce décalage est similaire au décalage observé dans la translation du centre de la sphère de solubilité. Le changement de polarité se produit de manière linéaire dans l'espace de Hansen, permettant ainsi une prédiction simple pour les autres membres de ces familles. L'organogélation dépend certainement de l'interaction entre la surface d'une fibre de gel et le liquide, aussi, pour qu'une modification structurelle dans une molécule gélifiante ait un effet sur les propriétés de gélification, cette modification doit présenter un changement dans la composition de la surface de la fibre. Il a également été observé que l'empilement moléculaire au sein des fibres de gels reste bien semblable entre les gélifiants testés. Pour établir le

lien entre la structure moléculaire et la morphologie des cristaux, de nouvelles études de simulation moléculaire sont nécessaires, mais nous pouvons supposer que lorsque les chaînes alkyles d'un gélifiant sont augmentées, l'exposition des chaînes alkyles à la surface de la fibre évolue proportionnellement. Si tel est le cas, l'augmentation de la longueur des chaînes alkyle entraîne une diminution de la polarité de la surface des fibres de gel, ce qui entraîne une dérive du centre du domaine de gélification vers une zone de polarité inférieure dans l'espace de Hansen.

Le deuxième comportement de gélification observé n'est présent que dans l'un des cinq groupes de gélifiants étudiés. Dans ce groupe de gélifiants, nous avons observé que l'augmentation de la longueur des chaînes alkyles linéaires n'avait pas d'effet significatif sur les domaines de gélification. Bien que nous ne puissions pas proposer un modèle exact qui corresponde aux données de rayons X, la nature symétrique des molécules de gélifiant et la présence de trois fonctions amide responsables de fortes liaisons hydrogène facilite la rationalisation du possible empilement moléculaire de ce gélifiant. La liaison hydrogène est l'interaction non covalente la plus forte possible pour ces molécules et est donc très probablement le moteur de la formation des fibres de gel. De petites variations d'orientation des groupes amides sont possibles, mais la liaison hydrogène est toujours préservée. Par conséquent, quel que soit l'empilement exact de cette famille de gélifiants, les côtés des fibres ne sont recouverts que de chaînes alkyles (probablement désordonnées) et leur allongement ne devrait pas affecter de manière significative la composition de la surface des fibres. En conséquence, la longueur des chaînes alkyles ne doit pas influencer les interactions avec le liquide environnant. Ceci explique l'absence d'évolution du domaine de gélification.

Le troisième comportement observé est présent dans les deux groupes restants d'organogélateurs étudiés. Ces organogélifiants présentent un comportement de gélification complexe dans l'espace de Hansen. L'augmentation de la longueur de la chaîne alkyle provoque un déplacement non monotone du centre de la sphère de gélification, rendant impossible la détermination d'une tendance. Le premier groupe qui a présenté ce comportement complexe ne comporte qu'un membre de la famille présentant un empilement légèrement différent de celui des autres membres de la famille. Même en excluant ce membre, les données de gélification restent très complexes. Une explication possible pourrait être la présence de différentes morphologies cristallines au sein de la famille. Même si la maille cristalline semble évoluer régulièrement au sein de la famille, on ne peut exclure la formation de cristaux ayant des faces cristallographiques différentes. Si cette altération ne se produit pas de manière continue, l'énergie de surface d'une fibre de gel peut changer brusquement, ce qui entraîne un comportement erratique du centre de la sphère de gélification. Le deuxième groupe de gélifiants présentant un comportement complexe en matière de gélification contient en fait deux membres dont la structure ou la stabilité des cristaux sont légèrement différentes de celles des autres membres. Si ces derniers sont retirés de l'étude, une tendance linéaire est obtenue pour les membres restant du groupe.

Au bilan, cette thèse a apporté de nouvelles connaissances dans le domaine de la chimie supramoléculaire et de l'organogélation et a dévoilé de nouveaux défis pour la rationalisation de l'organogélation à l'aide des HSP. Les principales contributions de cette thèse peuvent être divisées en quatre parties: 1- compilation d'outils pour une méthode de résolution de l'empilement moléculaire à partir de fibres de gel; 2 - amélioration du traitement des données pour la rationalisation des organogels à partir des paramètres de solubilité de Hansen; 3 - découverte que la variation de longueur d'une chaîne alkyle d'un organogélateur peut entraîner trois comportements de gélification différents; et 4 - résolution de la structure cristalline de plusieurs organogélateurs, ce qui peut être utilisé pour mieux comprendre les mécanismes d'auto-assemblage qui entraînent la gélification.

Il reste encore à comprendre le comportement de gélification complexe (dans certains cas) causé par la variation de la longueur de chaînes alkyles. Cette question nécessite l'utilisation de méthodologies avancées de chimie théorique pour déterminer des modèles d'empilement moléculaires et de morphologies cristallines des fibres.

# 2. Acknowledgements

First of all, I would like to thank Pierre-Antoine Albouy and Laurent Bouteiller for directing this PhD project. Both helped my grow scientifically and personally through this period of my life.

I would like to thank the ANR for the financial support.

I would like to thank all the members of the jury. Franck Artzner and David Canevet for the reports given, Philippe Roger for accepting the position of president of the jury and Amparo Ruiz-Carretero and Nathalie Guillou for fulfilling the position of examiners.

I would like to thank Ahmad Hammoud, Quentin Sallembien, Laura Luiz, Richard Albiges, Océane Fort and Dorian Rabaud for allowing the best possible work environment that a PhD student can ask for and all the friendship.

I would like to thank Pascale Foury-Leylekian and Stéphan Rouzière for all the help in the structure resolution methods.

I would like to thank all permanent members, post-doc and PhD students of the Matrix group of the Laboratoire de Physique des Solides and the polymer chemistry team of the Institut Parisien de Chimie Moléculaire for all the help in this project.

I would like to thank Soleil synchrotron, particularly Erik ELKAIM for the pair distribution function measurements.

I would like to thank the Laboratory for Chemistry of Novel Materials in the University of Mons, particularly Patrick Brocorens, Roberto Lazzaroni and Manuel Reche for the computational modeling done for the ANR project.

I would like to thank Aalto university particularly Olli Ikkala and Emilie Ressouche for the mobility period in MOLMAT.

Finally, I would like to thank everybody that provided emotional support and good moments that

helped this journey. Particularly André Pontes da Costa and João Gonçalves for mentoring and friendship. My mother Ana Rosa for helping me the person that I am today. And Nina Pitkänen for being always there.

# 1. Contents

# 3. Introduction

## 1. What are gels

Gels are semi-solid materials, formed by a non-fluid network that is expanded throughout the whole volume of a fluid. The transition from liquid to solid state of these materials is called gelation and is driven by the formation of an internal network, which normally represents less than 5 % of the entire system. Gels can sustain shear stress and can range from soft to hard or from brittle to stretchable materials. These heterogeneous materials are at the frontier between a solid and a fluid and are sometimes called "Jelly-like".[1,2]

The invention of the term gel is ultimately credited to Scottish chemist Thomas Graham in 1899,[3] by a derivation of the word gelatin that by itself comes from the Latin word *gelatus* which means to be frozen, to be chilled or cause to freeze.[4]

The oldest records of these materials are collagen-based gels that acted as glue, used by the Egyptians approximately 8000 years ago.[5] They were used in daily use objects such as rope baskets, embroidered fabrics, nets and wooden arrowheads. In the XVIII century gels started being massively used by the population in the form of gelatin, thanks to the invention of the steam digester by French physicist Denis Papin. This early version of a pressure cooker made it possible to transform bones and skin from animals into an eatable sub product, that at the time helped feed the poor population that had difficult access to animal-based nutrients.[6,7]

Nowadays gels have gained more applications and can be seen every day. The food industry continues to be one of the greatest users of these materials, producing wide quantities of gelatin and jelly. In the field of cosmetic products gels usually serve as a base for the transport of active ingredients to the skin and can also be seen in products such as lipstick, tooth paste and hair gel. With a more medicinal approach, the pharmaceutical industry uses special engineered gels as drug delivery agents due to the high tunability of the sol-gel transition or in medical devices due to their good wettability while remaining a solid (i.e. contact lenses). The materials industry also uses gels in the formulation of paints and adhesive materials. The applications of these materials are countless and with the discovery of new ways to better tune the sol-liquid properties and introduce new functions in these materials the applications will only tend to increase.

## 2. Classification of gels

The internal network that is responsible for the transformation of a fluid into a gel can be divided in several categories according to the network structure. Paul Flory organized these categories in 1974 in his introductory lecture given to Faraday Discussions of the Chemical Society about Gels and Gelation.[8] This organization is still mostly followed today, as observed in the IUPAC recommendations.[9] According to this a gel can be made from:

I. a covalent polymer network. It is formed by crosslinking polymer chains or by nonlinear polymerization. This can also be called a chemical gel, since the polymerization process occurs thanks to chemical reaction;
II. a supramolecular polymer network formed through the physical aggregation of small molecules, caused by non-covalent interactions, that results in regions of local order acting as the network junction points. The resulting swollen network may be termed a "thermoreversible gel" if the regions of local order are thermally reversible. Also called a physical gel, since no chemical phenomenon occurs in the formation of the network;[10]
III. a polymer network formed through glassy junction points. Normally based on triblock copolymers were the central block presents a high solubility and the outer blocks do not. This leads to the segregation of the non-soluble blocks forming spherical, glassy microdomains, forming this way a network of solid spheres, cross linked by the solvated blocks. These systems can also be called "thermoreversible gels" or physical gels; [11–13]
IV. lamellar structures. Lamellar gel networks, were not present in the original definition given by Flory. They are multiphase colloidal structures, that comprise a lamellar gel phase and a bulk water phase. Usually the lamellar phase is formed with surfactants below their Krafft temperature at a much higher concentration than the solubility limit. These systems can also be called "thermoreversible gels" or physical gels (i.e. soap gels, phospholipids, and clays);[14]
V. particulate disordered structures, e.g., a flocculent precipitate usually consisting of particles with large geometrical anisotropy, such as in $V_2O_5$ gels and globular or fibrillar protein gels.).

Another type of classification of gels is based on the medium that gels are formed. Hydrogels are formed in water and organogels are supramolecular gels formed in organic solvents. This last group will be further explained in the next section.

# 3. Organogels

Organogels mainly differ from other classes of gels due to the nature of their network. Low molecular weight gelators (LMWG) tend to self-aggregate in a preferential single direction. This leads to the formation of elongated structures, mainly fibers, that by continuous evolution of the assembly process form an entangled Self-Assembled Fibrillar Network (SAFIN).[15–18] This particular mechanism of self-assembly is led by non-covalent interactions like hydrogen-bonding, π–π stacking, donor–acceptor interactions, metal coordination and van der Waals interactions. Forming a network only based on weak interactions highly affects the structural integrity, making organogels metastable and thermoreversible.

Typically, organogels are formed by adding LMWGs to the organic liquid to be gelated. The LMWGs are not soluble in the organic liquids to be gelated, so at first the mixture of both components forms a suspension. To promote solubility the suspension mixture is heated until dissolution and then left to cool down to room temperature, reaching a super saturated condition. As the temperature of the system decreases, also does the solubility. When this happens, most materials tend to simply precipitate or crystalize, but due to the preferential unidirectional crystallization of LMWGs the formation of a network of fibers and a gel occurs instead. This procedure is illustrated in figure 1.

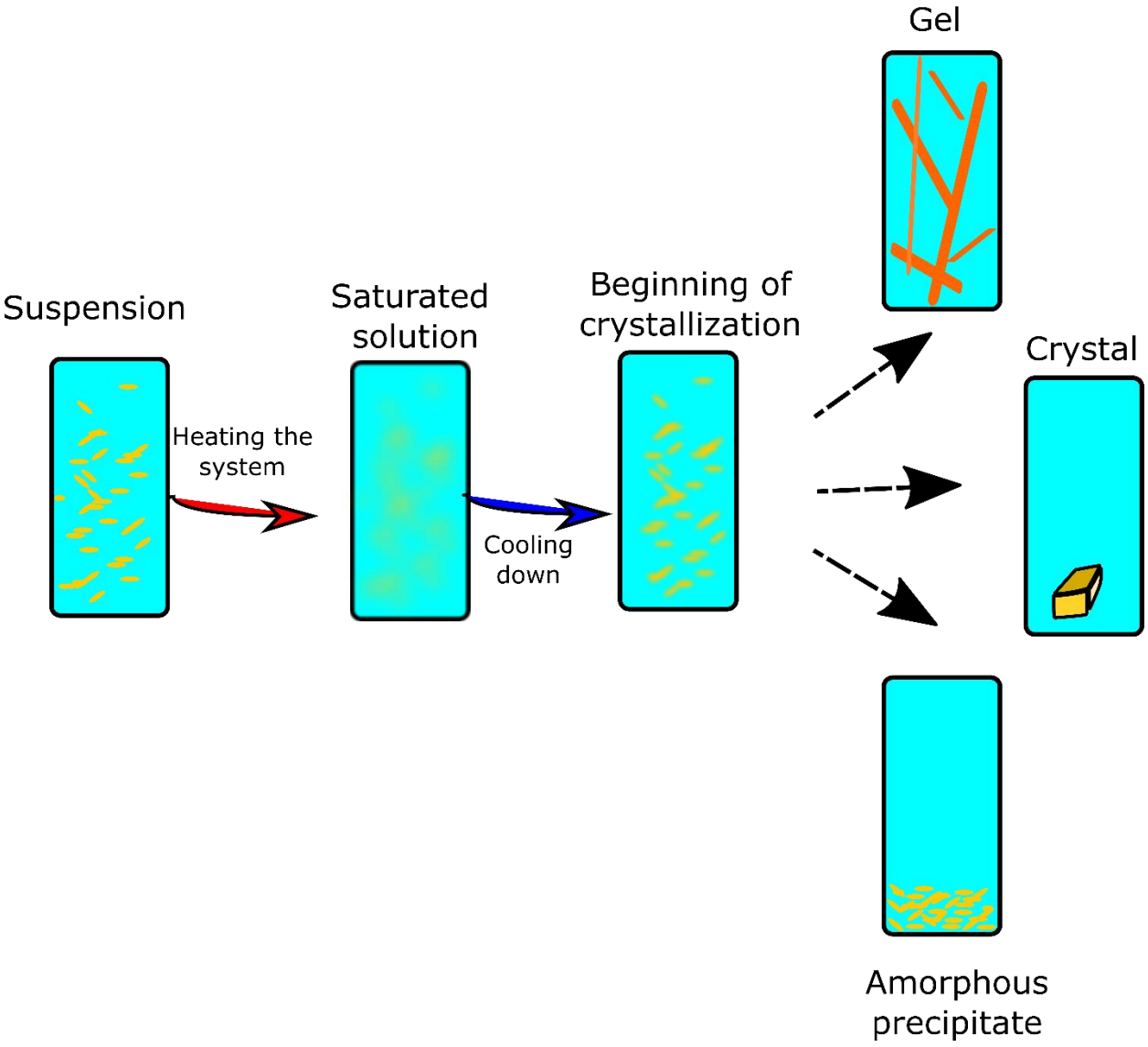

*Figure 1. Organogel preparation path.*

# 4. Applications of organogels

During the last 30 years the interest on the organogelation field has hugely increased, as seen by the number of publications that use the term “organogel”, “molecular gels”, “LMWG” or “SAFIN” found in a search performed in Web of Knowledge (Figure 2).

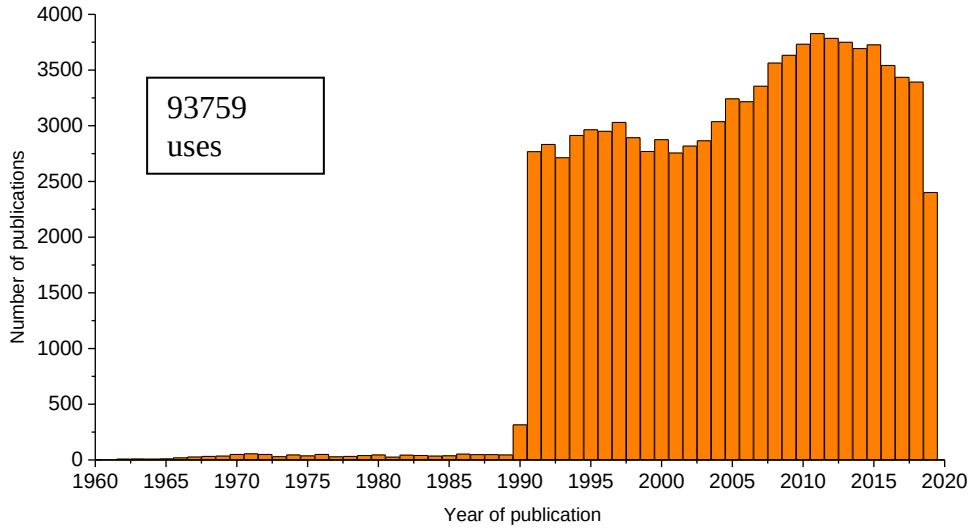


*Figure 2. Number of references found by searching the term "organogel" in Web of Knowledge.*

The structures of small organic molecules are highly tunable, and this allows the introduction of a variety of different properties in organogels. This coupled with the thermoreversibility of these materials are some of the main reasons for the increasing interest that also lead to a wide range of

potential applications reported. Figure 3 illustrates a variety of organogels reported in the literature designed for different applications. Examples of these applications are described below alongside with an explanation of why organogels are good candidates for each application.

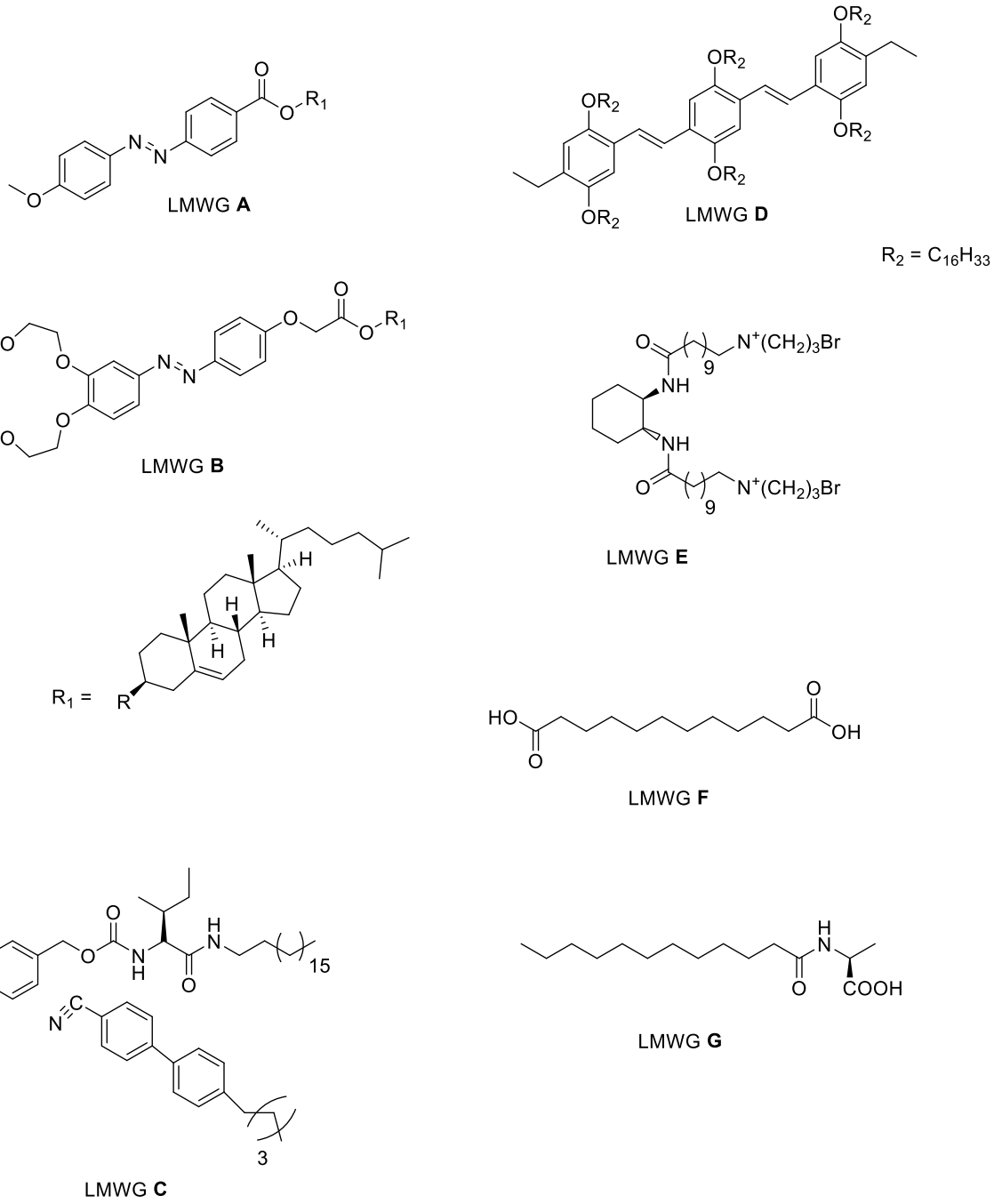


*Figure 3. Examples of organogelators used for different applications.*

## 4.1. Stimuli responsiveness and sensing materials

The intrinsic property of reversible sol to gel phase transition that organogels exhibit, makes them ideal materials for sensing. Also called smart materials, they can transition from gel state to solution and vice versa when certain alterations occur in the medium. The most basic application is to indicate a difference in temperature, since organogels form solutions when there is an increase of temperature.[10] More interestingly some organogels are designed to trigger the transition between solution and gel by differences in the pH of the medium, application of different light sources or presence of certain chemicals. One of the earliest examples of a photoresponsive organogel was synthesized using the structure of cholesterol end-functionalized with an azobenzyl (**LMWG A** figure 3).[19] This gelator was able to transition from the gel state to solution when subject of UV-light and from solution to gel when subject to visible light. This was archived by designing a gelator that could only self-assemble in the trans isomer, thus, when applied UV-light the compound photoisomerizes to the cis conformation yielding a poor gelator. An example of organogel as sensing materials is **LMWG B** (figure 3), an azacrown derivative of cholesterol. This gelator increases the gel–sol transition temperature (Tgel) of the gel when in the presence of alkali metal or ammonium ions (such as $Li^+$, $Na^+$, $K^+$, $Rb^+$ and $NH_4^+$).[19]

## 4.2. Optical properties

Liquid crystalline organogels are microphase-separated composites comprising a fibrous network of gel formed with a low molecular weight gelator, and the entrapped liquid crystal molecules (mesogens). These materials can have two thermoreversible phase transitions independent from each other, isotropic liquid-isotropic gel and isotropic gel-liquid crystalline gel. This allows the formation of a gel that can interchange between isotropic and anisotropic, changing in particular the ability to scatter light, only by applying an electric field. **LMWG C** is an example of a liquid crystalline

organogelator with tunable light scattering properties when applying an electric field.[20,21]

## 4.3. Light harvesting

Some organogels have been reported to mimic the light harvesting capability of some photosynthetic organisms. Light harvesting consists in complexes that absorb sunlight and transfer energy to the reaction center where the photoinduced redox processes are initiated. **LMWG D** present in figure 3 is an example of an organogel with such capability. Derived from p-phenylenevinylene and mixed with an organic dye (Rhodamine B), this organogel system was reported to form self-assembled superstructures during gelation that are capable of thermoreversible transferring fluorescence resonance energy to the acceptor Rhodamine B.[22]

## 4.4. Structure directing agents for the synthesis of other materials

Mainly due to the formation of SAFIN that can take the shape of rods, ribbons, tapes, tubes or helices, organogels can serve as a template for formation of several tailor-made inorganic particles. The example **LMWG E** represented in figure 3 is reported to allow the formation of silica nanostructures. This is achieved by incorporating tetraethyl orthosilicate (TEOS) amongst the gel fibers. After adding a catalyst that allows the hydrolysis of TEOS followed by polycondensation of the silicate around the gel fibers, it is possible to wash the organic gel matrix and maintain a porous silica matrix.[23]

## 4.5. Material modifiers

In the field of material sciences, organogels have also been used to as an additive to change the properties of several systems. It has been reported their application as surface modifiers of glass surface,[24] by creating a superhydrophobic surface on glass that allows water contact angles greater

than 150°. It has also been reported the application of organogels as bitumen additives. **LMWG F** (figure 3) is an example of an organogelator that is able to self-assemble in a bitumen matrix forming crystalline fibers.[25] This additive resulted in an increase of the temperature range where the bitumen is solid while increasing the hardness and elastic modulus at room temperature, without increasing the melt viscosity, thus allowing easy processing.

## 4.6. Oil spill

Organogels can also have the property of being selective in the type of solvents in which self-assembly occurs and thus gelation. This becomes particularly interesting when organogelators are able to gelate a particular liquid present in a mixture of liquids, creating a heterogeneous system composed by the gelated liquid and the non-gelated liquids physically separated. **LMWG G** (figure 3) is such an example of an organogelator with phase-selective gelation. This gelator was capable of selectively forming a gel in a water-oil mixture, creating a two-phase system containing water and a gel, allowing an easier removal of oil-components.[26] This may be useful in cases of environment catastrophes that result in oil spill in the ocean, were the use of organogels could allow an easier removal of oil product minimizing this way the environmental impact.

# 5. Difficulty to design a new organogelator

Figure 3 exemplifies the wide variety of molecular structures that can self-assemble and form a gel in organic solvents. This rich variety is what makes organogels such an interesting type of materials since, as mentioned above, this allows for a wide range of properties and applications. The problem with organogels is in fact knowing which organic molecules are capable of gelating which liquids. It is known that normally a gelator needs to have functional groups that provide a strong non-covalent interaction between molecules and that its solubility needs to be adapted, but this is not enough to predict gelation. Due to the lack of predictive methodology, the discovery of new organogelators is still mainly the result of serendipity and their gelation abilities are usually probed by exhaustive trial and error processes. Thus, arises a need to develop a methodology capable to decrease time and expenses when researching new organogelators or tuning their properties.

# 6. Objectives and outline

This aim of this work is to develop a previously proposed method to rationalize organogelation, based on the Hansen solubility parameters. The first version of this method rationalized gelation with empirical thermodynamic parameters.[27–29] Despite showing good results when proposing a model to predict what liquid could be gelated by a single molecule, this model could not fully explain how gelation could vary depending on the molecular structure of the gelator.

In an attempt to fill this gap, we studied the molecular packing of gel fibers with the hope to better understand certain phenomena of organogelation. Molecular periodic structures are more commonly obtained from X-ray diffraction of small single crystal structures. Since gels are materials with physical characteristics different from crystals the same methodology could not be applied. Thus, there was the need to develop a standard procedure to measure and resolve molecular packing of organic molecules within gels.

After proposing gel/fiber molecular packing solving methodology (chapter 1) and presenting a correction on the initial method to rationalize organogelation of a single molecule with the Hansen solubility parameters (Chapter 2) we perform an in-depth study on the effect that a small structure variation has on the gelation properties. To do this we focus our efforts on the study of the effect of the length of linear alkyl chains in the organogelator structure. Five groups of molecules [30–34] with reported organogelator properties were chosen, each with shared molecular structure only varying the length of the alkyl chains (Figure 4).

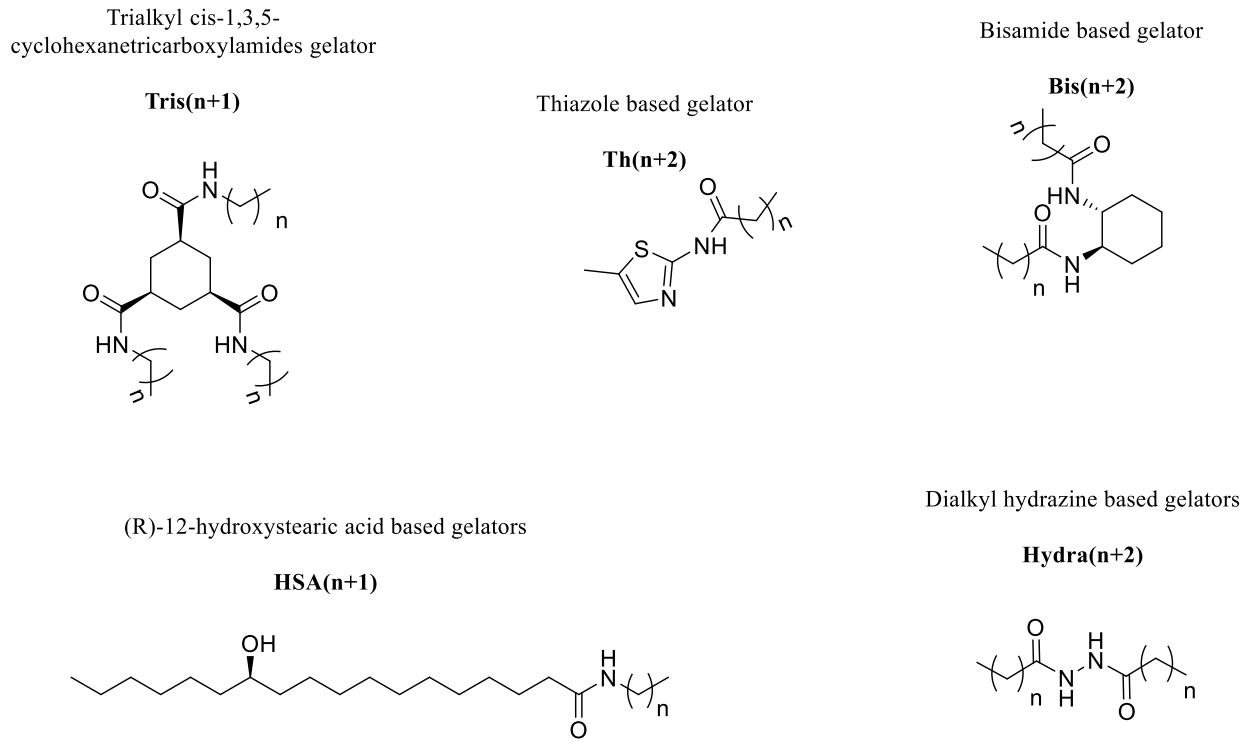


*Figure 4. Family of organogelators used to probe the effect of the length of an alkyl chain on its gelation domain in the Hansen Space.*

After studying the Hansen space and molecular packing of each family of molecules, the results are then divided into two chapters. Chapter three includes all family of gelators that show a simple gelation behavior in the Hansen space when correlated with the increase in length of the linear alkyl chain and chapter four by opposition shows all family of gelators with a more complex behaviour. Both chapters will include morphology studies of gel fibers as well as computation modeling work done with the aim of clarifying the molecular packing. All results from these analyses are compared with the gelation behavior of the different gelator families in the Hansen space with the aim of finding a correlation. Consequently, this will provide new insights in the organogelation field to the scientific community and leave us one step closer to obtain a fully realized prediction system for gelation properties.

# 7. References

1 R. G. Jones, E. S. Wilks, W. V. Metanomski, J. Kahovec, M. Hess, R. Stepto and T. Kitayama, Eds., *Compendium of Polymer Terminology and Nomenclature*, Royal Society of Chemistry, Cambridge, 2009.

2 S. Slomkowski, J. V. Alemán, R. G. Gilbert, M. Hess, K. Horie, R. G. Jones, P. Kubisa, I. Meisel, W. Mormann, S. Penczek and R. F. T. Stepto, *Pure Appl. Chem.*, 2011, **83**, 2229–2259.

3 D. A. Harper, Online Etymology Dictionary: gel, https://www.etymonline.com/word/gel.

4 P. G. W. Glare, *Oxford Latin dictionary*, 1968.

5 A. A. Walker, *Archaeol. Online News*.

6 C. Viel and J. Fournier, *Rev. Hist. Pharm. (Paris).*, 2012, **94**, 7–28.

7 D. Papin, *La manière d'amolir les Os...*, 1721.

8 C. S. (Great B. F. Division and R. S. of C. (Great B. F. Division, *Faraday Discussions of the Chemical Society*, Faraday Division, Chemical Society, 1972.

9 J. V. Alemán, A. V. Chadwick, J. He, M. Hess, K. Horie, R. G. Jones, P. Kratochvíl, I. Meisel, I. Mita, G. Moad, S. Penczek and R. F. T. Stepto, *Pure Appl. Chem.*, 2007, **79**, 1801–1829.

10 N. M. Sangeetha and U. Maitra, *Chem. Soc. Rev.*, 2005, **34**, 821.

11 T. Sato, H. Watanabe and K. Osaki, *Macromolecules*, 2000, **33**, 1686–1691.

12 T. Sato, H. Watanabe and K. Osaki, *Macromolecules*, 2002, **29**, 6231–6239.

13 H. Watanabe, S. Kuwahara and T. Kotaka, *J. Rheol. (N. Y. N. Y).*, 2002, **28**, 393–409.

14 T. Iwata, *Lamellar gel network*, Elsevier Inc., 2017.

15 P. Terech and R. G. Weiss, *Chem. Rev.*, 1997, **97**, 3133–3160.

16 M. George and R. G. Weiss, *Acc. Chem. Res.*, 2006, **39**, 489–497.

17 P. Dastidar, *Chem. Soc. Rev.*, 2008, **37**, 2699.

18 D. J. Abdallah and R. G. Weiss, *Adv. Mater.*, 2000, **12**, 1237–1247.

19 K. Murata, M. Aoki, T. Nishi, A. Ikeda and S. Shinkai, *J. Chem. Soc. Chem. Commun.*, 1991, 1715.

20 N. Mizoshita, K. Hanabusa and T. Kato, *Adv. Mater.*, 1999, **11**, 392–394.

21 N. Mizoshita, Y. Suzuki, K. Kishimoto, K. Hanabusa and T. Kato, *J. Mater. Chem.*, 2002, **12**, 2197–2201.

22 A. Ajayaghosh, S. J. George and V. K. Praveen, *Angew. Chemie Int. Ed.*, 2003, **42**, 332–335.

23 J. H. Jung, Y. Ono, K. Hanabusa and S. Shinkai, *J. Am. Chem. Soc.*, 2000, **122**, 5008–5009.

24 M. Yamanaka, K. Sada, M. Miyata, K. Hanabusa and K. Nakano, *Chem. Commun.*, 2006, 2248.

25 B. Isare, L. Petit, E. Bugnet, R. Vincent, L. Lapalu, P. Sautet and L. Bouteiller, *Langmuir*, 2009, **25**, 8400–8403.

26 Y. Ohsedo, *Polym. Adv. Technol.*, 2016, **27**, 704–711.

27 M. Raynal and L. Bouteiller, *Chem. Commun.*, 2011, **47**, 8271.

28 J. Bonnet, G. Suissa, M. Raynal and L. Bouteiller, *Soft Matter*, 2014, **10**, 3154.

29 J. Bonnet, G. Suissa, M. Raynal and L. Bouteiller, *Soft Matter*, 2015, **11**, 2308–2312.

30 K. Hanabusa, A. Kawakami, M. Kimura and H. Shirai, *Chem. Lett.*, 1997, **26**, 191–192.

31 N. Zweep, A. Hopkinson, A. Meetsma, W. R. Browne, B. L. Feringa and J. H. Van Esch, *Langmuir*, 2009, **25**, 8802–8809.

32 P. Yadav, D. Kour, V. K. Gupta, Rajnikant and A. Ballabh, *RSC Adv.*, 2013, **3**, 8417–8421.

33 K. Tomioka, T. Sumiyoshi, S. Narui, Y. Nagaoka, A. Iida, Y. Miwa, T. Taga, M. Nakano and T. Handa, J. Am. Chem. Soc., 2001, 123, 11817–11818.

34 V. A. Mallia, M. George, D. L. Blair and R. G. Weiss, *Langmuir*, 2009, **25**, 8615–8625.

4.

5.

# 6. Chapter 1

# Characterization of soft matter

A material can be described as soft material if it can be easily deformed when subjected to a small stimulus, such as differences in temperature or applied pressure. These materials are organized on the mesoscopic lengthscale, with structures bigger than an atom but much smaller than the overall object. The size of the formed structures and the weak interactions responsible for giving consistency to the system are responsible for the ‘’softness’’ characteristics of the materials. The dynamics of these materials is a time frame of seconds to minutes in contrast to hard matter, that are considered static systems because their dynamics occur in time frame of months or years. All of this creates challenges when characterizing any soft material.[1]

Organogels are a prime example of soft materials, not only because of the softness and dynamic nature of the non-covalent bonds inherent to the system, but also due to the challenges in characterization that these materials present. Organogels are also very diverse materials, ranging from highly organized and periodic materials to highly disorganized with lack of periodicity, which brings the need for different characterization techniques for different organogels.

# 1. Microscopic network observation

A common characterization technique of gel systems is to obtain images of the network phase of the system for direct observation. For this there is a need for a technique capable of enough magnification to analyse objects in the range of several nanometers to a few tens of micrometers. One of the easiest and most accessible way to do this is by using a scanning electron microscopy (SEM). A SEM is an electronic microscope that scans a small area of the sample using an electron beam. The interaction of the beam with the sample produces various signals that can be used to obtain information about the composition and topography of the material. The SEM is capable of a large depth of field, due to the very narrow electron beam used, that allows a large area to be focused at one time while yielding a characteristic 3-dimensional appearance and the high resolution up to several nanometers.[2] The biggest handicap of this technique when applied to gels is that the network needs to be separated from the liquid, since an SEM operates in vacuum. This extraction of the network from the gel system may cause some artifacts on the morphology of the networks. Even though, SEM continues to be the most used observation technique to characterize gel networks. All SEM images presented in this work were recorded using a Zeiss Sigma VP microscope and the gel networks were prepared by freeze-drying the gel samples in liquid nitrogen and vacuum-pumping the solvent.

Overall microscopy techniques provide useful information about the morphology of the structures formed in the mesoscopic scale but using only imaging techniques it is difficult to discriminate similar organogel systems.

# 2. From measure to molecular packing

To extract more information from organogel systems we had the need to study the molecular packing within gels fibers. This will provide data best suited to study very similar gel systems while giving at the same time important information about the molecular interactions that are responsible for the formation of the gel network. The study of the molecular conformation also brings more conclusive information for the possible existence of gel polymorphism caused by the interaction of LMWG with different liquids.

X-ray diffraction techniques can be used to study the atomic packing within a gel network. Under the influence of the incident X-ray beam, each atom reemits a spherical wavelet with similar wavelength. Interferences between these wavelets give rise to intensity maxima and minima. The crystalline state is characterized by long-range order between atoms and in that case conditions for constructive interferences are very strict: diffracted intensity is only observed in some specific directions, that correspond to the so-called Bragg reflections. It may be convenient to visualize Bragg reflections as

the reflection of the incident beam on a family of equidistant atomic planes. The condition for possible reflection on the atomic planes is given by the Bragg Equation (Eq1).[3]

$$(Eq1) \quad \lambda = 2\, d\, sin\, \theta$$

In the Bragg equation λ represents the wavelength of the used X-ray beam, 2θ represents the angle between the origin of the X-ray beam and the diffracted signal and *d* is the distance between atomic planes. Due to the information that can be collected from X-ray diffraction, this technique is not only used to solve molecular structures but also to identify phases, preferred crystal orientations, average grain size, crystallinity and crystal defects.

The standard method to solve the molecular packing of a material is by performing single crystal diffraction. As mentioned above, when an X-ray beam passes by a crystal the recorded resulting diffraction forms a diffraction pattern composed by small spots. Each spot represents a 2D slice in a 3-dimensional space. The sum of all these 2D slices are then used to construct a model that represents the atomic positions of the system in study.

For some LMWG, the crystal structure derived from single-crystal diffraction is already published. When this is the case the first step when studying the molecular packing within gel fibers is to directly compare the measured powder X-ray pattern from the gel fibers with the computed powder X-ray pattern of the crystal structure. In the case that both X-ray patterns match we can assume that the molecular packing within the gel fiber is the same as in the crystal state. This method is the most efficient and reliable to solve the molecular packing within a gel fiber.

Unfortunately, due to the tendency of LMWG to form fibers, forming crystals with these molecules with enough quality for single crystal X-ray diffraction is a challenging task. Because of this the majority of LMWGs do not have structural information in the form of single crystal. When this is the case, the only diffraction information that can be measured is in the form of powder diffraction. Contrary to single crystal diffraction, in powder diffraction the X-ray beam passes through a powder sample containing many small crystals in random orientations. This results in a diffraction pattern where Bragg spots are replaced by diffraction circles. One difficulty is the indexation that is less easy than for single-crystals. A second problem arises from the possible overlap of diffraction circles with different indexations.

Since obtaining a model for the molecular packing from powder X-ray is not as straightforward as with a single crystal, we breakdown the methodology to solve structure from powder diffraction diagrams used in this work, step by step and in some steps with multiple alternatives.

## 2.1. Sample Preparation

Ideally measurements should be done directly on a gel. As already discussed, the network represents normally less than 5% of the system. Due to the small amount of LMWG in a system, the contribution of the liquid to the measure is major, dwarfing any contribution from the LMWG. To overcome this problem and obtain an X-ray pattern of the LMWG network, the gel fibers were extracted by filtration and dried overnight at room temperature and room pressure. The extracted fibers were then grinded to avoid possible preferential orientation effects. Figure 5 illustrates the measure of **Bis4** gel formed in toluene (a) and the respective extracted fibers (xerogel) (b). While the gel only yielded the signal of the liquid phase, the xerogel presented a full diffraction pattern that matched the diffraction pattern of the single crystal structure of **Bis4** (Figure 5 b and c). The matching patterns indicate that the used method to extract gel fibers does not create artifacts in the packing structure.

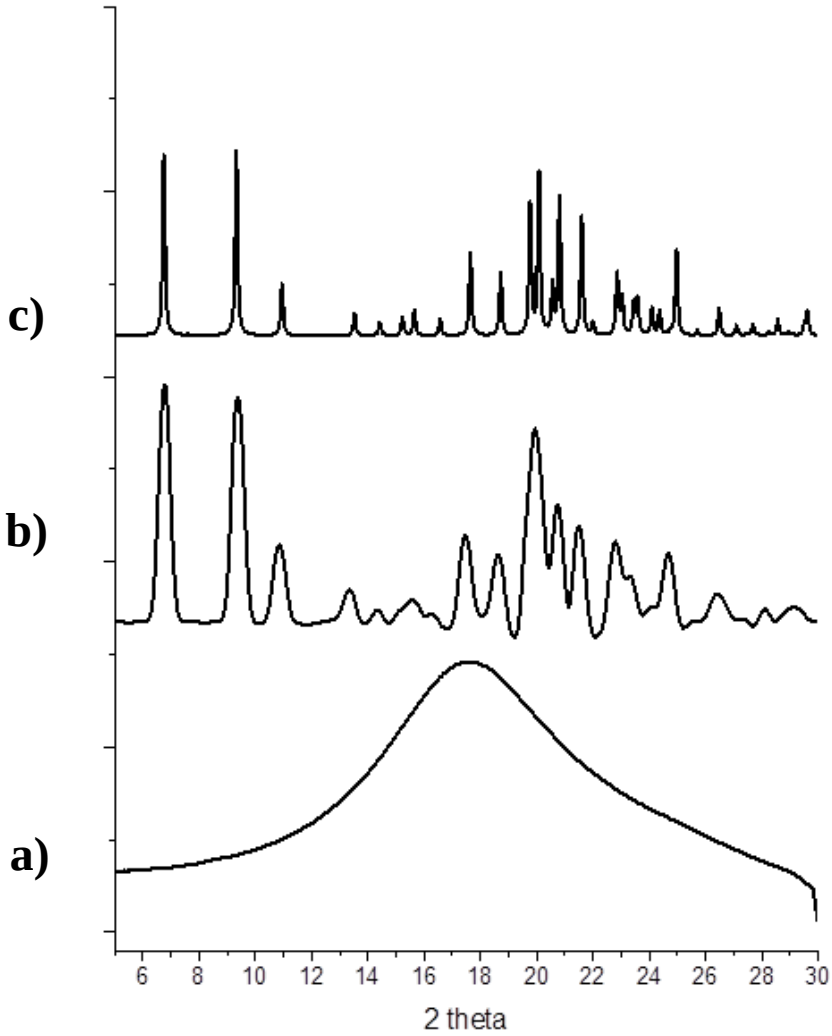


*Figure 5. a) X-ray measurement of Bis 4 gel in toluene. b) X-ray measurement of Bis 4 xerogel extracted from toluene c) simulated powder pattern of the single crystal structure of Bis4 (see figure 4 for the structure of Bis 4).*

## 2.2. X-ray measuring apparatus

Most measurements were performed in transmission geometry, in order to avoid the effect of preferential orientation. Then two different types of powder diffractometer setups were used. The first can be described as a low definition but quick measurement apparatus. Low definition because the obtained powder patterns do not have enough definition to apply the structure solving protocol described in this chapter. Measures performed with this setup are used to quickly scan several xerogels formed in different liquids. This is useful to quickly identify the presence of polymorphs formed due to the interaction of the LMWG and different liquids.

Measurements in the low definition setup were performed as follow: all xerogels were measured in sodaglass capillaries with 1 mm diameter. The two-dimensional wide-angle X-ray scattering (WAXS) patterns were collected on a MAR345 detector using Cu-K□ radiation (wavelength: 1.542 Å) of a rotating anode X-ray source (40 kV, 40 mA; multilayer graded monochromator). Exposure time was 1200 s.

The other types of setups used are considered high definition setups. The powder patterns recorded using these setups contain enough definition to solve the structure. The acquisition time of these setups is in average 2 to 4 times higher than the low definition setup. In this class of high definition measures two different equipments were used depending on availability. The first setup used was a home-made powder diffractometer (Figure 6) in parallel beam geometry and mounted on a rotating anode generator using Cu-K□ radiation (wavelength: 1.542 Å, 40 kV, 40 mA). All xerogels were also measured in sodaglass capillaries with 1 mm diameter. Exposure time was 3600 s. The second setup used was a commercial Rigaku SmartLab configured for paralleled beam geometry. In this setup all xerogels were measured in Kapton tape and using an anode generator using Cu-K□ radiation (wavelength: 1.542 Å, 40 kV, 200 mA). The equipment was configured with incident and receiving soller slits of 5 deg.

Figure 7 shows a comparison of the diffractograms obtained with all three equipments measuring the same sample of a xerogel of **Th12** extracted from toluene.

*Figure 6. Home-made powder diffractometer (Gonio).*

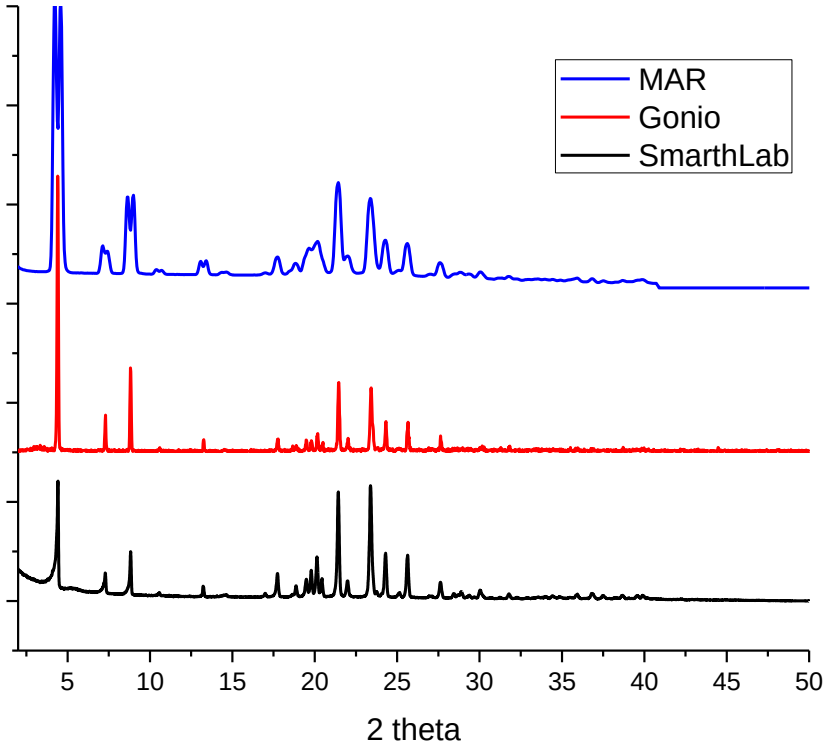


*Figure 7.Comparison of Th 12 xerogel X-ray patterns measured with different equipments, x-ray wavelength of 1.5406 Å.*

## 2.3. Structure resolution method from powder X-ray

### 2.3.1. Indexation

The first step when solving the molecular packing is to find the unit cell parameters of the system. The unit cell can be defined as the smallest volume that repeats itself and has the full symmetry of the model. This step highly depends on the accuracy of the data recovered, definition of the pattern and d-spacing information present on the pattern (number of diffractions on the pattern). Currently there are several tools to perform a relatively quick and reliable indexation. In our case Dicvol[4] was used as indexation software. Reported the first time by Louër & Louër [5], this software uses a dichotomy algorithm based on an exhaustive search of solution, working in the parameter space through crystal systems in decreasing order of symmetry. This method was created to work with orthorhombic and higher symmetry systems and later adapted to work with lower symmetry systems (i.e. monoclinic systems). This is of importance since organic molecules mostly organize periodically in monoclinic systems.[6] Dicvol is present on a wide variety of structural solving software suites such as Fullproof,[7] Expo,[8] and Materials Studio,[9] indicating its preference by the community.[10] Much of the above-mentioned suites contain an automatic peak finder option to facilitate the user's work, but in the case of solving LMWG structures from powder the use of this option is highly discouraged. Manual selection is preferable since the quality of the data recovered in organic systems is normally not compatible with auto selection.

The next tool used in this methodology is the CheckGroup software present in the Fullprof suite.[7] This tool when given a unit cell and a list of extracted intensities can propose a list of possible symmetry groups organized according to their figure of merit. Besides the figure of merit, the calculated density can also be a good criterium to help select the symmetry group. Organic materials have normally a density close to 1 g/cm$^3$, so that symmetry groups that do not result in such value can be excluded, even if they have a high figure of merit.

After obtaining good candidates for unit cell and symmetry groups, the Le Bail Fit [11] technique is applied to fine tune unit cell, instrumental and peak width parameters and extract intensities for further structure resolution.

### 2.3.2. Atomic position

The next step after obtaining a unit cell and a space group, is to find atomic positions of the molecules within the system. The traditional ab initio (direct methods)[12] procedure used to solve structures from single crystal diffraction data is based on the analysis of the electronic density map derived from the Bragg reflection intensities. When working with powder diffraction problems like peak overlapping, nonlinear background, preferred orientation and overall poor data quality cause ambiguities in the extraction of the integrated intensities. These problems together with the complexity of organic molecules that normally contain a large number of atoms in the asymmetric unit and normally accompanied by poor resolution make the use of direct methods not suitable to solve a organic molecule crystal packing.

#### 2.3.2.1. Direct space approach

In order to solve organic structures more information is introduced to the prediction methodology. Instead of trying to find independently the position of individual atoms, an expected structure is input in the system. This molecular structure will adopt different conformations and different positions within the unit cell, respecting the unit cell boundaries and symmetry rules, following a global optimization method. The degrees of freedom of the molecular system can be controlled by the user according to the knowledge in the system. The best solution is indicated by a cost function that compares the observed powder X-ray pattern with the calculated X-ray pattern from the simulated structure. This method called direct space method[13,14] is achieved by using a simulated annealing algorithm present in the Expo software package.[8]

#### 2.3.2.2. Polymorph approach

An alternative method also used was developed by our collaborators from the Laboratory of Chemistry of Novel Materials from the university of Mons. This method involves finding atomic positions using the Polymorph module, implemented in the Materials Studio software.[9] This module searches low-energy crystals in selected space groups for the selected molecule of the asymmetric unit. The Monte Carlo procedure randomly changes the torsions, the relative orientation of the molecules, and the relative orientation of the lattice vectors. The generated molecular packings were then optimized by Molecular Mechanics (MM). All the MM calculations were performed with the Dreiding force field (in which the hydrogen bond parameters have been adapted to properly reproduce van der Waals interactions in the solid state) and assigning PCFF atomic charges. The Metropolis

acceptance/rejection test was based on density (rejection if density lower than 0.3 g/cm$^3$) and energy. Because of periodic conditions, the long-range interactions were treated by the Ewald method, with an accuracy criterion of $10^{-5}$ kcal/mol. Thousands of generated candidates were optimized by MM using energy and force criteria of $2 \cdot 10^{-5}$ kcal/mol and $10^{-3}$ kcal/mol/Å, respectively. Redundant molecular packings were removed using Polymorph Clustering, and the remaining candidates were sorted by energy. Then, the possible crystal structures were selected within the lowest energy structures with cell parameters closest to the values derived from the indexation of the XRD patterns.

### 2.3.3. Refinement

After obtaining a suitable model the last step of every structural solution is the refinement step.

#### 2.3.3.1. Rietveld

The Rietveld refinement is the most used refinement methodology in periodic structure. This method performs small adjustments in the structure (unit cell, atom position, atomic occupancy), the fitting profile (zero, scale, peak shape) and also correction of preferential orientation using the March-Dollase approach, in order to obtain a better correlation between measured and calculated X-ray pattern. [15]

#### 2.3.3.2. Refinement + force field

Despite optimizing the sample for measurement in order to obtain the best definition possible, sometimes the information that can be obtained from a powder pattern might not be enough to fine tune complex models like organic molecules. To overcome this, our collaborators from the Laboratory of Chemistry of Novel Materials from the university of Mons applied a Rietveld refinement coupled with the force field to avoid unrealistic changes in the molecular geometry. This technique was applied using the Reflex module present in the Materials Studio software.[9] This module refines the simulated XRD structure using the Rietveld refinement procedure coupled with force field energy criteria, allowing small changes of the atomic positions while avoiding unrealistically high energy structures. The user can select the weight given to the energy contribution penalty in the combined figure of merit.

## 2.4. Local structure

The previously described methodology is based on the analysis of Bragg diffraction peaks to characterize the molecular packing of a material. Some materials present a broadening and reduction of the number of diffraction peaks which complicates the study of the system. This indicates the material is to some extent amorphous. An amorphous compound can be considered as an arrangement of locally ordered domains, with only short-range order.[16] To analyze such materials there is a need of a method that takes into account not only existent Bragg diffraction but also diffuse diffraction.

### 2.4.1. Pair distribution function

The analysis of the total scattering by the Pair Distribution Function (PDF)[17] is until this moment one of the best methods to analyze the atomic arrangements of amorphous structures. PDF gives the probability of finding two atoms separated by a distance *r*. This analysis takes into account not only Bragg diffraction but also diffuse scattering. The diffuse scattering is often ambiguous to interpret in reciprocal space, but after conversion to PDF this analysis becomes more straightforward to analyze. To transform a diffraction pattern into PDF one applies a Fourier transform to the reduced total scattering structure function, where the background from the capillary and the Compton scattering has previously been subtracted, and diffraction intensities are normalized.

### 2.4.2. Data acquisition and transformation

The main priority when collecting data for PDF is to record the scattered intensity with a good statistics up to a scattering vector Qmax at least equal to 16 $Å^{-1}$. Despite the fact PDF measurement can be acquired with in-house X-ray sources (Mo and Ag), our measurements were obtained using synchrotron radiation (lambda = 0.58171 Å) in order to increase data resolution. All data were collected at synchrotron Soleil beamline Cristal and converted using the software PDFgetX.[18]

To convert a total scattering pattern ($I_m(Q)$) the software PDFgetX first converts the pattern to the reduced structure function. The coherent scattering $I_c(Q)$ is obtained from Eq2. Here $a(Q)$ and $b(Q)$ are multiplicative and additive corrections to the measured intensity, which do not contain structural information, but correct for sample self-absorption and incoherent background, respectively.[18]

$$I_m(Q) = a(Q)I_c(Q) + b(Q) \qquad (Eq2)$$

The $I_c(Q)$ obtained from Eq2 is then used to obtain the structure function, $S(Q)$ according to Eq3. Here $f(Q)$ is the atomic scattering factor and the angle brackets indicate an average over all the atom types in the sample. [19]

$$(Eq3) \quad S(Q) = \frac{I_c(Q) - \langle f(Q)^2 \rangle + \langle f(Q) \rangle^2}{\langle f(Q) \rangle^2}$$

The structure function $S(Q)$ is then transformed to the reduced structure function $F(Q)$ according to Eq4.[20]

$$(Eq4) \quad F(Q) = Q[S(Q) - 1]$$

Finally, to obtain the PDF the reduced structure function is Fourier transformed according to Eq5.[21]

To exemplify this conversion, we use the total scattering pattern of **HSA10** xerogel extracted from toluene. This total scattering pattern is a perfect example to illustrate this conversion since the pattern contains a small number of Bragg diffractions with broad peaks and diffuse scattering. Figure 8 exemplifies this conversion from total scattered pattern to reduced structure function and then to PDF.

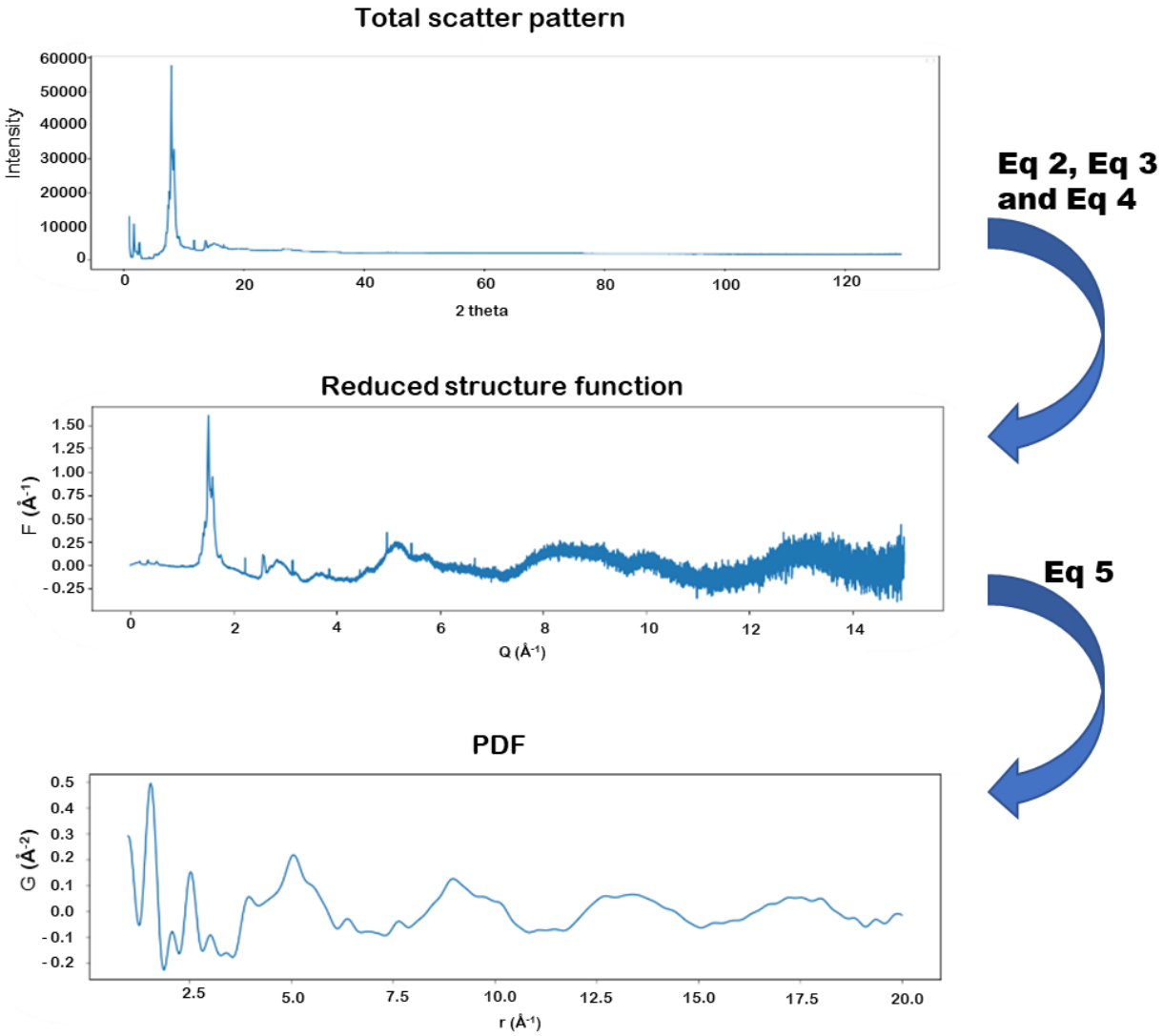


*Figure 8. Example of conversion of total scattering pattern of **HSA10** xerogel extracted from toluene into PDF.*

### 2.4.2.1. Qmax

After collection of the total scattering data it is important to choose the Qmax of the Fourier transform that can be used for conversion to PDF. In an optimal case the Qmax is the highest possible value measured, but this may cause artifacts. Figure 9 exemplifies the PDF of **Bis4** xerogel extracted from toluene using a Qmax of 12 $Å^{-1}$, 15 $Å^{-1}$ and 20 $Å^{-1}$. If one compares 12 $Å^{-1}$ with 15 $Å^{-1}$, it is visible that at small distances (below 6 Å) we lose details. When comparing 20 $Å^{-1}$ with 15 $Å^{-1}$, we can observe that at large periodicities (higher than 6 Å) the baseline of the PDF starts to become distorted. For this reason, we selected a Qmax of 15 $Å^{-1}$ to perform all conversion from total scattering pattern to PDF.

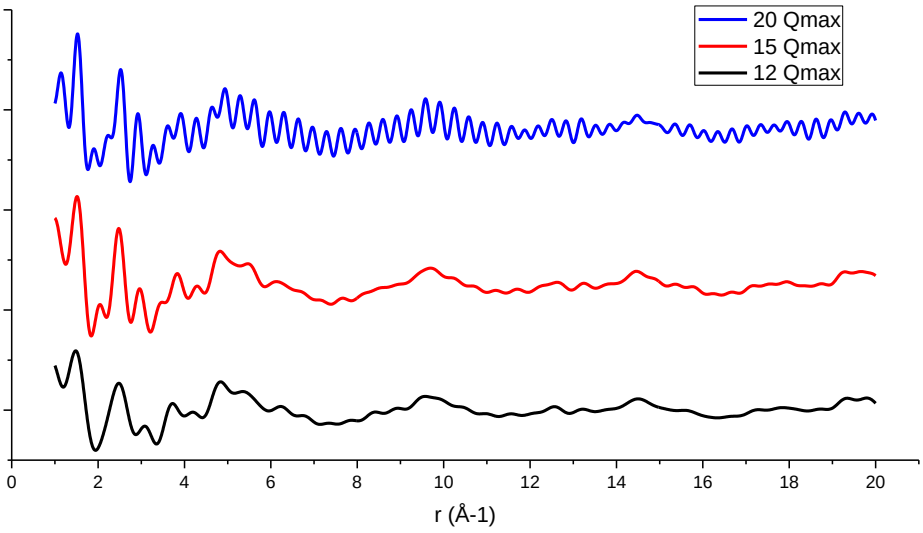


*Figure 9. Comparison of PDF of **Bis4** xerogel extracted from toluene at different Qmax.*

## 2.4.3. Comparing molecular conformations

One of biggest uses of PDF is the study of the local molecular structure when a unit cell cannot be accurately determined or in the case of amorphous materials where there is a lack of long-range periodicity. PDF is highly sensitive to changes in molecular conformation, particularly in the intra-molecular region (between 0 and 8 $Å^{-1)}$, thus this technique allows us to directly compare different gel fibers and determine if there are significative differences of the local structure within gel fibers. To illustrate how different molecular conformations can result in different PDF, we simulated the theoretical PDF of **Bis4** in the single crystal conformation (Figure 10 red) and compared to the theoretical PDF of a randomly generated conformation of **Bis4** (Figure 10 blue) using the PDFgui software22. By overlapping both PDF we can observe the differences in the intra-molecular region.

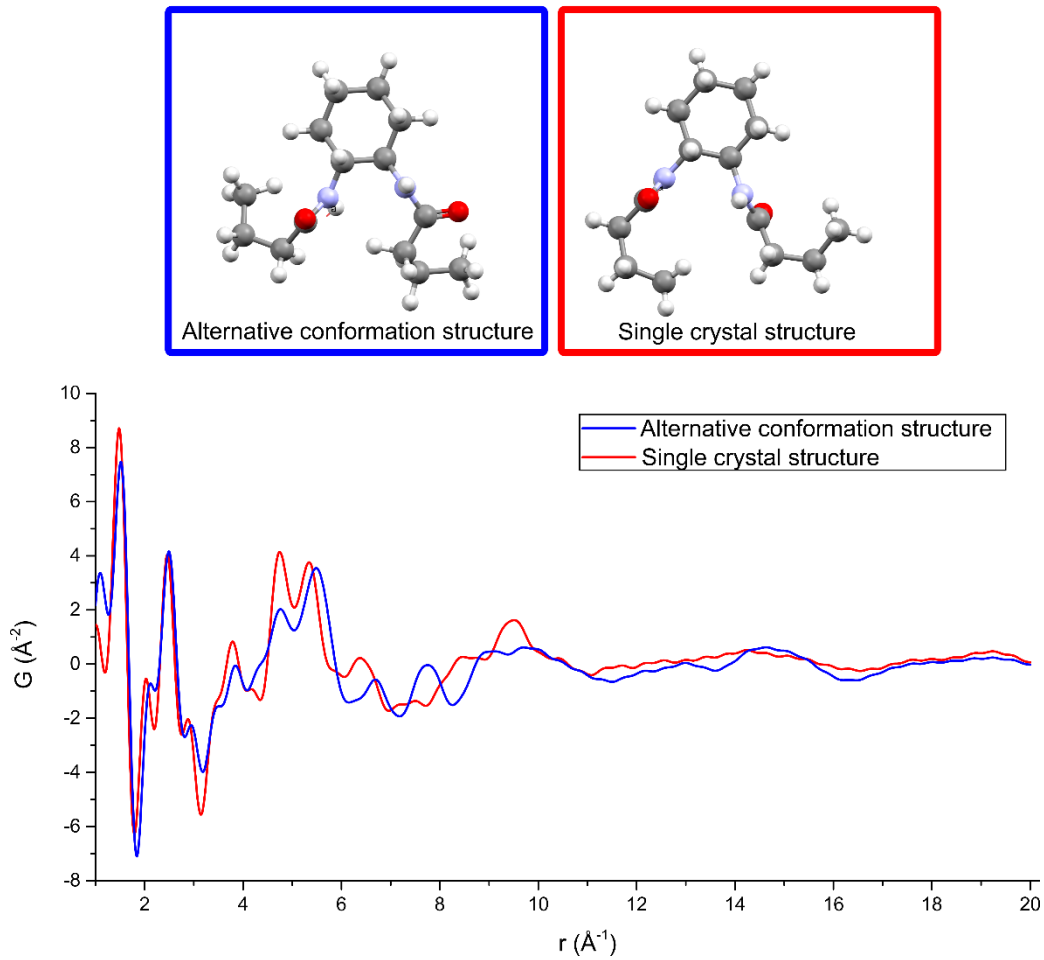


*Figure 10. Comparison of the theoretical PDF of **Bis4** in the single crystal conformation (red) and in a randomly generated conformation (blue).*

## 2.4.4. Comparing experiment with simulation

In order to use PDF to validate if a given molecular packing model accurately represents a given gelator we need to simulate the PDF of the model and compare with the measured PDF of the system in study. To do so, we first need to tune the different simulation parameters to obtain a PDF pattern that would match the measured PDF. The aim is that the only differences between simulated and measured PDF should come from the model itself and not from instrumental variables. We used the single crystal structure of **Bis4** to simulate PDF and fine tune the simulation parameters that are not related with structure until we obtained the best match with the measured PDF of **Bis4** xerogel extracted from toluene. We chose **Bis4** because of the available single crystal structure in the literature and also because it was already demonstrated in this chapter that the molecular packing within gel fibers is the same as the single crystal structure. We adjusted scale factors and Qbroad values using the PDFgui software[22] in order to obtain the best match. The scaling factor should always be set to adapt freely in every refinement cycle and the optimal Qbroad value found for these materials was 0.5. Figure 11 illustrates the match between the computed and measured PDF of **Bis4**.

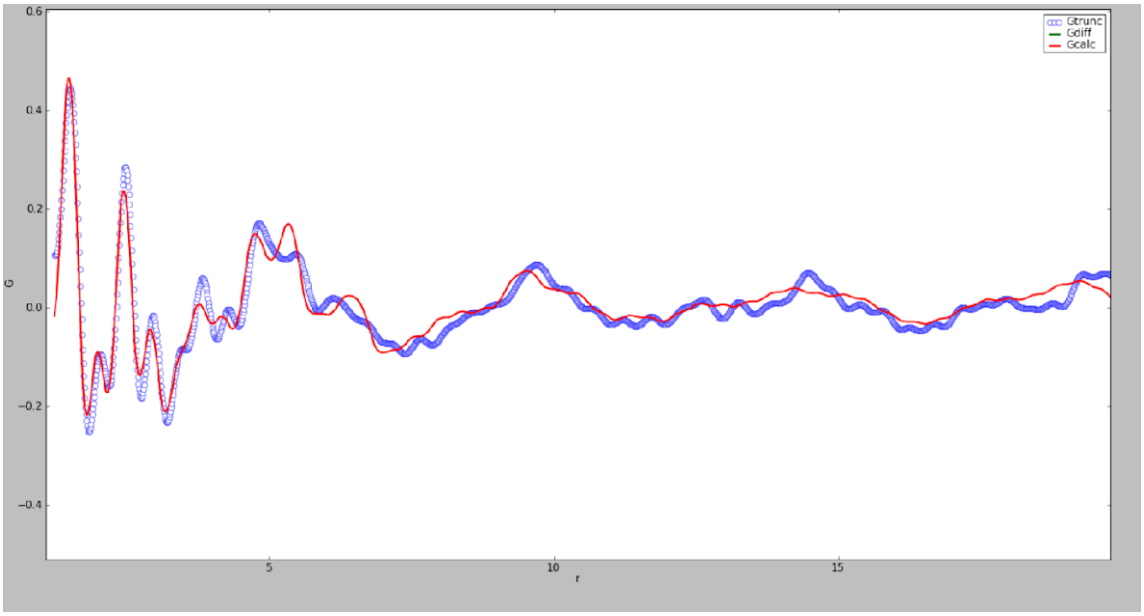


*Figure 11. Comparison of calculated PDF from **Bis4** crystal structure (red) and measured PDF of **Bis4** xerogel extracted from toluene (blue).*

Full structure solving methodologies only using PDF as a basis are still not widely available, thus for structures that present few and broad diffractions we apply a hybrid procedure based on the previously presented methodologies based on Bragg diffractions. Indexation and simulated annealing occur normally but instead of performing Rietveld refinement (with or without energies), the best model is energetically optimized using only force field. Within this exercise for each target molecule several conformational models are generated and then imported to the PDFgui software. After importing all models, the corresponding simulated PDFs are generated and compared to the measured PDF. The best model is then chosen based on the fit between simulated and measured PDF.

# 3. Remarks

This chapter presents a breakdown of the methods used in this work to provide additional information about the organogelator systems. A brief description of the microscopy techniques and equipment used to characterize the morphology of gel fibers is provided as well as in depth explanation of the methods used to study the molecular structure within gel fibers. The study of the molecular packing is based on X-ray diffraction techniques with the aid of computational modeling techniques. The nature of the methodology adopted to study the molecular packing in the gel fibers depends on X-ray powder pattern measured from the xerogels. If the gelators assemble in a highly organized fashion with well-defined periodicities, the X-ray powder pattern presents a considerable number of diffraction peaks with narrow widths and thus it is possible to extract data from the pattern itself to perform computational modeling (in this case called direct space method). If the gelator assembles in a less organized fashion, the resulting X-ray pattern presents a reduced number of diffraction peaks with large widths. When this is the case extraction of information from the X-ray pattern becomes complicated and the use of the PDF becomes the only alternative to extract information from the molecular packing. With the PDF the emphasis is more on the local structure (conformation and neighbor molecules) instead of periodicity and symmetry groups. With these techniques we were able to provide explanatory models of the molecular packing for most of the studied families of gelators. Such models provided insight of the mechanism of self-assembly that leads to gelation.

# 4. Bibliography


1 J. van der Gucht, Front. Phys.,2018, 6, 87

2 G. Yu, X. Yan, C. Han and F. Huang, Chem. Soc. Rev., 2013, 42, 6697.

3 W. H. Bragg and W. L. Bragg, Proc. R. Soc. A Math. Phys. Eng. Sci., 1913, 88, 428–438.

4 A. Boultif and D. Louër, J. Appl. Crystallogr., 2004, 37, 724–731.

5 D. Louër and M. Louër, J. Appl. Crystallogr., 1972, 5, 271–275.

6 N. Padmaja, S. Ramakumar and M. A. Viswamitra, Acta Crystallogr. Sect. A, 1990, 46, 725–730.

7 J. Rodríguez-Carvajal, Phys. B Condens. Matter, 1993, 192, 55–69.

8 A. Altomare, C. Cuocci, C. Giacovazzo, A. Moliterni, R. Rizzi, N. Corriero and A. Falcicchio, J. Appl. Crystallogr., 2013, 46, 1231–1235.

9 D. S. BIOVIA, 2011.

10 D. G. Porob and T. N. G. Row, J. Chem. Sci., 2001, 113, 435–444.

11 A. Le Bail, H. Duroy and J. L. Fourquet, Mater. Res. Bull., 1988, 23, 447–452.

12 A. Altomare, C. Cuocci, A. Moliterni and R. Rizzi, J. Appl. Crystallogr., 2013, 46, 476–482.

13 M. Falcioni and M. W. Deem, J. Chem. Phys., 1999, 110, 1754–1766.

14 A. Altomare, N. Corriero, C. Cuocci, A. Moliterni and R. Rizzi, J. Appl. Crystallogr., 2013, 46, 779–787.

15 H. M. Rietveld, J. Appl. Crystallogr., 1969, 2, 65–71.

16 S. Bates, G. Zografi, D. Engers, K. Morris, K. Crowley and A. Newman, Pharm. Res., 2006, 23, 2333–2349.

17 D. Prill, P. Juhás, M. U. Schmidt and S. J. L. Billinge, J. Appl. Crystallogr., 2015, 48, 171–178.

18 P. Juhás, T. Davis, C. L. Farrow and S. J. L. Billinge, J. Appl. Crystallogr., 2013, 46, 560–566.

19 C. L. Farrow and S. J. L. Billinge, arXiv Prepr. arXiv1211.4284.

20 B. E. Warren, X-ray Diffraction, Courier Corporation, 1990.

21 C. L. Farrow and S. J. L. Billinge, Acta Crystallogr. Sect. A Found. Crystallogr., 2009, 65, 232–239.

22 C. L. Farrow, P. Juhas, J. W. Liu, D. Bryndin, E. S. Božin, J. Bloch, T. Proffen and S. J. L. Billinge, J. Phys. Condens. Matter, 2007, 19, 335219.

# 7. Chapter 2

# 8. Rationalizing Organogelation

Several groups already attempted to rationalize organogelation by applying different methodologies. In this chapter such methodologies will be discussed with a focus on the rationalization of organogelation using Hansen solubility parameters. This will include the theoretical background of the method, its limitations and the proposition of a comprehensive revision of the method.

# 1. Literature review of the rationalization attempts on organogelation

## 1.1. Dielectric constant (ε)

M. Zinic et al.[1] proposed one of the first attempts of rationalizing organogelation properties. In his work a bis(amino acid) oxalylamine gelator was synthesized and used to gelate several alcohols. Upon gelation the thermally reversible gel-sol transition temperature (Tgel) of all gels was measured and correlated with the dielectric constant (ε) of each alcohol. A direct correlation was observed between the Tgel values of gels formed in linear alcohols ranging from one to six carbons (methanol to 1-hexanol), but also of some cyclic and branched alcohols, showing a linear correlation with an $r^2$ >0.99. In these cases, the Tgel decreased with an increase of ε. It implies that better solubility and less efficient network assembly occurs for the gelator in the alcohols of higher dielectric constant. However, for the alcohols with longer linear alkyl chains (1-heptanol to 1-dodecanol), no Tgel/ε correlation was observed at all. In each case much lower Tgel values than expected were measured on the basis of their ε values. The explanation for this phenomenon provided by the author was that, the dispersive interactions between the gelator and long and foldable alkyl chains of higher n-alcohols enhance its solubility in these solvents, breaking the linear correlation. Whatever the reason, it is clear that such correlation is not general.

## 1.2. ET polarity scale

In another attempt to rationalize organogelation D.K. Smith et al.[2] compared the Tgel of a two-component gelator (diaminododecane with dendritic L-lysine-based peptide) in different liquids with different solubility parameters. In this study D.K. Smith attributes the solvent effect to its polarity. [3] When comparing the Tgel with the ε of the solvents a poor correlation was obtained, thus other polarity scales were tested. The *E*t polarity scale is derived from the solvatochromic behavior of Reichardt's dye.[4] In this case, a better correlation was found where the Tgel decreased with the increase of the *E*t. Indeed, protic solvents (*E*t 0.5-1.0) resulted in optically transparent solutions whereas dipolar non-hydrogen bond donor (*E*t 0.3-0.5) and apolar non-hydrogen bond donor (*E*t 0.0-0.3) solvents formed gels with higher Tgel. Despite showing a better correlation that ε, using the *E*t scale is far from ideal. As an example, it was observed that chloroform (*E*t 0.259) did not allow gel formation, while 1,2-dichloroethane (*E*t 0.327) did, breaking the trend proposed by the author.

## 1.3. Hildebrandt solubility parameter

In contrast from the two previous methodologies reported that used polarity of a solvent as the main parameter to rationalize organogelation, C. Friedrich et al. [5] proposed to rationalize Tgel with the Hildebrandt solubility parameter. The Hildebrandt solubility parameter is defined by the square root of the cohesive energy density of a solvent, which is derived from the enthalpy of vaporization.[6] By studying the organogelation of different polymeric matrixes by 1,3,2,4-dibenzylidene-d-sorbitol an average correlation was achieved: Tgel increased when the difference of the Hildebrandt solubility parameter between gelator and polymer increased. C. Friedrich also proposed that a better correlation could not be obtained due to the lack of accuracy of the Hildebrandt solubility parameter given for the polymer matrixes.

## 1.4. Kamlet–Taft parameters

Upon realizing the rationalization of organogelation with a single solubility parameter did not yield the best results, D.K Smith[7] tested a multi parameter solubility parameter, the Kamlet–Taft parameters. The Kamlet–Taft parameters[8] measure separately the hydrogen bond donor (α), hydrogen bond acceptor (β), and dipolarity/polarizability (π*) properties of solvents as contributing to overall solvent polarity. Using a family of L-lysine bis-urea gelators with variable peripheral groups in different solvents, D.K. Smith concluded that the α parameter of a solvent appears to have the highest importance in controlling whether a hydrogen bond network of gelators can be established and thus gelation occurs, since solvents with a α different from zero did not form gels. The β parameter was thought to tune the thermal stability of the gel by modulating gelator–gelator interactions and the π* parameter was thought to control the interactions of the peripheral groups of the gelator with solvent, and tune gel stability and the ability of the gelator to establish fiber–fiber interactions. Obviously, these conclusions are only valid for this particular family of gelators.

## 1.5. Hansen Solubility Parameters

Some authors [9-12] attempted to rationalize organogelation with the Hansen Solubility Parameters (HSP). [13–15] The HSP decompose the cohesive energy density into three different parameters: dispersive interactions (δd), polar interactions (δp) and hydrogen bonds (δh). The first attempts considered each parameter individually and did not provide a good correlation with organogelation. Bouteiller et al.[16,17] improved the correlation by considering that all 3 HSP parameters (δd, δp, δh) should be used simultaneously to correlate with the gelation properties. They proved this by applying his methodology to several organogelators described in the literature.

Mainly, the HSP are widely used in polymer science to predict solubility. To do this the HSP work

by the principle of similarity: if the HSP value of a target polymer is close to the HSP of a liquid, the target polymer should be soluble in the liquid. It is to be noted that HSP are a predictive methodology that is only based on thermodynamics and not kinetic, this means that the HSP can predict if a polymer is soluble in a liquid but cannot predict how long solubilization will take. In practice the HSP of a polymer are determined by performing solubility tests with liquids that already have their HSP published in the literature ($\delta d^S$, $\delta p^S$, $\delta h^S$). The results are then plotted in a 3D diagram with the three HSP as axes. This diagram is called Hansen space. The solvents that solubilize the polymer tend to from a cluster and in order to simplify data treatment the smallest sphere that contains the majority of liquids that solubilize the polymer is determined. This sphere is called the solubility sphere. The center of this sphere defines the HSP value of the tested polymer ($\delta d$, $\delta p$, $\delta h$). The distance between a liquid and the center of the solubility sphere in the Hansen space is given by Eq 6.

$$Eq\ 6 \quad R = \sqrt{4(\delta d - \delta d^S)^2 + (\delta p - \delta p^S)^2 + (\delta h - \delta h^S)^2}$$

For an untested liquid, if the R value is smaller than the radius of the solubility sphere, then there is a high probability of the liquid being a good solvent for the tested polymer. Figure 12 represents the Hansen space of Bis 6,[18] illustrating liquids that solubilize the compound by blue points clustered in the same region and the liquids that do not solubilize the compounds represented by red points surrounding the clustered region of blue points.

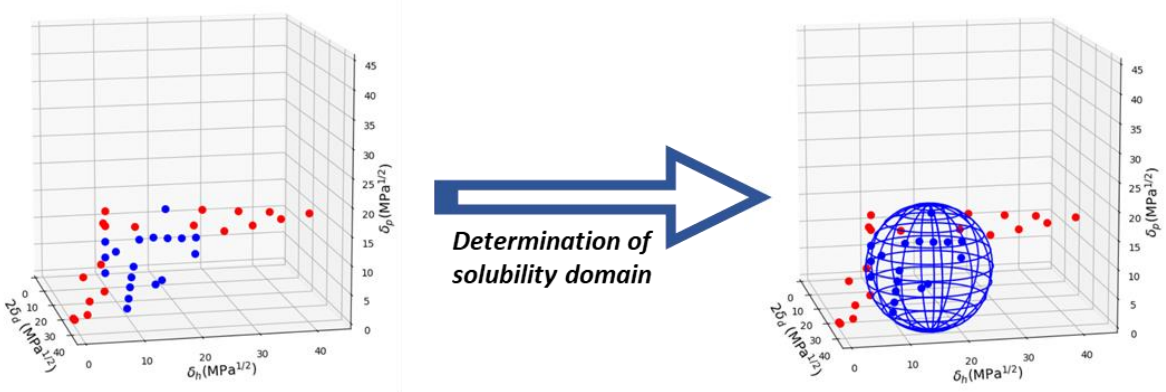


*Figure 12. Hansen space of Bis 6. Liquids that solubilize the compound are represented by blue points. Liquids that do not solubilize it are represented by red points. The solubility sphere is represented by a blue meshed sphere.*

In a first global attempt to rationalize organogelation with the HSP, Bouteiller et al.[16] selected 8 LMWG reported in the literature[19–26] that provide an extensive set of solubility data. The selected LMWG included various molecular structures, with the main interaction ranging from hydrogen bond

or ionic bond to π-staking, dipolar and van der Waals interactions. The results were then plotted in the Hansen space, being this time divided in three classes: S (forming a solution), I (either insoluble or formation of a precipitate after cooling) and G (gel formation). For all the tested examples, it was observed a clustering of the majority of S points, similar to what is observed for polymers, and a clustering of the majority of G points in a distinct area of the Hansen space. Thus, a gelation sphere was calculated in addition to the solubility sphere. Therefore, as long as a sufficient solubility dataset is available, this method allows to predict if an untested liquid will be gelated by a given gelator.

The correlation of HSP with the gelation ability of LMWGs has since then been applied in numerous publications, with varied approaches to data treatment and presentation. Some studies performed a simple qualitative description of the Hansen space (without determining a gelation sphere) or used a 1D or 2D projection of Hansen space (Teas Plot) to simplify the data treatment and representation.[27–41] The use of the Teas Plot avoids the need for a software that generates 3D plots, since it uses a specific 2D projection (Figure 13). Despite facilitating data representation, this approach is not fit to plot big data sets and can lead to misleading interpretations. If two point are close in the Hansen space, they with also be close in the Teas Plot, but the reverse is not true. For instance, diethyl ether ($\delta d = 14.5$, $\delta p = 2.9$, $\delta h = 4.6$ $MPa^{1/2}$) and chloroform ($\delta d = 17.8$, $\delta p = 3.1$, $\delta h = 5.7$ $MPa^{1/2}$) are far apart in the Hansen space, which reflects their well-known solubility differences, but they are nearly at the same location in the Teas plot.

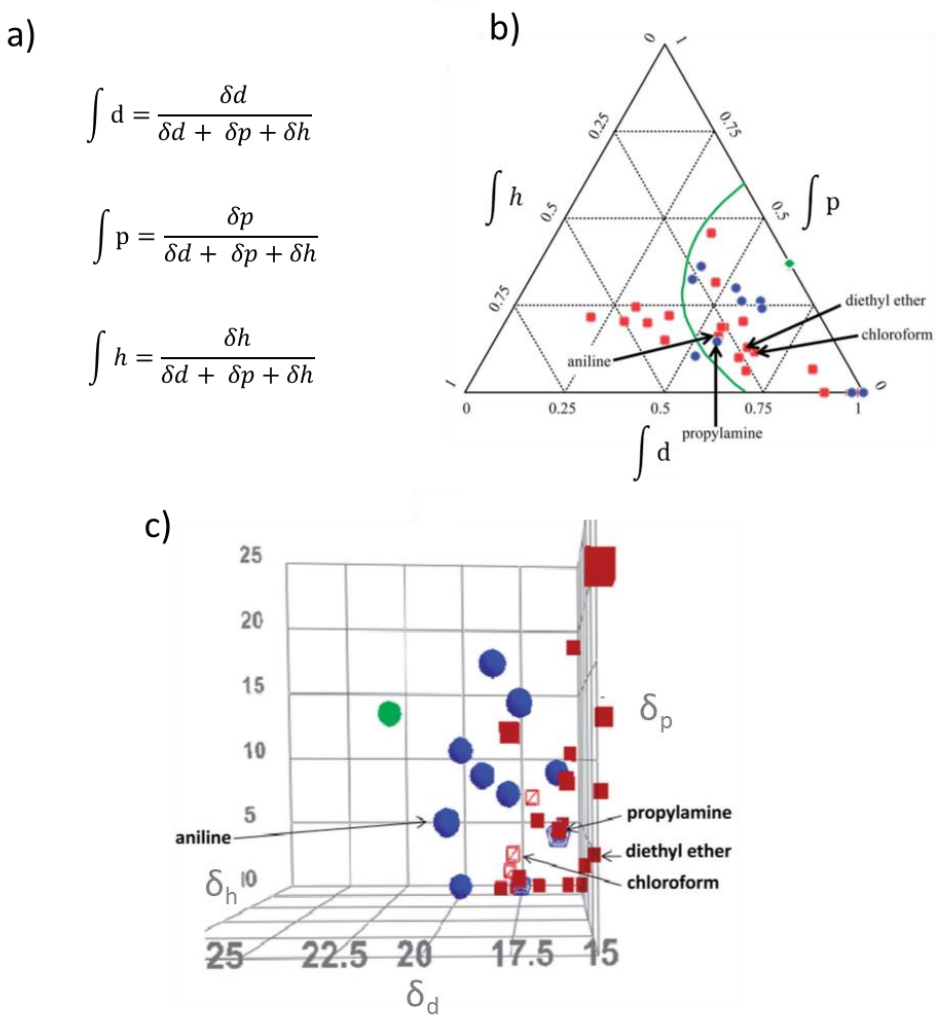


*Figure 13. a) formula for normalizing HSP for Teas plot. b) Teas plot representing the proximity of diethyl ether and chloroform. c) Hansen space representing the distance between diethyl ether and chloroform.*

More interestingly, some studies proposed alternative procedures to determine a gelation domain in the Hansen space from a particular set of experimental data.[42–50] While these alterations in data treatment are certainly well suited to particular datasets, the natural question that arises is whether they are of general applicability.

Therefore, the next part[51] presents my contribution to the revision of the initial methodology to calculate the gelation domain, with the necessary changes to account for the new data and to allow an easy comparison between different experimental studies.

# 2. Rationalizing organogelation with the Hansen Solubility Parameters

## 2.1. The initial method

The accepted methodology to determine the *solubility* sphere of any kind of solute is to find the centre and radius of a sphere so that most **S** points should lie inside the sphere and most other points (**P** and **G** in the case of a LMWG) should lie outside. [13–15] By analogy, in the initial method to calculate the *gelation* domain,[16,17] the centre and radius were determined in such a way that most **G** points should lie inside the sphere and most **S** and **P** points should lie outside. The consequence of this procedure is that no or very little overlap of the gelation and solubility spheres is expected. We call this procedure NO (for No Overlap). The solubility and gelation spheres obtained with this NO procedure presented a good description of the data of several LMWGs available in the literature.[16,17] The same methodology was also successfully used in a comprehensive gelation study of amide derivatives of (R)-12-hydroxystearic acid gelators.[52]

## 2.2. Do gelation and solubility spheres share the same center?

Since the first approach was published, other methods to determine the gelation sphere have appeared. In particular, Weiss et al.[47,48] proposed an approach that resulted in concentric spheres (CS), with the solubility sphere being enclosed by the gelation sphere. This was achieved by taking into account the center of the solubility sphere and force fitting the gelation sphere to have the same center. This CS method presented a good fit in the Hansen space of some LMWGs and made less complex the data interpretation.[47,48] However, it was proven to be not general, since Weiss and Rogers et al in later studies[42,44,45,49,50] showed several cases where this CS treatment is not the best alternative. Indeed, there are LMWG where the **G** points are not uniformly distributed around the solubility sphere in Hansen space. To clearly exemplify this lack of generality, the CS method was applied to the data obtained in a previous study [52], using the LMWG **HSA4** (Figure 14).

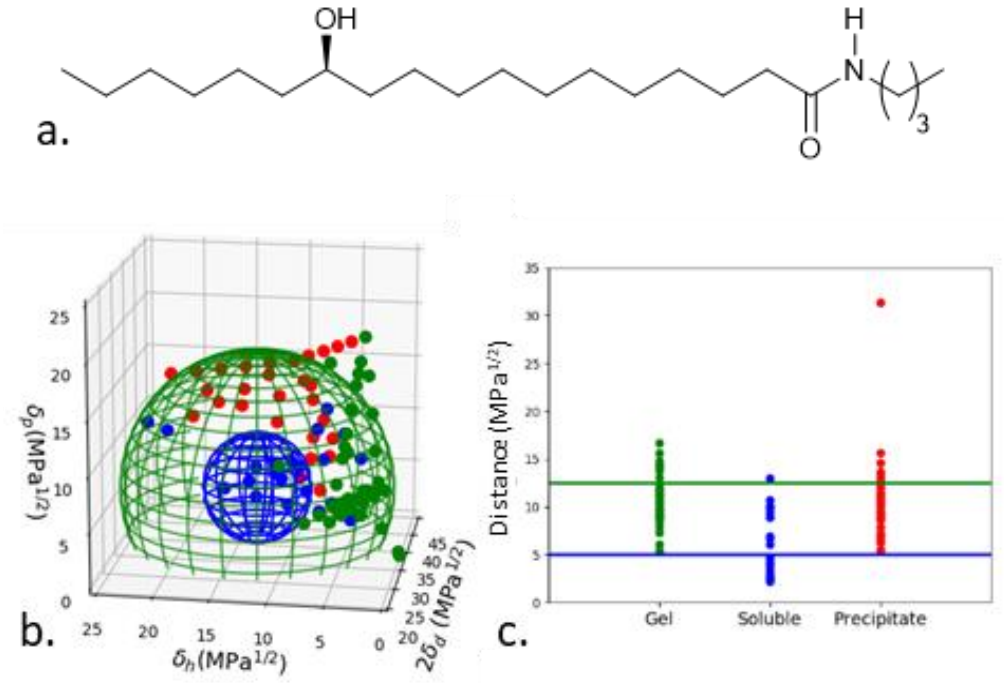


*Figure 14. a) LMWG **HSA4** b) Data for **HSA4** at 2 wt/v % represented in Hansen space. Liquids are represented by full circles and calculated domains are represented by meshed spheres. Green: gel; Red: precipitate. Blue: soluble. The solubility and gelation spheres are forced to have the same centre (CS method). c) Distances in HSP space of the liquids tested to the centre of the gelation and solubility spheres, highlighting the radius of the spheres by a green (gelation) or blue (solubility) line. 31 outlying points (8 **G** points outside the gel sphere and 23 **P** points inside the gel sphere) are created with this method. [Solubility sphere: δd = 17.57; δp = 4.89; δh = 13.29; $R_{Sol}$ = 5.0 MPa$^{1/2}$, Gelation sphere: $R_{Gel}$ = 12.5 MPa$^{1/2}$]*

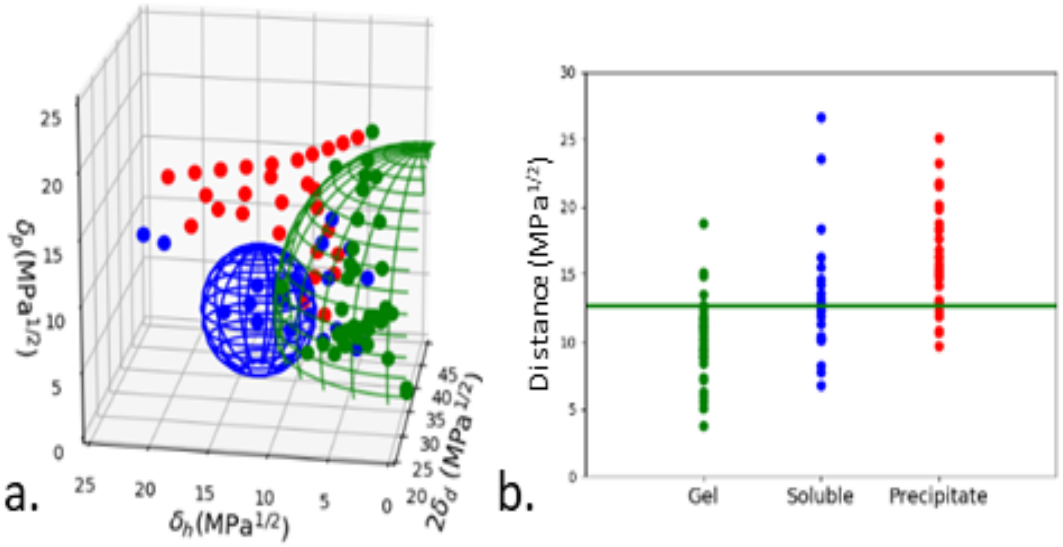

*Figure 15. a) Same data as in Fig. 14. The solubility and gelation spheres are not forced to have the same centres (NO method). b) Distances in HSP space of the liquids tested to the centre of the gelation sphere, highlighting the radius of the gelation sphere by a green line. 9 outlying points (4 **G** points outside the gel sphere and 5 **P** points inside the gel sphere) are created with this method. [Gelation sphere: δd = 20.57; δp =3.71; δh = 0.00; $R_{Gel}$ = 12.7 $MPa^{1/2}$]*

The determination of a gelation sphere for **HSA4** that has the same centre as the solubility sphere results in a poor fit to the experimental data, with 23 **P** points and 8 **G** points as outliers. In contrast, if the centre of the gelation sphere is not imposed to be the same as the centre of the solubility sphere, a better fit is obtained with only 4 **P** points and 5 **G** points as outliers (Figure 15).

## 2.3. Do gelation and solubility spheres overlap?

Although force fitting the centre of the gelation sphere may not be the best general method for domain determination, we cannot discard the hypothesis that some LMWG could show a better fit of the data if the gelation and solubility spheres are allowed to overlap (fully or partially). This was actually observed by several authors, [42,44,45,49,50] and we investigate this issue with the following example: LMWG **Bis6**, a bisamide based LMWG[18] (Figure 16a) was synthesized and its gelation ability was tested.

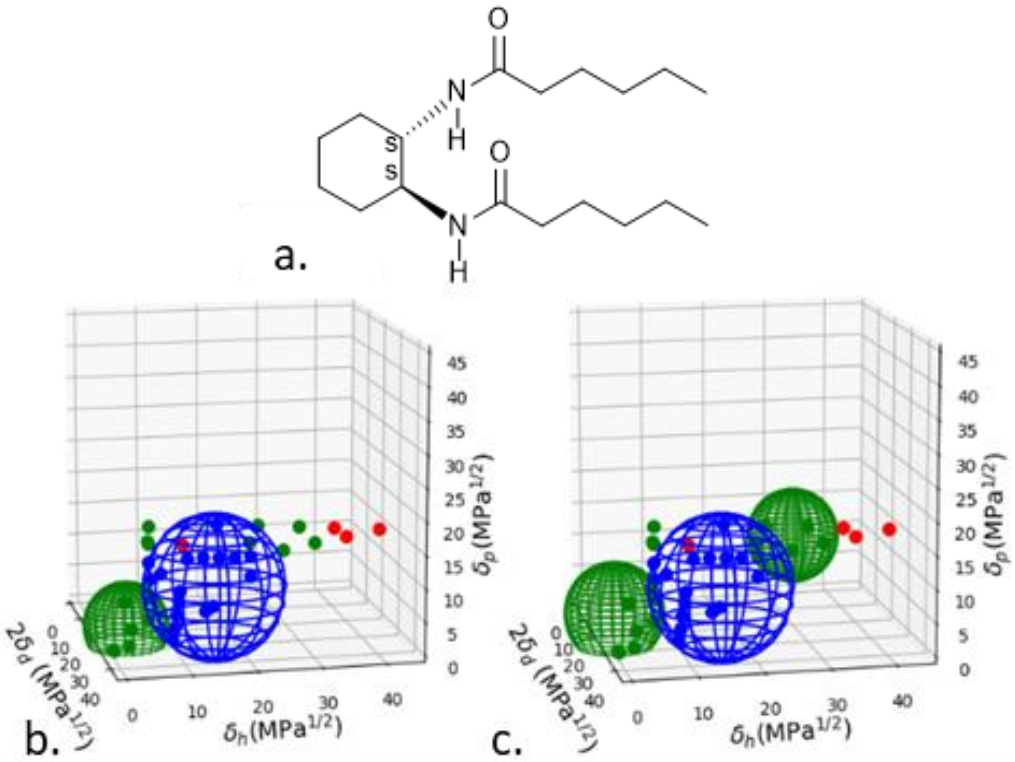


*Figure 16. a) LMWG **Bis6** b) Data for **Bis6** at 1 wt/v % with a single gelation sphere. Liquids are represented by full circles and calculated domains are represented by meshed spheres. Green: gel; Red: precipitate. Blue: soluble. The spheres are determined according to the NO method [Gelation sphere: δd = 15.93; δp = 3.33; δh = 2.31; $R_{Gel}$ = 6.5 MPa$^{1/2}$] c) Same data with two gelation spheres. [Gelation sphere 1: δd = 15.41; δp = 5.24; δh = 0.0 ; $R_{Gel}$ = 7.5 MPa$^{1/2}$, Gelation sphere 2 : δd = 16.34; δp = 16.11; δh = 26.99; $R_{Gel}$ = 6.8 MPa$^{1/2}$]. [Solubility sphere: δd = 18.56; δp = 9.82; δh = 15.08; $R_{Sol}$ = 10.9 MPa$^{1/2}$]*

Using the original NO methodology in which the gelation and solubility spheres are not allowed to overlap, it was not possible to obtain a good fit to the experimental data (figure 16b). This procedure resulted in 8 **G** points as outliers. As previously proposed,[17] this bad fit drove us to test whether the use of two gelation spheres would be more suitable. Of course, this approach results in a better fit showing only 3 **G** points as outliers (figure 16c).

A possible reason why two gelation spheres might exist, is if each one is associated to a specific crystalline packing.[53,54] Therefore, X-ray measures (figure 17) were performed on xerogels obtained from different liquids in order to test this point.

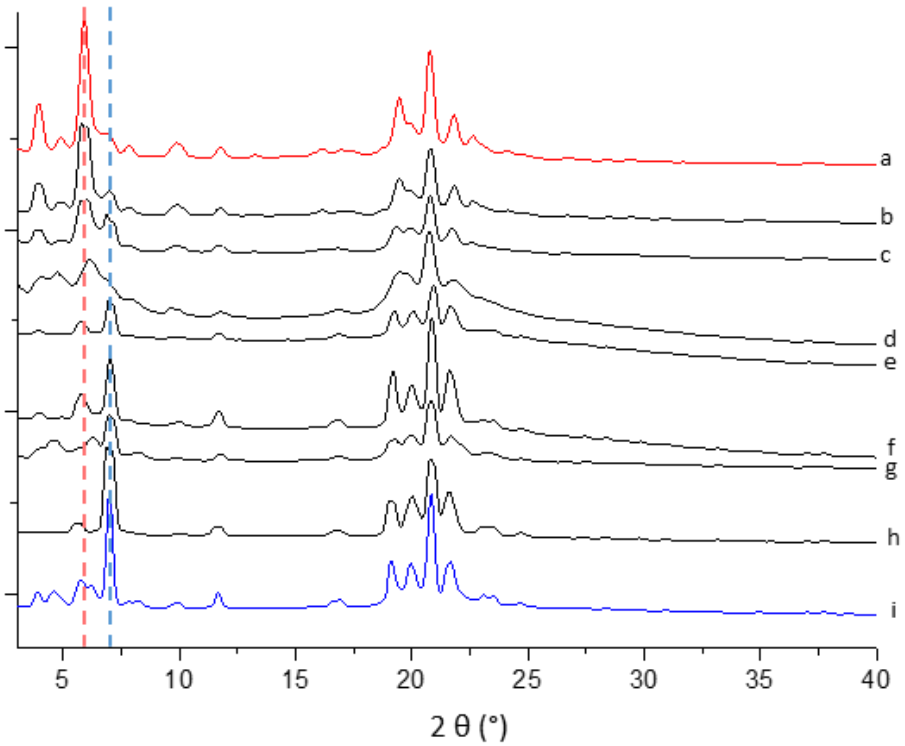


*Figure 17. X-ray patterns of xerogels of **Bis6**, a - toluene, b - t-butylacetate, c – 1-chloropentane, d - acetonitrile, e - cyclohexane, f - chlorobenzene, g - methylethylketone, h - methanol/water (composition:75/25), i - methanol/water (composition:50/50). Diffractograms a to g (respectively h to i) correspond to gels included in the low δh (respectively high δh) gelation sphere of Fig. 16. Dashed red line (respectively blue) highlight the peak representative of phase 1 (respectively phase 2). X-ray wavelength of 1.5406 Å.*

Indeed, significant differences in the patterns indicate that more than one phase is present. We propose that two phases coexist, one of them being prominent in the xerogel formed in toluene (Figure 17a) while the other one is prominent in the xerogel obtained from the methanol water mixture (50:50) (Figure 17i). A precise indexation of both phases is still under investigation, but it is sufficient to notice at this point that the coexistence is observed for both spheres. It means that this polymorphism is not a discriminant factor between the two gelation spheres (Figure 17c), thus not supporting the existence of more than one gelation sphere.

Rogers and Weiss [42,49] presented an alteration of Weiss original CS methodology [47,48] to determine the gelation sphere where they showed the gelation and solubility spheres sharing a common volume

in the Hansen space, without sharing the same center. Following this idea, the original methodology is adapted to allow overlapping gelation and solubility spheres (AO method stands for Allowed Overlap). We propose to calculate the gelation sphere so that most **G** points lie inside the sphere and most **P** points lie outside, with no consideration of where the **S** points are placed. When this new AO methodology is applied to the data of **Bis6**, a large gelation sphere is obtained that encloses the solubility sphere (Figure 18). It results in a good description of the experimental data with only a single outlier (Figure 19).

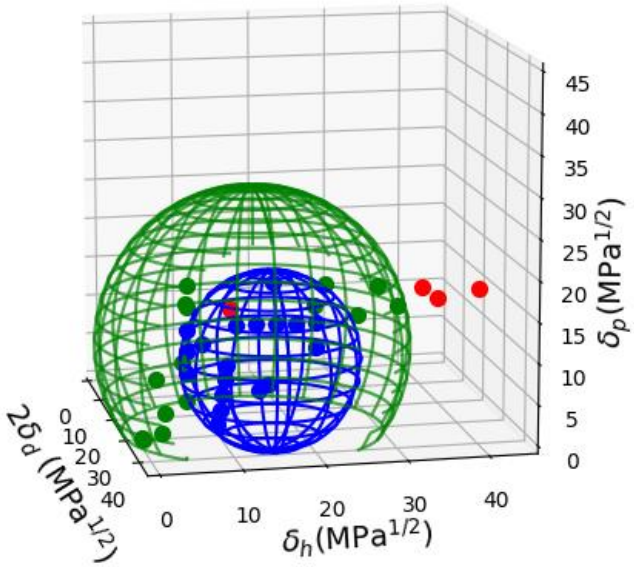


*Figure 18. Same data as in Fig. 16. Liquids are represented by full circles and calculated domains are represented by meshed spheres (AO method). Blue: soluble; Green: gel; Red: precipitate. [Gelation sphere: δd = 16.25; δp = 10.94; δh = 13.76; $R_{Gel}$ = 19.91 MPa$^{1/2}$; Solubility sphere: δd = 18.56; δp = 9.82; δh =15.08; $R_{Sol}$ = 10.9 MPa$^{1/2}$]*

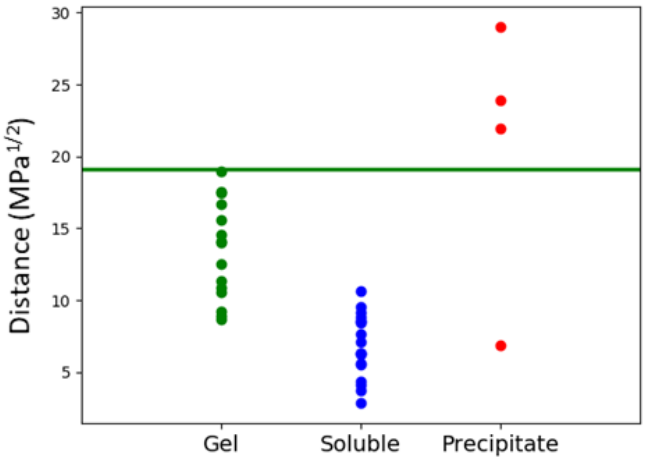


*Figure 19. Same data and spheres (AO method) as in Fig. 18. Distances in HSP space of the liquids tested to*

*the centre of the gelation sphere, highlighting the radius of the sphere by a green line. Green: gel; Red: precipitate. Blue: soluble.*

When this new AO method is applied to LMWGs that had been previously studied by Bouteiller et al., [17] we obtain similar outcomes as with the NO method (annexes at the end of this manuscript). Indeed, these previously studied LMWGs, do not show **G** points uniformly distributed around **S** points, so that the AO method yields non-overlapping gelation and solubility spheres, with similar center, radius and number of outliers as the originally proposed NO method. [16,17] Moreover, this AO method was also tested with success on all recent gelation data dealing with the HSP-based rationalization of gelation (see data in the Annexes chapter [28–33,35,37–40]).
This indicates that using a methodology that allows but does not force the gelation sphere to share a common volume with the solubility sphere is the most suitable option for a general method for the determination of the gelation domain.

## 2.4. The need for a dedicated algorithm

Finally, it is important to use a precise optimization procedure to determine the center and radius of the spheres (gelation and solubility). Indeed, the ideal situation where all **G** points lie inside the gel sphere and all **P** points lie outside is rather rare. Therefore, a quantitative criterion must be chosen to measure the quality of the fit. Examples of such criterion and minimization algorithm have been proposed by Gharagheizi et al[55] or in the HSPiP[13–15] or UMD[48] software.
An alternative approach called the minimal enclosing sphere has been proposed.[42] In this method, the gelation sphere is the smallest sphere that contains all the **G** points. The problem with this admittedly simple method is that a single **G** point that lies far from the other points will considerably and artificially displace the gel sphere.
To illustrate the need of a minimization algorithm we determined the gelation sphere of **HSA18**[52], using either the minimal enclosing sphere method (Figure 20) or a dedicated fitting algorithm (Figure 21). The principle of the algorithm is to minimize the objective function in order to get a sphere which includes a maximum of **G** points and a minimum of **P** points. In this case the comparison is clear, showing that the minimal enclosing sphere resulted on an overall of 54 outliers compared with only 10 outliers when using the dedicated fitting algorithm.

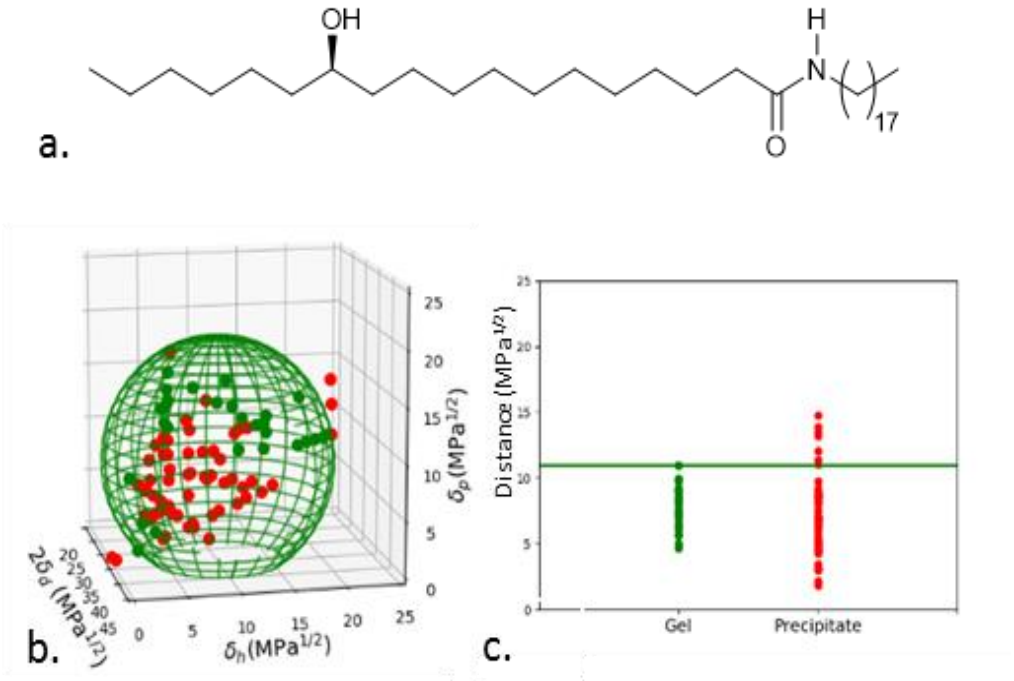


*Figure 20. a) LMWG **HSA18** b) Data for **HSA18** at 2 wt/v % with the gelation sphere calculated using the BoundingRegion function from Wolfram Mathematica 11 (minimal enclosing sphere). Green: gel; Red: precipitate. Liquids are represented by full circles and the gelation sphere is represented by a meshed sphere. The present dataset does not include any S points. [Gelation sphere: δd = 18.19; δp = 9.25; δh = 9.62; $R_{Gel}$ = 10.95 MPa$^{1/2}$] c) Distances in HSP space of the liquids tested to the centre of the gelation sphere, highlighting the radius of the sphere by a green line. 54 outlying points (**P** points inside the gel sphere) are created with this method.*

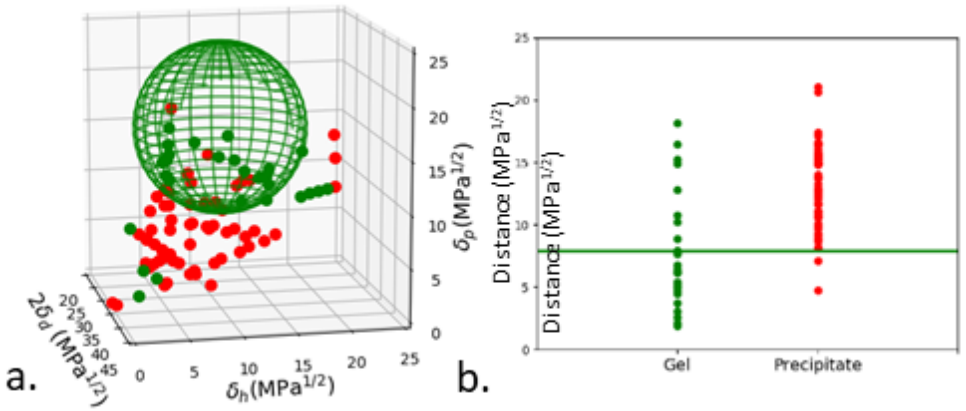


*Figure 21. Same data as in Fig. 20. a) The gelation sphere was calculated using the HSPiP software. Green: gel; Red: precipitate. [Gelation sphere: δd = 19.65; δp = 9.05; δh = 17.76; $R_{Gel}$ = 7.9 MPa$^{1/2}$] b) Distances in HSP space of the liquids tested to the centre of the gelation sphere, highlighting the radius of the sphere by a green line. 10 outlying points (8 **G** points outside the gel sphere and 2 **P** points inside the gel sphere) are created with this method.*

# 3. Experimental

## 3.1. Solubility tests

Gels were prepared by adding the desired amount of LMWG and 1 mL of liquid in a screw-cap vial. The suspensions were heated until dissolution and left to cool to room temperature on the bench. After 24 hours the vials were inverted, and the aspect of the samples was noted as gel (G), solution (S) or precipitate (P). A material is considered a gel if no deformation is observed after inverting the vial.

Data of LMWGs **HSA4 and HSA18** were previously described.[52]

## 3.2. Hansen Spheres determination

All solubility and gelation spheres with the exception of the minimal enclosing gelation sphere were calculated using the generic algorithm provided in the HSPiP software.[13–15] The solubility sphere was calculated in a way that as many S points as possible lie inside the sphere, but as many G and P points as possible lie outside. The gelation sphere determined according to the NO methodology contained as many G points as possible inside the sphere, but as many S and P points as possible outside. Following the new AO methodology, the gelation sphere was determined so that as many G points as possible lie inside the sphere, but as many P points as possible lie outside. In other words, the S points are not taken in consideration for the gelation sphere determination in the AO methodology.

Minimal enclosing sphere was computed using the BoundingRegion formula from Wolfram Mathematica 11.

## 3.3. Data representation

All data visualization was done with a Python script that makes use of the SciPy Python library. An executable version of our data plotting method with easy-to-use features can be obtained from this reference.[51]

## 3.4. X-ray scattering analysis

Gel samples were dried under vacuum in order to obtain xerogels and subsequently ground to a powder. All xerogels were measured in sodaglass capillaries with 1mm diameter. The two-

dimensional wide-angle X-ray scattering (WAXS) patterns were collected on a MAR345 detector using Cu-K□ radiation (wavelength: 1.542 Å) of a rotating anode X-ray source (40 kV, 40 mA; multilayer graded monochromator). Exposure time was 1200s.

# 4. Remarks

By modifying the previous methodology, it was possible to develop a general way of determining the gelation domain of LMWGs that is compatible with all the published data. The exclusion of **S** points from the gelation sphere determination allows (but does not force) gelation and solubility spheres to share a common volume. This AO methodology yields a good fit to the data, whether the experimental **G** and **S** points lie in disjoined or imbricated regions. The use of a dedicated algorithm is also necessary for a general methodology since some LMWGs have complex Hansen profiles and a minimal enclosing sphere of the **G** points is not robust enough. By presenting a general method for the gelation sphere determination we hope that future comparison between studies that correlate gelation data with HSP will become easier. This methodology has been used throughout this PhD project.

# 5. Bibliography


1 J. Makarević, M. Jokić, B. Perić, V. Tomišić, B. Kojić-Prodić and M. Žinić, Chem. - A Eur. J., 2001, 7, 3328–3341.

2 A. R. Hirst and D. K. Smith, Langmuir, 2004, 20, 10851–10857.

3 A. R. Katritzky, D. C. Fara, H. Yang, K. Tämm, T. Tamm and M. Karelson, Chem. Rev., 2004, 104, 175–198.

4 V. G. Machado and C. Machado, J. Chem. Educ., 2001, 78, 649.

5 W. Fräßdorf, M. Fahrländer, K. Fuchs and C. Friedrich, J. Rheol. (N. Y. N. Y)., 2003, 47, 1445–1454.

6 J. Burke, 1984

7 W. Edwards, C. A. Lagadec and D. K. Smith, Soft Matter, 2011, 7, 110–117.

8 In IUPAC Compendium of Chemical Terminology, IUPAC, Research Triagle Park, NC.

9 A. R. Hirst and D. K. Smith, Langmuir, 2004, 20, 10851.

10 W. Frassdorf, M. Fahrlander, K. Fuchs and C. Friedrich, J. Rheol., 2003, 47, 1445.

11 W. Edwards, C. A. Lagadec and D. K. Smith, Soft Matter, 2011, 7, 110.

12 K. Hanabusa, M. Matsumoto, M. Kimura, A. Kakehi and H. Shirai, J. Colloid Interface Sci., 2000, 224, 231.

13 C. M. Hansen, HANSEN SOLUBILITY PARAMETERS A User's Handbook HANSEN SOLUBILITY PARAMETERS A User ' s Handbook Second Edition, 2007.

14 S. Abbott and C. M. Hansen, Hansen Solubility Parameters in Practice, 2008.

15 M. J. Louwerse, A. Maldonado, S. Rousseau, C. Moreau-Masselon, B. Roux and G. Rothenberg, ChemPhysChem, 2017, 18, 2999–3006.

16 M. Raynal and L. Bouteiller, Chem. Commun., 2011, 47, 8271.

17 J. Bonnet, G. Suissa, M. Raynal and L. Bouteiller, Soft Matter, 2014, 10, 3154.

18 N. Zweep, A. Hopkinson, A. Meetsma, W. R. Browne, B. L. Feringa and J. H. Van Esch, Langmuir, 2009, 25, 8802–8809.

19 N. Amanokura, K. Yoza, H. Shinmori, S. Shinkai and D. N. Reinhoudt, J. Chem. Soc. Perkin Trans. 2, 1998, 0, 2585–2592.

20 K. Murata, M. Aoki, T. Suzuki, T. Harada, H. Kawabata, T. Komori, F. Ofaseto, K. Ueda and S. Shinkai, J. Am. Chem. Soc., 1994, 116, 6664–6676.

21 R. Mukkamala and R. G. Weiss, Langmuir, 1996, 12, 1474–1482.

22 D. R. Trivedi, A. Ballabh, P. Dastidar and B. Ganguly, Chem. - A Eur. J., 2004, 10, 5311–5322.

23 M. Fang, J. Long, W. Zhao, L. Wang and G. Chen, Langmuir, 2010, 26, 16771–16774.

24 K. Hanabusa, H. Kobayashi, M. Suzuki, M. Kimura and H. Shirai, Colloid Polym. Sci., 1998, 276, 252–259.

25 O. Gronwald and S. Shinkai, Chem. - A Eur. J., 2001, 7, 4328–4334.

26 J. W. Liu, J. T. Ma and C. F. Chen, Tetrahedron, 2011, 67, 85–91.

27 J. Gao, S. Wu and M. A. Rogers, J. Mater. Chem., 2012, 22, 12651.

28 H. Xu, J. Song, T. Tian and R. Feng, Soft Matter, 2012, 8, 3478.

29 Y. Huang, Y. Yuan, W. Tu, Y. Zhang, M. Zhang and H. Qu, Tetrahedron, 2015, 71, 3221–3230.

30 Y. Li, X. Ran, Q. Li, Q. Gao and L. Guo, Chem. - An Asian J., 2016, 11, 2157–2166.

31 T. L. Lai, D. Canevet, N. Avarvari and M. Sallé, Chem. - An Asian J., 2016, 11, 81–85.

32 T. Wang, X. Yu, Y. Li, J. Ren and X. Zhen, ACS Appl. Mater. Interfaces, 2017, 9, 13666–13675.

33 T. Xiao, X. Zhang, J. Wu, J. Yang and Y. Yang, Chempluschem, 2017, 82, 879–887.

34 F. Aparicio, F. García and L. Sánchez, Chem. - A Eur. J., 2013, 19, 3239–3248.

35 W. Edwards and D. K. Smith, J. Am. Chem. Soc., 2013, 135, 5911–5920.

36 S. Wu, J. Gao, T. J. Emge and M. A. Rogers, Soft Matter, 2013, 9, 5942.

37 V. C. Edelsztein, A. S. Mac Cormack, M. Ciarlantini and P. H. Di Chenna, Beilstein J. Org. Chem., 2013, 9, 1826–1836.

38 T. Ando and K. Ito, J. Incl. Phenom. Macrocycl. Chem., 2014, 80, 285–294.

39 S. He, H. Zhao, X. Guo, X. Xu, X. Zhou, J. Liu, Z. Xing, L. Ye, L. Jiang, Q. Chen and Y. He, Chem. - A Eur. J., 2014, 20, 15473–15481.

40 C. Tong, K. Fan, L. Niu, J. Li, X. Guan, N. Tao, H. Shen and J. Song, Soft Matter, 2014, 10, 767–772.

41 H. Shen, L. Niu, K. Fan, J. Li, X. Guan and J. Song, Langmuir, 2014, 30, 9176–9182.

42 Y. Lan, M. G. Corradini, X. Liu, T. E. May, F. Borondics, R. G. Weiss and M. A. Rogers, Langmuir, 2014, 30, 14128–14142.

43 Y. Yin, Z. Gao, Y. Bao, B. Hou, H. Hao, D. Liu and Y. Wang, Ind. Eng. Chem. Res., 2014, 53, 1286–1292.

44 M. Zhang, S. Selvakumar, X. Zhang, M. P. Sibi and R. G. Weiss, Chem. - A Eur. J., 2015, 21, 8530–8543.

45 C. Liu, M. Corradini and M. A. Rogers, Colloid Polym. Sci., 2015, 293, 975–983.

46 N. Yan, Z. Xu, K. K. Diehn, S. R. Raghavan, Y. Fang and R. G. Weiss, Langmuir, 2013, 29, 793–805.

47 N. Yan, Z. Xu, K. K. Diehn, S. R. Raghavan, Y. Fang and R. G. Weiss, J. Am. Chem. Soc., 2013, 135, 8989–8999.

48 K. K. Diehn, H. Oh, R. Hashemipour, R. G. Weiss and S. R. Raghavan, Soft Matter, 2014, 10, 2632.

49 Y. Lan, M. G. Corradini and M. A. Rogers, Cryst. Growth Des., 2014, 14, 4811–4818.

50 A. Singh, F.-I. I. Auzanneau, M. G. Corradini, G. Grover, R. G. Weiss and M. A. Rogers, Langmuir, 2017, 33, 10907–10916.

51 D. Rosa Nunes, M. Raynal, B. Isare, P.-A. Albouy and L. Bouteiller, Soft Matter, 2018, 14, 4805–4809.

52 J. Bonnet, G. Suissa, M. Raynal and L. Bouteiller, Soft Matter, 2015, 11, 2308–2312.

53 J. Gao, S. Wu, T. J. Emge and M. A. Rogers, CrystEngComm, 2013, 15, 4507.

54 C. Zhao, H. Wang, B. Bai, S. Qu, J. Song, X. Ran, Y. Zhang and M. Li, New J. Chem., 2013, 37, 1454.

55 F. Gharagheizi, J. Appl. Polym. Sci., 2007, 103, 31–36.

# 9. Chapter 3

# 10. Smooth influence of the gelator structure on the gelation sphere

The first part of this work described a methodology that rationalizes the gelation behaviour of any given organogelator. This methodology has proven to be a good predictive tool when used to identify if an untested liquid would be gelated by a particular LMWG. The next challenge in the field is to evaluate how changes in the structure of a LMWG can affect the gelation domain. This is a vast problem: when picking a gelator, there are several components of the molecular structure that can be altered to study the influence on gelation. In order to keep our first attempt as simple as possible, we chose to vary the length of a linear alkyl chain present in the gelator. To do so, a gelator with one or more linear alkyl chain was selected from the literature and several analogues with various lengths of alkyl chain were synthesized. Finally, the contribution of this alteration on the gelation domain was studied. In order to probe the generality of the conclusions, we actually applied the same structure alteration to several gelators.

# 1. Thiazole based gelators

The first attempt to characterize the Hansen space and correlate the molecular structure with the gelation domains of a group of LMWG was performed using a family of amide-based thiazole derivatives bearing a long aliphatic chain (Figure 22). In these gelators the amide group is expected to provide supramolecular H-bond interactions while the long alkyl chain contributes to dispersion interactions. This group of LMWGs was first reported by Ballabh et al.[1,2] together with the single-crystal structure of two members of the family.

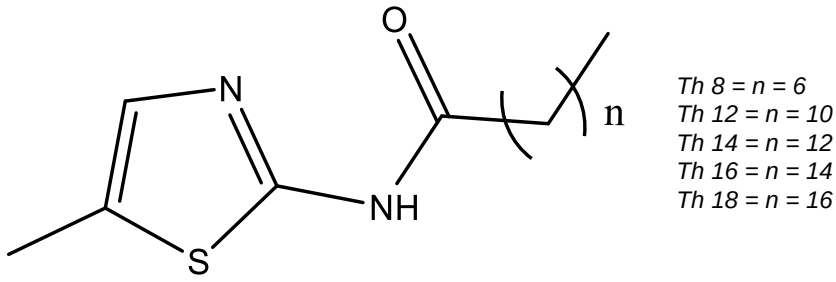


*Figure 22. Chemical structure of the thiazole-based LMWGs.*

The gelation domain of several members of this family were determined, with the alkyl chain length ranging from 6 to 16 $CH_2$ groups, together with a structural characterization (X-ray diffraction measurements and scanning electronic microscopy). To study the molecular packing within gel fibers, the molecular modeling protocol described in chapter 1 was applied, including the indexation software Dicvol, average atom position finder software Polymorph and the structures were refined using Rietveld together with energy optimization. The most probable packing structure was identified by comparing the simulated patterns of dozens of candidates to the experimental data.

## 1.1. Influence of concentration on Hansen space

First, the gelation domain in the Hansen space of LMWG **Th12** was determined at different concentrations to help select an ideal concentration for the entire family of LMWG. The gelation domains were determined using the methodology explained in chapter 2. For each liquid tested the desired amount of LMWG and 1 mL of liquid were added to a screw-cap vial. The suspensions were heated up to 100°C until dissolution and left to cool to room temperature on the bench. After 24 hours the vials were turned upside-down, and the aspect of the samples was noted as gel (G), solution (S) or precipitate (P). A material is considered a gel if no deformation is observed after turning the vial upside-down.

We determined the gelation domain of **Th12** at concentrations between 3 and 0.75 wt% (Figure 23). We observed that an increase of concentration decreased the radius of the solubility sphere and increased the radius of the gelation sphere (Table 1). In principle, the centers of the Hansen spheres should remain similar at different concentrations and only the radius should differ. The solubility sphere respects this expectation between 2 and 1 wt% and the gelation sphere between 3 and 1.5 % wt. The center of the solubility sphere at 0.75 wt% and gelation sphere at 1 wt% are apparently affected by concentration due to a lack of points to reliably construct the Hansen spheres. Below 1 wt% **Th12** formed very few gels in the tested liquids and at 3 wt% almost none of the tested liquids fully solubilized the LMWG. Therefore, we selected an intermediate concentration (2 wt%) to be able to detect any effect of the length of the alkyl chain on the gelation domain.

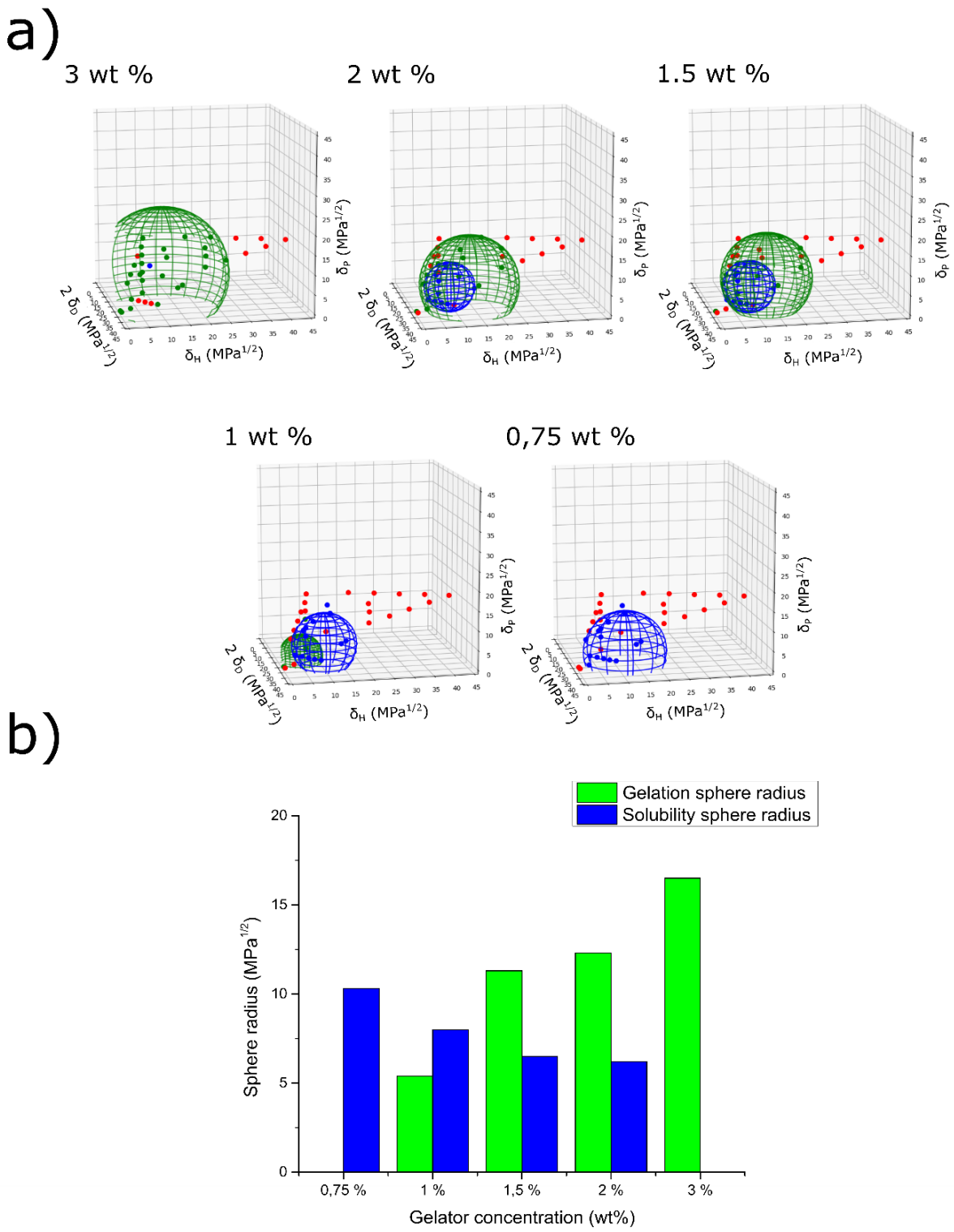


*Figure 23.a) Gelation data plotted in Hansen space for the LMWG **Th12** at different concentrations. The tested liquids are represented by full circles and the calculated domains are represented by meshed spheres. Green: gel; red: precipitate; blue: soluble. b) Radius of the solubility (blue) or the gelation (green) spheres for **Th12** at different concentrations.*

*Table 1. Coordinates of the center and radius of Th12 Hansen spheres at different concentrations*

| | Solubility sphere | | | | Gelation sphere | | | |
|---|---|---|---|---|---|---|---|---|
| wt % | $\delta_D$ ($MPa^{1/2}$) | $\delta_P$ ($MPa^{1/2}$) | $\delta_H$ ($MPa^{1/2}$) | r ($MPa^{1/2}$) | $\delta_D$ ($MPa^{1/2}$) | $\delta_P$ ($MPa^{1/2}$) | $\delta_H$ ($MPa^{1/2}$) | r ($MPa^{1/2}$) |
| 3 | | | | | 17.1 | 9.7 | 10.3 | 16.5 |
| 2 | 18.8 | 7.2 | 7.5 | 6.2 | 17.7 | 7.1 | 12.8 | 12.3 |
| 1.5 | 18.7 | 7.1 | 7.6 | 6.5 | 17.4 | 8.6 | 12.4 | 11.3 |
| 1 | 18.4 | 6.2 | 9.5 | 8.0 | 15.5 | 2.2 | 4.7 | 5.4 |
| 0.75 | 17.4 | 4.0 | 11.3 | 10.3 | | | | |

## 1.2. Hansen space of thiazole based gelators

The evolution of the size of the solubility and gelation spheres is represented in Figure 24 and summarized in Figure 25. The solubility sphere dramatically shrinks with an increase in alkyl chain length, in such a way that for **Th16** and **Th18**, solubility is no longer observed. The center of the solubility sphere shifts gradually to a less polar region (smaller $\delta_H$ and $\delta_P$) and to a less polarizable region of the Hansen space (smaller $\delta_D$) as the alkyl chain length increases (Figure 25b).

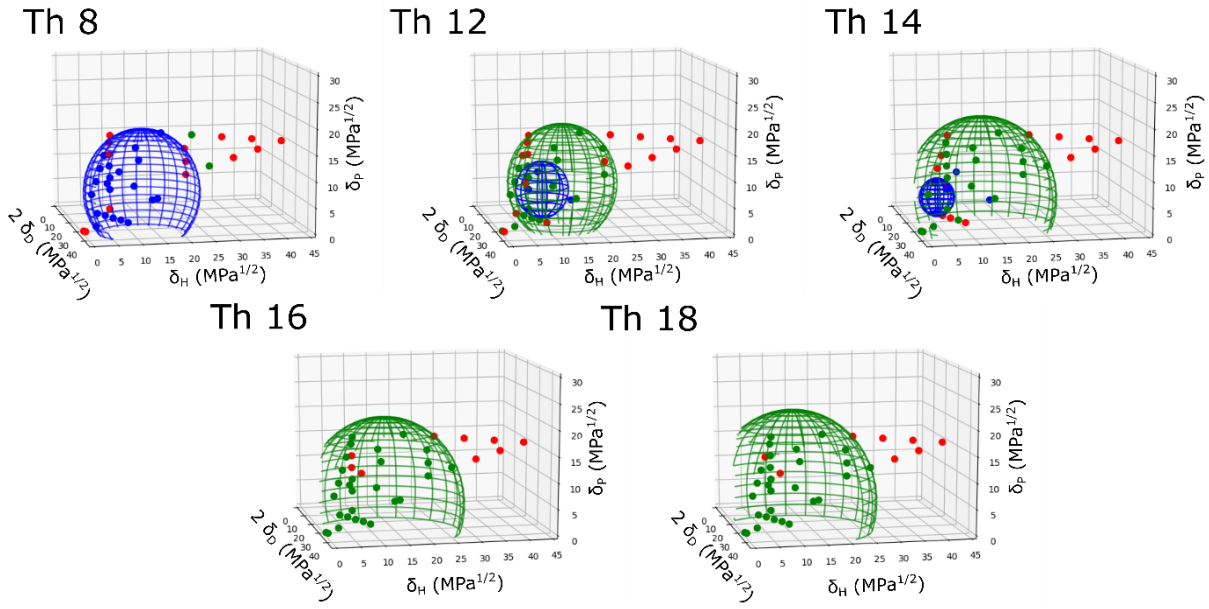


*Figure 24. Gelation data plotted in Hansen space for the thiazole-based LMWGs at 2wt%. The tested liquids are represented by full circles and the calculated domains are represented by meshed spheres. Green: gel; red: precipitate; blue: soluble.*

To better follow the shift of the Hansen spheres we calculated the trend lines by considering the

general vector equations in the HSP space (Eq 7) where x = $\delta_D$; y = $\delta_P$; z= $\delta_H$; t = number of carbons in each alkyl chain.

Eq 7: [x,y,z] = [x0,y0,z0] + t [a,b,c] , $8 \leq t \leq 18$

The values of [x0,y0,z0] and [a,b,c] were adjusted to minimize the overall distance of the experimental points to the trend line.

The trend of the center of LMWG solubility spheres **Th8** and **Th12** yields the following vector equation:

Eq 8: [$\delta_D$, $\delta_P$, $\delta_H$] = [21.3, 10.2, 12.3] + t[-0.21, -0.25, -0.40]

It can be seen from the trend lines that adding one $CH_2$ decreases the parameters for the center of the solubility sphere by $\delta_D$ = -0.21; $\delta_P$ = -0.25; $\delta_H$ = -0.40 $MPa^{1/2}$. The solubility sphere of **Th14** was not taken in account when calculating the trend of solubility since it was obtained with a very small number of solubility points (4 in a total of 37 studied liquids).

We also plotted the theoretical HSP values of each LMWG (Table 3) in Figure 25b, which also shift to a less polar region of the Hansen space. These theoretical values are obtained using the HSPiP software [3-4] and is based on an empirical group contribution method. The trend of the theoretical values of the solubility parameters yields the following vector equation:

Eq 9: [$\delta_D$, $\delta_P$, $\delta_H$] = [18.6, 12.1, 10.0] + t[-0.08, -0.29, -0.26]

In the theoretical values, adding one $CH_2$ decreases the parameters for the center of the solubility sphere by $\delta_D$ = -0.08; $\delta_P$ = -0.29; $\delta_H$ = -0.26 $MPa^{1/2}$. Considering the fact that Eq 8 was determined from only 2 points, the agreement between Eq 8 and 9 is quite good.

In clear contrast, the increase in length of the alkyl chain leads to an expansion of the gelation sphere from **Th12** to **Th18** (Figure 25 a). More interestingly, the parameters for the center of the gelation sphere shift by $\delta_D$ = -0.26; $\delta_P$ = -0.23; $\delta_H$ = -0.41 $MPa^{1/2}$ with the increase in length of the alkyl chain, yielding a very similar trend when compared with the solubility sphere. The trend of the center of LMWG gelation spheres yields the following vector equation:

Eq 10: [$\delta_D$, $\delta_P$, $\delta_H$] = [20.8, 9.9, 17.8] + t [-0.26, -0.23, -0.41]

Therefore, a longer alkyl chain increases the contribution of the non-polar group with respect to the

contribution of the polar one, both on the solubility sphere and on the gelation sphere. Finally, one can notice that the shift of the center of the gelation sphere to a less polar region is not accompanied by a loss of gelation in the polar region because the shift in the center occurs together with the increase of the radius of the gelation sphere.

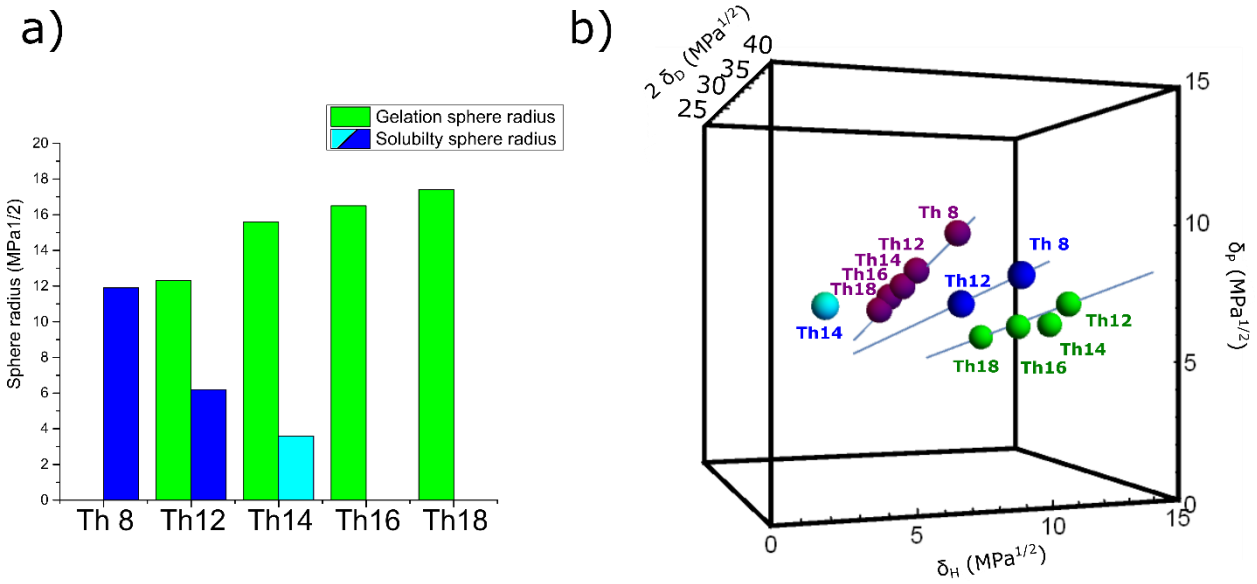


*Figure 25. a) Radius of the solubility (blue) or the gelation (green) spheres for the thiazole-based LMWGs. b) Center of the solubility spheres (blue), center of the gelation spheres (green) and simulated HSP parameters of each thiazole-based gelator (purple). Data from Figure 24; for* ***Th14****, a light blue color has been selected to highlight the limited precision of that particular data (only 4 S points);*

*Table 2. Coordinates of the center and radius of Hansen spheres for thiazole based LMWGs (2 wt%)*

| | Solubility sphere | | | | Gelation sphere | | | |
|---|---|---|---|---|---|---|---|---|
| LMWG | $\delta_D$ ($MPa^{1/2}$) | $\delta_P$ ($MPa^{1/2}$) | $\delta_H$ ($MPa^{1/2}$) | r ($MPa^{1/2}$) | $\delta_D$ ($MPa^{1/2}$) | $\delta_P$ ($MPa^{1/2}$) | $\delta_H$ ($MPa^{1/2}$) | r ($MPa^{1/2}$) |
| Th8 | 19.6 | 8.3 | 9.1 | 11.9 | | | | |
| Th12 | 18.8 | 7.2 | 7.5 | 6.2 | 17.7±0.8 | 7.1±0.5 | 12.8±0.4 | 12.3±0. |
| Th14 | 18.9 | 7.3 | 2.6 | 3.6 | 17.3±2.0 | 6.3±2.6 | 12.4±1.4 | 15.6±1. |
| Th16 | | | | | 17.9±0.4 | 5.7±0.4 | 11.7±0.4 | 16.5±0. |
| Th18 | | | | | 16.2±0.5 | 5.7±0.4 | 10.3±0.9 | 17.4±0. |

***Table 3. Coordinates of the theoretical HSP values calculated by the HSPiP software[3-4] for thiazole based LMWGs.***

| **LMWG** | $\delta_D$ ($MPa^{1/2}$) | $\delta_P$ ($MPa^{1/2}$) | $\delta_H$ ($MPa^{1/2}$) |
|---|---|---|---|
| **Th8** | 18.0 | 9.8 | 7.9 |
| **Th12** | 17.5 | 8.4 | 6.6 |
| **Th14** | 17.4 | 7.8 | 6.1 |
| **Th16** | 17.2 | 7.4 | 5.7 |
| **Th18** | 17.2 | 6.9 | 5.3 |

To confirm the accuracy of the experimentally obtained trends we tried to estimate the uncertainty in the determination of the gelation spheres. The larger source of uncertainty is clearly the unperfect nature of the gelation data. Indeed, if the number of gelation tests (i.e. the number of points on figure 24) is too low, then the gelation sphere cannot be determined with precision. In order to quantify this effect, we started by removing one point from the gelation dataset and re-calculated the coordinates of the sphere. This was done systematically with each point of the original dataset and then the standard deviation was determined for each coordinate ($\delta_D$, $\delta_P$ and $\delta_H$) of the center of the gelation sphere over this global analysis. In fact, this procedure measures the uncertainty that would be introduced if we removed one point (chosen randomly) from the dataset. We can consider it also provides a relative estimation of the reliability of the full dataset. The values obtained are given in table 2 and plotted as ellipsoids in the Hansen Space (Figure 26).

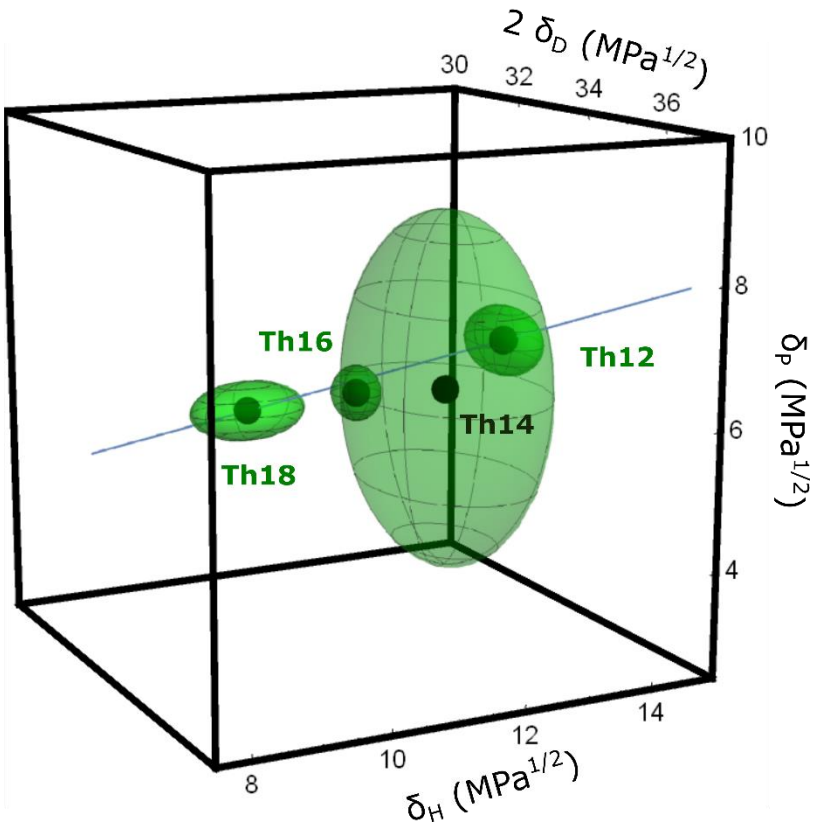


*Figure 26. Center of the gelation spheres (dark green) and the standard deviation (meshed green ellipsoids) represented in Hansen space.*

All centers of the gelation sphere with the exception of **Th14** presented small values of standard deviation (< 0.9 $MPa^{1/2}$), indicating a high accuracy in the experimental data determination. The high values obtained for the standard deviation of **Th14**, particularly $\delta_P = 6.3 \pm 2.6$ $MPa^{1/2}$, indicate a lack of accuracy of the gelation sphere for this particular gelator. Therefore, the trend for the center of LMWG gelation spheres was determined again, but the previously unweighted minimization was now weighted inversely by the standard deviations. Equation 11 shows the result which is similar to the unweighted result (equation 10). It shows that the less reliable **Th14** data does not affect the previous conclusions.

Eq 11: $[\delta_D, \delta_P, \delta_H] = [20.7, 9.8, 17.9] + t\,[-0.25, -0.23, -0.42]$

## 1.3. SEM observation of fibers

In order to try and rationalize these observations, we investigated the morphology and the structure of the fibers.

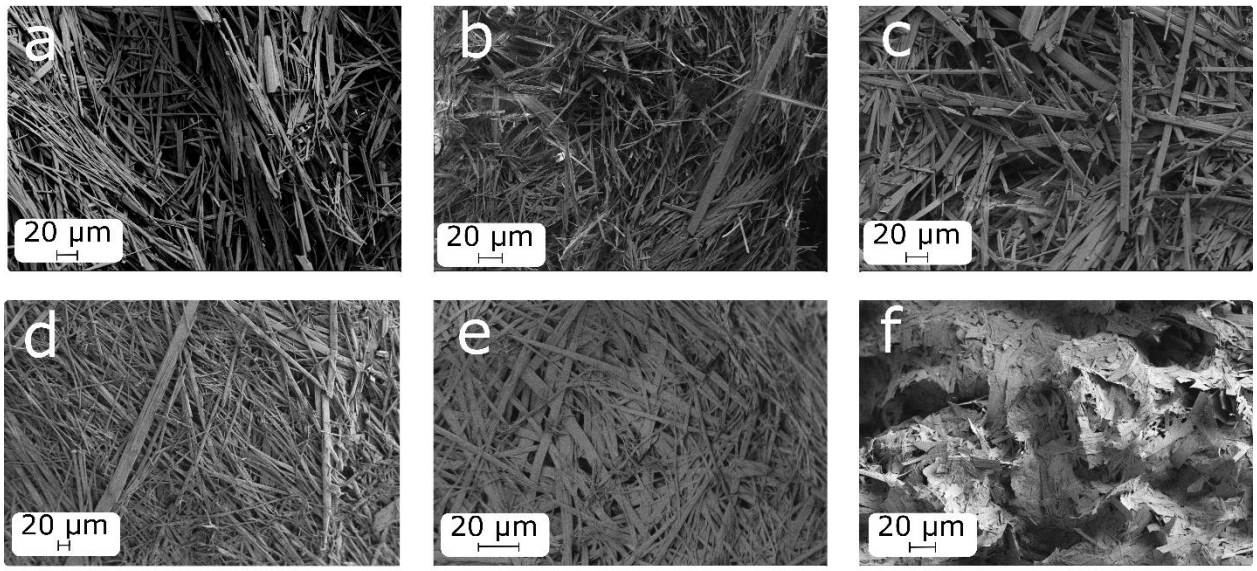


*Figure 27. SEM images of the thiazole-based xerogels: a - Th12 from toluene, b - Th12 from cyclohexane, c - Th12 from 1-butanol, d - Th14 from toluene, e - Th16 from toluene, f - Th18 from toluene.*

The morphology of **Th12** to **Th18** gel fibers was observed by scanning electronic microscopy (SEM). All **Th12** xerogels obtained from various liquids (toluene, cyclohexane and 1-butanol) (Figure 27.a to c) show rectilinear shaped fibers with very few differences in size, indicating that the different liquids do not affect the morphology of the fibers. Moreover, the fibers of the various gelators **Th12** to **Th18** (Figure 27.a and d to f) obtained from toluene also share a very similar morphology, even if the **Th18** sample appears more blurred than the others. Therefore, no major effect is detected at this length scale.

## 1.4. X-ray measurements in transmission

X-ray measurements were performed on xerogels obtained from **Th12** to **Th18** from various liquids to determine whether the nature of the liquid influences the packing within the fibers. Xerogels were grinded to obtain a fine powder and then measured in transmission mode with the X-ray beam set-up in the parallel beam configuration. The data from the **Th12** and **Th14** xerogels were compared to the powder pattern simulated from the previously published single-crystal structure. [1,2]

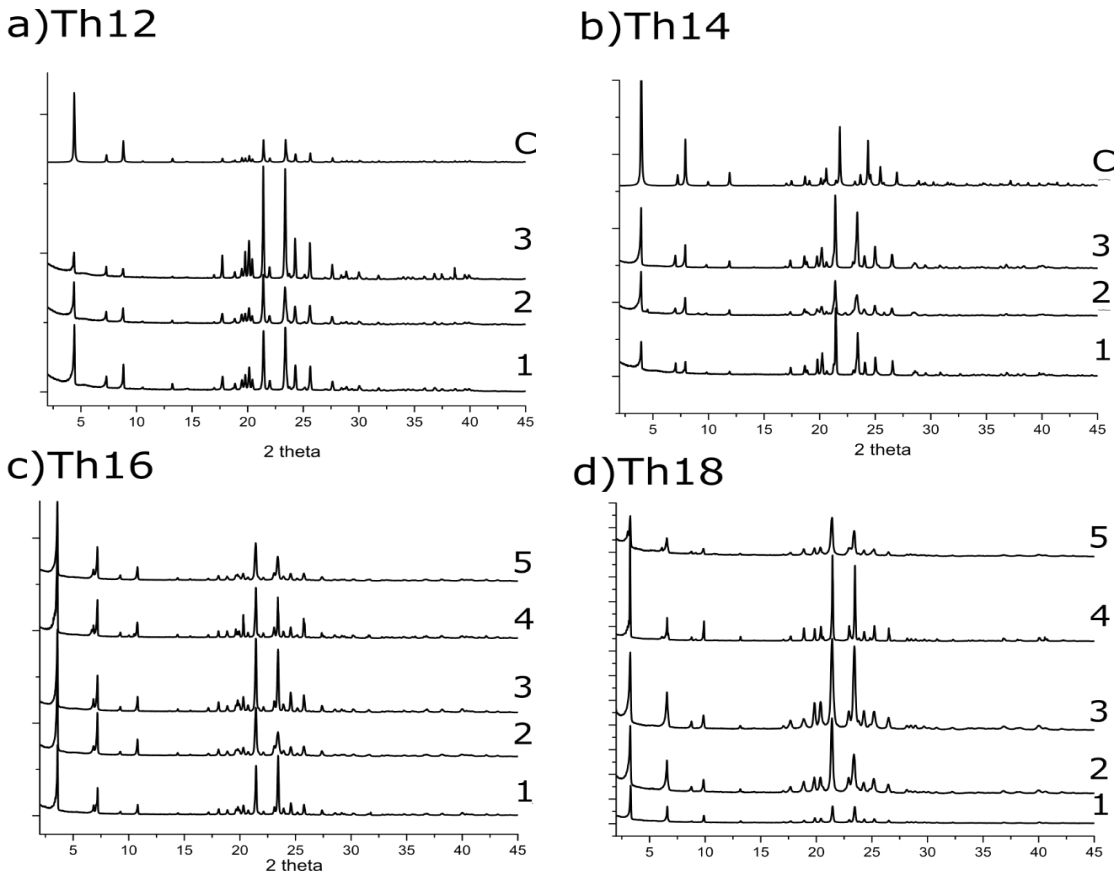


*Figure 28. X-ray patterns of xerogels of the thiazole-based gelators obtained from (1) toluene, (2) cyclohexane, (3) 1-butanol, (4) acetonitrile, (5) 1,4-dioxane. Pattern simulated from the single-crystal structure (C). X-ray wavelength of 1.5406 Å.*

Similar X-ray powder patterns were obtained from the **Th12** xerogels regardless of the liquid in which they were formed (Figure 28 a 1,2,3). Small differences in diffraction peak intensity can be attributed to weak effects of preferential orientation within the samples. This observation also applies to **Th14**, **Th16**, and **Th18** (Figure 28 b, c, d). This indicates that in this family of LMWGs, the molecular packing within the fibers is independent of the liquid in which the gel is formed. In fact, different patterns for a given gelator were only observed for **Th12** when precipitates were obtained instead of gels (Figure 29). Thus, within each gelation sphere the molecular packing can be considered to be

similar. The xerogels obtained from **Th12** also present a high resemblance with the powder pattern simulated from the published single-crystal structure of **Th12** (Figure 28 a C). This indicates that the gel fibers of **Th12** share the same packing as the corresponding single-crystal.

**Th14** shows the same X-ray pattern for all the measured xerogels (Figure 28 b 1,2,3) but small differences appear with respect to the powder pattern simulated from the single-crystal data (Figure 28 b C): the measured xerogels show a good match to the single-crystal pattern in the small angle region (0 ° to 15°) and a constant small shift of +0.5 degrees in the wide-angle region (above 15°).

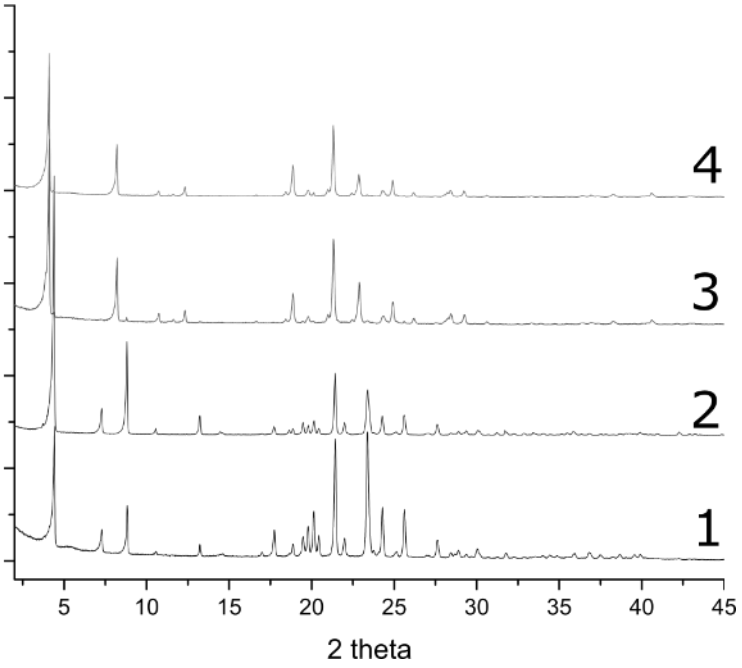


*Figure 29. X-ray patterns of thiazole **Th12**. Xerogel obtained from 1-butanol (1). Precipitates obtained from 1.4-dioxane (2), acetonitrile (3), or methanol (4). X-ray wavelength of 1.5406 Å.*

## 1.5. Molecular packing

To better understand how the length of the alkyl chain affects the crystal structure within the gel fibers, the molecular packing was determined based on the powder patterns measured on the xerogels and molecular modelling simulations (Figure 30). The validation of the methodology was performed by comparing the structure obtained for **Th12** with the published single-crystal structure of the same molecule. Overlaying the two structures, it was found that they are similar, with cell parameters differing by less than 0.05 Å and 0.1 °, and atoms overlapping almost perfectly (Figure 31 a). The very good agreement between the modelled and published single-crystal structure validates the applicability of the procedure established to determine the molecular packing within the gel fibers. The structure proposed for the **Th14** xerogels also presents a conformation similar to the previously published single-crystal structure (Figure 31 b), despite the differences shown in the X-ray patterns (Figure 28 b). This small difference in the X-ray pattern is due to a slightly denser packing (3.9%) in the case of the single crystal (see Table 4).

The indexation of the powder patterns for all these thiazole-based gelators points to monoclinic unit cells, with the cell parameter "*a*" increasing with the length of the alkyl chain and the other cell parameters remaining constant (see Table 5). The fitted XRD patterns are given in table 5 and figures 32, 33, 34 and 35.

Figure 30 illustrates the high structural similarity between gelators **Th12** to **Th18**, suggesting that differences in the length of the alkyl chain do not change the packing of these gelators within the gel fibers. These calculated structures are characterized by the presence of H-bonded dimers forming a cyclic H-bond topology (Figures 36 and 37), where the amide group is the donor of hydrogen bond and the nitrogen of thiazole is the acceptor (NH…N bonds), as reported previously. [1,2] To check the carbonyl oxygen is not involved in hydrogen bonding, infrared spectroscopy was performed (Figure 38). With this analysis we can compare the signal of the LMWG as it is packed in the gel fiber with the one of the same molecules in solution, either in a protonated solvent (methanol) and or in a non-protonated solvent (toluene). In methanol, the carbonyl oxygen is hydrogen bonded to the solvent while it remains free in toluene, giving different signals in the infrared spectrum. We observed that the signal of the carbonyl oxygen in the xerogel is the same as in the toluene solution, which is a clear indication that the carbonyl oxygen remains free in the gel fibers. According to the calculated structure, the thiazole moieties of the dimers form planar objects that organize in a π packing, i.e., a combination of a parallel-displaced arrangement along the [001] direction and a herringbone arrangement along the [010] direction (Figure 36). The sulfur atoms of neighboring stacks are in van der Waals contact, with a distance of 3.57 Å. All alkyl chains organize in an extended all-trans conformation, interdigitating along the (100) plane (Figure 30).

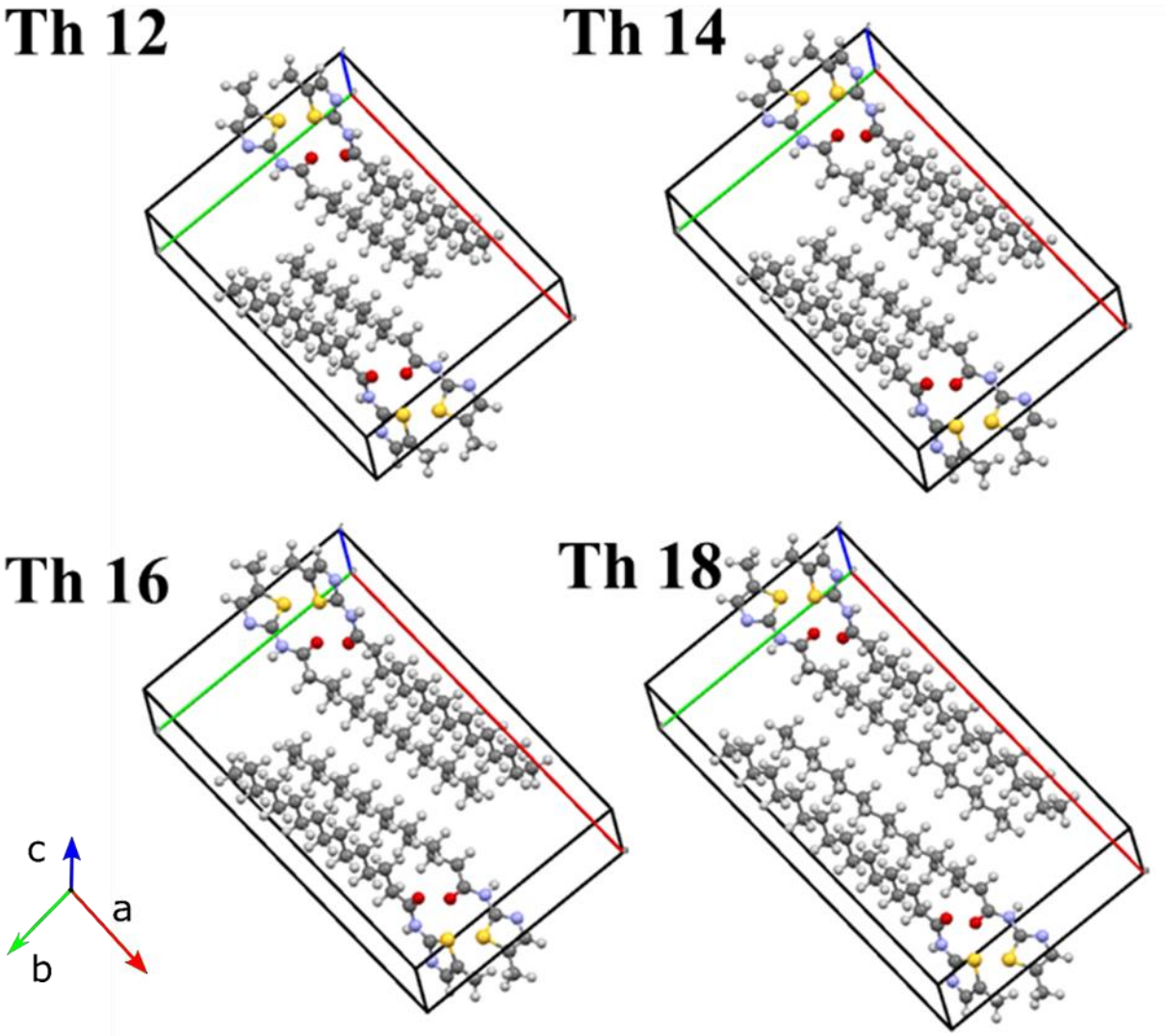


*Figure 30. Molecular packing of thiazole-based LMWG obtained with the methodology described in chapter 1, with cell parameters "a" in red, "b" in green and "c" in blue.*

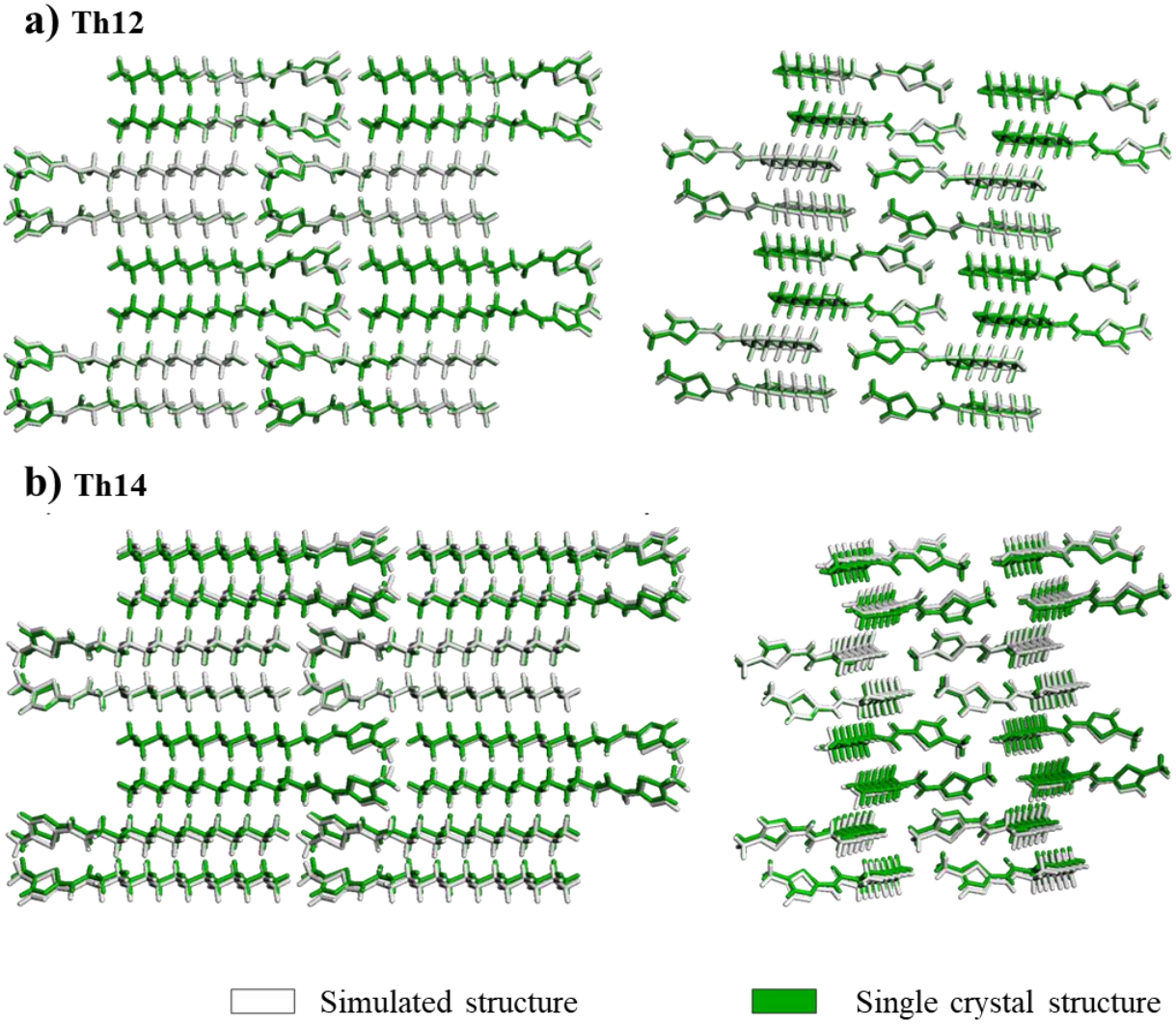


*Figure 31. a) Th12 modelled structure (white) compared with published **Th12** single-crystal molecular packing (green).[1] Root mean square value of 0.2 Å. b) Th14 modelled structure (white) compared with published **Th14** single-crystal molecular packing (green).[1] Root mean square value of 0.6 Å.*

*Table 4. Densities calculated for gelators **Th12** and **Th14***

| | **calculated from the modelled structure** | **calculated from the single-crystal data** |
|---|---|---|
| *Th12* | 1.173 | 1.171 |
| *Th14* | 1.147 | 1.192 |

*Table 5. Proposed unit cell parameters of the thiazole-based gelators.*

| LMWG | **Th12** | **Th14** | **Th16** | **Th18** |
|---|---|---|---|---|
| crystal system | monoclinic | monoclinic | monoclinic | monoclinic |
| space group | $P2_1/c$ | $P2_1/c$ | $P2_1/c$ | $P2_1/c$ |
| a(Å) | 20.00 | 22.30 | 24.60 | 26.99 |
| b(Å) | 15.17 | 15.18 | 15.19 | 15.19 |
| c(Å) | 5.54 | 5.55 | 5.55 | 5.56 |
| α(deg) | 90 | 90 | 90 | 90 |
| β(deg) | 92.37 | 90.86 | 93.54 | 95.74 |
| γ(deg) | 90 | 90 | 90 | 90 |
| volume ($Å^3$) | 1697.4 | 1889.6 | 2081.9 | 2274.1 |
| Z | 4 | 4 | 4 | 4 |
| Density $gcm^{-3}$ | 1.173 | 1.147 | 1.132 | 1.115 |
| formula weight | $C_{16}H_{28}N_2OS$ | $C_{18}H_{32}N_2OS$ | $C_{20}H_{36}N_2OS$ | $C_{22}H_{40}N_2OS$ |
| 2θinterval(deg) | 2-60 | 2-60 | 2-60 | 2-60 |
| step size (deg) | 0.005 | 0.005 | 0.005 | 0.005 |
| counting time(s) | 3 | 3 | 3 | 3 |
| Rp | 7.731 | 7.955 | 9.203 | 6.618 |
| Rwp | 12.103 | 12.682 | 13.441 | 9.137 |
| $X^2$ | 1.946 | 1.367 | 2.141 | 1.000 |

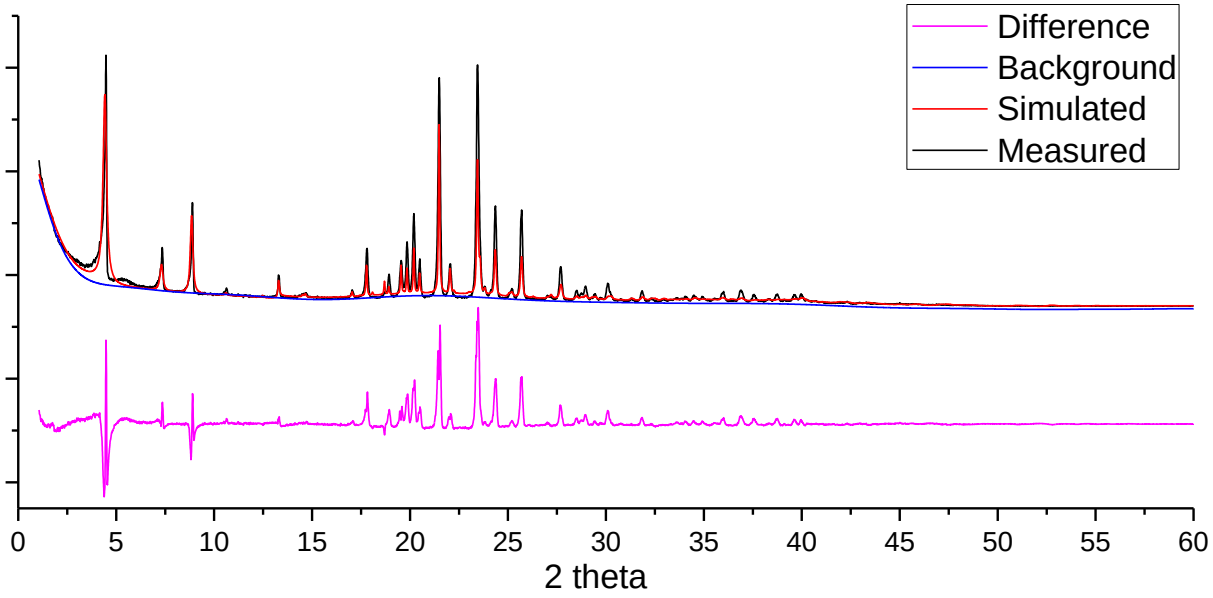


*Figure 32. Comparison between simulated X-ray pattern from simulated structure of* ***Th12*** *and measured pattern from* ***Th12*** *xerogel extracted from toluene. X-ray wavelength of 1.5406 Å.*

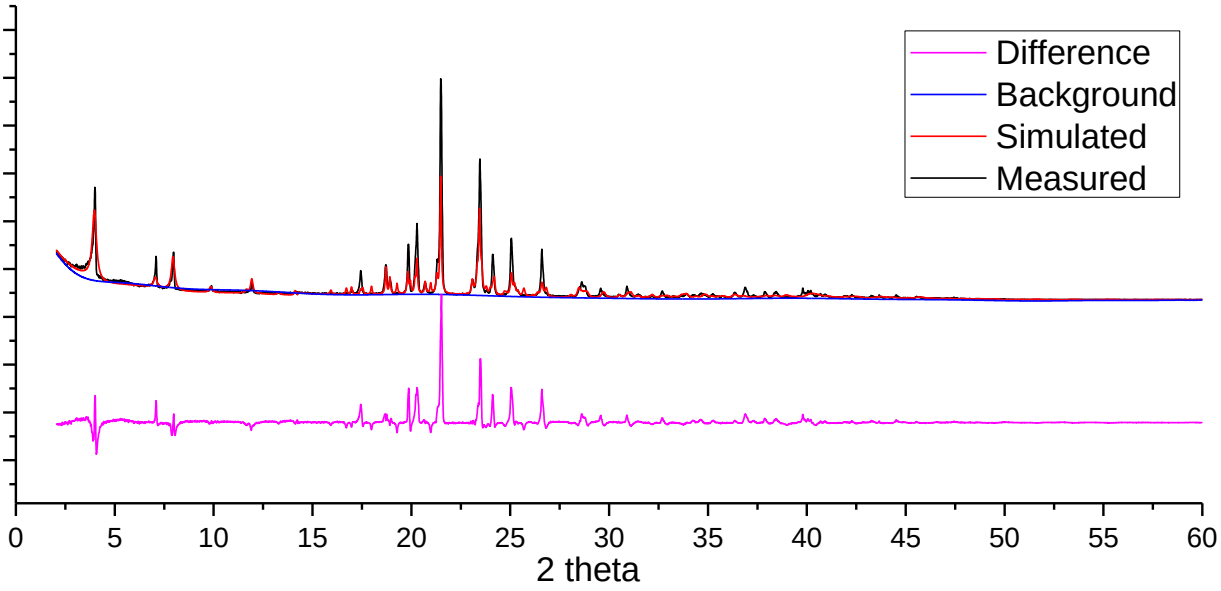


*Figure 33. Comparison between simulated X-ray pattern from simulated structure of* ***Th14*** *and measured pattern from* ***Th14*** *xerogel extracted from toluene. X-ray wavelength of 1.5406 Å.*

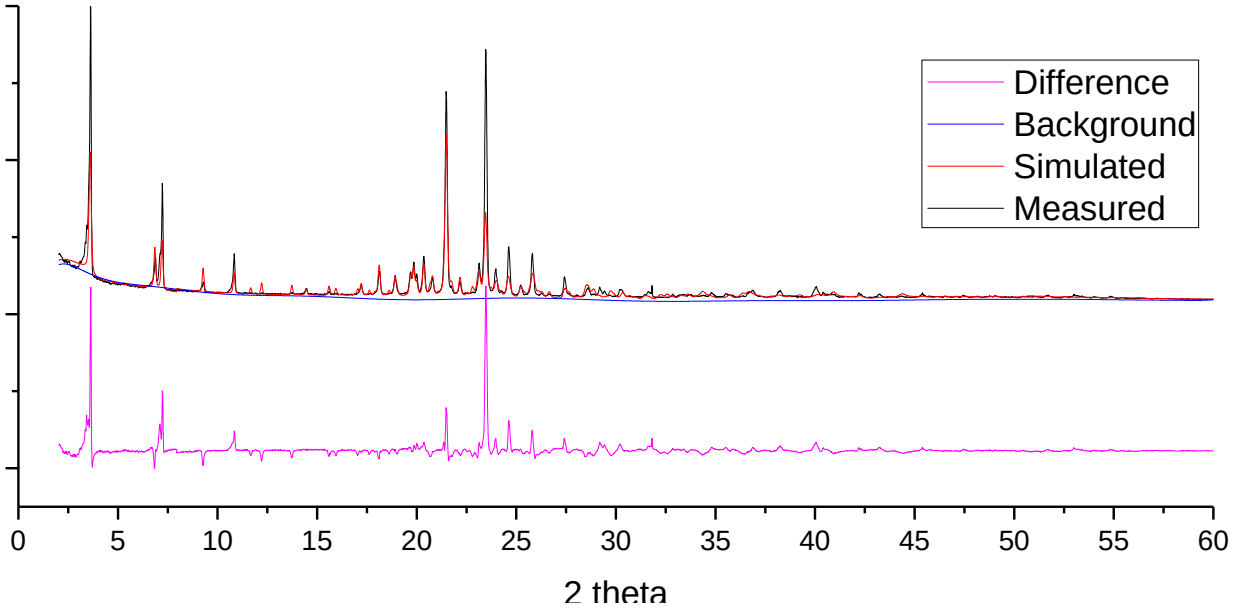


*Figure 34. Comparison between simulated X-ray pattern from simulated structure of* ***Th16*** *and measured pattern from* ***Th16*** *xerogel extracted from toluene. X-ray wavelength of 1.5406 Å.*

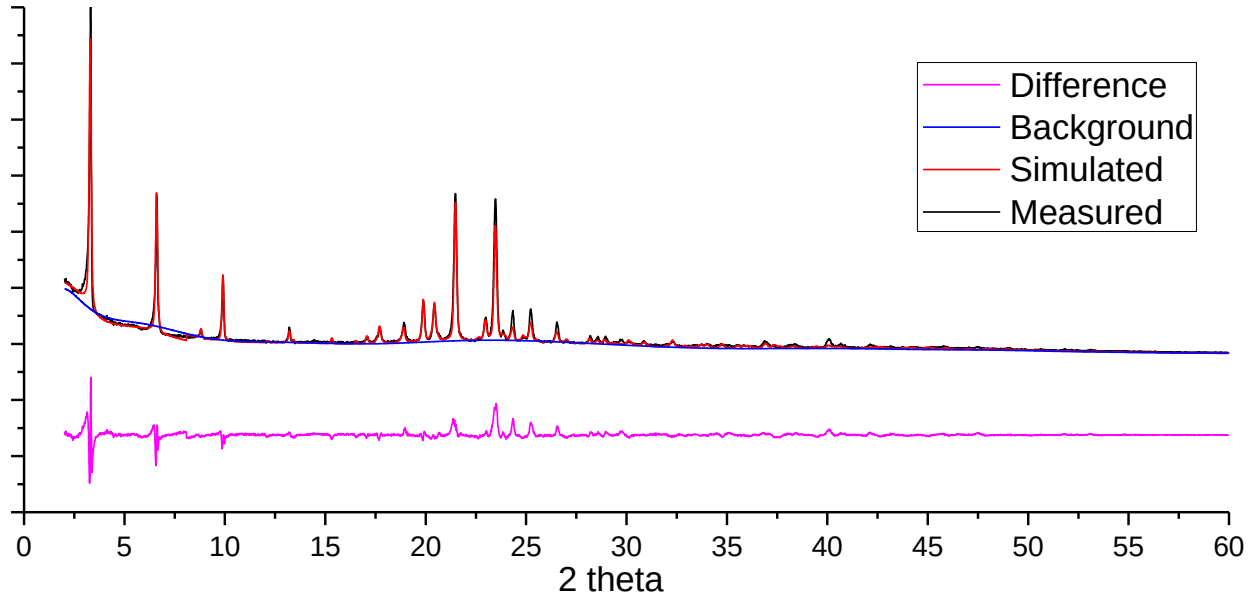


*Figure 35. Comparison between simulated X-ray pattern from simulated structure of* ***Th18*** *and measured pattern from* ***Th18*** *xerogel extracted from toluene. X-ray wavelength of 1.5406 Å.*

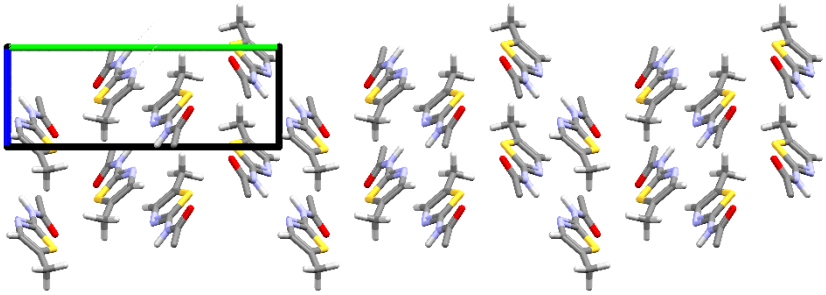

*Figure 36. View along the "a" parameter of six cells of* ***Th12****, where the alkyl chains were removed for clarity. The thiazole dimers organize in π packing with sulfur…sulfur contacts of 3.57Å (cell parameters b in green, c in blue).*

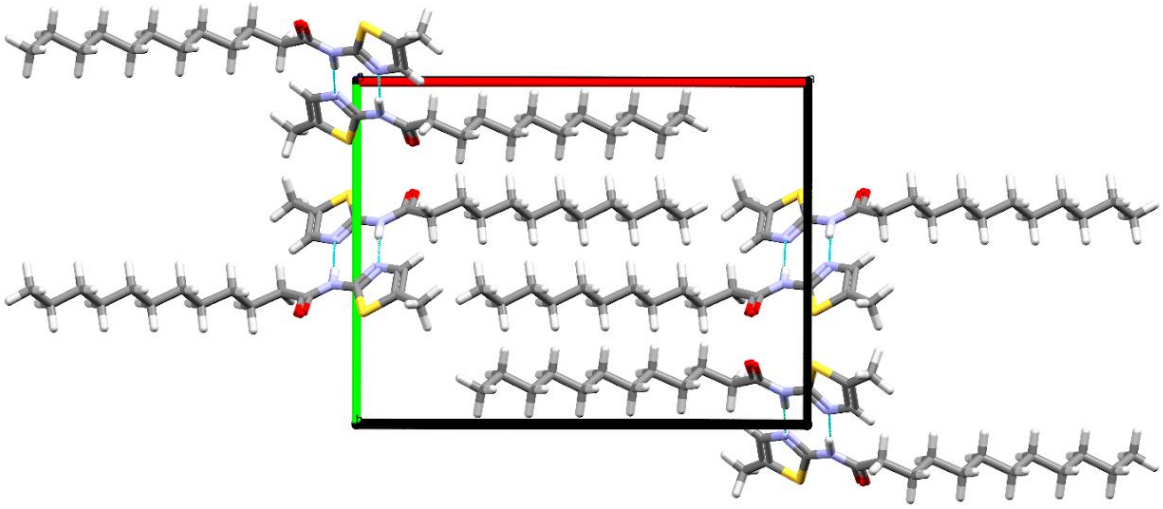

*Figure 37. View of* ***Th12*** *highlighting the presence of dimers formed by H-bond (cell parameters a in red, b in green).*

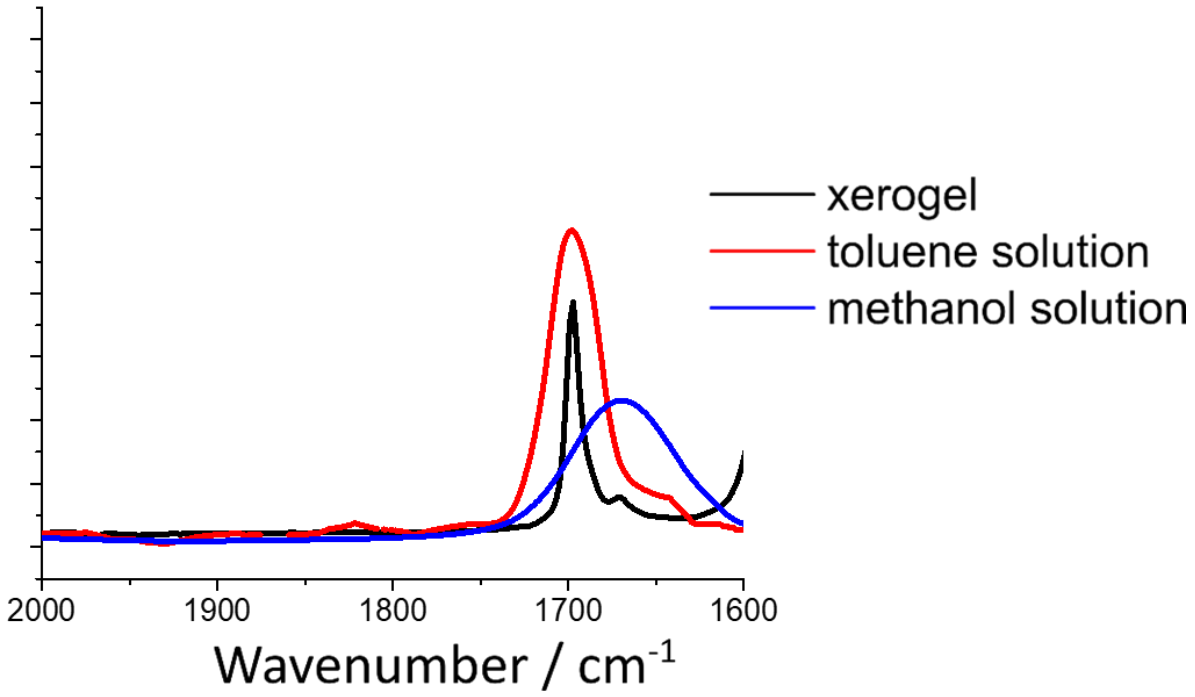


*Figure 38. IR spectra of* ***Th12*** *xerogel, compared to its solution in toluene or methanol. Free amide I: 1696 cm$^{-1}$; bonded amide I: 1668 cm$^{-1}$.*

## 1.6. X-ray measurements on oriented fibers

Usually, a strong directional interaction is responsible for the anisotropic growth of the organogel fibers. Here, this feature is not obvious since the amide groups are involved in dimer formation instead of forming chains of hydrogen bonds. To unambiguously identify which axis of the unit cell lies along the fiber growth direction, we performed X-ray diffraction on oriented fibers. By keeping the gel fibers intact (i.e., no grinding was performed) and compacting them as a film on a flat surface, we expect that most fibers lie parallel to the substrate. In these conditions, only reflections associated to lattice planes parallel to the fiber axis can be visualized in symmetric diffraction geometry (see Figure 39, which shows the difference in the experimental setup between the measurements performed on randomized crystals and oriented fibers).

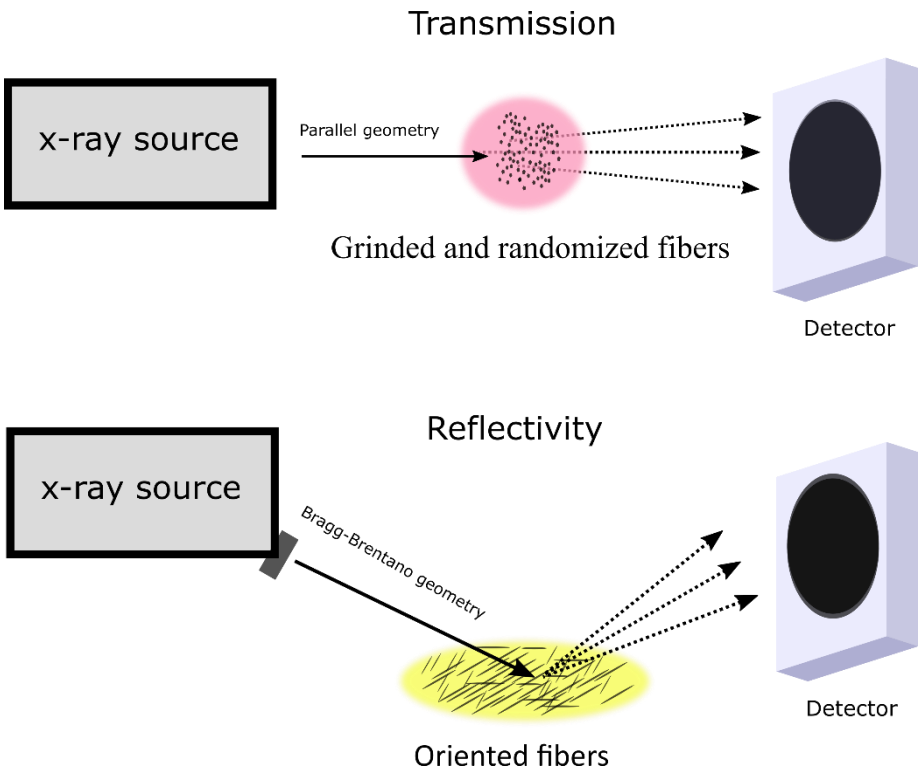


*Figure 39. Comparison of the X-ray methodology to measure randomized or oriented gel fibers.*

Figure 40 illustrates the difference between the patterns obtained from randomized and oriented fibers for **Th12** in toluene. The diffraction peaks that are present in both patterns can be easily identified as due to diffraction by (hk0) lattice planes. Reflections of the type 00L corresponding to the diffraction of the (00L) planes are not present in the oriented fibers pattern. Thus the (00L) planes are never in reflection condition which means that the [00L]* direction, which deviates from the [00L] axis by only few degrees, is never orthogonal to the sample plane. This is an indication of a preferred orientation of the fibers in a 2D powder, where the [00L] axis is in the sample plane and should thus correspond to the fiber axis. This point is illustrated in Figure 41 where some (hk0) planes are represented. We can conclude that the non-covalent interaction responsible for the elongation of the fibers is the π- π stacking between the thiazole aromatic rings and possibly the weak hydrogen bond between $CH_3$ and thiazole nitrogen, as reported by Ballabh et al[1,2] .

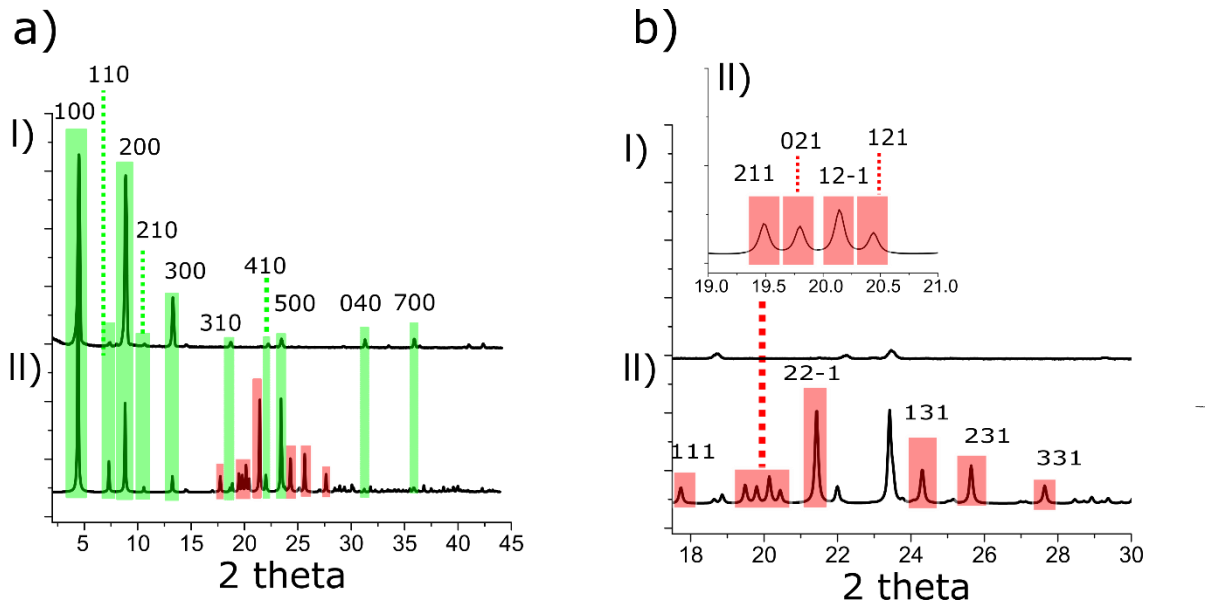


*Figure 40. Comparison between the X-ray patterns of oriented (top) and randomized (bottom) gel fibers of Th12. a) full range pattern. b) Close-up in the 17.5 - 30 2-theta range; the inset is a further zoom on the 19 – 21 2-theta range. Green highlighting corresponds to the diffraction peaks present in both X-ray patterns. Red highlighting corresponds to diffraction peaks only present in randomized fibers. X-ray wavelength of 1.5406 Å.*

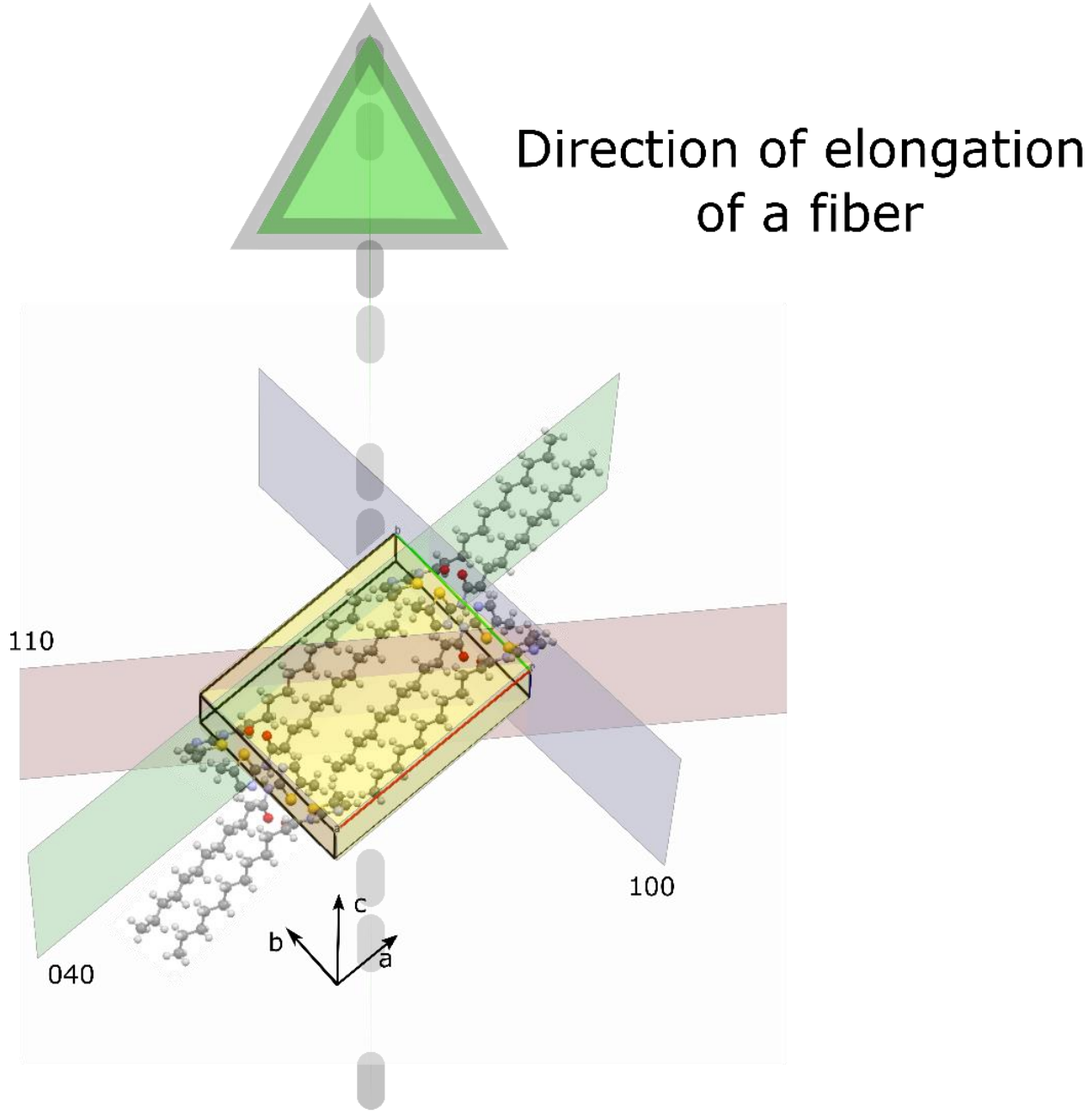


*Figure 41. Representation of the diffraction planes observed in the X-ray patterns of the oriented fibers.*

## 1.7. Conclusion for the thiazole based gelators

The study of this family of thiazole-based gelators presented a clear and simple trend. Increasing the length of the alkyl chain results in an increase of the radius of the gelation domains and a linear drift of the center of the gelation sphere to an area of the Hansen space of lower polarity (lower $\delta_P$ and $\delta_H$). It was also determined that the molecular packing within the gel fibers is conserved independently of the length of the alkyl chain. We can thus assume that the surface of the gel fibers involves a facet presenting alkyl chains that interact with the solvent. If the crystal habit is conserved within the family, we can expect that the surface of the fibers becomes less polar when the alkyl chain grows, which explains why the center of the gelation sphere drifts to an area of lower polarity in the Hansen space.

# 2. Bisamide based gelators

The following family of LMWGs is a bisamide organogelator derived from commercially available (1*S*,2*S*) -(+)-1,2-Diaminocyclohexane (Figure 42). This LMWG was first reported by Zweep et al,[5] where the length of the alkyl chains from the LMWGs was correlated with the gel-sol transition temperature and the minimum gelation concentration. The same model gelator is now used to correlate the effect of the alkyl chain in the Hansen space. Nine members of this group of LMWG were synthesized, with each alkyl chain varying between one (**Bis3**) to sixteen (**Bis18**) $CH_2$. After characterizing the Hansen space, X-ray measurements were performed to study the existence of polymorphism caused by the formation of gels in different liquids and molecular packing within gel fibers.

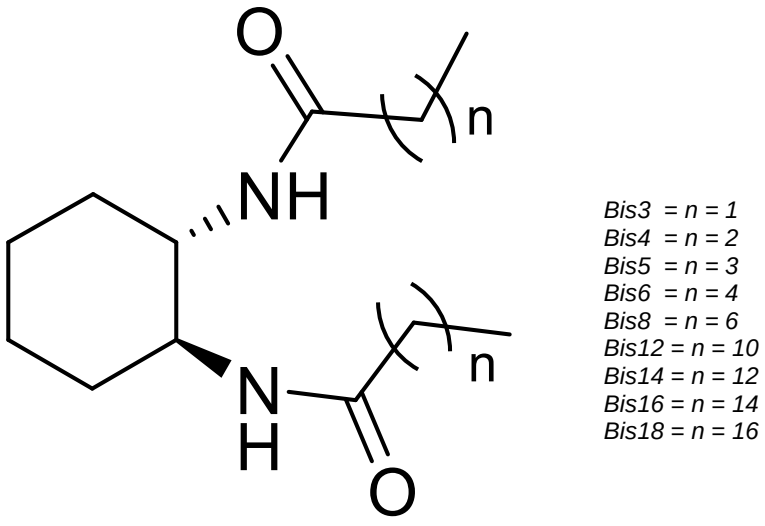


*Figure 42. Chemical structure of the bisamide-based LMWGs.*

## 2.1. Influence of concentration on Hansen space

Before comparing the Hansen space of different bisamide based LMWGs, **Bis5** was chosen to perform an in-depth study of the Hansen space at different concentrations (from 3 wt% to 0.15 wt%) (Figure 43). All Hansen domains were calculated following the methodology described in chapter 2. While at 0.15 wt % and 0.3 wt% we were not able to highlight any gelation domain, as we increase the amount of LMWG we can observe the shrinking of the solubility sphere giving space to a gelation domain. As expected, the center of solubility sphere remains relativity constant and the radius decreases with the increase of the gelation concentration (Table 6). The center of the gelation sphere remains without major changes between 3 wt % and 1 wt% and shifts to lower $\delta_H$ values at 0.75 wt% and 0.5 wt%. This shift of the center of the gelation sphere is unexpected since only the radius of the sphere should be affected by the concentration (similarly to the thiazole based LMWG). A possible explanation is the lack of solvent with high $\delta_H$ used in the solubility test, that gives a lower definition of the Hansen space at high $\delta_H$ values.

Based on the solubility tests on **Bis5** at different concentration we chose a standard concentration of 1 wt% to characterize the remaining LMWGs. This value was chosen due to the ratio of almost 2:1 of the gelation sphere compared to the solubility sphere, representing a good starting point to observe changes in the proportion of the spheres.

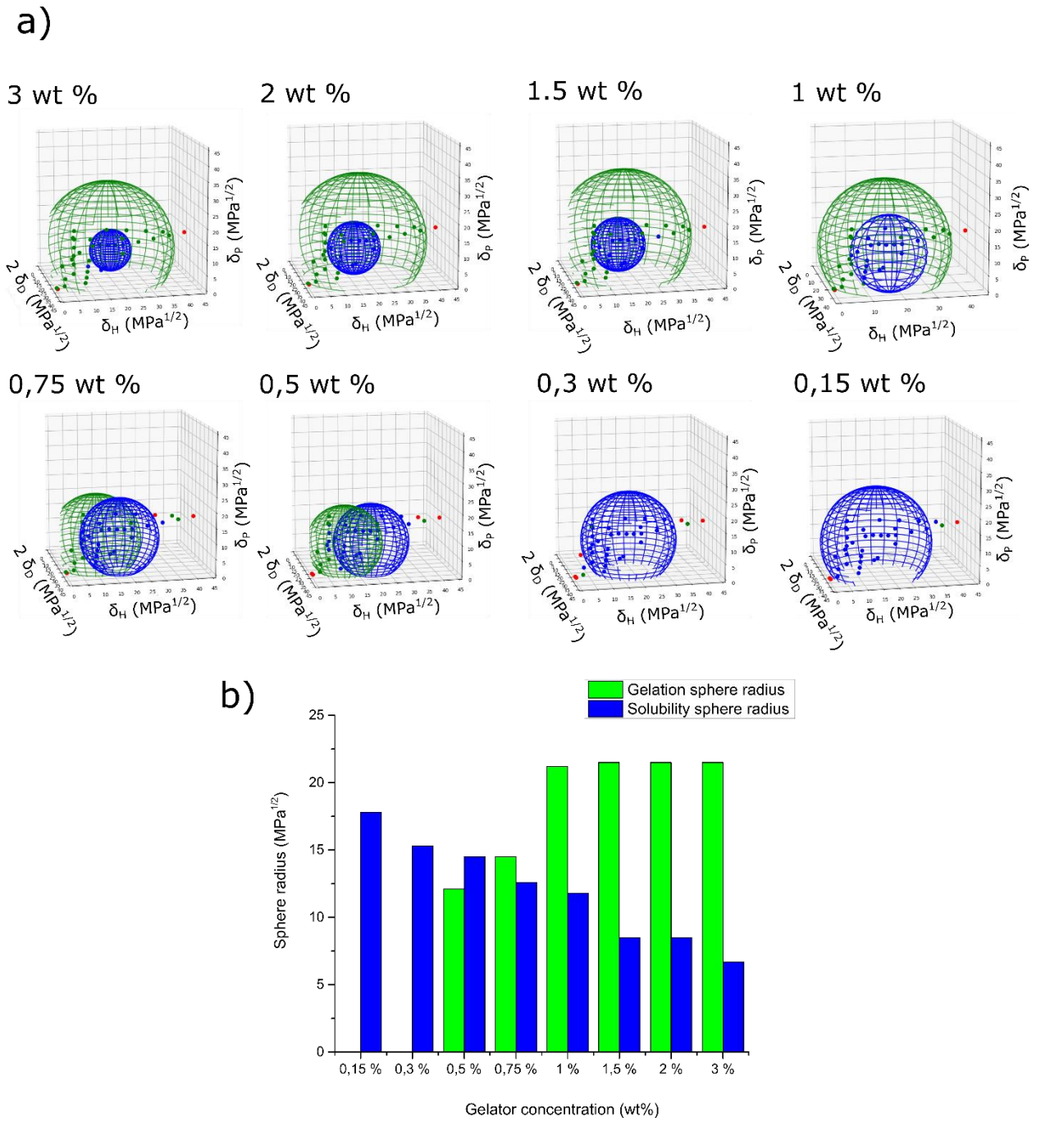


*Figure 43. a) Gelation data plotted in Hansen space for the LMWG **Bis5** at different concentrations. The tested liquids are represented by full circles and the calculated domains are represented by meshed spheres. Green: gel; red: precipitate; blue: soluble. b) Radius of the solubility (blue) or the gelation (green) spheres for **Bis5** at different concentrations.*

*Table 6. Coordinates of the center and radius of Bis5 Hansen spheres at different concentrations.*

| | Solubility sphere center | | | | Gelation sphere center | | | |
|---|---|---|---|---|---|---|---|---|
| wt % | $\delta_D$ ($MPa^{1/2}$) | $\delta_P$ ($MPa^{1/2}$) | $\delta_H$ ($MPa^{1/2}$) | r ($MPa^{1/2}$) | $\delta_D$ ($MPa^{1/2}$) | $\delta_P$ ($MPa^{1/2}$) | $\delta_H$ ($MPa^{1/2}$) | r ($MPa^{1/2}$) |
| 3 | 16.3 | 9.6 | 17.3 | 6.7 | 14.1 | 11.6 | 17.6 | 21.5 |
| 2 | 17.6 | 10.9 | 15.0 | 8.5 | 14.3 | 12.4 | 17.6 | 21.8 |
| 1.5 | 15.3 | 11.4 | 14.0 | 8.7 | 14.6 | 13.8 | 16.2 | 21.6 |
| 1 | 17.0 | 10.6 | 17.3 | 12.0 | 14.8 | 12.1 | 16.8 | 21.1 |
| 0.75 | 18.1 | 11.4 | 16.8 | 12.6 | 15.2 | 10.0 | 10.2 | 14.5 |
| 0.5 | 17.1 | 10.0 | 19.0 | 14.5 | 17.1 | 9.87 | 10.5 | 12.1 |
| 0.3 | 16.0 | 11.4 | 17.5 | 15.3 | | | | |
| 0.15 | 16.6 | 11.3 | 15.1 | 17.8 | | | | |

## 2.2. Hansen space of bisamide based gelators

Figure 44 shows the 3D representation in the Hansen space for **Bis3, Bis4, Bis5, Bis6, Bis8, Bis12, Bis14, Bis16** and **Bis18** at 1 wt%. The gelation sphere for **Bis3** was not determined due to lack of gelated liquids. LMWG **Bis14, Bis16** and **Bis18** were not soluble in any liquids and thus no solubility domain could be calculated for these LMWG.

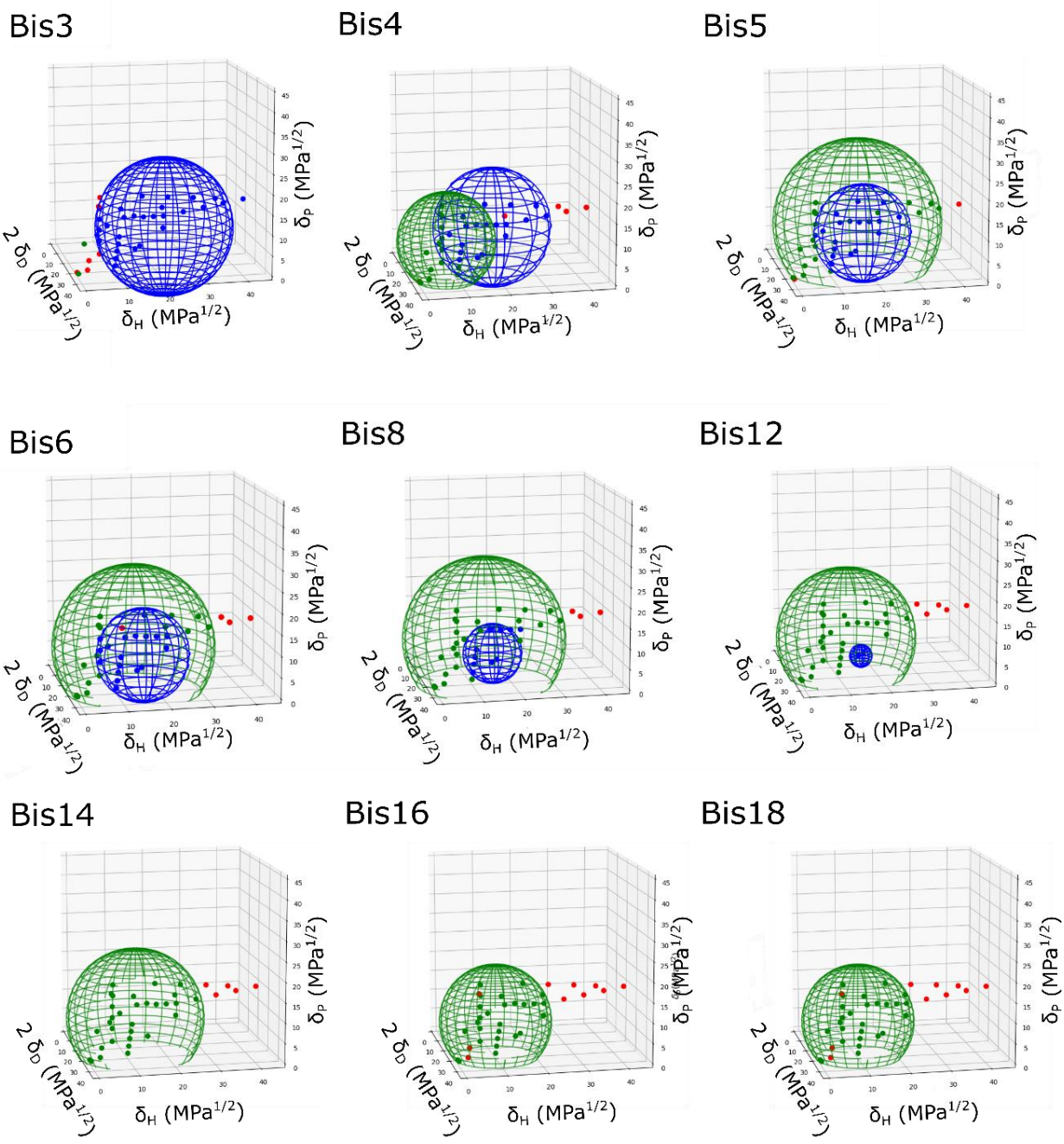


*Figure 44. Gelation data plotted in Hansen space for the bisamide-based LMWGs at 1 wt%. The tested liquids are represented by full circles and the calculated domains are represented by meshed spheres. Green: gel; red: precipitate; blue: soluble.*

The increase in the length of the alkyl chain leads to a decrease of the radius of the solubility sphere (Figure 45a) and to a shift of the center of the solubility sphere (Table 7) to lower values of $\delta_P$ and $\delta_H$

(Figure 45b). The trend of the center of LMWG solubility spheres **Bis3** and **Bis12** yields the following vector equation:

Eq 12: $[\delta_D, \delta_P, \delta_H] = [16.8, 14.2, 19.2] + t\,[0.04, -0.73, -0.37]$

Adding one $CH_2$ to each alkyl chain causes the center of the solubility spheres to drift by $\delta_D = 0.04$; $\delta_P = -0.73$; $\delta_H = -0.37$ $MPa^{1/2}$.
The theoretical HSP values of the bisamide-based gelators (Table 8) and the trend lines were also added to figure 45b. The trend of the theoretical values of HSP yields the following vector equation:

Eq 13: $[\delta_D, \delta_P, \delta_H] = [17.8, 13.8, 8.7] + t\,[-0.09, -0.43, -0.29]$

Similar to what was observed with the thiazole-based gelators, the slope in the trend line of the theoretical HSP values is consistent with the slope in the trend line of experimental center of solubility spheres, despite the theoretical occupying a region at lower $\delta_H$.
A behavior similar to the evolution of the solubility spheres can be observed with the gelation sphere where the increase of the length of the alkyl chain leads to the decrease of the radius of the sphere from **Bis5** to **Bis18** (Figure 45a) while the center of the sphere (Table 7) also shifts to lower values of $\delta_P$ and $\delta_H$ (Figure 45b). The gelation sphere of **Bis4** is outside of this trend because the number of G points is not sufficient to fully characterize the Hansen space. **Bis4** is the only gelator in this family that does not present a gelation sphere enclosing the solubility sphere (when it exists) and this points to a lack of definition of the sphere of this gelator at high $\delta_H$. Thus, **Bis4** was not taken in consideration for the calculation of the trend line of the center of the gelation spheres. The trend of the center of LMWG gelation spheres yields the following vector equation:

Eq 14: $[\delta_D, \delta_P, \delta_H] = [16.1, 12.0, 16.2] + t\,[0.02, -0.17, -0.42]$

Adding one $CH_2$ to each alkyl chain causes the center of the gelation spheres to drift by $\delta_D = 0.02$; $\delta_P = -0.17$; $\delta_H = -0.42$ $MPa^{1/2}$. One important remark is that despite the center of the gelation spheres drifts to an area of lower polarity in the Hansen space, the slope of the trend line differs from the slope observed in the trend line of the center of solubility spheres. In this family of LMWG the increase in length of the alkyl chains has a minor effect on $\delta_P$ and a major effect on $\delta_H$ of the center of the gelation spheres when compared to the solubility spheres.

.

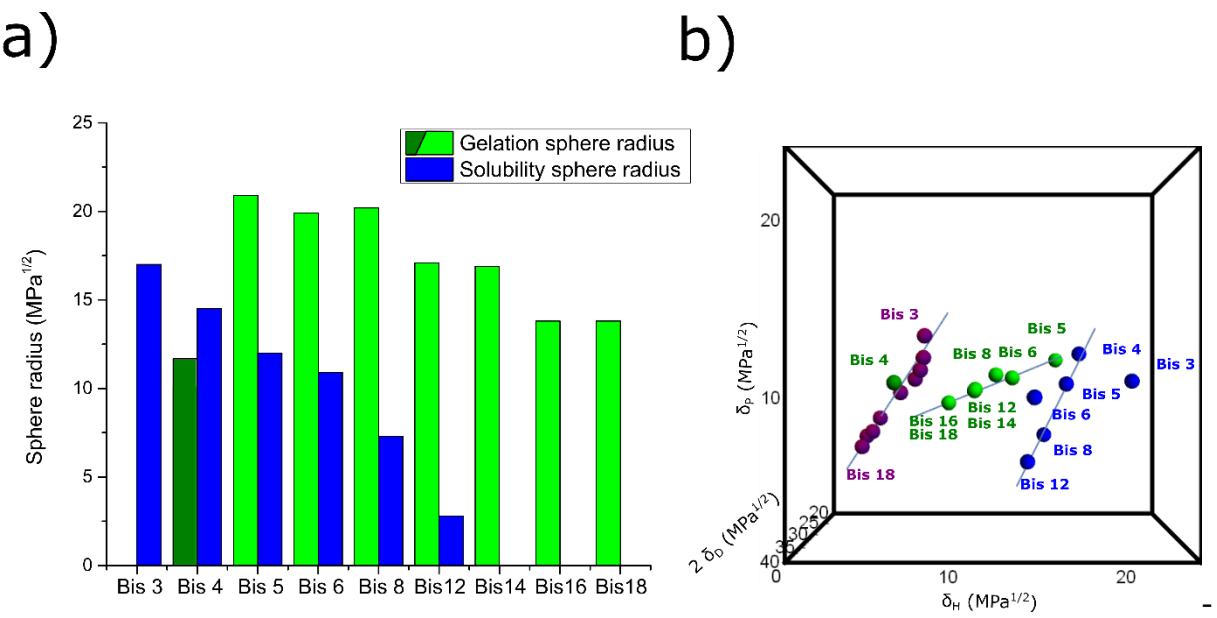


*Figure 45. a) Radius of the solubility (blue) or the gelation (green) spheres for the bisamide-based LMWGs. b) Center of the solubility spheres (blue), center of the gelation spheres (green) and simulated HSP parameters of each bisamide-based gelator (purple) represented in Hansen space. Data from Figure 44; for **Bis4**, a dark green color has been selected to highlight the limited precision of that particular dataset.*

*Table 7. Coordinates of the center and radius of Hansen spheres for bisamide-based LMWGs at 1 wt %.*

| | Solubility sphere centre | | | | Gelation sphere centre | | | |
|---|---|---|---|---|---|---|---|---|
| LMWG | $\delta_D$ ($MPa^{1/2}$) | $\delta_P$ ($MPa^{1/2}$) | $\delta_H$ ($MPa^{1/2}$) | r ($MPa^{1/2}$) | $\delta_D$ ($MPa^{1/2}$) | $\delta_P$ ($MPa^{1/2}$) | $\delta_H$ ($MPa^{1/2}$) | r ($MPa^{1/2}$) |
| Bis3 | 17.0 | 10.8 | 21.6 | 17.0 | | | | |
| Bis4 | 16.3 | 12.5 | 18.2 | 14.5 | 17.5±1.4 | 10.1±0.7 | 6.4±1.4 | 12.0±0.7 |
| Bis5 | 17.0 | 10.6 | 17.3 | 12.0 | 14.8±0.4 | 12.1±0.6 | 16.8±0.4 | 21.1±0.4 |
| Bis6 | 18.6 | 9.8 | 15.1 | 10.9 | 16.3±0.3 | 10.9±0.3 | 13.8±0.3 | 19.9±0.4 |
| Bis8 | 15.8 | 7.1 | 14.9 | 7.3 | 16.3±0.3 | 11.4±0.3 | 12.7±0.2 | 20.1±1.8 |
| Bis12 | 17.3 | 5.5 | 14.7 | 2.8 | 16.8±0.3 | 10.1±0.3 | 11.3±0.2 | 17.1±0.3 |
| Bis14 | | | | | 16.8±0.3 | 10.2±0.3 | 11.3±0.3 | 16.9±0.3 |
| Bis16 | | | | | 16.4±0.2 | 9.3±0.3 | 9.5±0.2 | 13.8±0.2 |
| Bis18 | | | | | 16.4±0.2 | 9.3±0.3 | 9.5±0.2 | 13.8±0.2 |

*Table 8. Coordinates of the theoretical HSP values calculated by the HSPiP* software[3-4] *for bisamide-based LMWGs*

| LMWG | $\delta_D$ ($MPa^{1/2}$) | $\delta_P$ ($MPa^{1/2}$) | $\delta_H$ ($MPa^{1/2}$) |
|---|---|---|---|
| Bis3 | 17.9 | 13.7 | 8.1 |
| Bis4 | 17.7 | 12.3 | 8.0 |
| Bis5 | 17.3 | 11.5 | 7.8 |
| Bis6 | 17.2 | 10.9 | 7.4 |
| Bis8 | 16.9 | 10.0 | 6.4 |
| Bis12 | 16.6 | 8.3 | 5.0 |
| Bis14 | 16.6 | 7.4 | 4.5 |
| Bis16 | 16.5 | 7.1 | 4.1 |
| Bis18 | 16.6 | 6.4 | 3.8 |

To confirm the accuracy of the experimentally obtained centers of the gelation spheres and the trend obtained we calculated the uncertainty in the determination of the gelation spheres. The values were then plotted as ellipsoids in the Hansen space together with the center of the spheres in figure 46. All gelators from **Bis5** to **Bis18** presented a low standard deviation value (< 0.6 $MPa^{1/2}$) indicating a good accuracy of the domain determination and trend line. **Bis4**, the gelator that resides outside of the gelation trend of this family presented a standard deviation significantly higher (≈ 1.4 $MPa^{1/2}$) than all other members. This higher standard deviation value may be due to the lack of definition at high $\delta_H$ in the Hansen space of **Bis4** that was already mentioned.

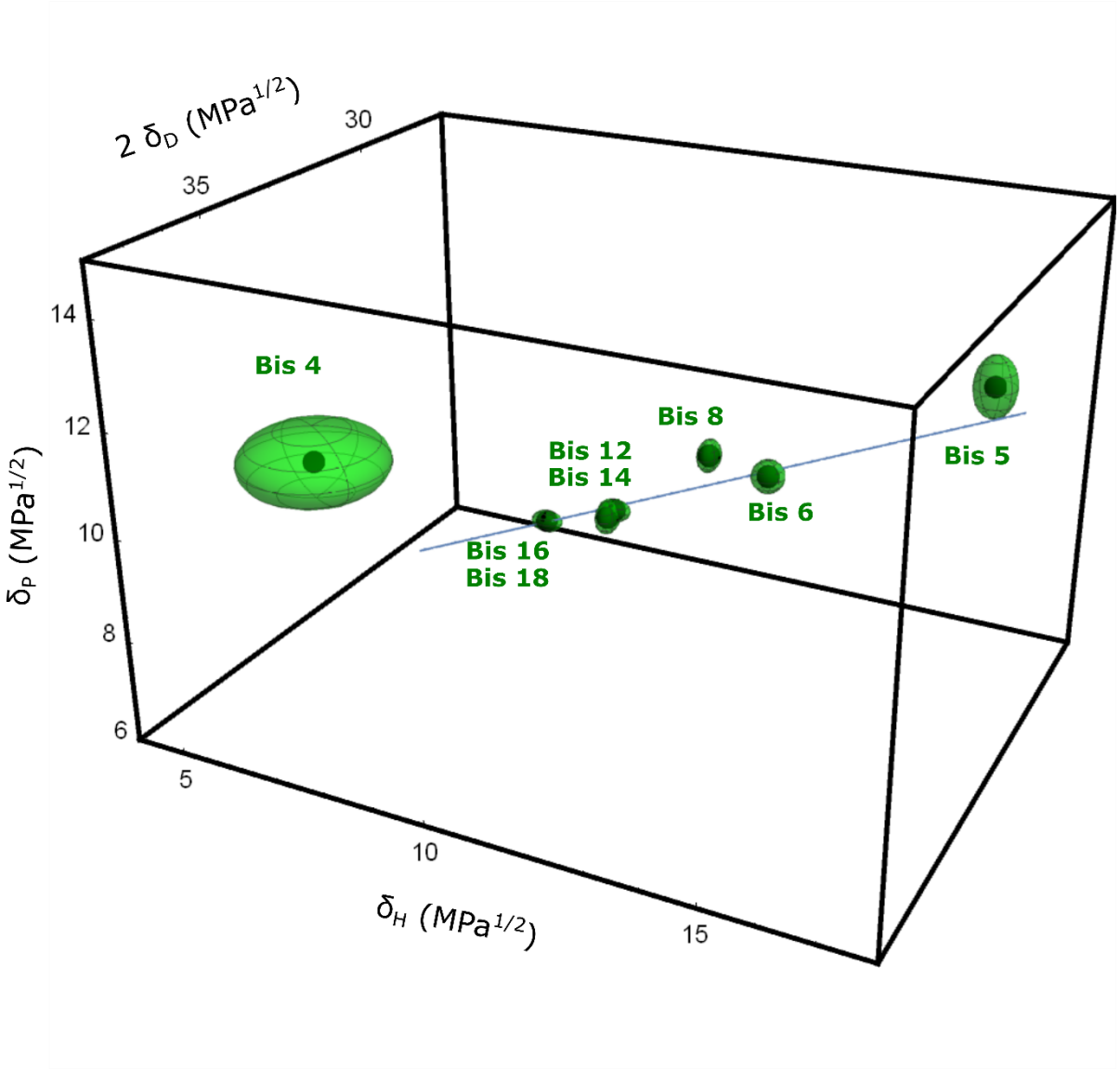


*Figure 46. Center of the gelation spheres (dark green) and the standard deviation (meshed green ellipse) represented in Hansen space.*

## 2.3. X-ray measurements for xerogels from toluene

X-ray analysis was performed on xerogels of all bisamide LMWG extracted from toluene (Figure 47). The main phenomenon observed when comparing all diffraction patterns is the decrease of crystallinity with the increase of the alkyl chain length. **Bis3, Bis4, Bis5** and **Bis6** present several sharp diffraction peaks but the sharpness and number of diffraction peaks drastically decrease for **Bis8, Bis12, Bis14, Bis16** and **Bis18**. This indicates that from **Bis6** to **Bis8** there is an abrupt loss of long-range organization.

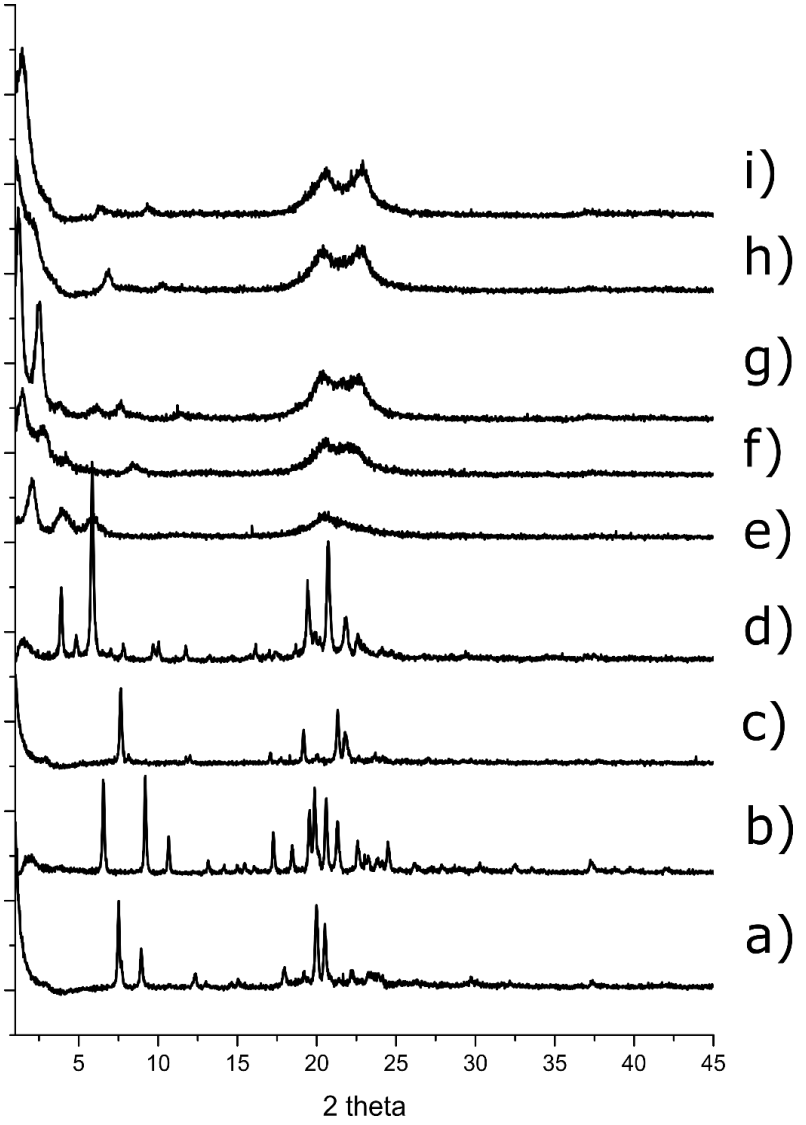


*Figure 47. X-ray patterns of bisamide-based LMWGs xerogels extracted from toluene. a)* ***Bis3****, b)* ***Bis4****, c)* ***Bis5****, d)* ***Bis6****, e)* ***Bis8****, f)* ***Bis12****, g)* ***Bis14****, h)* ***Bis16*** *and i)* ***Bis18****. X-ray wavelength of 1.5406 Å.*

As this group of LMWG presents a decrease of organization as the length of the alkyl chain increases, PDF measurements were performed on the xerogel of **Bis4** (organized molecules inside fibers) and **Bis8, Bis12, Bis16** and **Bis18** (disorganized molecules inside fibers) (figure 48). The PDF measurement is very similar between all measured gelators in figure 48, indicating that the local molecular structure is very similar between LMWG with and without long-range periodicities.

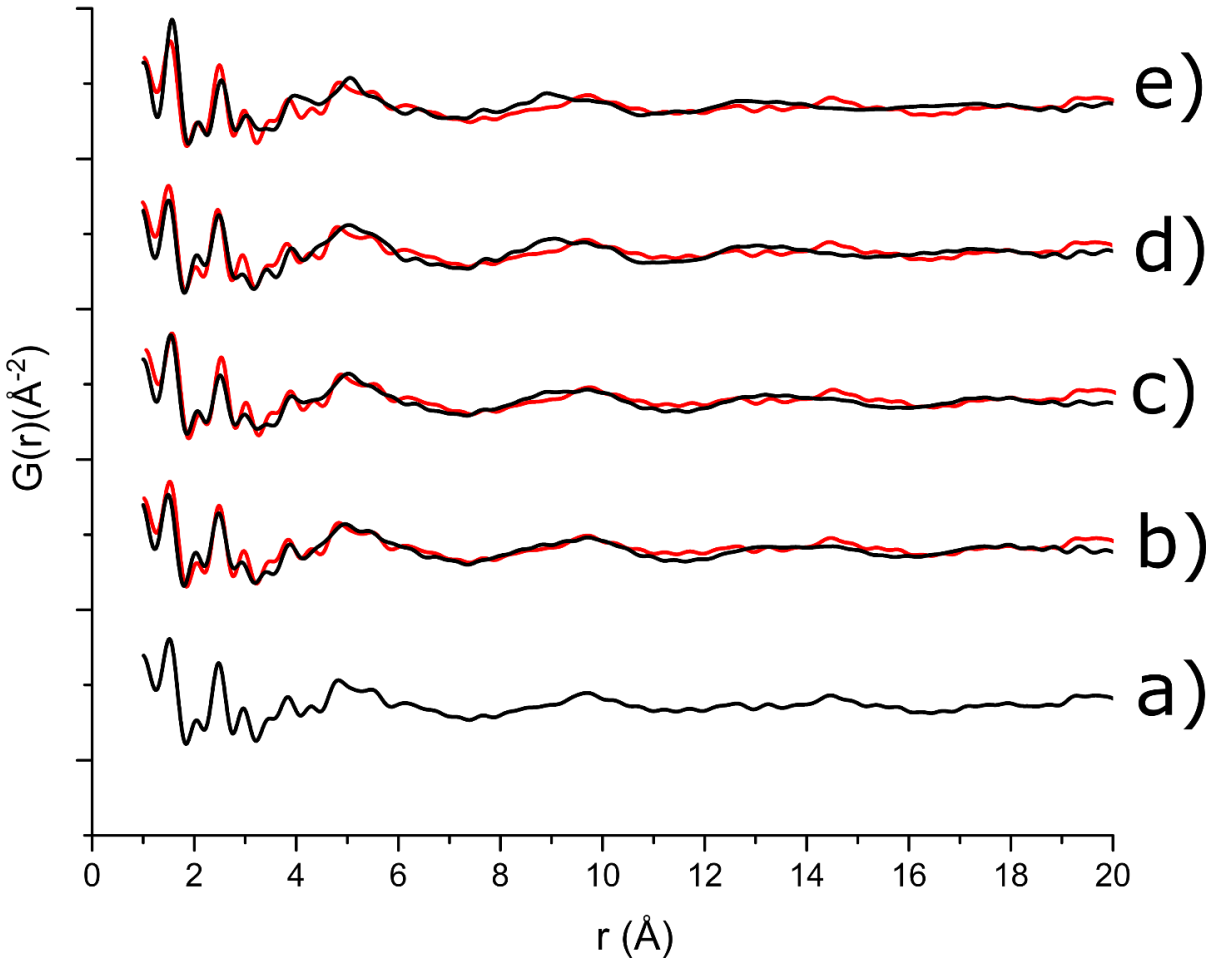


*Figure 48. PDF measurements of bisamide-based LMWGs xerogels extracted from toluene. a)* ***Bis4****, b)* ***Bis8*** *c)* ***Bis12****, d)* ***Bis16*** *and e)* ***Bis18*** *represented in black with* ***Bis4*** *overlayed in red.*

## 2.4. Bisamide polymorphism

Another interesting information provided by X-ray diffraction about this group of LMWG is the possibility of forming polymorphs depending on the liquid that is gelated. This phenomenon was already briefly mentioned in chapter 2 but will be further explored here. The X-ray powder pattern of a material serves as a sort of molecular fingerprint of the crystal structure. This means that if an organogelator self-assembles in two different ways, the powder patterns of these two different forms will be different.

To probe the existence of polymorphism within this group of LMWGs we performed X-ray diffraction measurements on xerogels of LMWGs formed in different liquids and that demonstrate some degree of crystallinity. The first LMWG to be studied was **Bis4**. Seven **Bis4** gels formed in different liquids scattered across the Hansen space were prepared and their xerogels were measured (Figure 49). All the measured xerogels of **Bis4** presented almost identical powder patterns, indicating that for **Bis4** the molecular packing of the gel fibers is independent from the liquid that is gelated. The measured xerogels were also compared with the simulated powder pattern obtained from the single crystal structure of **Bis4** found in the literature.[5] The difference in peak width between the simulated and measured powder pattern is due to the low definition setup used in this measurement. Beside the already mentioned peak width, peak position and intensities are very similar. This indicates that **Bis4** has the same molecular packing in single crystal and gel fibers independently of the liquid gelated.

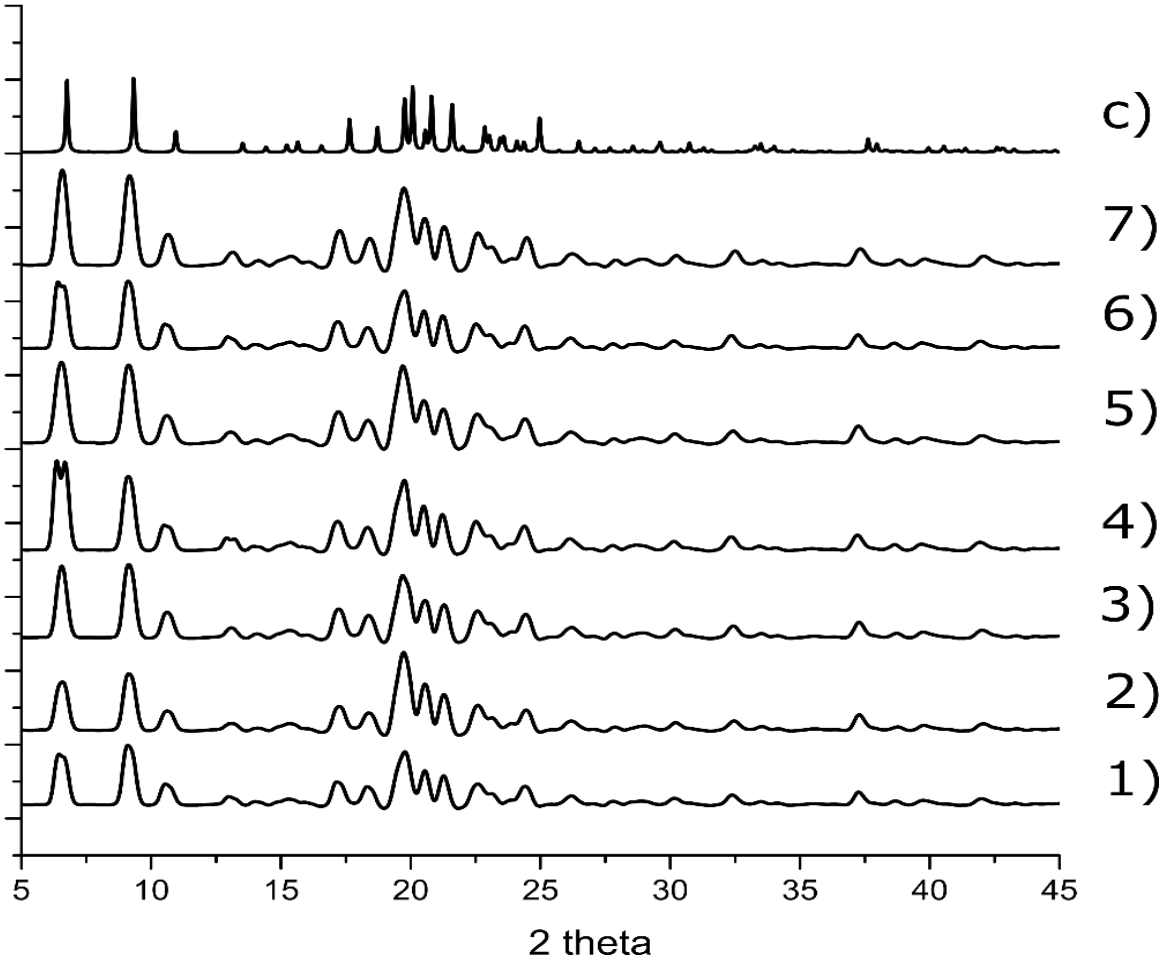


*Figure 49. X-ray patterns of xerogels of **bis4** obtained from (1) acetonitrile, (2) t-butyl acetate, (3) 1-chloropentane, (4) chlorobenzene, (5) cyclohexane, (6) MEK, (7) toluene. Pattern simulated from the single-crystal structure (C). X-ray wavelength of 1.5406 Å.*

The same exercise was performed with **Bis5**. In that case it was possible to observe two different types of powder pattern depending on the liquid that was used to form a gel (Figure 50a). The first type of powder pattern is highlighted in green in figure 50a) and is called polymorph **1**. The second type of powder pattern is highlighted in red in figure 50a) and is called polymorph **2**. The main points used to differentiate these patterns are that polymorph **1** possesses at small angle a weak diffraction peak at 6.0 º and a strong one at 7.6 º whereas polymorph **2** contains two strong diffractions peaks at 5.2 º and 6.5 º, and completely different profiles between 15 º and 30 º. We represented in Figure 50b the position of the liquids from which the gels were formed in the Hansen space. This figure shows that the different polymorphs do not originate from separated clusters in the Hansen space.

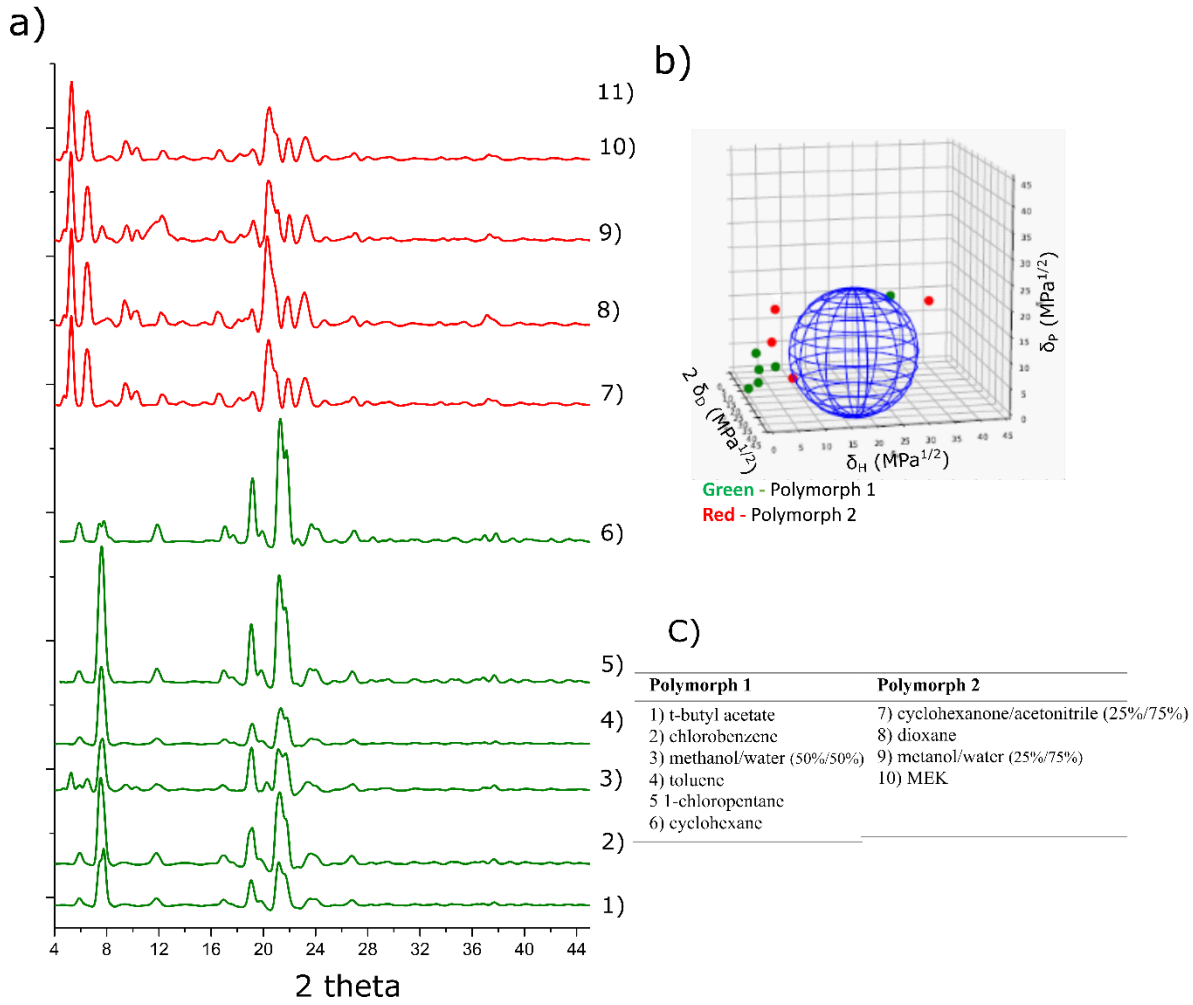


*Figure 50. a) X-ray patterns of **Bis5** xerogels, polymorph **1** represented by green and polymorph **2** represented by red. X-ray wavelength of 1.5406 Å. b) Hansen space of **Bis5** indicating the position of polymorphs **1** and **2** surrounding the solubility sphere. c) indication of the different solvents that form the different polymorphs.*

Differential scanning calorimetry (DSC) provided further proof that the different powder patterns represented different polymorphs. Polymorph **1** and **2** present a first endotherm at 105°C and 147°C, respectively and both showed the melting point at the same temperature (243°C) (Figure 51). After melting and crystallization, both samples show a transition temperature at 91°C: after thermal treatment the gelator molecules lose the conformation acquired when self-assembling in gel fibers and assemble again but this time in bulk conditions.

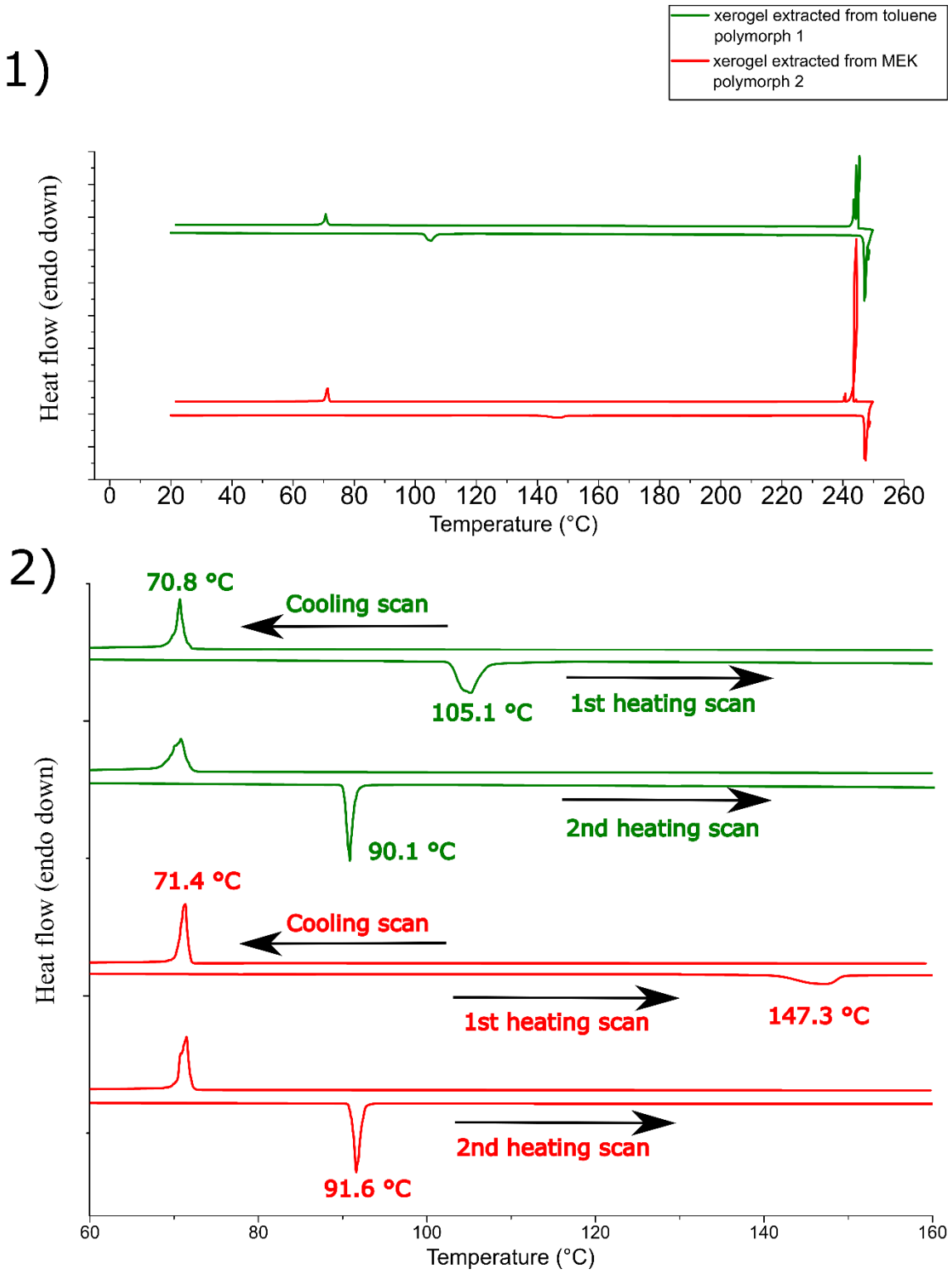


*Figure 51. DSC analysis of **Bis5** xerogels extracted from MEK (red) or toluene (green).1) first heating/cooling cycle 2) amplification of the temperature region where transitions occur. First and second cycles (10°C/min).*

**Bis6**[6] presented a phenomenon similar to **Bis5**. Here also it was possible to identify two different

types of powder patterns depending on the liquid used to form the gel. The patterns for polymorph **a** are highlighted in red in Figure 52a, and in green for polymorph **b**. Polymorph **a** contains a strong diffraction peak at 7° and polymorph **b** contains a medium intensity diffraction peak at 3.7° degree and a strong one at 6°. Both patterns show slight differences between 18° and 24 °. Again, both polymorphs were plotted in the Hansen space, but no clustering of the polymorphs was observed, being randomly dispersed in the Hansen space.

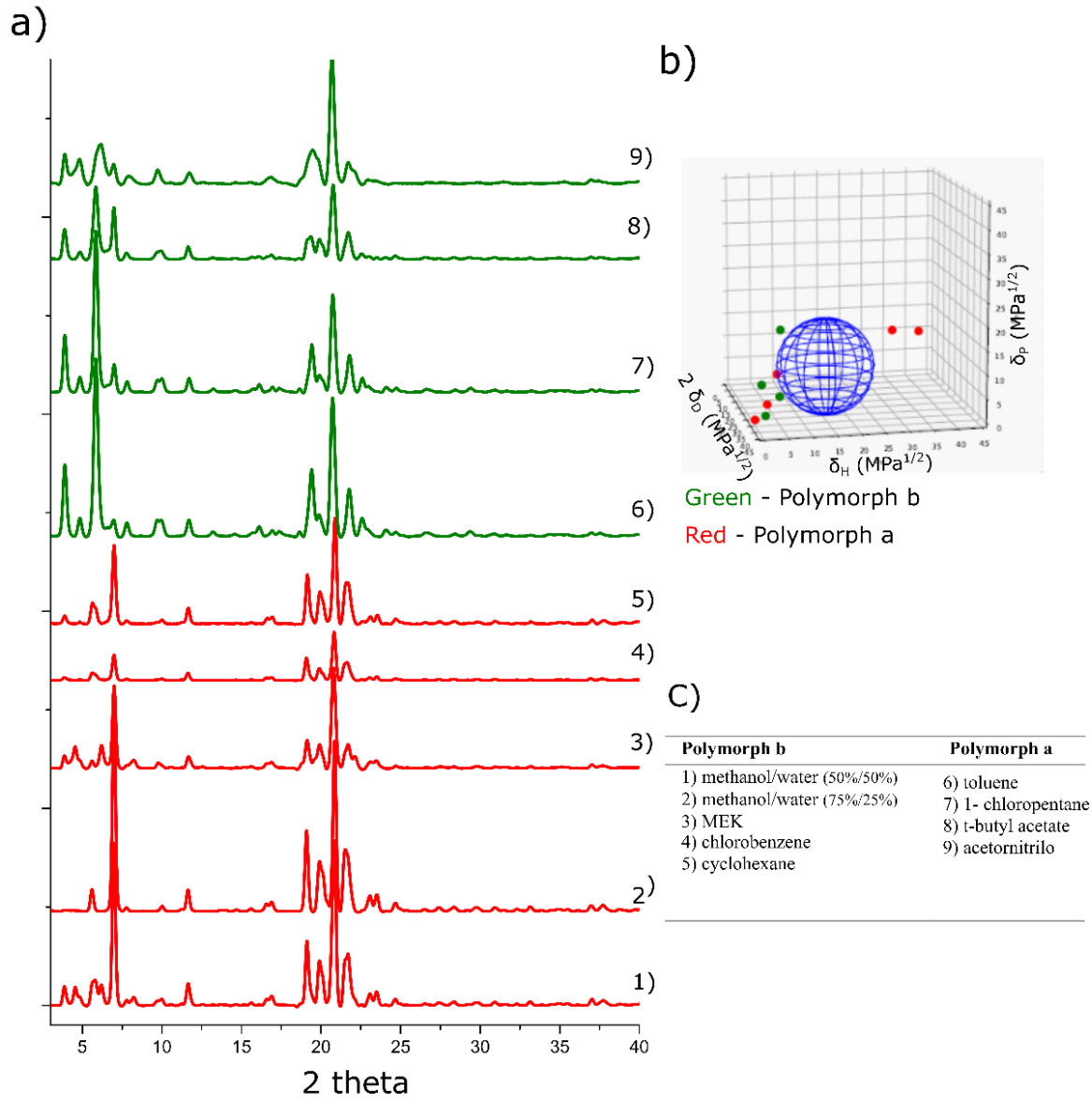


*Figure 52. a) X-ray patterns of **Bis6** xerogels, polymorph **b** represented by green and polymorph **a** represented by red. X-ray wavelength of 1.5406 Å. b) Hansen space of **Bis6** indicating the position of polymorphs **a** and **b** surrounding the solubility sphere. c) indication of the different solvents that form the different polymorphs.*

Again, DSC traces demonstrate the existence of polymorphism, with polymorph **a** having a transition

temperature of 125°C and polymorph **b of** 121 °C (Figure 53) and both presenting the melting point at the same temperature (231°C).

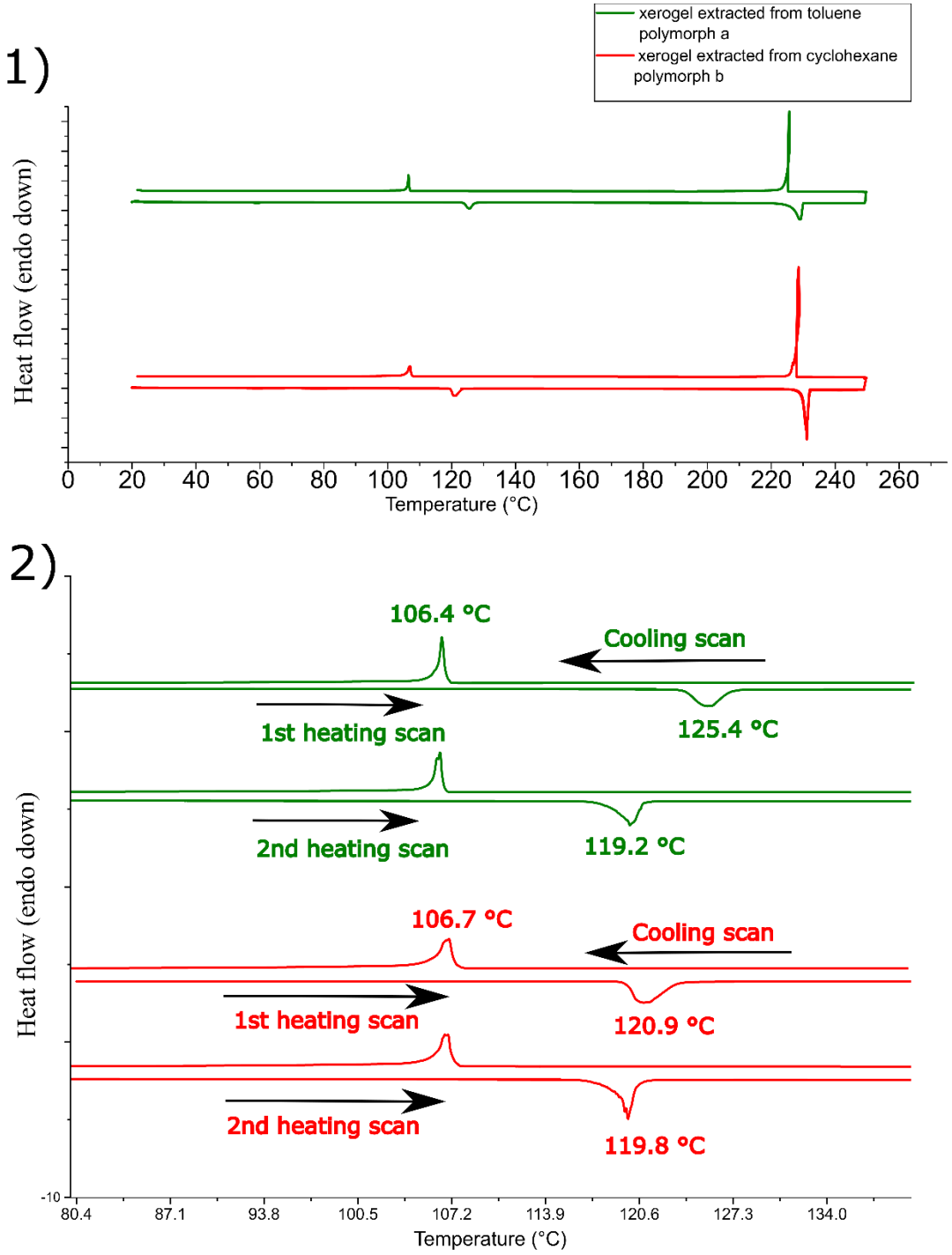


*Figure 53. DSC analysis of **Bis6** xerogels extracted from cyclohexane (green) or toluene (red). 1) first heating/cooling cycle 2) amplification of the temperature region where transitions occur. First and second cycles (10°C/min).*

Another important fact to mention is that it is not always the same groups of liquids that form different polymorphs between **Bis5** and **Bis6**. For example, in **Bis5** toluene and cyclohexane give xerogels

with the same type of powder pattern while the same two liquid give different powder patterns with **Bis6**.

When comparing the X-ray patterns of **Bis8** xerogel extracted from different solvents (figure 54), only a few differences in peak intensities were observed while all peak position remained the same. This gives an indication that no polymorphism exists in this gelator, or at least that they cannot be discriminated based on the broad the X-ray patterns available.

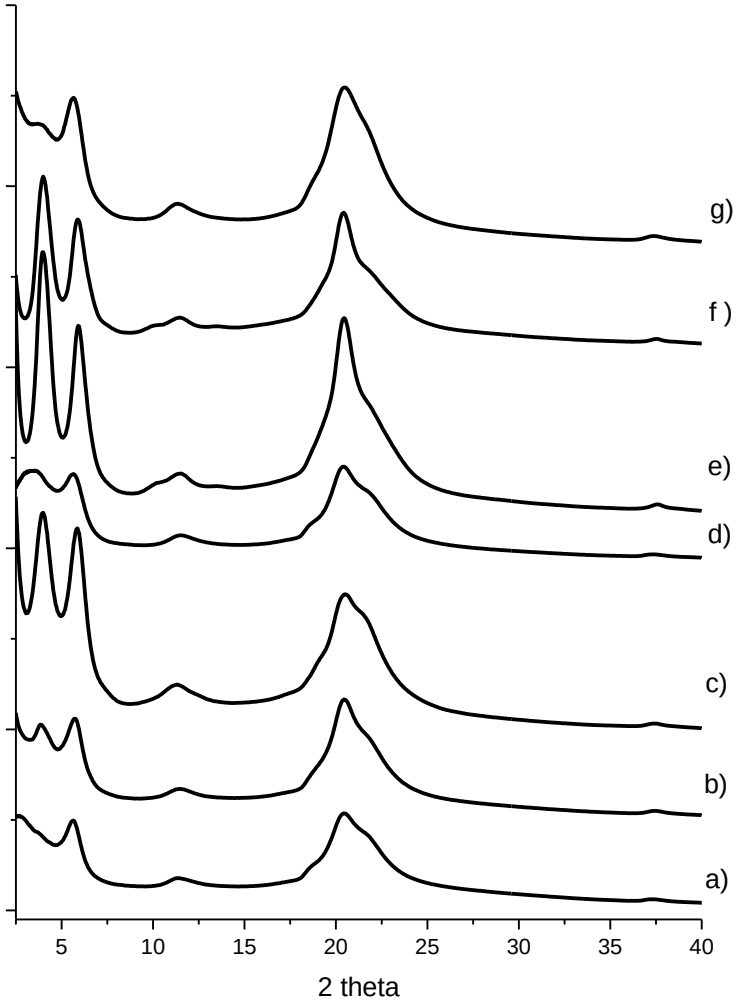


*Figure 54. X-ray patterns of **Bis8** xerogels a) dioxane, b) MEK, c) toluene, d) acetonitrile, e) t-butyl acetate, f) 1-chloropentane and g) chlorobenzene. X-ray wavelength of 1.5406 Å.*

Based on the date collected we identified that the increase in length of the bisamide based gelators causes the molecular packing within the fibers to evolve. **Bis4** assembles in highly organized

structures whatever the gelated liquid. A slight increase of the length of the alkyl chains (**Bis5** and **Bis6**) resulted in the presence of polymorphs within the gel fibers depending on the liquid gelated. Further increase in length of the alkyl chains (**Bis8**, **Bis12**, **Bis14**, **Bis16** and **Bis18**) resulted in the loss of periodicity in the gel fibers (Table 9).

*Table 9. Summary of the molecular packing within bisamide-based gel fibers.*

| | ***Bis4*** | ***Bis5*** | ***Bis6*** | ***Bis8*** | ***Bis12*** | ***Bis14*** | ***Bis16*** | ***Bis18*** |
|---|---|---|---|---|---|---|---|---|
| ***number of polymorphs*** | *1* | *2* | | | | | | |
| ***long range order*** | *yes* | | | *no* | | | | |

## 2.5. Microscopy observation of fibers

Figure 55 illustrates SEM pictures of bisamide based LMWG fibers extracted from toluene. **Bis4, Bis6** and **Bis18** present cylindrical fibers with a similar diameter. The main difference between them is that LMWG **Bis4 and Bis6** are made of long rigid fibers while **Bis18** contains short and highly entangled fibers. Here we can deduce that the increase in the length of the alkyl chains of the LMWGs increases the degree of entanglement of the fibers. The lack of long-range order revealed by X-ray measurements for **Bis18** is probably responsible for the lower rigidity of the fibers.

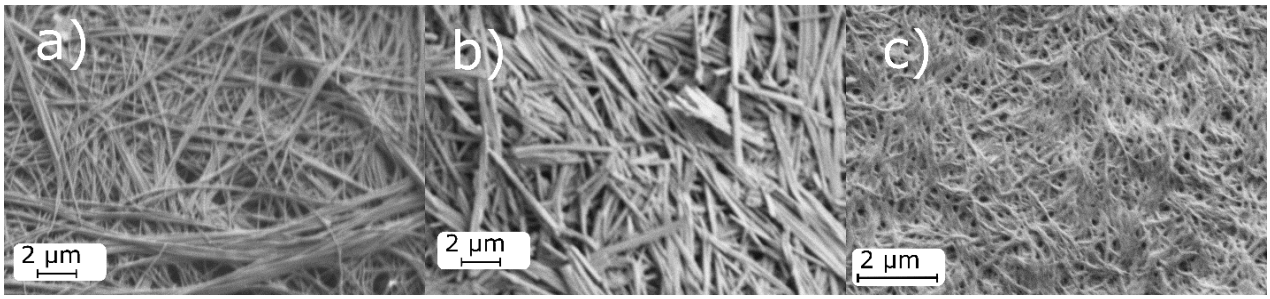


*Figure 55. SEM images of the bisamide-based xerogels extracted from toluene. a) **Bis4**, b) **Bis6**, c) **Bis18**.*

When the fibers of the same LMWG **Bis6** extracted from different liquids are compared, one can observe small differences in morphology. Fibers of **Bis6** (Figure 56a) extracted from toluene (i.e.

polymorph **a**) are cylindrical and linear with a low degree of entanglement. The fibers of **Bis6** extracted from cyclohexane (polymorph **b**, Figure 56b) are also present as cylinders but aggregate in tape-like objects, which have average cross sections significantly larger than the fibers extracted from toluene. This suggests that some solvents may promote aggregation of bisamide fibers.

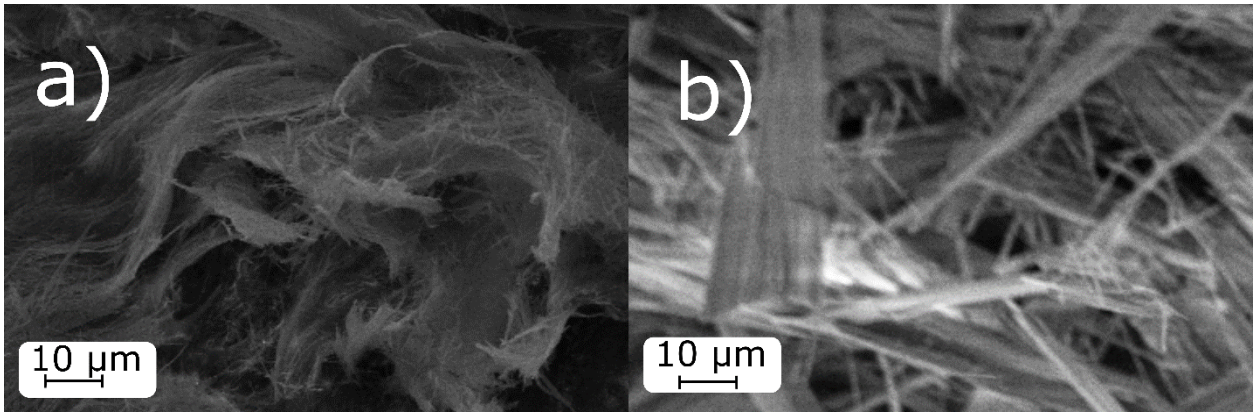


*Figure 56. SEM images of the **Bis6** xerogels extracted from a) toluene, b) cyclohexane.*

Microscopy under polarized light (POM) analysis was performed directly on gel samples of **Bis4, Bis6, Bis8, Bis12** and **Bis18** in toluene. The advantage of POM is that under polarized light only birefringent structures are visible, appearing as white objects. Birefringence is an inherent property of many anisotropic crystals and is caused by structure ordering in a specific direction. In **Bis4** and **Bis6** the fibers appear as sharp needles (Figure 57a and c) and when observed under polarized light, the same fibers are still observable as white bright objects (Figure 57b and d), indicating that the gelator molecules are ordered within the gel fibers. Contrary to **Bis4** and **Bis6**, the gel network of **Bis8**, **Bis12 and Bis18** are presented as a continues aggregation of small fiber that are barely observable under the optical microscope (Figure 57e, g and i). When observed under cross polarized light nothing can be observed indicating that the matter is poorly organized within the fibers of **Bis8**, **Bis12 and Bis18** or that they are too small (Figure 57f, h an j). Therefore, optical and electron microscopies provide a coherent description of the fiber morphology and show that the longer members of the bisamide family form less rigid and less organized fibers than the shorter members of the family.

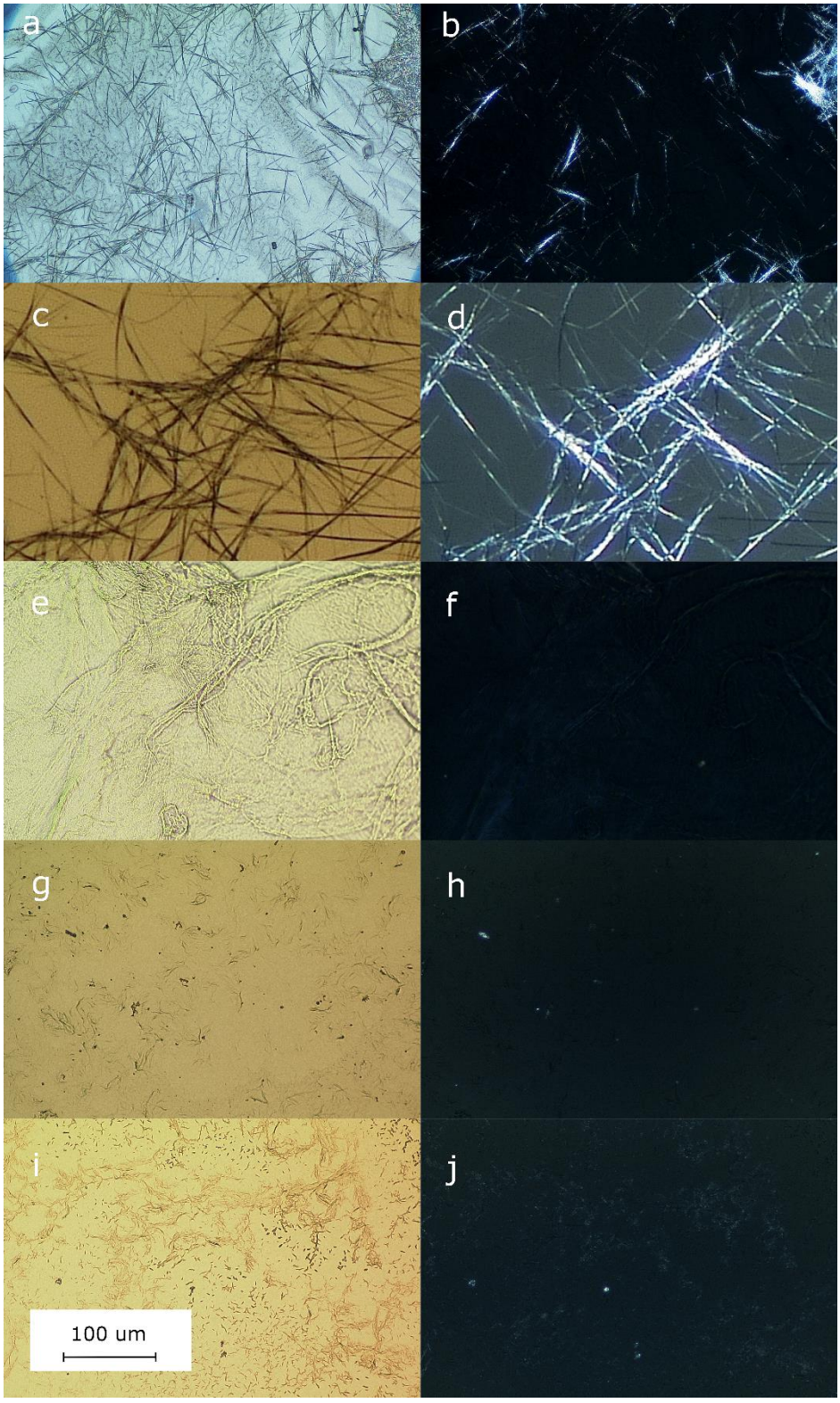


*Figure 57. Optical microscopy images of **Bis4** (a,b) , **Bis6** (c,d), **Bis8** (e,f), **Bis12** (g,h) and **Bis18** (i, j) gels in toluene with (b, d, f, h and j) or without (a ,c, e, g or i) crossed polarizers.*

## 2.6. Molecular packing

The same methodology used to solve the molecular packing of the thiazole based LMWG was applied to the crystalline members of the bisamide based LMWGs (**Bis3, Bis4, Bis5** and **Bis6**). High definition patterns were recorded from xerogels extracted from toluene and used to solve the molecular packing. To address the phenomenon of polymorphism exhibited by this family of LMWG, patterns of the other polymorph of **Bis5** (extracted from MEK) and **Bis6** (extracted from cyclohexane) were also recorded. Figure 58 shows the molecular packing structures that were obtained from the powder patterns, where the structure of **Bis5** polymorph **2** is absent since no acceptable result could be obtained.

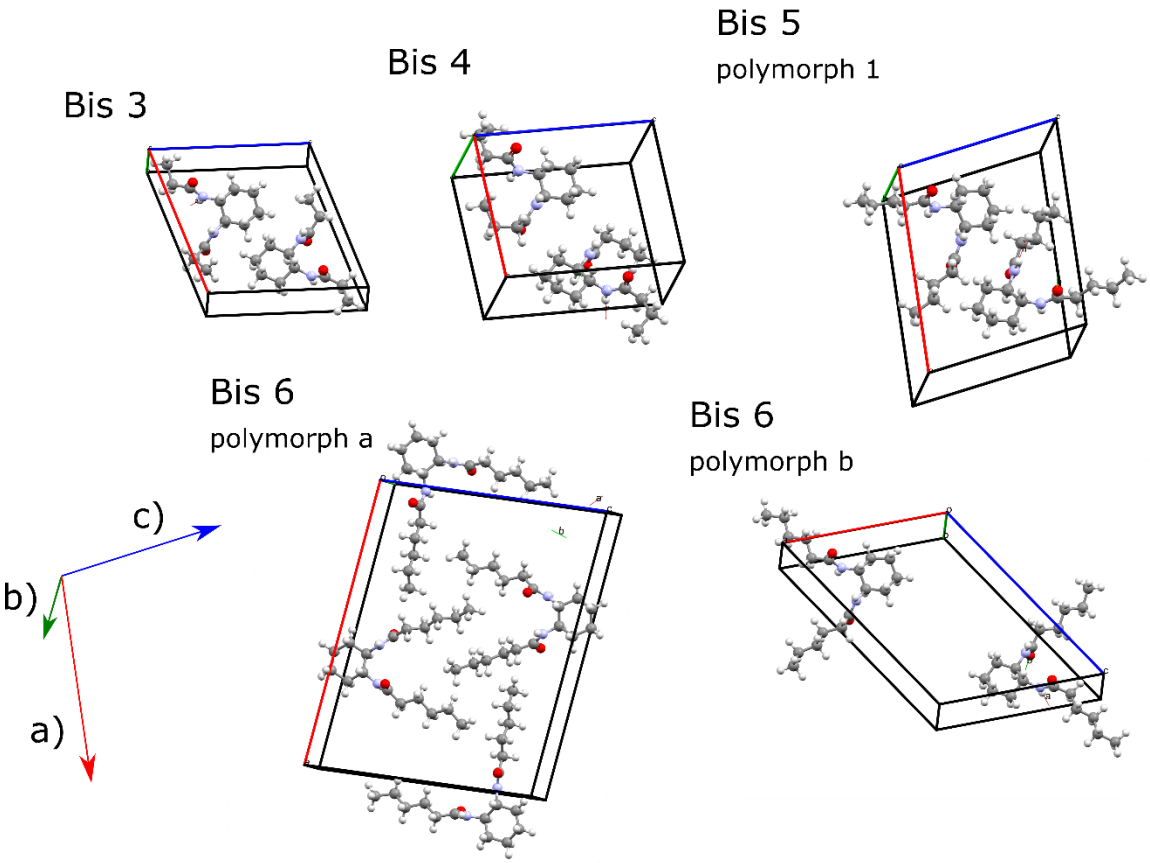


*Figure 58. Molecular packing of bisamide-based LMWG obtained with the methodology described in chapter 1 with cell parameters "a" in red, "b" in green and "c" in blue.*

The detailed structures and fitted XRD patterns are given in table 10 and figures 59, 60, 61, 62 and 63.

Table 10. *Proposed unit cell parameters of the bisamide-based gelators.*

| LMWG | **Bis 3** | **Bis 4** | **Bis 5 .1** | **Bis 6.a** | **Bis 6.b** |
|---|---|---|---|---|---|
| crystal system | monoclinic | monoclinic | monoclinic | monoclinic | monoclinic |
| space group | $P2_1$ | $P2_1$ | $P2_1$ | $P2_1$ | $P2_1$ |
| a(Å) | 12.2840 | 11.9112 | 12.121 | 22.7536 | 13.0200 |
| b(Å) | 4.7957 | 4.8118 | 4.8664 | 4.3677 | 4.8560 |
| c(Å) | 12.0110 | 13.5498 | 15.7359 | 18.3314 | 18.0500 |
| α(deg) | 90 | 90 | 90 | 90 | 90 |
| β(deg) | 108 | 98.3260 | 107.2210 | 96.8210 | 119.5650 |
| γ(deg) | 90 | 90 | 90 | 90 | 90 |
| volume ($Å^3$) | 672.359 | 768.412 | 885.199 | 1808.9 | 992.623 |
| Z | 2 | 2 | 2 | 4 | 2 |
| Density $gcm^{-3}$ | 1.137 | 1.117 | 1.073 | 1.115 | 1.052 |
| formula weight | $C_{12}N_2O_2H_{26}$ | $C_{14}N_2O_2H_{30}$ | $C_{16}N_2O_2H_{34}$ | $C_{18}N_2O_2H_{38}$ | $C_{18}N_2O_2H_{38}$ |
| 2θinterval(deg) | 2-60 | 2-60 | 2-45 | 2-60 | 2-60 |
| step size (deg) | 0.010 | 0.010 | 0.010 | 0.010 | 0.005 |
| counting time(s) | 0.500 | 0.500 | 0.500 | 0.500 | 3 |
| Rp | 24.513 | 23.566 | 16.544 | 9.093 | 21.485 |
| Rwp | 31.463 | 31.640 | 21.593 | 12.875 | 28.697 |
| $X^2$ | 2.923 | 3.112 | 1.868 | 7.271 | 2.169 |

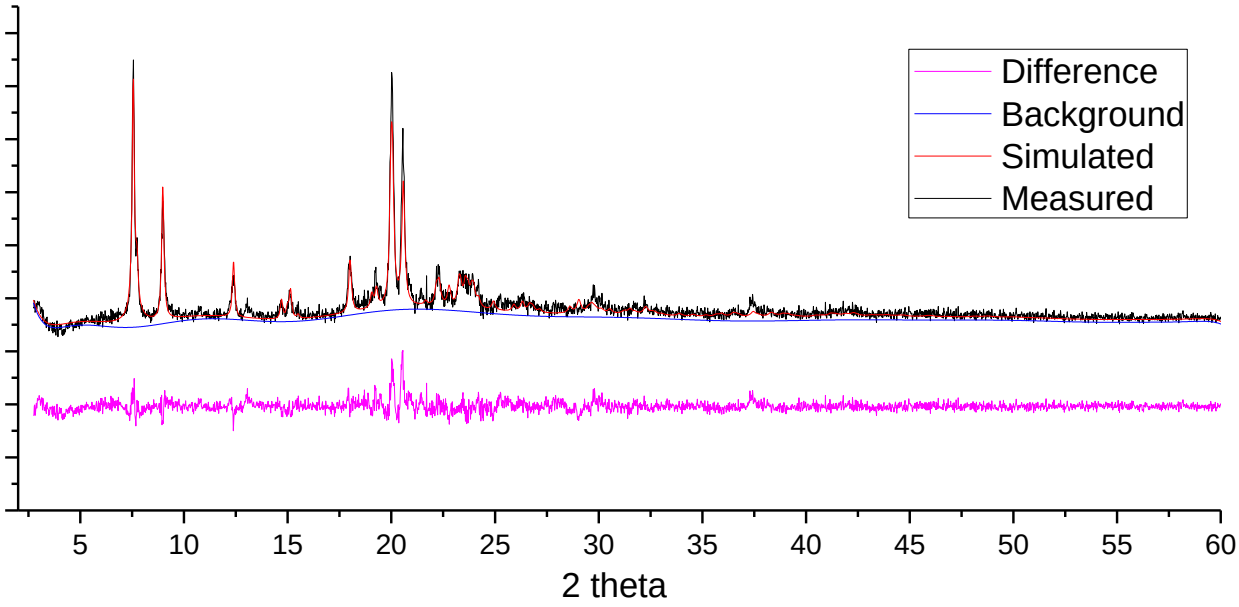


*Figure 59. Comparison between calculated X-ray pattern from simulated structure of* ***Bis3*** *and measured pattern from xerogel extracted from toluene. X-ray wavelength of 1.5406 Å.*

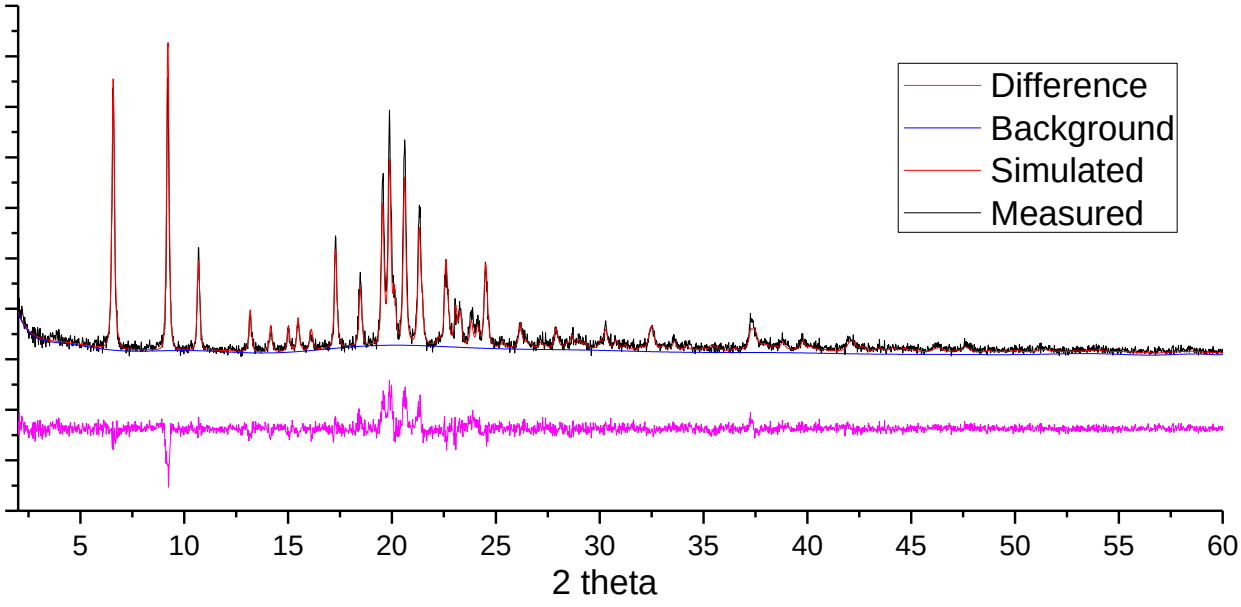


*Figure 60. Comparison between calculated X-ray pattern from simulated structure of* ***Bis4*** *and measured pattern from xerogel extracted from toluene. X-ray wavelength of 1.5406 Å.*

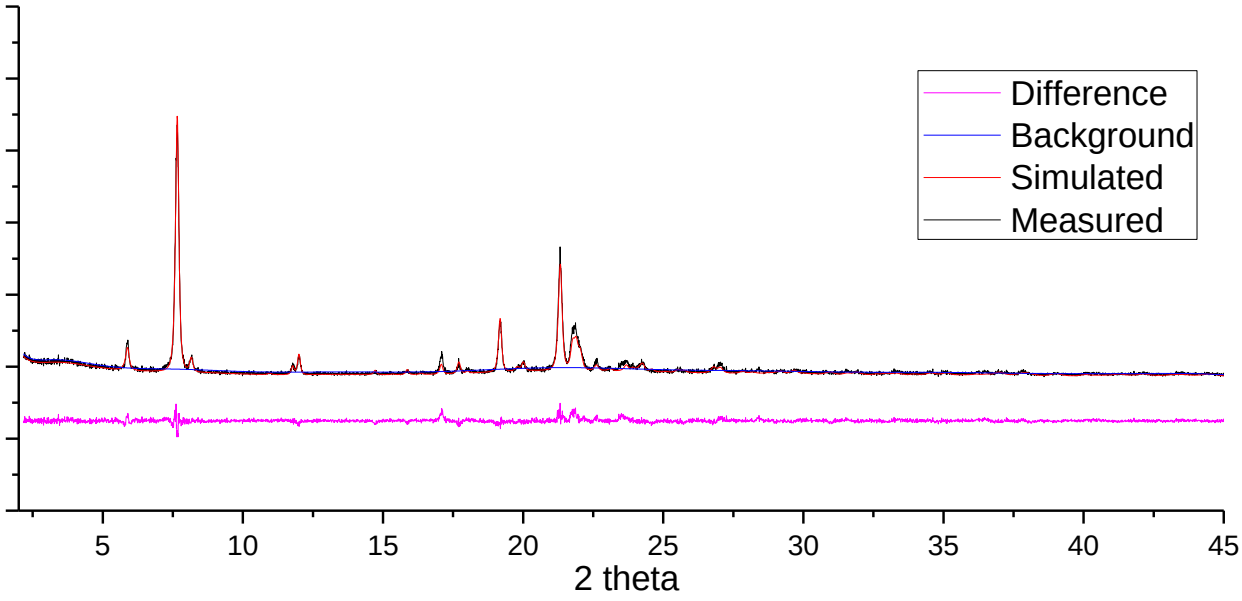


*Figure 61. Comparison between calculated X-ray pattern from simulated structure of* ***Bis5*** *and measured pattern from xerogel extracted from toluene (polymorph* ***1****). X-ray wavelength of 1.5406 Å.*

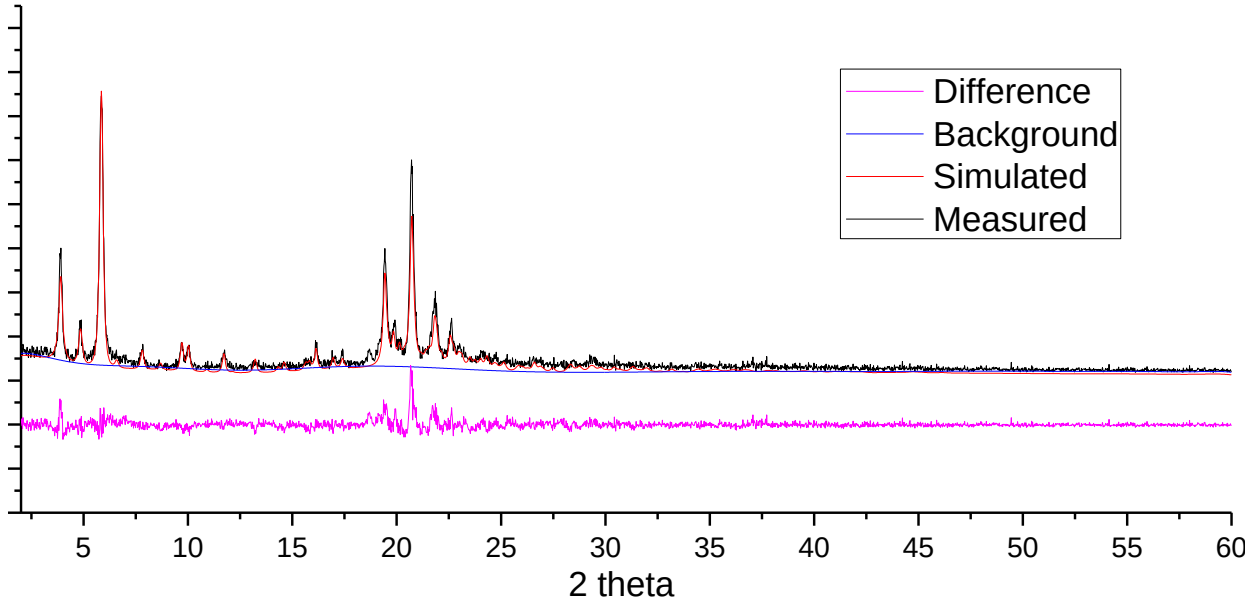


*Figure 62. Comparison between calculated X-ray pattern from simulated structure of* ***Bis6*** *and measured pattern from xerogel extracted from toluene (polymorph* ***a****). X-ray wavelength of 1.5406 Å.*

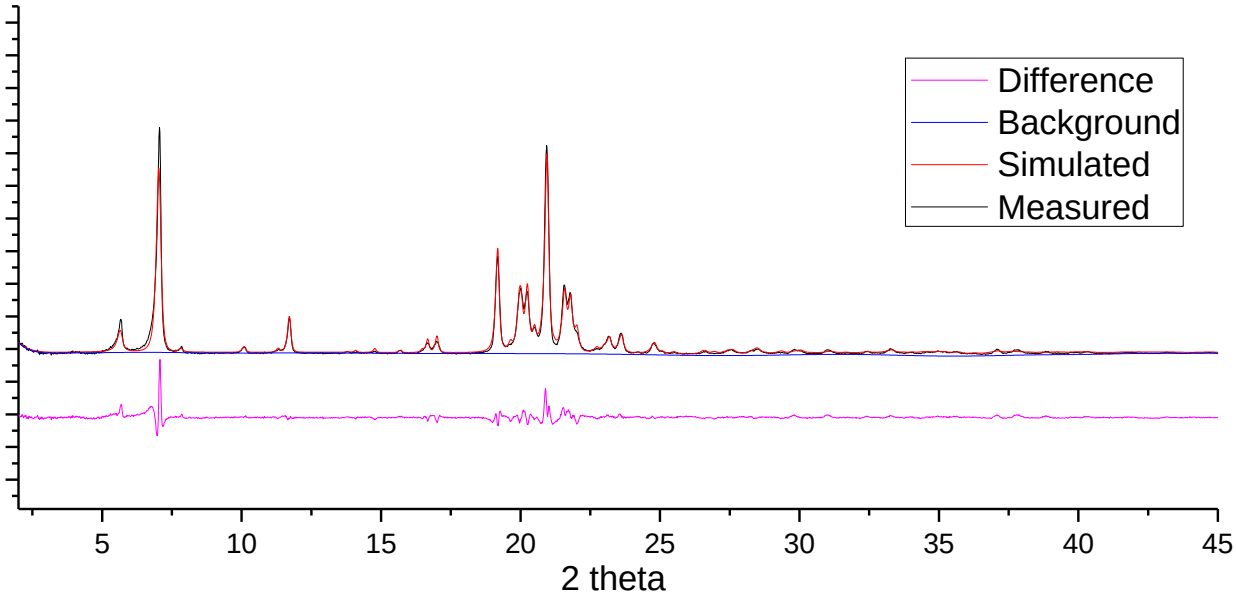


*Figure 63. Comparison between calculated X-ray pattern from simulated structure of* ***Bis6*** *and measured pattern from xerogel extracted from cyclohexane (polymorph* ***b****). X-ray wavelength of 1.5406 Å.*

The methodology was again validated by comparing a simulated structure with an existing crystal

structure for **Bis4**.[5] The measured powder patterns and the simulated powder pattern from the single crystal structure indicate that the molecular packing is virtually the same. In fact, both structures are found similar when overlaid, with cell parameters differing by less than 0.3 Å and 0.1 °, and atoms overlapping almost perfectly (Figure 64).

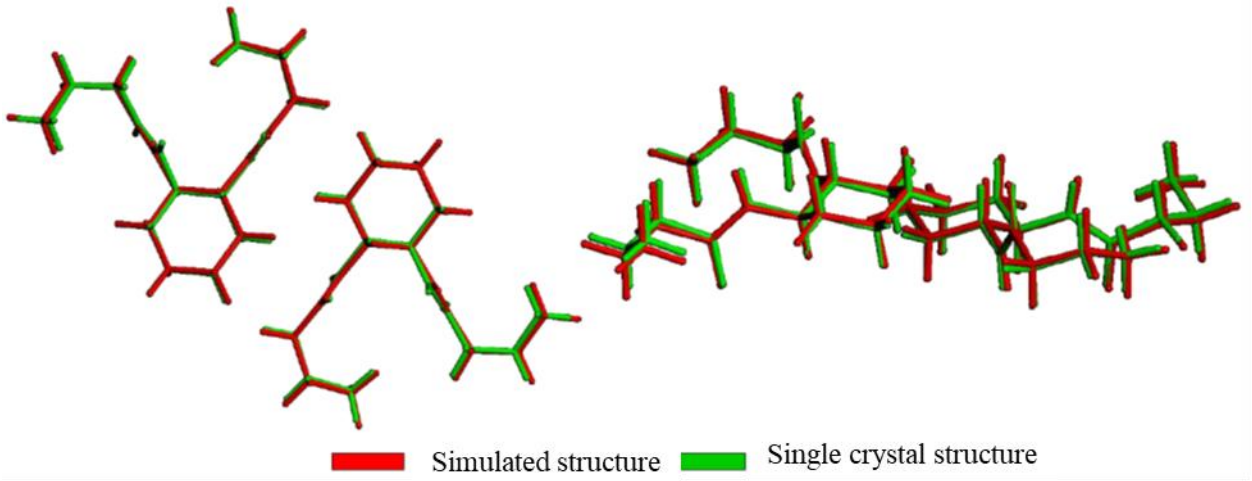


*Figure 64.* ***Bis4*** *modelled structure (red) compared with published*[5] ***Bis4*** *single-crystal molecular packing (green). Root mean square value of 0.1Å.*

All LMWGs presented monoclinic unit cells with a $P2_1$ symmetry group (Figure 58). Parameter c increases with the increase of the alkyl chain while parameters a and b maintain a similar value in all bisamide based LMWG (excluding **Bis6.a** whose unit cell contains twice as many molecules) (Table 10). Although the exact packing of these LMWG differ, they are all characterized by hydrogen bonding between the amide groups, forming a column of molecules along the b axis (Figure 65). All observed hydrogen bonding is intermolecular and with a very similar conformation. The hydrogen bonding between molecules in a single direction is commonly observed in the self-assembly of an organogelator.[7–9]This strong non-covalent interaction is probably responsible for the self-assembly of this LMWG into fibers, since the hydrogen bonding promotes a faster crystallization along the b axis.

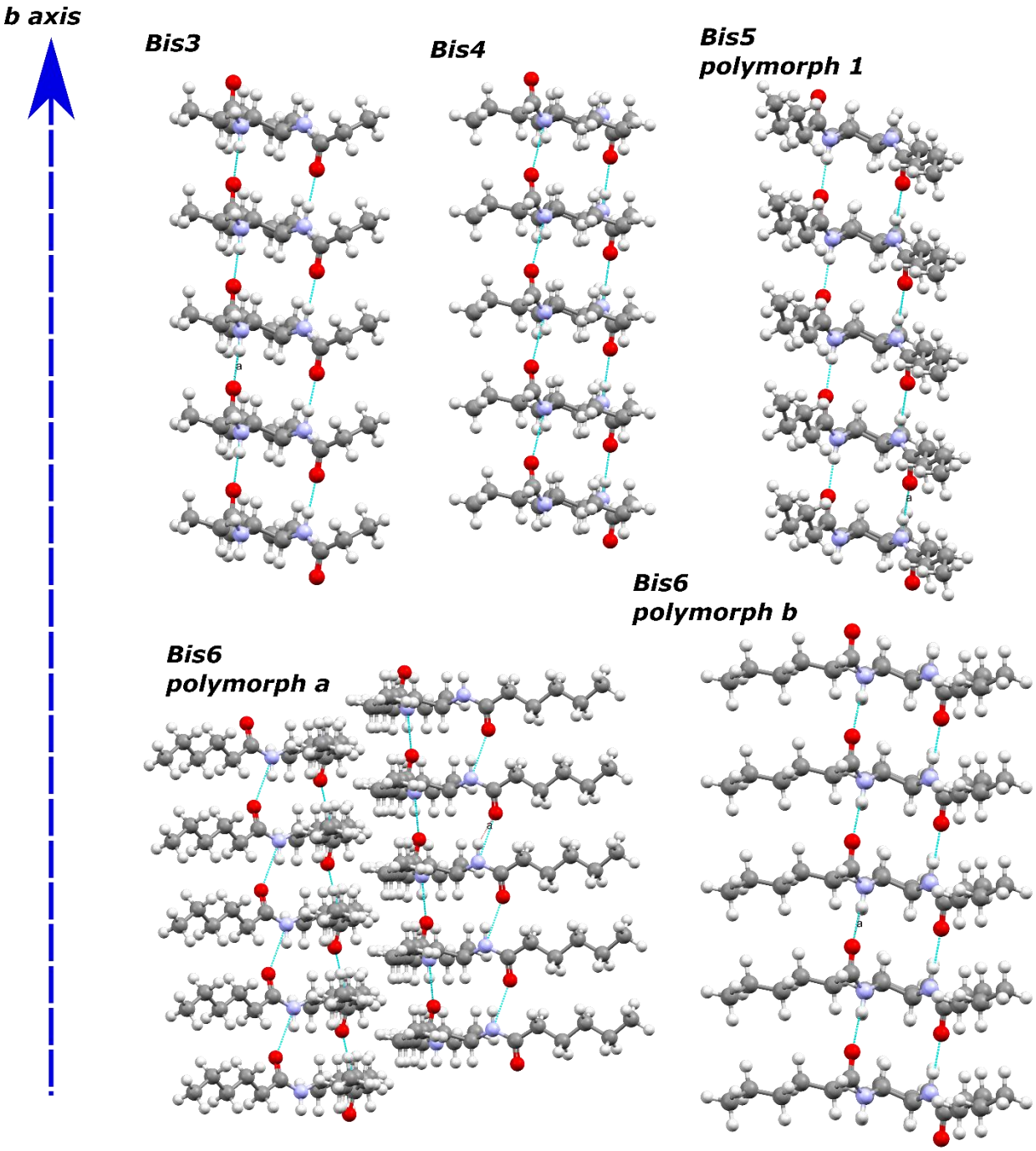


*Figure 65. Molecular packing of bisamide-based gelators. Same data as figure 64 but showing the hydrogen bonding pattern along b axis.*

Even in the case of **Bis6** polymorphs all molecules present similar conformations. Figure 66 presents

both molecules of **Bis6 polymorph a** present in the asymmetric unit and the single molecule of **Bis 6 polymorph b** present in the asymmetric unit overlapped for comparison.

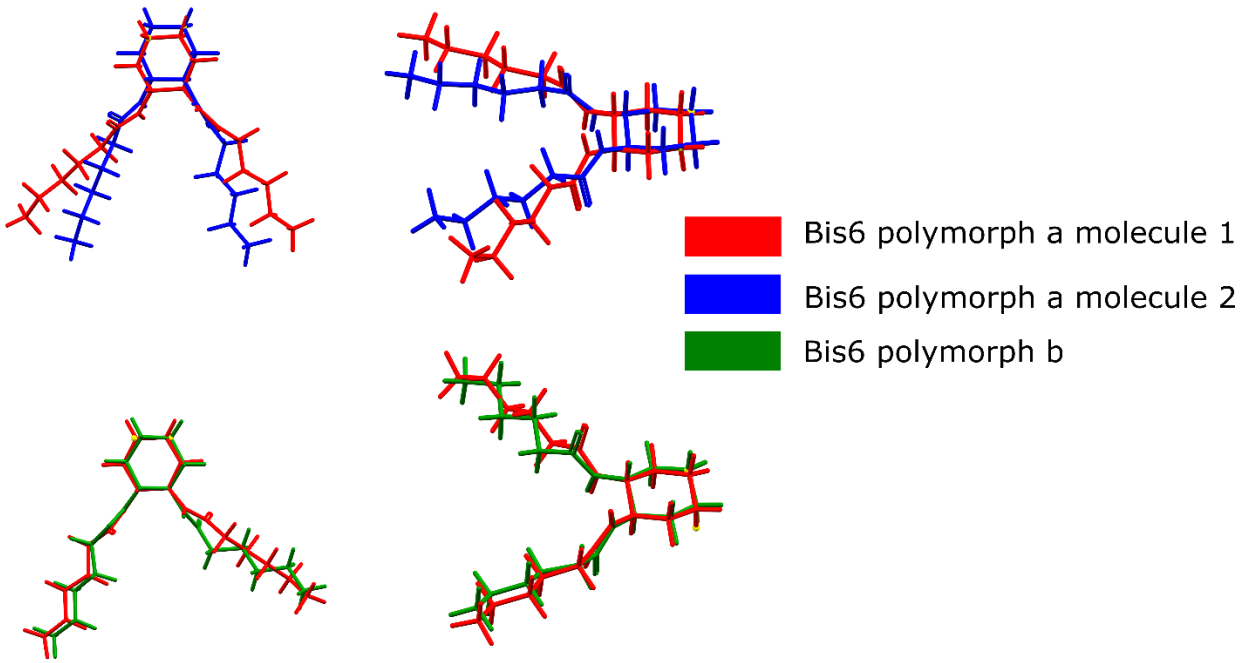


*Figure 66. All conformations of **Bis6** overlapped.*

## 2.7. Conclusion for the bisamide based gelators

The center of the gelation spheres drifts linearly to lower $\delta_P$ and $\delta_H$ values in the Hansen space with the elongation of the alkyl chains, as seen with the thiazole-based gelators. However, the increase in length of the alkyl chains of the bisamide-based gelators resulted in a complex evolution of the molecular packing within gel fibers. At small alkyl chain lengths (**Bis5** and **Bis6**) the molecular packing within gel fibers is well organized but present polymorphism among the different liquids. At higher alkyl chain lengths (**Bis8**, **Bis12**, **Bis14**, **Bis16** and **Bis18**) the molecular packing within gel fiber loses long range periodicity. Despite this complex behavior in the molecular packing we observed that the local molecular conformation remains similar throughout all gelators with different alkyl chains lengths. Therefore, the gradual shift of the center of the gelation spheres is possibly a result of a decrease in polarity of the surface of the gel fibers caused by the increase of the length of the alkyl chains. In other words, even if the crystal packing is not identical within this family, it is possible that the crystal habit and thus the composition of the facets of the fibers evolve gradually with the length of the alkyl chain.

# 3. General remarks

We studied the effect of elongating alkyl chains on the gelation of the thiazole and bisamide-based gelators. For both families, the increase of the linear alkyl chains results in the preferential gelation of less polar liquids. The shift in polarity occurs in a linear way in Hansen space, thus allowing a straightforward prediction for other members of these families. Organogelation certainly depends on the interaction between the surface of a gel fiber and the liquid, so, for a structural alteration in a gelator molecule to have an effect in the gelation properties, this alteration needs to present a shift in the composition of the surface of the fiber. It was also observed that the molecular packing within gels fibers remained constant for the thiazole family and quite similar in the case of the bisamide family. To establish the link between the molecular packing and the crystal habit, further molecular simulation studies are required, but we can assume that when the alkyl chains of a gelator are increased, the exposition of alkyl chains at the surface of the fiber evolves in proportion. If this is the case, the increase of the length of the alkyl chains leads to a decrease in polarity of the surface of the gel fibers which leads to a drift of the center of the gelation domain to a lower polarity zone in the Hansen space.

# 4. References and notes


1 P. Yadav, D. Kour, V. K. Gupta, Rajnikant and A. Ballabh, *RSC Adv.*, 2013, **3**, 8417–8421.

2 P. Yadav and A. Ballabh, *New J. Chem.*, 2015, **39**, 721–730.

3 C. M. Hansen, Hansen solubility parameters A User's Handbook Second Edition, 2007.

4 S. Abbott and C. M. Hansen, Hansen Solubility Parameters in Practice, 2008.

5 N. Zweep, A. Hopkinson, A. Meetsma, W. R. Browne, B. L. Feringa and J. H. Van Esch, *Langmuir*, 2009, **25**, 8802–8809.

6 Bis6 was briefly mentioned in chapter 2, and the fact that polymorphs do not cluster in the Hansen space was an indication for the formation of a single gelation sphere instead of a model with multiple spheres.

7 D. J. Abdallah and R. G. Weiss, *Adv. Mater.*, 2000, **12**, 1237–1247.

8 P. Terech and R. G. Weiss, *Chem. Rev.*, 1997, **97**, 3133–3160.

9 M. George and R. G. Weiss, *Acc. Chem. Res.*, 2006, **39**, 489–497.

# 11. Chapter 4

# 12. Limited influence of the gelator structure on the gelation sphere

After identifying one type of gelation behavior we continued studying different families of organogelators with different molecular structures. This chapter will describe a different gelation behavior observed when increasing the length of linear alkyl chains.

# 1. *Cis*-1,3,5-cyclohexanetricarboxamide based gelators

Self-assembly of cyclohexane tricarboxylic acids derivatives (CTA) has been widely studied.[1-8] Hirofusa Shirai et al.[9] discovered that trialkyl *cis*-1,3,5-cyclohexanetricarboxamides were able to gelate organic solvents. Within this group of LMWG, the main force that drives self-assembly is the intermolecular hydrogen bonding from each of the three amide functional groups. To study the effect of the length of the alkyl chain in the Hansen space we prepared four members of this group of LMWGs with alkyl chains ranging from 11 $CH_2$ (**Tris12**) to 17 $CH_2$ (**Tris18**). (Figure 67)

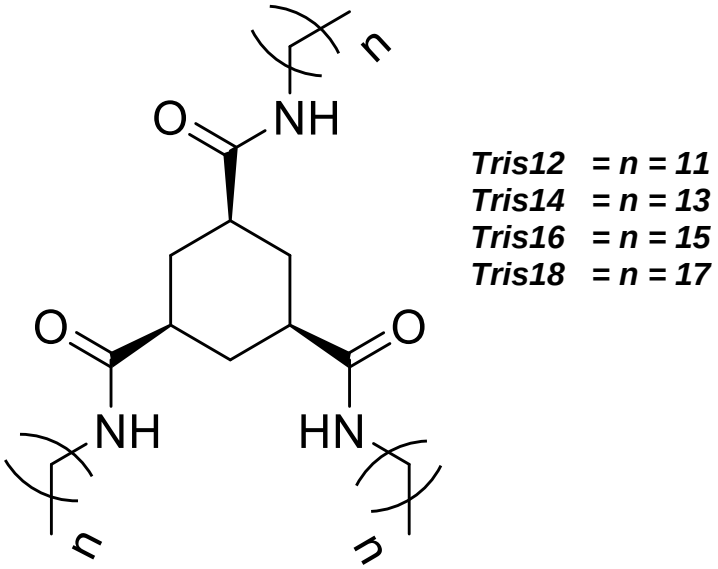


*Figure 67. Chemical structures of the trialkyl cis-1,3,5-cyclohexanetricarboxamide gelators studied in this chapter.*

## 1.1. Hansen space of trialkyl *cis*-1,3,5-cyclohexanetri-carboxamides

In the original work of Hirofusa Shirai et al.[9] where this group of LMWG was first reported, the solubility table showed that the minimum gelation concentration of these gelators is on average below 1 wt %, positioning this group of LMWG in the class of super-organogelators. Based on Shirai's work, the concentration of 1wt% was chosen to characterize their Hansen space.

The gelation domains were determined using the methodology explained in chapter 2. For each liquid tested the desired amount of LMWG and 1 mL of liquid were added to a screw-cap vial. The suspensions were heated up to 120° C until dissolution and left to cool to room temperature on the

bench. After 24 hours the vials were turned upside-down, and the aspect of the samples was noted as gel (G) or precipitate (P). In this group of LMWG very few liquids solubilized the gelator at room temperature. Figure 68 illustrates the Hansen space with the calculated gelation domains of all trisamide-based gelators and Figure 69 illustrates a comparison of the radius and centers of all gelation domains.

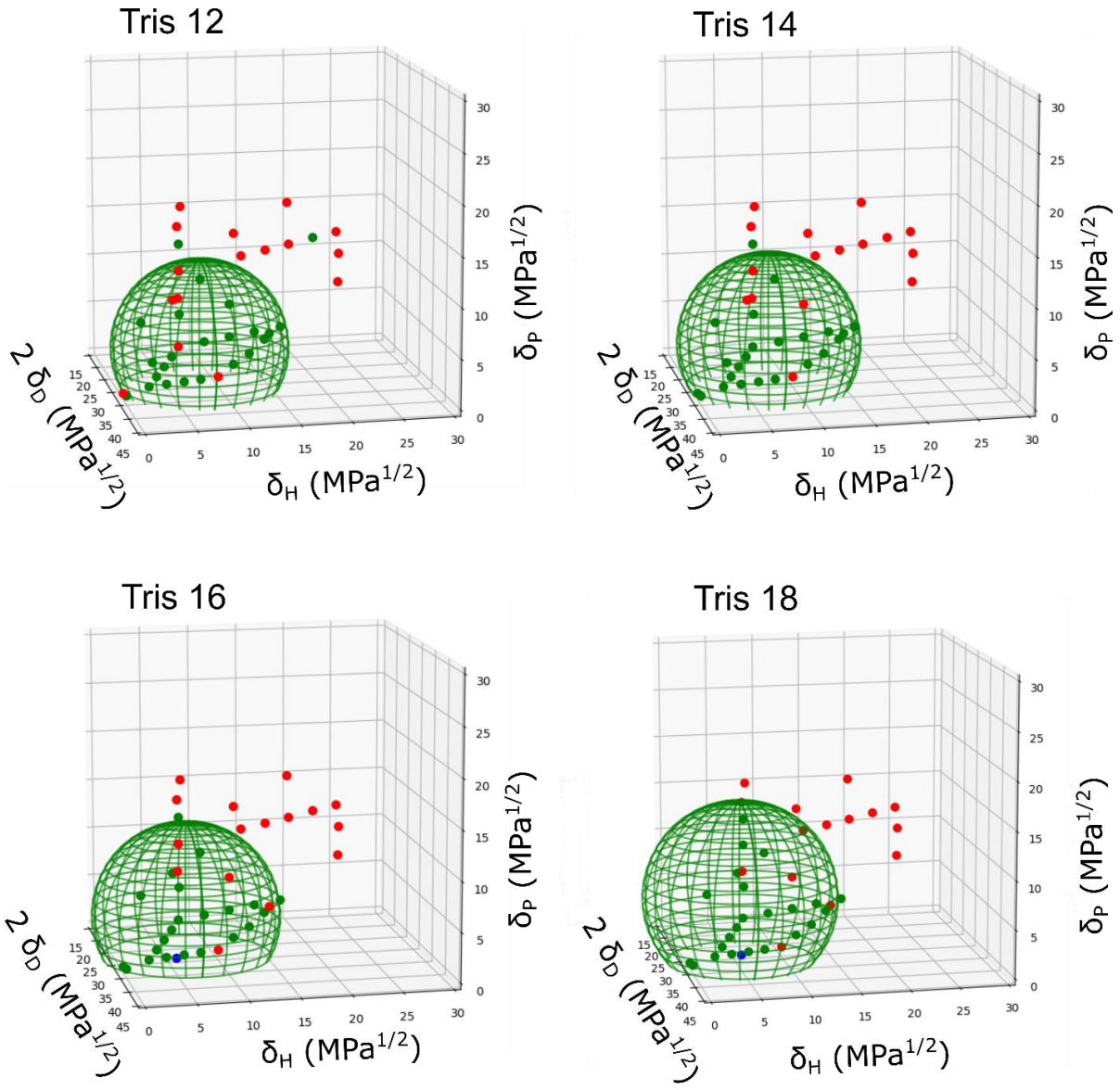


*Figure 68. Gelation data plotted in Hansen space for the trisamide gelators at 1 wt%. The tested liquids are represented by full circles and the calculated domains are represented by meshed spheres. Green: gel; red: precipitate; blue: soluble.*

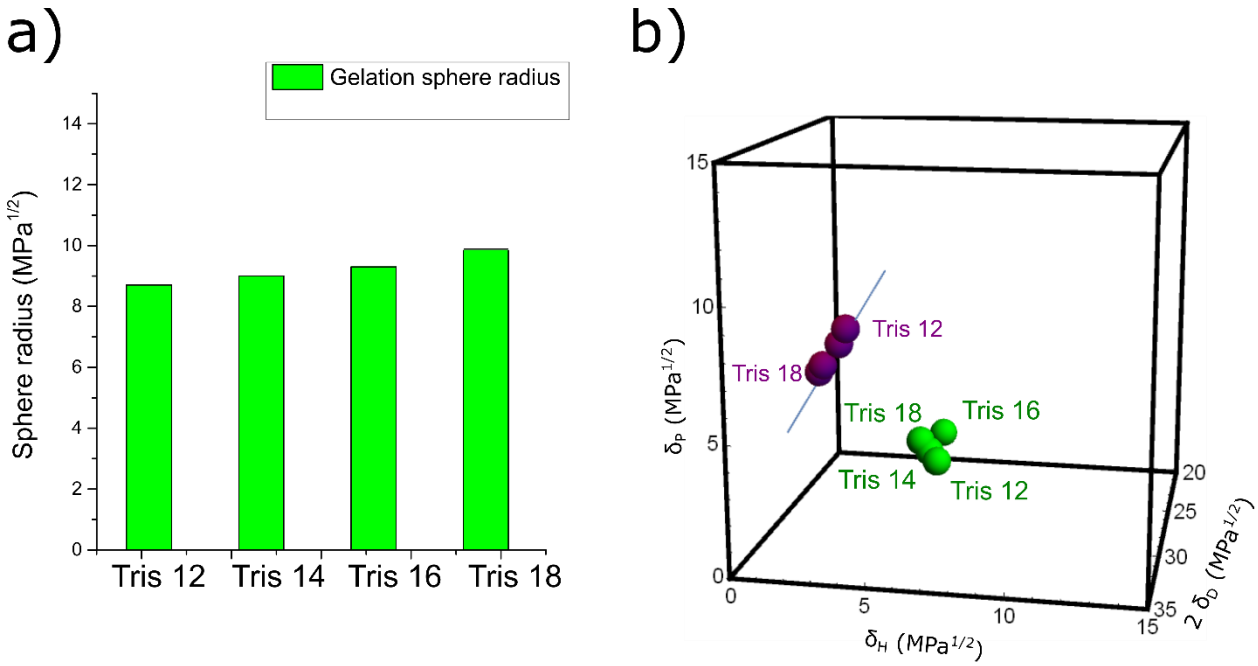


*Figure 69. a) Radius of the gelation (green) spheres for the trisamide gelators. b) Center of the gelation spheres (green) represented in Hansen space and simulated HSP parameters of each trisamide-based gelator (purple).*

*Table 11. Coordinates of the center and radius of the Hansen gelation sphere for trisamide gelators at 1wt % and theoretical values for the solubility of the same molecules.*

| | Gelation sphere | | | | theoretical solubility sphere | | |
|---|---|---|---|---|---|---|---|
| LMWG | $\delta_D$ ($MPa^{1/2}$) | $\delta_P$ ($MPa^{1/2}$) | $\delta_H$ ($MPa^{1/2}$) | r ($MPa^{1/2}$) | $\delta_D$ ($MPa^{1/2}$) | $\delta_P$ ($MPa^{1/2}$) | $\delta_H$ ($MPa^{1/2}$) |
| **Tris12** | 17.0±1.0 | 4.6±0.2 | 7.4±0.4 | 8.7±0.3 | 17.2 | 9.3 | 4.3 |
| **Tris14** | 16.8±0.4 | 4.8±0.5 | 7.1±0.6 | 9.0±0.4 | 17.1 | 8.7 | 4.0 |
| **Tris16** | 15.3±1.3 | 4.3±0.9 | 6.7±0.7 | 9.3±1.2 | 17.1 | 7.9 | 3.4 |
| **Tris18** | 16.8±2.2 | 5.1±0.5 | 6.7±1.2 | 9.9±1.2 | 17.0 | 7.6 | 3.2 |

Since this group of LMWG did not present enough soluble (blue) points to form solubility spheres the only alternative is to compare the trend of the center of the gelation spheres with the theoretical HSP values simulated with the HSPiP software. These simulated values are presented in purple in figure 69.

The trend of the theoretical values of HSP yields the following vector equation (where t is the number of carbons in each alkyl chain):

Eq 15 : $[\delta_D, \delta_P, \delta_H] = [17.8, 14.1, 7.5] + t\ [-0.05, -0.36, -0.23]$

The increase in length of the alkyl chains resulted in a drift of the theoretical HSP values of trisamide-based gelators to an area of lower polarity as observed in the previous families of gelators. Adding a $CH_2$ to each alkyl chain reduced the HSP values by $\delta_D = 0.05$ $MPa^{1/2}$, $\delta_P = 0.36$ $MPa^{1/2}$ and $\delta_H = 0.23$ $MPa^{1/2}$.

Curiously, the increase in length of the alkyl chains of the trisamide-based gelators only has a minor effect on the radius and center of the gelation sphere. The radius of the gelation spheres presented a limited increase from **Tris12** ($r = 8.7$ $MPa^{1/2}$) to **Tris18** ($r = 9.9$ $MPa^{1/2}$), and all the centers of the gelation spheres presented similar HSP values. This is confirmed by the standard deviations (Figure 70 and Table 11). Thus, with the obtained center of gelation spheres it was not possible to deduce a linear trend. Given the HSP uncertainties, we can conclude that all gelation spheres have approximately the same center.

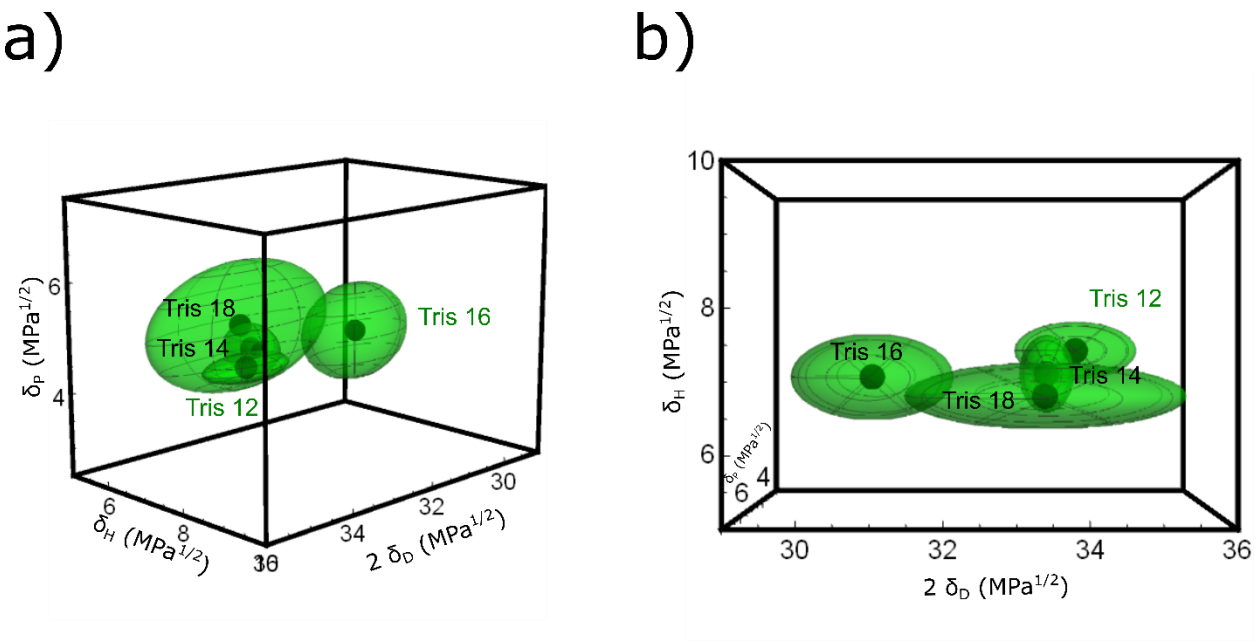


*Figure 70. Center of the gelation spheres (dark green) and the standard deviation (meshed green ellipse) represented in Hansen space. a) lateral view, b) top view.*

## 1.2. Structural analysis

X-ray measurements of trisamide xerogels extracted from toluene (Figure 71) all showed X-ray patterns with broad diffraction peaks until approximately 24º and set of sharp peaks from 24º to 33º. These fine peaks are due to an unknown inorganic impurity present in a quantity of about 10 wt% (see annex). We assume its presence does not affect the gelation results and molecular packing.

.

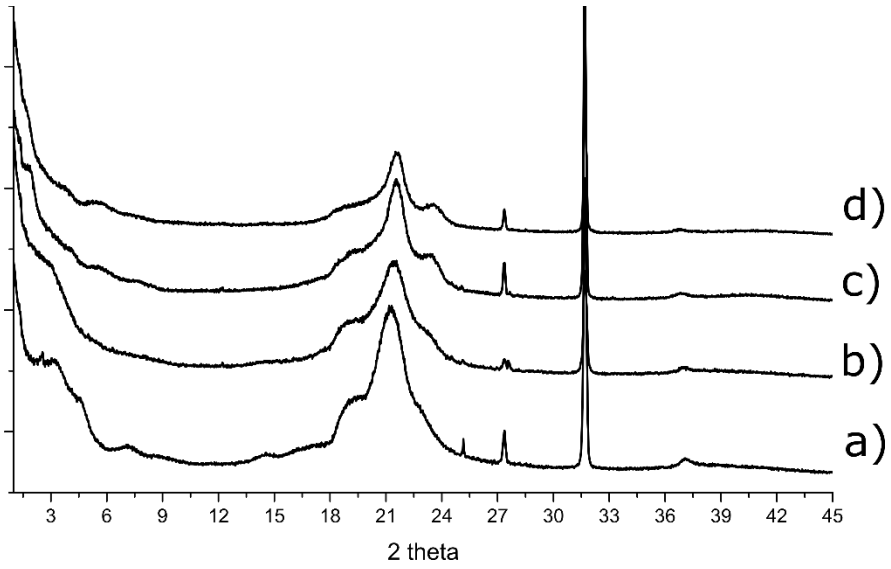

*Figure 71. X-ray patterns of trisamide based gelators extracted form toluene. a)* ***Tris12****, b)* ***Tris14****, c)* ***Tris16*** *and d)* ***Tris18****. X-ray wavelength of 1.5406 Å.*

After exclusion of the fine diffraction peaks, the remaining X-ray patterns do not provide enough information to apply the methodology explained in chapter one, and it is not possible to extract much information. However, very few differences can be observed between the different patterns a high angle, (between 14° and 25° in 2θ) which indicates similar structures. The differences observed at low angles can be attributed to the difference in size of the objects formed after self-assembly (i.e. fiber cross-section). As the alkyl chains increase in length the signal at low angles shifts to smaller 2 θ values indicating thicker objects.

According to Albuquerque et al.[10] trialkyl *cis*-1,3,5-cyclohexanetricarboxamides assemble in columns with all three carbonyl groups pointing to the same direction to form hydrogen bonding (model 3:0) or with two of the carbonyls pointing to the same direction and the third one pointing to the opposite direction (model 2:1). To correlate locally the structure to the X-ray patterns, models 3:0 and 2:1 were built using computational modelling and the structures were optimized using a DFT software package. Both models were built and fitted in a tetragonal unit cell with a and b parameters equal to 30Å and parameter c equal to 5 Å, with symmetry group *P1*. The unit cell values were chosen to roughly fit the structure. After building the model, we used the periodic DFT software package Quantum espresso to optimize the cell unit and atomic position. The optimization was carried using the VC-relax function until convergence was reached. Figure 72 illustrates the packing obtained after optimization.

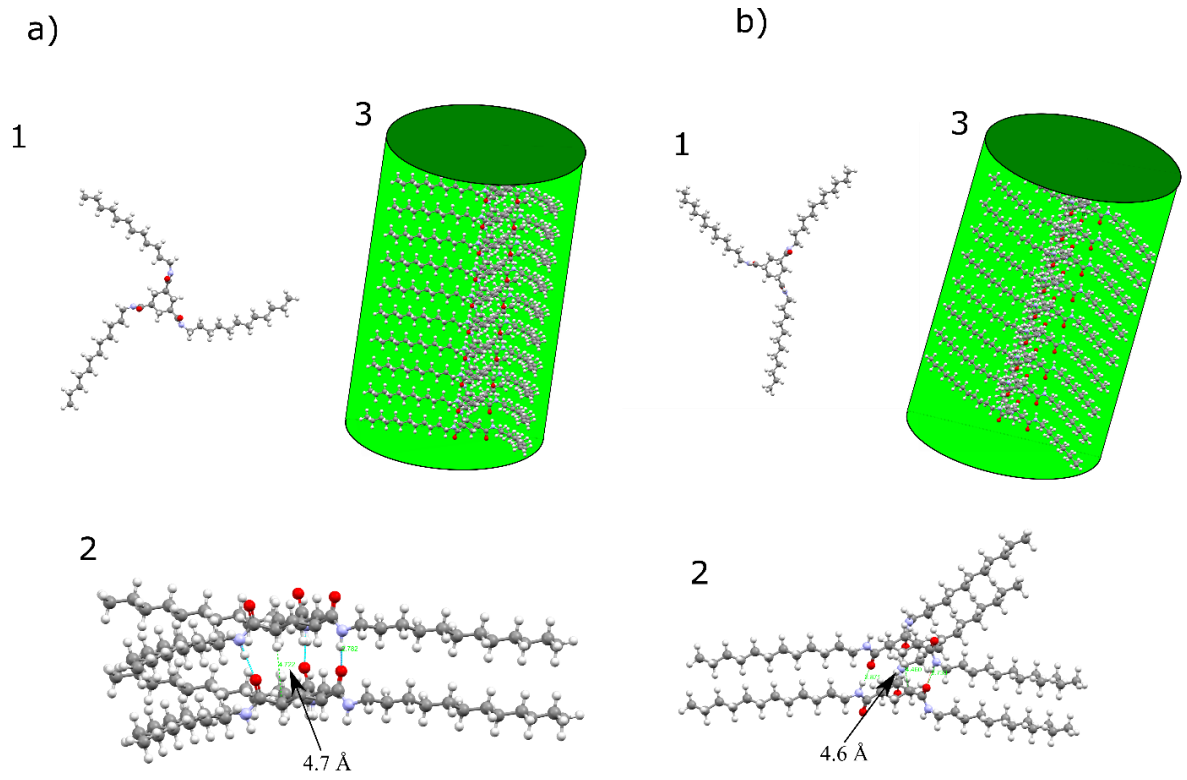


*Figure 72. Representation of a) model 3:0 and b) model 2:1. 1) represents a single molecule of* ***Tris12****, 2) represents a set of 2 gelator molecules with the distance between the cyclohexane highlighted and 3) represents a column that results from the self-assembly of these gelators.*

The optimized models showed an inter-cyclohexane distance of 4.7Å in the 3:0 model and 4.6Å in the 2:1 model. These distances correspond roughly to the peak at 19° in the X-ray powder patterns present in Figure 71.

Infrared spectroscopy performed in trisamide-based xerogels extracted from toluene (Figure 73) provided further proof of hydrogen bonding between gelators. All xerogels present a similar spectrum with a single observed frequency observed for N-H (3290 $cm^{-1}$) and C=O (1640 $cm^{-1}$) which are in agreement with the results demonstrated by Shirai et al.[9] and can be assigned to hydrogen bonded amides.

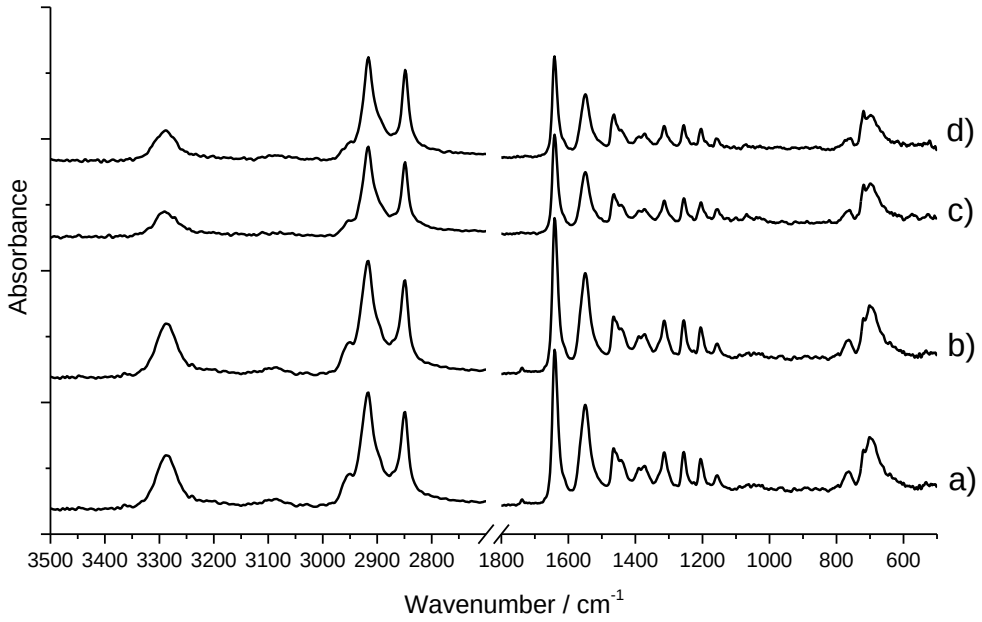


*Figure 73. Infrared absorbance spectrum of trisamide-based xerogel extracted from toluene. a)* ***Tris12****, b)****Tris14****, c)****Tris16*** *and d)****Tris18****.*

Coming back to the X-ray results, the broad peak observed at 22° (4.0 Å) (Figure 70) can be attributed to the presence of poorly organized alkyl chains.

Despite the X-ray patterns not presenting enough definition to apply the methodologies described in chapter 1, the modeled structures match the main diffraction peaks at high angles present in the xerogels powder patterns indicating that the trialkyl *cis*-1,3,5-cyclohexanetricarboxamides gelators most probably self-assemble in either models 3:0 and 2:1 or their mixture.

# 2. Correlations of gelation and structural data for the trisamide based gelators

Increasing the length of all three linear alkyl chains of the trisamide-based gelator did not present a significant effect in their gelation domains. Despite not being able to propose an exact model that would fit the X-ray data, the symmetrical nature of the gelator molecules coupled with three amide functional groups responsible for strong hydrogen bonding, makes for an easy rationalization of the possible molecular packing of this gelator. Hydrogen bonding is the strongest non-covalent interaction possible for these molecules thus it is most probably the driving force for the formation of the gel fibers. Small variations of the orientation of the amide groups are possible, but the hydrogen bonding is always preserved. Therefore, whatever the exact packing of this family of gelators the

sides of the fibers are covered by alkyl chains only (probably disordered) and their elongation is not expected to affect significantly the composition of the surface of the fibers. As a consequence, the length of the alkyl chains should not influence the interactions with the surrounding liquid. This might explain the lack of evolution of the gelation domain.

# 3. References


1 M. de Loos, J. H. van Esch, R. M. Kellogg and B. L. Feringa, Tetrahedron, 2007, 63, 7285–7301.

2 R. Q. Albuquerque, A. Timme, R. Kress, J. Senker and H.-W. Schmidt, Chem. - A Eur. J., 2013, 19, 1647–1657.

3 Y. Zhou, M. Xu, J. Wu, T. Yi, J. Han, S. Xiao, F. Li and C. Huang, J. Phys. Org. Chem., 2008, 21, 338–343.

4 A. Brizard, M. Stuart, K. van Bommel, A. Friggeri, M. de Jong and J. van Esch, Angew. Chemie Int. Ed., 2008, 47, 2063–2066.

5 E. Fan, J. Yang, S. J. Geib, T. C. Stoner, M. D. Hopkins and A. D. Hamilton, J. Chem. Soc. Chem. Commun., 1995, 1251.

6 M. Seitz, C. K. Park, J. Y. Wong and J. N. Israelachvili, Langmuir, 2001, 17, 4616–4626.

7 F. Versluis, D. M. van Elsland, S. Mytnyk, D. L. Perrier, F. Trausel, J. M. Poolman, C. Maity, V. A. A. le Sage, S. I. van Kasteren, J. H. van Esch and R. Eelkema, J. Am. Chem. Soc., 2016, 138, 8670–8673.

8 A. Timme, R. Kress, R. Q. Albuquerque and H. W. Schmidt, Chem. - A Eur. J., 2012, 18, 8329–8339.

9 K. Hanabusa, A. Kawakami, M. Kimura and H. Shirai, *Chem. Lett.*, 1997, **26**, 191–192.

10 M. Pereira Oliveira, H. W. Schmidt and R. Queiroz Albuquerque, *Chem. - A Eur. J.*, 2018, **24**, 2524.

# 13. Chapter 5

# 14. Complex relationship between gelator structure and gelation sphere

This chapter presents a different gelation behavior, resulting from the variation in the length of a linear alkyl chain in an organogelator. The two families of LMWG reported in this chapter contrary to the gelators described in the previous chapters, present a complex movement of the center of the gelation spheres in the Hansen sphere with the increase in length of linear alkyl chains. With the aim of understanding why some families of LMWG behave differently when subjected to the same structural alteration, we performed microscopy analysis and X-ray scattering characterization to study the gel morphology and molecular packing within fibers.

## 1. Dialkyl hydrazide based gelators

The LMWG family of dialkyl hydrazide based gelators has been previously reported in the literature by Handa et al.[1] In this original study, Handa studied the effect that a linear carbon bridge with variable length between two amides has on the gelation proprieties. It was observed that an odd or even number of carbons in the linear bridge was shown to alter the gel-sol transition temperature and fiber morphology. Among these systems, we selected a gelator with no carbon bridge and varied the length of the external alkyl chains. We synthesized six members of the dialkyl hydrazide gelators (Figure 74) with alkyl chain ranging from 7 $CH_2$ (**Hydra8**) to 17 $CH_2$ (**Hydra18**).

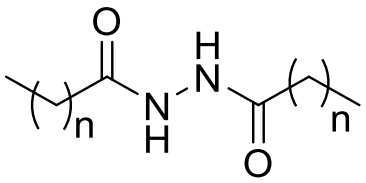


*Hydra 8 = n = 7*
*Hydra 10 = n = 9*
*Hydra 12 = n = 11*
*Hydra 14 = n = 13*
*Hydra 16 = n = 15*
*Hydra 18 = n = 17*

*Figure 74. Chemical structure of the dialkyl hydrazide based LMWGs*

## 1.1. Hansen space of dialkyl hydrazide based gelators

Based on the gelation data provided by Handa et al.[1] all gelation tests on this family of LMWG were performed at 3 wt%. The gelation domains were determined using the methodology explained in chapter 2. For each liquid tested 30 mg of LMWG and 1 mL of liquid were added to a screw-cap vial. The suspensions were heated up to 120°C until dissolution and left to cool to room temperature on the bench. After 24 hours the vials were turned upside-down, and the aspect of the samples was noted. Figure 75 illustrates the Hansen space with the calculated gelation domains of all hydrazide based gelators and figure 76 presents the extracted radius and center of the calculated gelation domains.

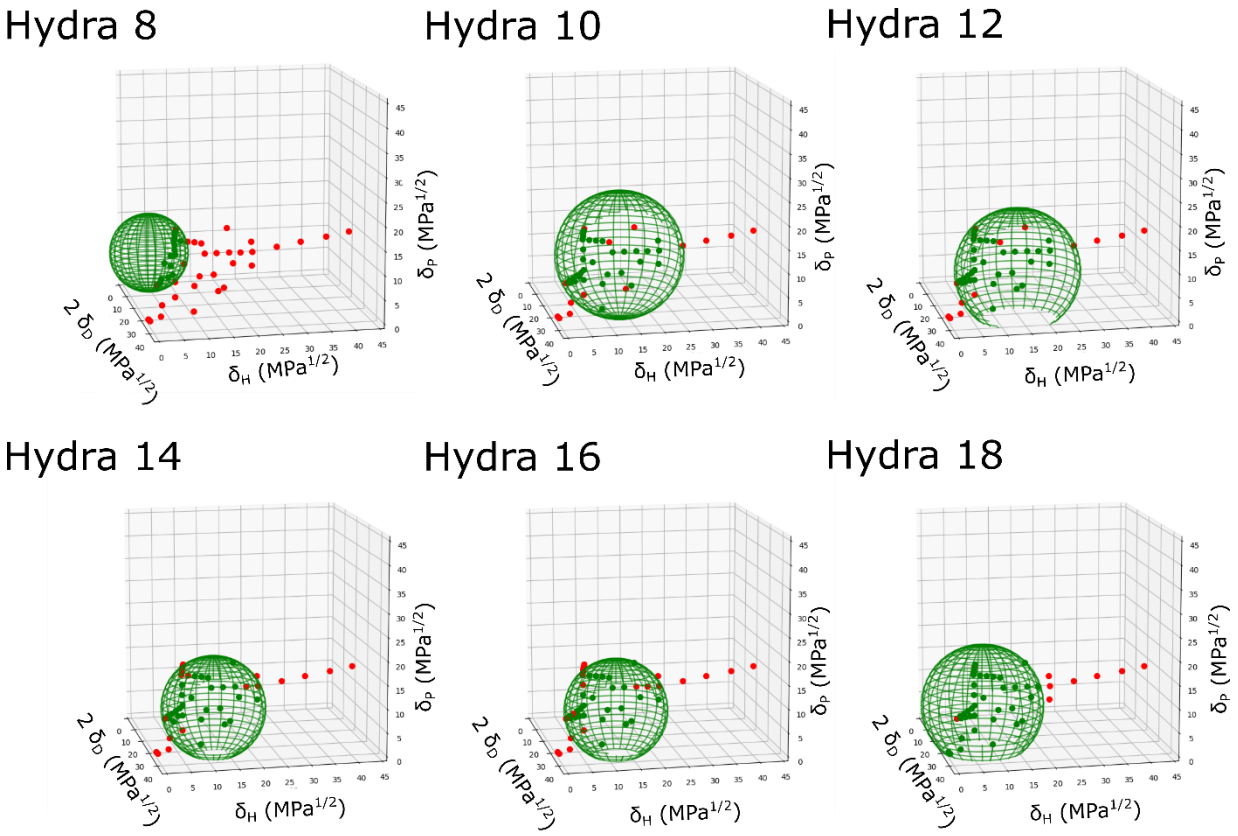


*Figure 75. Gelation data plotted in Hansen space for the hydrazide based LMWGs at 3 wt%. The tested liquids are represented by full circles and the calculated domains are represented by meshed spheres. Green: gel; red: precipitate.*

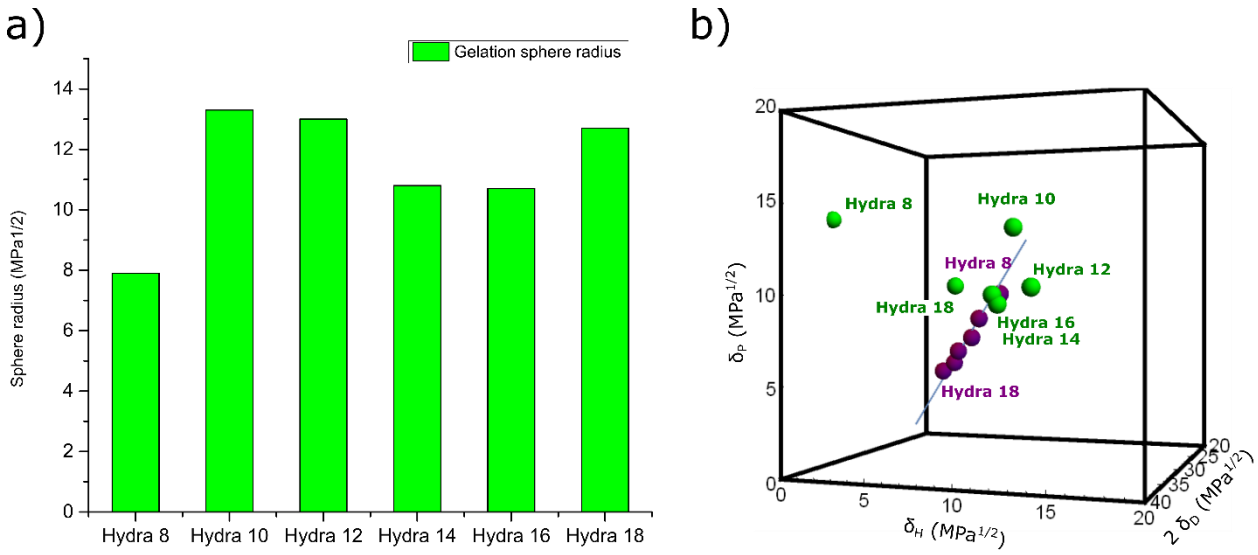


*Figure 76. a) Radius of the gelation spheres for the hydrazide based LMWGs. b) Center of the gelation spheres (green) represented in Hansen space and the simulated HSP parameters of each dialkyl hydrazide-based gelator (purple).*

Among all liquids tested with this family of LMWG none was found to solubilize the gelator, thus no solubility domains could be calculated. To have a reference to compare with the center of the gelation domains, we calculated the theoretical HSP values (obtained from the HSPiP software) of each gelator (Figure 76 b purple). The theoretical values present a linear shift, mostly decreasing $\delta_P$ and $\delta_H$ as the linear alkyl chain increases in length. It was possible to plot a trend line, which yields the following vector equation (t = number of carbons in each alkyl chain):

Eq 16: $[\delta_D, \delta_P, \delta_H] = [17.9, 13.0, 12.6] + t\,[-0.08, -0.43, -0.33]$

Regarding gelation, the increase of the length of the alkyl chain resulted in a non-monotonous variation of the radius and center of the Hansen domains. The radius of the gelation domains (Figure 76 a) increases from **Hydra8** to **Hydra10** (from 7.9 to 13.3 $MPa^{1/2}$), decreases from **Hydra10** to **Hydra16** (from 13.3 to 10.8 $MPa^{1/2}$) and increases again from **Hydra16** to **Hydra18** (from 10.8 to 12.7 $MPa^{1/2}$). This behavior is different from the previously studied families of gelators, that show a constant increase or decrease of the radius of the gelation spheres with the increase in length of the alkyl chain. Another non-monotonous variation can also be observed in the movement of the center of the gelation spheres as the length of the alkyl chains increases (Figure 76. b). The first major shift occurs from **Hydra8** to **Hydra10**, that moves the center of the gelation sphere mostly on the $\delta_H$ axes, from 0.17 to 12.3 $MPa^{1/2}$. From **Hydra10** to **Hydra12** it can be observed a decrease in $\delta_P$ of about 3 $MPa^{1/2}$. Then, the major shift observed from **Hydra12** to **Hydra18** is a decrease in $\delta_H$ (from 13.6 to 7.6 $MPa^{1/2}$).

We determined the standard deviation of calculated gelation spheres to investigate the existence of outliers that could explain the erratic variation of the center of the domains. The standard deviation obtained for each parameter ($\delta_D$, $\delta_P$, $\delta_H$) were plotted around the center of the gelation sphere as ellipsoids (figure 77) and listed in table 12 as uncertainties. All parameters presented a standard deviation lower than 0.6 $MPa^{1/2}$ except for **Hydra10** and **Hydra12** that presented a standard deviation as high as 1.4 $MPa^{1/2}$ for $\delta_P$. However, even if these two gelators are excluded, no regular trend can be identified.

***Table 12. Centre of Hansen spheres for all LMWG at 3 wt %.***

| | Gelation sphere | | | | Theoretical solubility sphere | | |
|---|---|---|---|---|---|---|---|
| **LMWG** | $\delta_D$ | $\delta_P$ | $\delta_H$ | r | $\delta_D$ | $\delta_P$ | $\delta_H$ |
| | ($MPa^{1/2}$) | ($MPa^{1/2}$) | ($MPa^{1/2}$) | ($MPa^{1/2}$) | ($MPa^{1/2}$) | ($MPa^{1/2}$) | ($MPa^{1/2}$) |
| **Hydra 8** | 17.2±0.4 | 14.5±0.5 | 0.17±0.5 | 7.9±0.4 | 17.3 | 10.1 | 10.7 |
| **Hydra 10** | 18.6±0.7 | 13.6±1.4 | 12.3±0.6 | 13.3±0.5 | 17.1 | 8.7 | 9.3 |
| **Hydra 12** | 19.1±0.8 | 10.4±1.3 | 13.6±0.6 | 13.0±0.5 | 16.9 | 7.6 | 8.7 |
| **Hydra 14** | 18.7±0.6 | 10.0±0.6 | 11.3±0.3 | 10.8±0.5 | 16.8 | 6.8 | 7.8 |
| **Hydra 16** | 18.7±0.3 | 9.5±0.2 | 11.5±0.3 | 10.7±0.2 | 16.6 | 6.1 | 7.4 |
| **Hydra 18** | 16.7±0.2 | 10.6±0.3 | 7.6±0.2 | 12.7±0.1 | 16.6 | 5.6 | 6.7 |

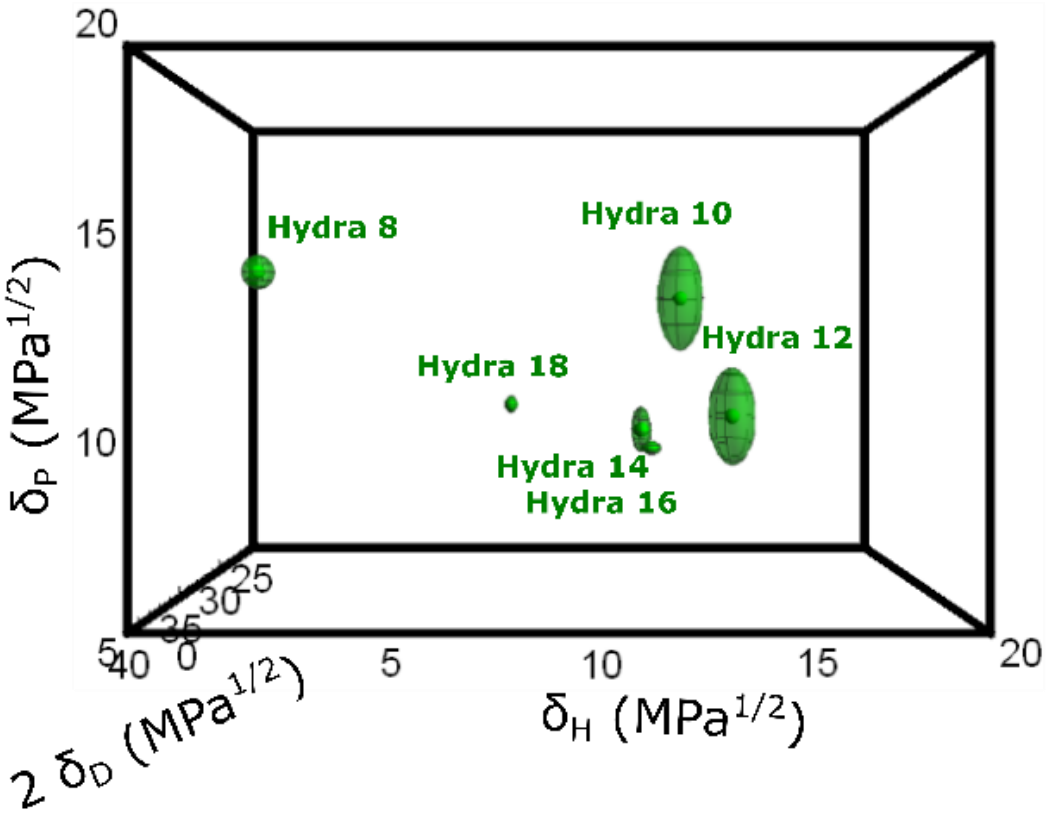


*Figure 77. Center of the gelation spheres (dark green) and the standard deviation (meshed green ellipsoids) represented in Hansen space.*

## 1.2. SEM observation of fibers

The morphology of **Hydra8** to **Hydra18** gel fibers was observed by scanning electron microscopy (Figure 78). All fibers presented a rigid tape-like morphology with very few differences in size, indicating that the different alkyl chain length does not affect the morphology of the fibers.

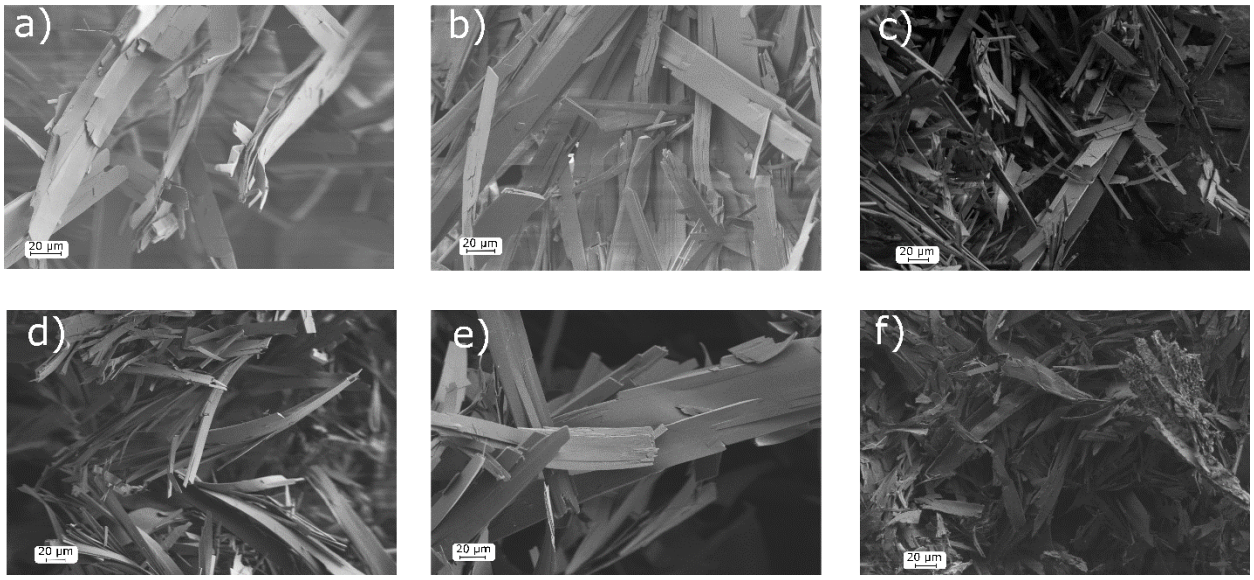


*Figure 78. SEM images of the hydrazide xerogels extracted from MEK: a)* ***Hydra8****, b)* ***Hydra10****, c)* ***Hydra12****, d)* ***Hydra14****, e)* ***Hydra16****, f)* ***Hydra18****.*

## 1.3. Single crystal structure of **Hydra12**

By forming a dilute solution (> 0.1 % wt) of **Hydra12** in 1-butanol and letting a slow crystallization for more than a month, it was possible to obtain a crystal with enough quality to perform single crystal diffraction. The structure was solved by the XRD platform of the Institut Parisien de Chimie Moléculaire.

The structure obtained by this process of slow crystallization consisted of 4 molecules per unit cell with $I_2/a$ symmetry group (Figure 79 and table 13). The alkyl chains are linearly placed along the c axes connected by the hydrazide moiety adopting a trans conformation. Carbonyl oxygen and amine hydrogen are oriented along the b axis of the unit cell forming a bridge of hydrogen bonding along the same axis.

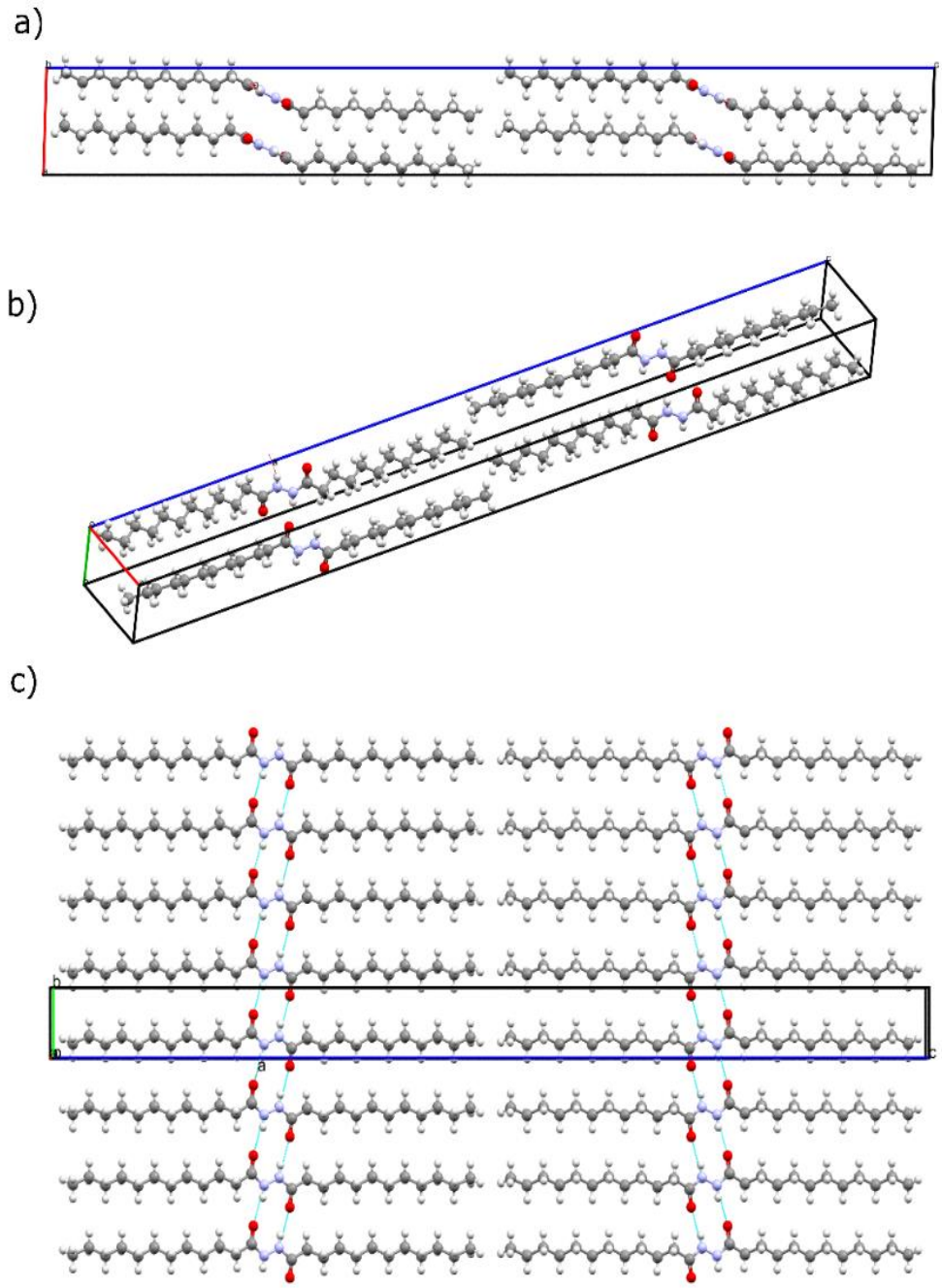


*Figure 79.* ***Hydra12*** *single crystal structure a) top view, b) full view and c) lateral view representing hydrogen bond formation along the b axes. Axes color: a (red), b (green) and c (blue)*

***Table 13. single crystal structure of Hydra12***

| | |
|---|---|
| **crystal system** | Monoclinic |
| **space group** | $I_2/a$ |
| **Cell unit (Å)** | **a** 7.280(3) **b** 4.860(2) **c** 68.491(18) |
| **Angles(deg)** | **α** 90 **β** 91.90(2) **γ** 90 |
| **volume (Å$^3$)** | 2421.93 |
| **Z** | 4 |
| **formula weight** | $C_{24}$ $H_{48}$ $N_2$ $O_2$ |
| **R-factor (%)** | 13.58 |

## 1.4. Structural analysis of gel fibers

To study the molecular packing within the gel fibers we performed X-ray diffraction in transmission mode on xerogel samples. First, we compared the X-ray pattern of **Hydra12** xerogel extracted from MEK with the simulated pattern from the previously obtained single crystal of **Hydra12** to check if gel fibers and single crystal possessed the same molecular packing. By stacking both X-ray patterns (Figure 80), it is clear that at small and wide angles there are big differences. At small angles the xerogel presents a strong diffraction peak at 3.15 theta (28 Å) while the single crystal pattern has a strong diffraction peak at 2.58 theta (34.2 Å)$^2$. This is a good indicator of differences between the two structures since the largest periodicity of each structure differs by about 6 Å. Since the single crystal structure presents the alkyl chains extended, occupying the entire length of the c axis of the unit-cell (largest periodicity) we can assume that the molecules within the gel fibers are slightly tilted, because they are confined in smaller periodicities (diffraction at small angles in figure 80. At wide angles we can also observe different diffraction peaks. This points to a different molecular packing within the gel fibers from the one present in the single crystal structure.

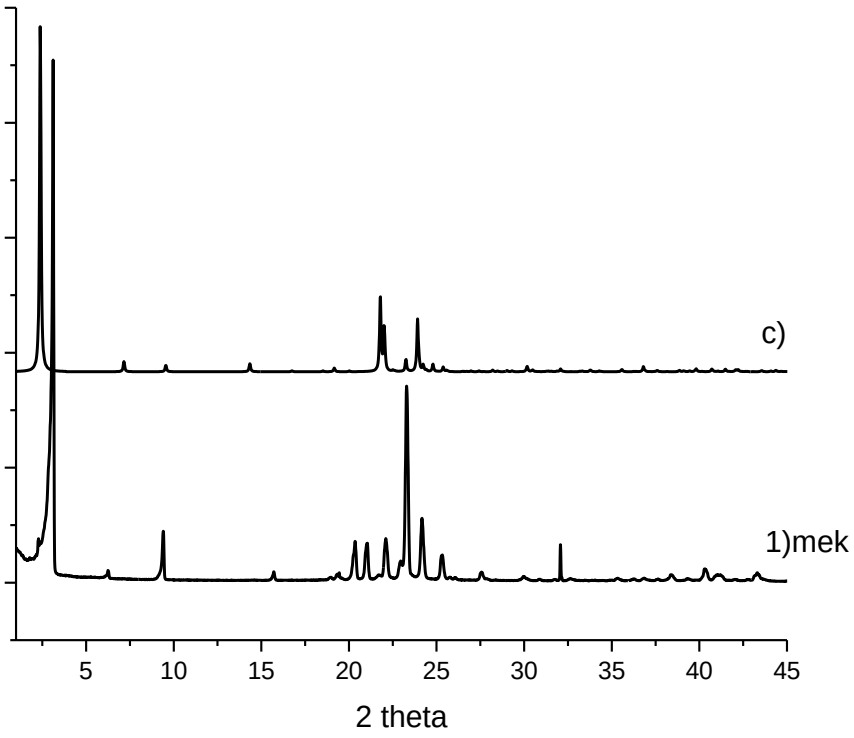


*Figure 80. Comparison of X-ray patterns of **Hydra12**: C) simulated from the single crystal structure and 1) measured on the xerogel extracted from MEK. X-ray wavelength of 1.5406 Å.*

Then, we set on to find out if the molecular packing could also differ based on the liquid that is gelated. To do so, we compared the X-ray patterns of the xerogels extracted from MEK and dioxane (Figure 81). For all LMWG, the xerogels extracted from the two liquids presented all diffraction peaks at the same position with some differences in intensity. Such differences in intensity can be attributed to preferential orientation obtained in the drying process of the gel fibers. Therefore, no influence of the liquid on the molecular packing in the gel fibers was detected.

Regarding the influence of the length of the alkyl chains on the X-ray patterns, we observed that the first observed diffraction peak at low angle (that corresponds to the largest dimension of the unit cell) shifted to lower angles as the length of the alkyl chains increased. In fact, figure 82 illustrates that this dimension increases linearly: every two $CH_2$ added to each alkyl chain, the first diffraction peak increases by 2.1 Å in real space.[3] This result is compatible with a regular evolution of the molecular packing in the family and does not give a hint for the erratic gelation behavior.

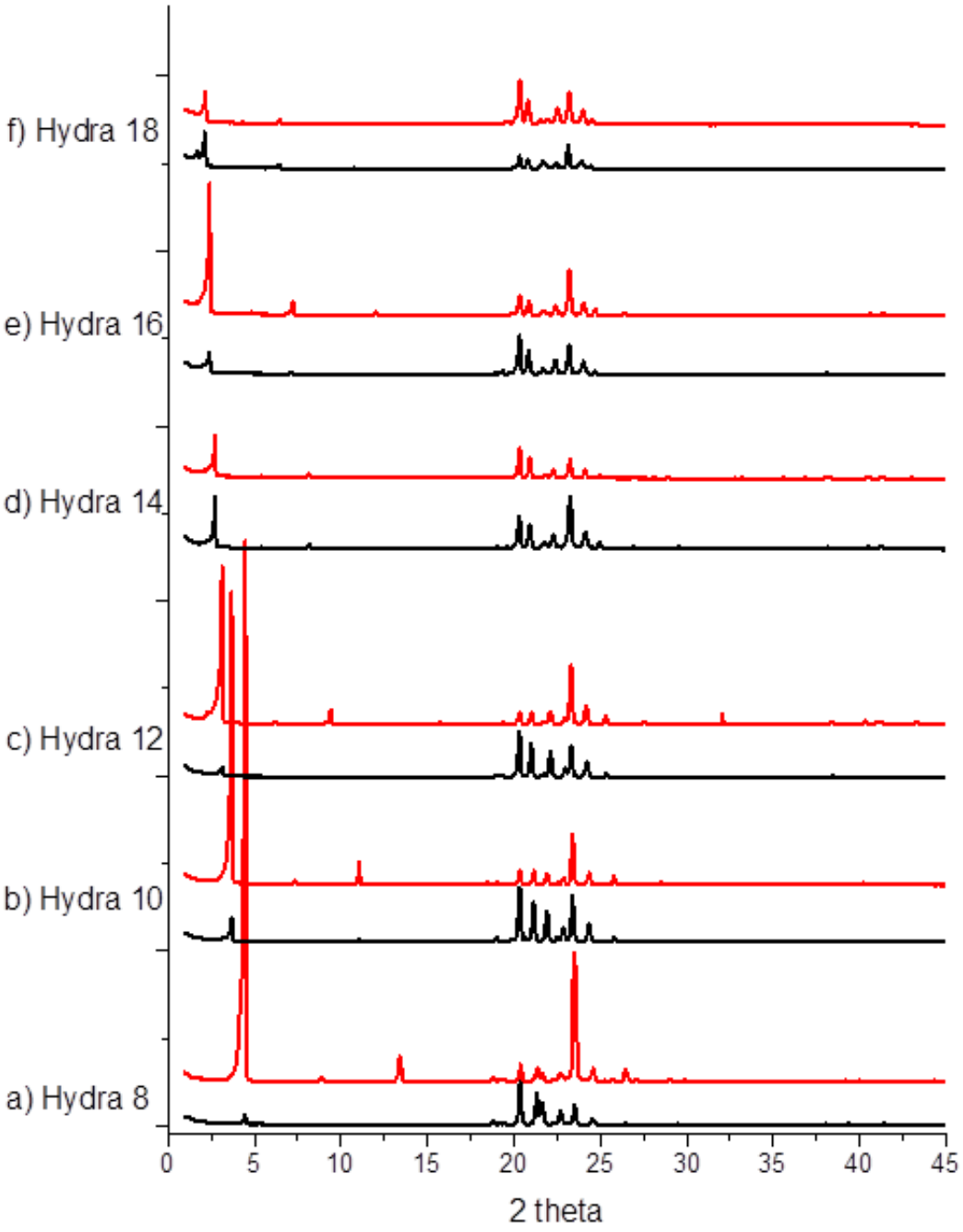


*Figure 81. Comparison of X-ray patterns for dialkyl hydrazide based gelators extracted from MEK (red) and dioxane (black). X-ray wavelength of 1.5406 Å.*

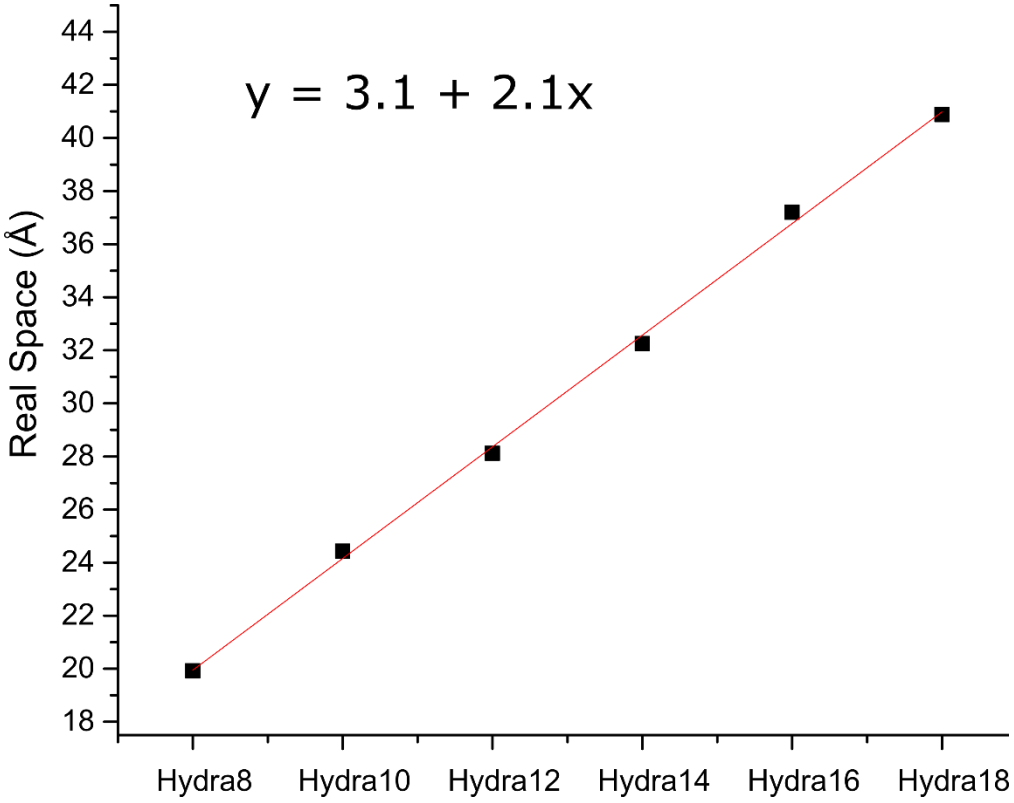


*Figure 82. Real space representation of the first observed diffraction at small angles in figure 81.*

We also studied other physical properties of the gel fibers, mainly melting point and infrared spectroscopy. The melting point of dialkyl hydrazide-based fibers extracted from MEK (Figure 83) presented a regular decrease in their melting point as the linear alkyl chains increased in length. The infrared spectrum of all dialkyl hydrazide-based xerogels (figure 84) presented a similar profile with in particular the same NH and C=O stretching bands (at 3220 and 1600 $cm^{-1}$, respectively) that are characteristic for hydrogen bonding (see Figure 85). However, subtle differences are observed at 2920 $cm^{-1}$ and in the region between 1280 $cm^{-1}$ and 1160 $cm^{-1}$ where **Hydra8** presents a slight discrepancy compared to the other members of the family. In particular, the shift to higher wavenumber at 2920 $cm^{-1}$ (antisymmetric $CH_2$ stretching) is characteristic for the presence of some disorder in the alkyl chain.[4] FTIR measurement therefore indicate a small difference of packing between **Hydra8** and the other members of the family.

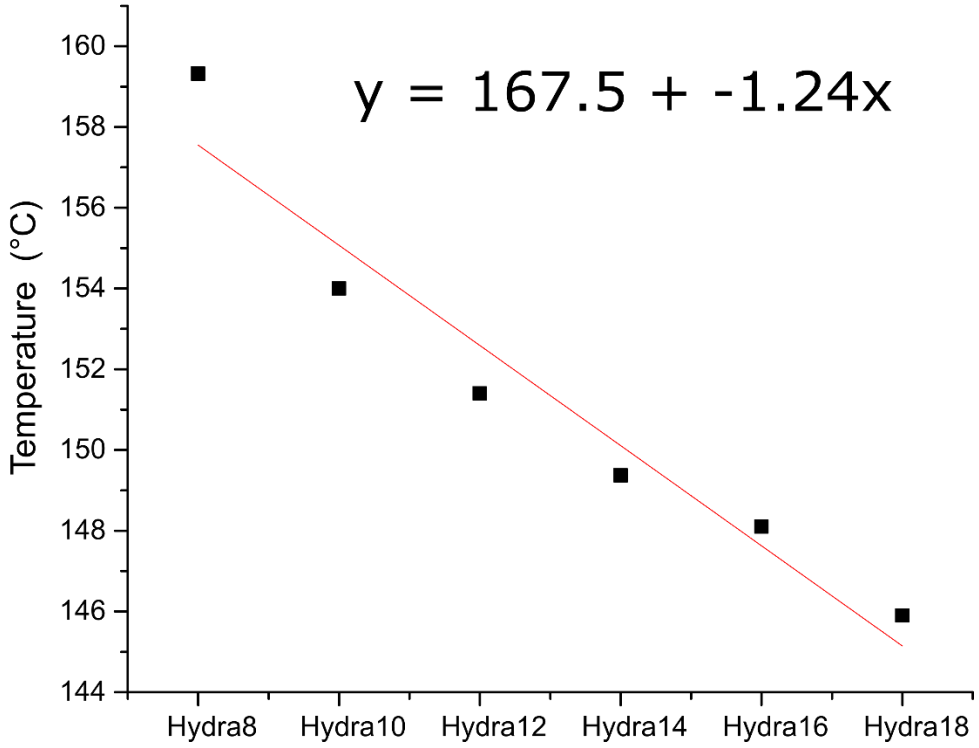


*Figure 83. Melting temperature of Hydra xerogels extracted from MEK.*

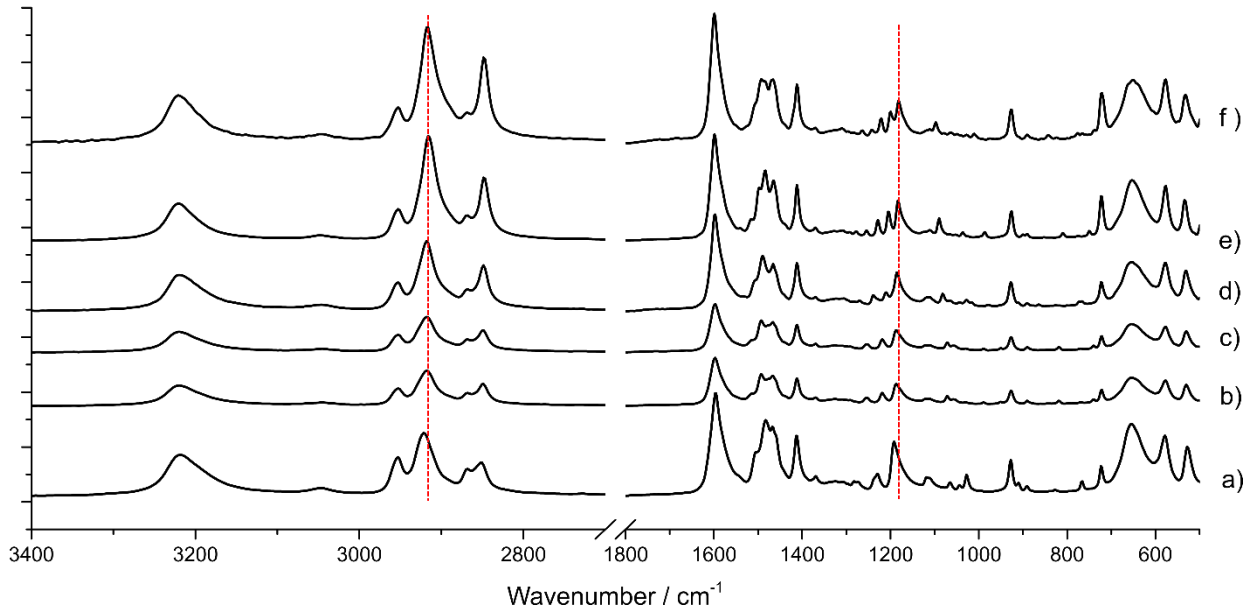


*Figure 84. Infrared absorbance spectrum of dialkyl hydrazide-based xerogel extracted from MEK. a)* ***Hydra8****, b)* ***Hydra10****, c)* ***Hydra12****, d)* ***Hydra14****, e)* ***Hydra16*** *and f)* ***Hydra18****.*

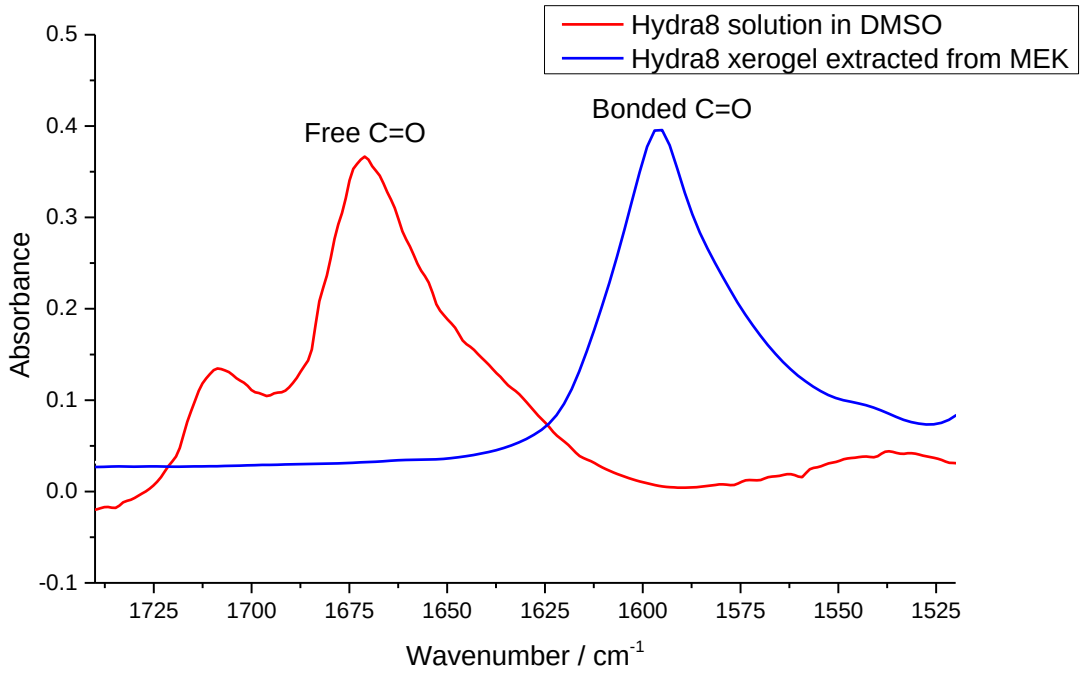


*Figure 85. Infrared absorbance spectrum comparison of **Hydra8** xerogel and solution.*

## 1.5. Molecular packing

Since the X-ray measurements indicate that the molecular packing within gel fibers differs from the one found on the single crystal structure, we used the direct space method described in chapter 1 to determine the packing within gel fibers. Within this family the direct space method was applied with indexation performed using Dicvol, Montecarlo simulation to find the average atom position and Rietveld refinement with energetic optimization to refine the final structure.

Unfortunately, the fitting values obtained from the molecular packing structures were not optimal. With Rp values close to 40 % and Rwp values close to 50%, the quality of the obtained structures was average at best. The inability to further improve these structures could be related to the acquired data, where possibly exists a strong effect of preferential orientation that could not be accounted for. The poor fitting of the XRD patterns is obvious on figures 88 to 93, where final refinements and fitting were performed without the diffraction peak presented a lower angle due to the high intensity compared to the rest of the patterns.

With the knowledge that the obtained structures can only be considered as proposals and not as exact models, the proposed molecular packing models for the different LMWG are represented in Figure 86. All models presented similar conformations despite different length of alkyl chains, with monoclinic unit cells and symmetry group $P2_1$. Axes b and c of the unit cell remain with similar values (4.3 Å and 9.4 Å) throughout all LMWG while the axes a increases as the alkyl chains increase

in length. The hydrazide moiety in the center of the LMWGs orientates the alkyl chain in a trans conformation. The oxygen carbonyls are orientated closely parallel to the b axis and form hydrogen bonds along the same axis (Figure 87).

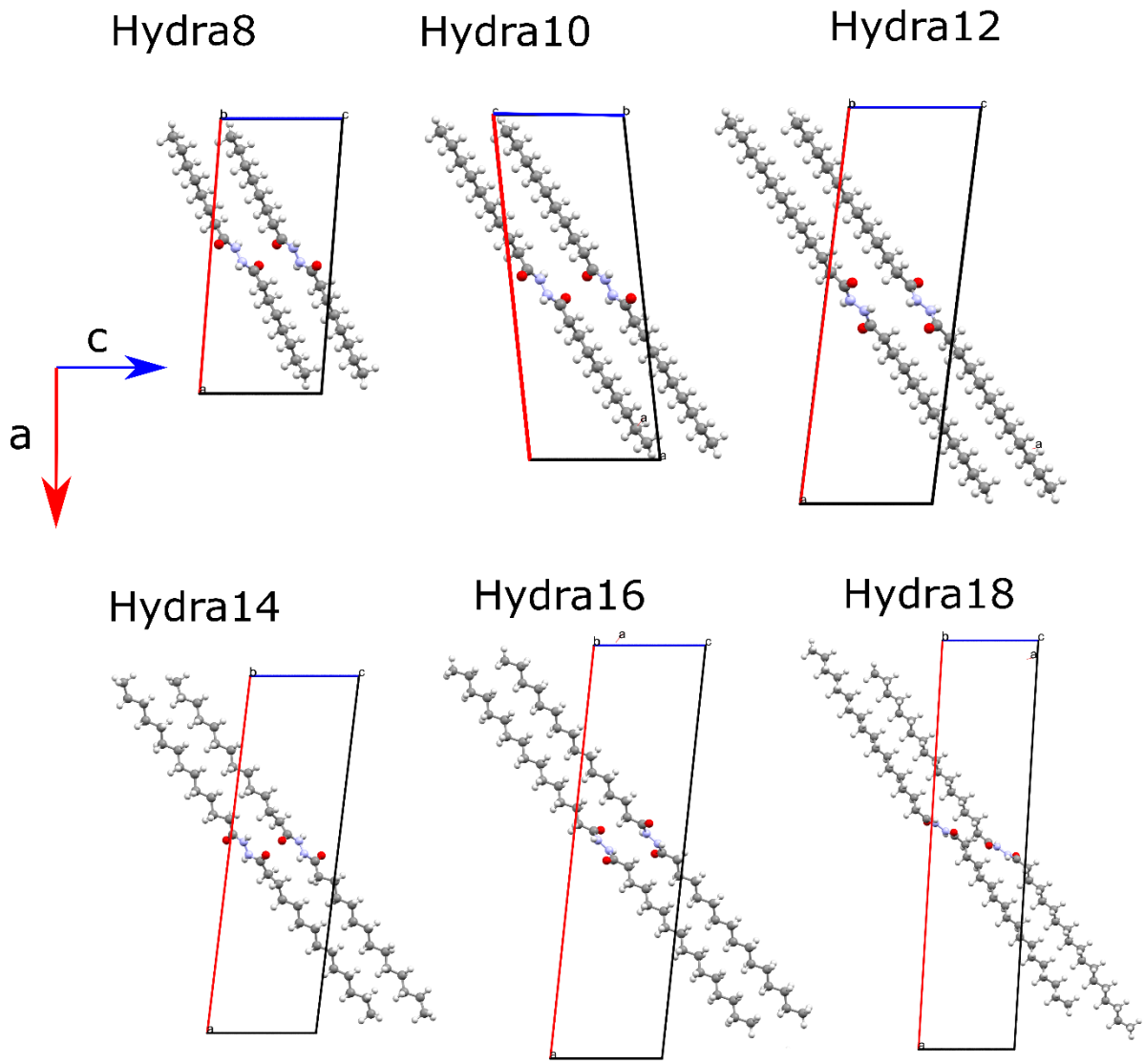


*Figure 86. Molecular packing of dialkyl hydrazide based LMWG obtained with the methodology described in chapter 1. Axes color: a (red), b (green) and c (blue)*

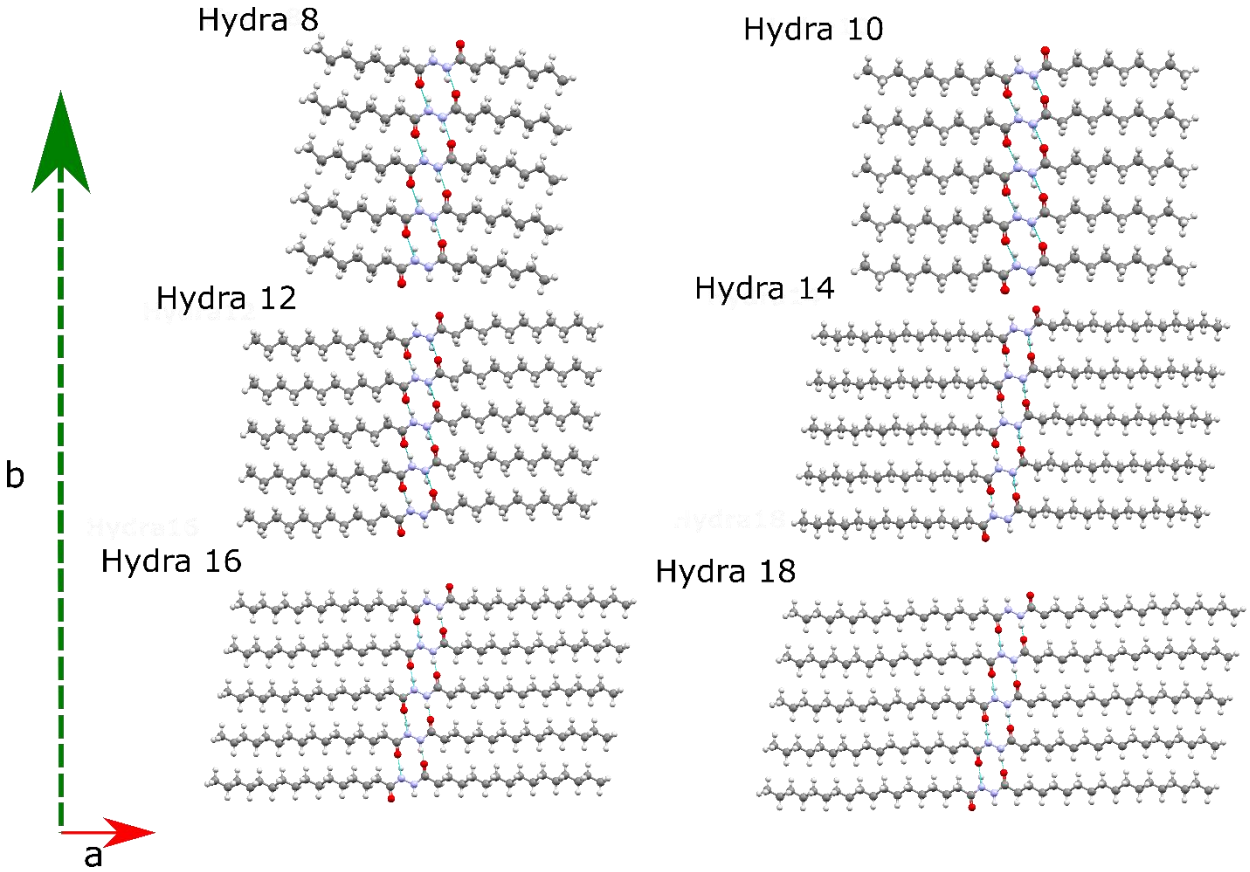


*Figure 87. Proposed molecular packing of dialkyl hydrazide-based gelators highlighting the formation of hydrogen bonds along the b axes.*

*Table 13. Proposed unit cell parameters of the dialkyl hydrazide-based gelators.*

| LMWG | **Hydra 8** | **Hydra 10** | **Hydra 12** | **Hydra 14** | **Hydra 16** | **Hydra 18** |
|---|---|---|---|---|---|---|
| crystal system | monoclinic | monoclinic | monoclinic | monoclinic | monoclinic | monoclinic |
| space group | P21 | P21 | P21 | P21 | P21 | P21 |
| a(Å) | 19.92 | 24.43 | 28.12 | 32.25 | 37.2 | 40.88 |
| b(Å) | 4.28 | 4.3 | 4.24 | 4.17 | 4.38 | 4.32 |
| c(Å) | 8.79 | 9.20 | 9.27 | 9.75 | 10.01 | 9.69 |
| α(deg) | 90 | 90 | 90 | 90 | 90 | 90 |
| β(deg) | 94.39 | 96.06 | 97.25 | 96.87 | 96.02 | 97.88 |
| γ(deg) | 90 | 90 | 90 | 90 | 90 | 90 |
| volume ($Å^3$) | 746.23 | 964.82 | 1112.45 | 1400.32 | 1656.37 | 1696.65 |
| Z | 2 | 2 | 2 | 2 | 2 | 2 |
| Density $gcm^{-3}$ | 1.12 | 1.07 | 1.12 | 1.03 | 0.98 | 1.07 |
| formula weight | $C_{16}H_{32}N_2O_2$ | $C_{20}H_{40}N_2O_2$ | $C_{24}H_{48}N_2O_2$ | $C_{28}H_{56}N_2O_2$ | $C_{32}H_{64}N_2O_2$ | $C_{36}H_{72}N_2O_2$ |
| 2θinterval (deg) | 5-60 | 5-60 | 5-60 | 5-60 | 5-60 | 5-60 |
| step size (deg) | 0.005 | 0.005 | 0.005 | 0.005 | 0.005 | 0.005 |
| counting time(s) | 3 | 3 | 3 | 3 | 3 | 3 |
| Rp | 62.735 | 52.068 | 54.297 | 37.447 | 67.534 | 47.701 |
| Rwp | 136.336 | 105.541 | 101.528 | 49.272 | 120.040 | 57.701 |

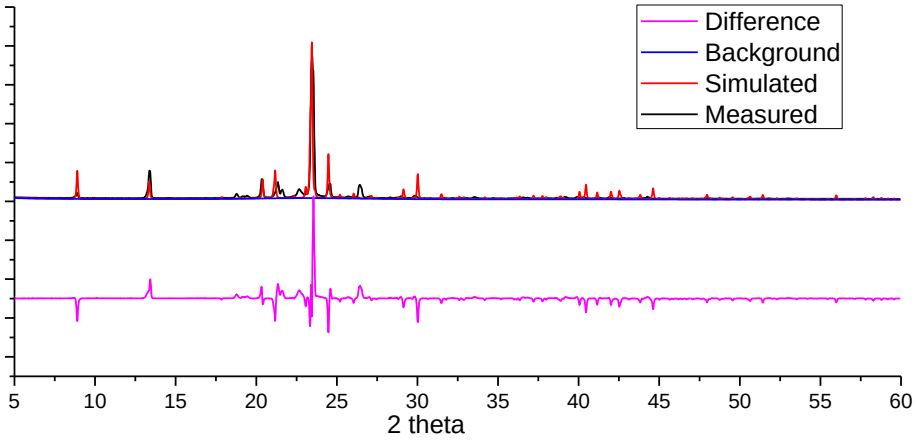


*Figure 88. Comparison between simulated X-ray pattern and measured pattern from **Hydra8** xerogel extracted from MEK. X-ray wavelength of 1.5406 Å.*

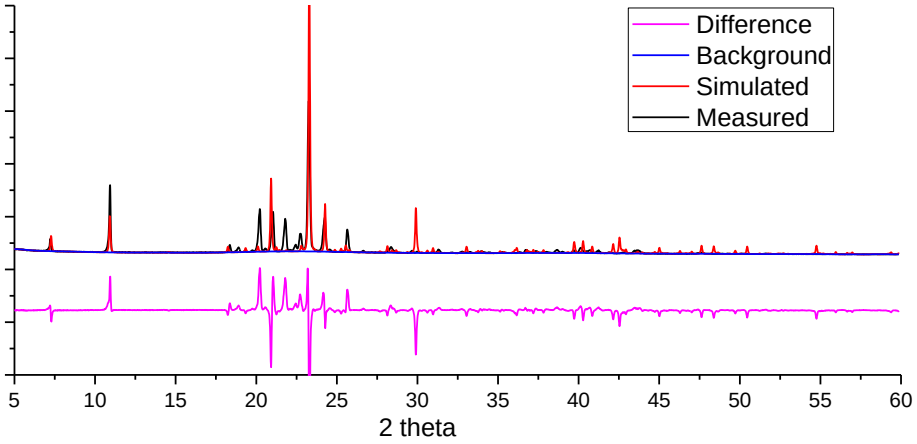


*Figure 89. Comparison between simulated X-ray pattern and measured pattern from **Hydra10** xerogel extracted from MEK. X-ray wavelength of 1.5406 Å.*

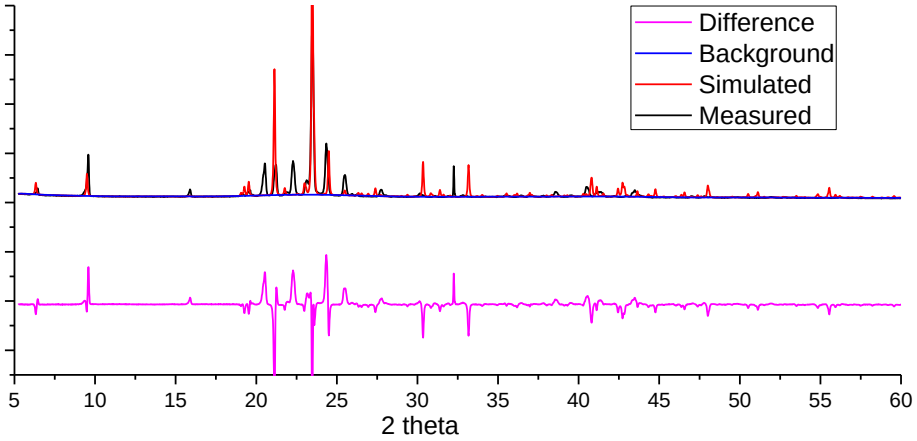


*Figure 90. Comparison between simulated X-ray pattern and measured pattern from **Hydra12** xerogel extracted from MEK. X-ray wavelength of 1.5406 Å.*

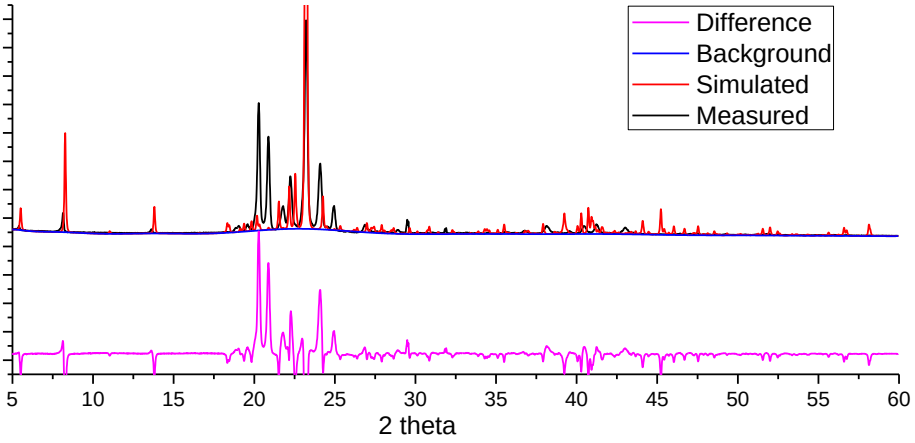


*Figure 91. Comparison between simulated X-ray pattern and measured pattern from* ***Hydra14*** *xerogel extracted from MEK. X-ray wavelength of 1.5406 Å.*

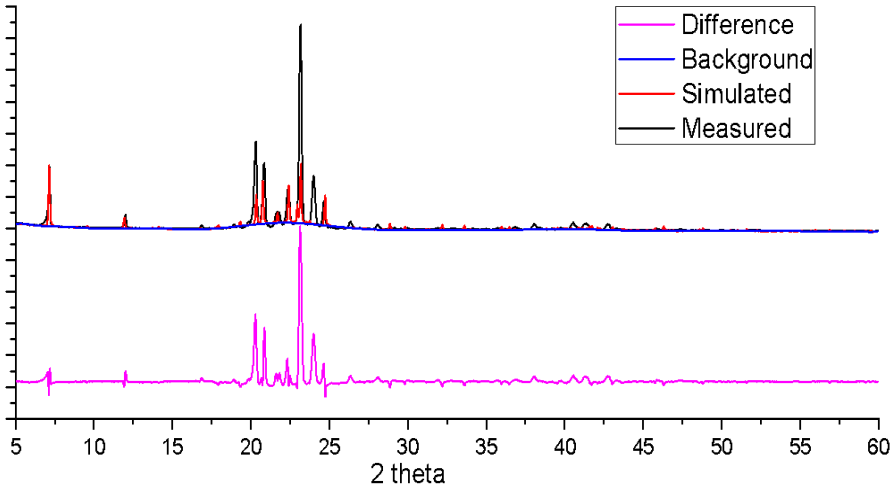


*Figure 92. Comparison between simulated X-ray pattern and measured pattern from* ***Hydra16*** *xerogel extracted from MEK. X-ray wavelength of 1.5406 Å.*

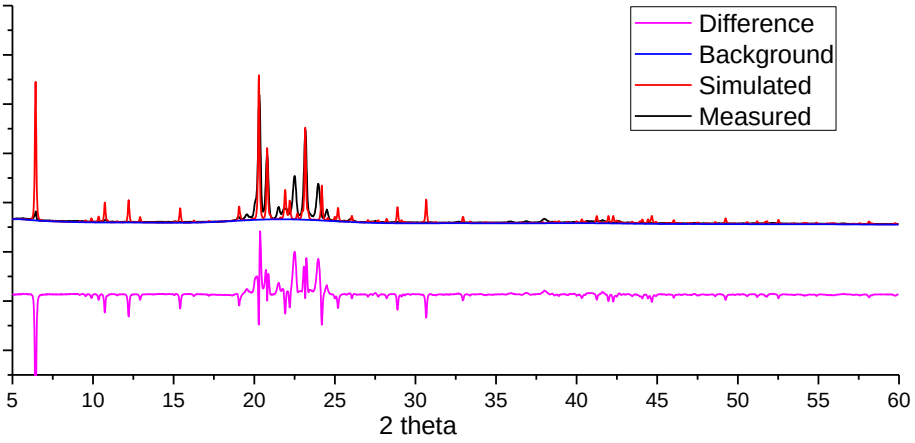


*Figure 93. Comparison between simulated X-ray pattern and measured pattern from* ***Hydra18*** *xerogel extracted from MEK. X-ray wavelength of 1.5406 Å.*

## 1.6. Conclusion for the dialkyl hydrazide based gelators

The dialkyl hydrazide-based gelators present an erratic behavior in the evolution of gelation sphere with an increase of the alkyl chains length. In an attempt to understand the reason for this erratic behavior we studied the molecular packing within gel fibers. Unfortunately, a reliable fit of the X-ray data was not possible thus the molecular packing structures presented are only an approximation of the packing within gel fibers.

FTIR spectroscopy hints at a slightly different packing for the shortest member of the family (**Hydra8**). However, even if this point is removed from the dataset, the remaining gelation data still presents an erratic behavior. A possible explanation is if the members of the family do not share the same crystal habit, i.e. if the most stable faces of the crystalline fibers are not the same.

# 2. (R)-12-hydroxystearic amide based gelators

The last family of gelator described in this chapter is the (R)-12-hydroxystearic amide (HSA) based gelators. This LMWG family was first reported by Richard Weiss et al.[5] and was obtained by reacting (R)-12-hydroxystearic acid with different linear alkyl amines. Later, Laurent Bouteiller et al.[6] prepared four members of this family (**HSA4, HSA8, HSA12** and **HSA18**) and studied their gelation in an attempt to correlate the gelation domains in the Hansen space with the length of the alkyl chains. They concluded that no clear trend was obtained. However, if **HSA12** is considered an outlier, then the three remaining gelation spheres are shifted to a more polar region while the alkyl chain length is increased. This trend is actually opposite to the ones demonstrated in the case of thiazole and bisamide families (see Chapter 3). The conflicting trend and the absence of any structural investigation in the initial HSA study prompted us to reinvestigate this family.

Therefore, the gelation of two new members of this family (Figure 94) close to **HSA12** (**HSA10** and **HSA14**) was investigated. The gelation domains of all members of this family were then determined using the optimized method explained in chapter 2 (the AO method). We also studied the macroscopic morphology of the gel fibers and proposed a model for the molecular packing within gel fibers.

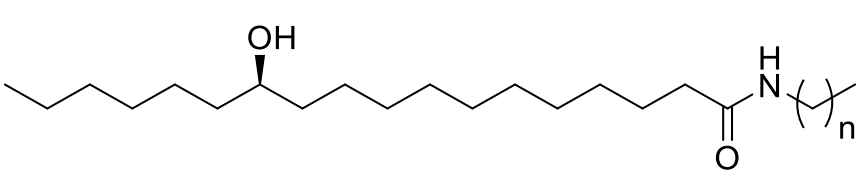


*HSA4 = n = 3*
*HSA8 = n = 7*
*HSA10 = n = 9*
*HSA12 = n = 11*
*HSA14 = n = 13*
*HSA18 = n = 17*

*Figure 94. Chemical structure of the HSA based gelators*

## 2.1. Hansen space of all HSA based gelators

**HSA10** and **HSA14** were subjected to the same set of solubility tests than all other members of the HSA based gelators of the previously mentioned study [6] and then the gelation domains were re-determined using the AO method (Figure 95).

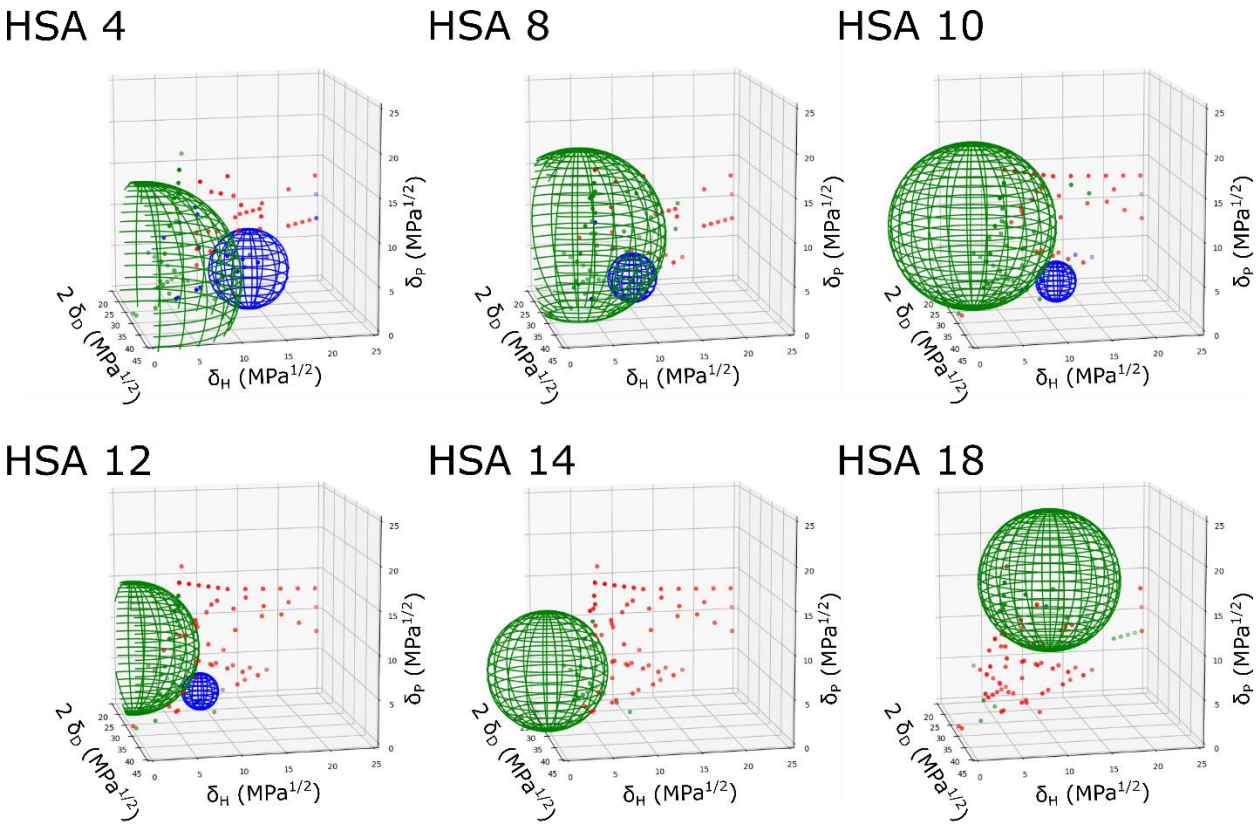


*Figure 95. Gelation data plotted in Hansen space for the HSA based gelators at 2 wt%. The tested liquids are represented by full circles and the calculated domains are represented by meshed spheres. Green: gel; red: precipitate; blue: soluble.*

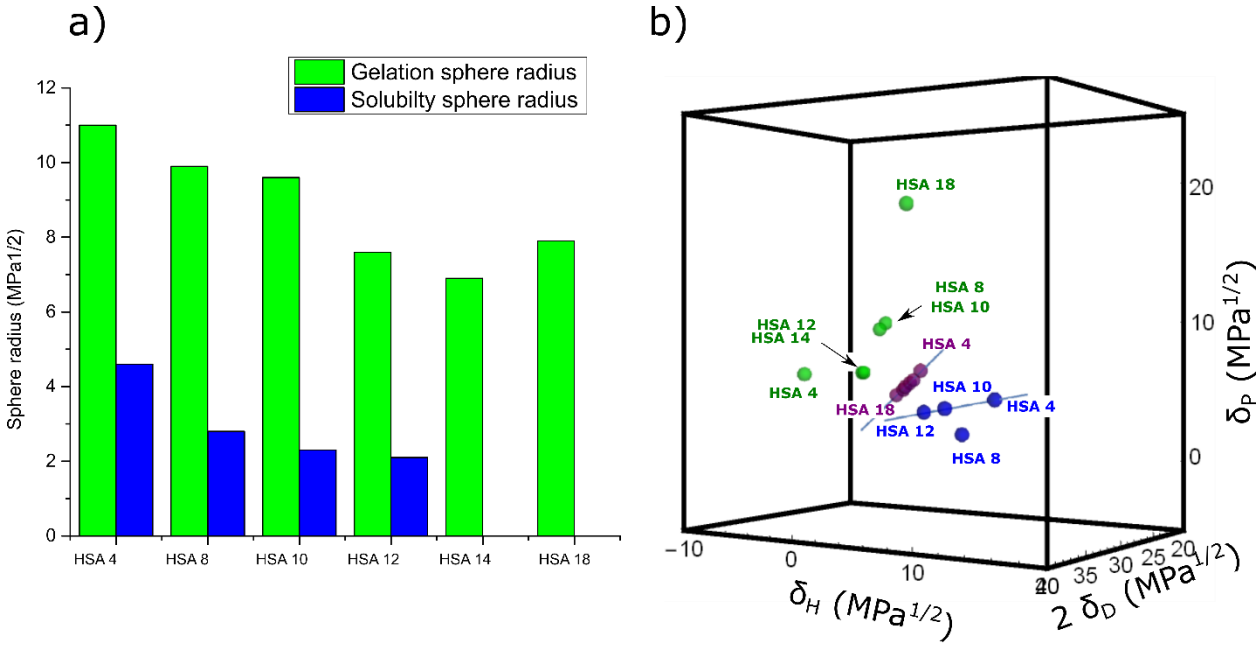


*Figure 95. a) Radius of the solubility (blue) or the gelation (green) spheres for the HSA based gelators. b) Center of the solubility spheres (blue), center of the gelation spheres (green) and simulated HSP parameters (purple) represented in Hansen space.*

After re-determining all gelation and solubility spheres, we could observe that the increase in the length of the linear alkyl chain resulted in the decrease of the radius of the solubility spheres (Figure 96 a) from **HSA4** up to **HSA12** while with **HSA14** and **HSA18** none of the tested liquids were able to dissolve the gelators so no solubility sphere could be determined. The center of the solubility spheres (Figure 96 b blue) tend to shift to less polar areas of the Hansen space, similar to what was observed with the solubility spheres of the previous gelators. Each $CH_2$ added to the alkyl chains lead the center of the gelation sphere to move by $\delta_D$ = -0.02; $\delta_P$ = -0.12; $\delta_H$ = -0.66 $MPa^{1/2}$. The vector equations of the trend in the Hansen space is given by (t = number of carbons in each alkyl chain):

Eq 17 : $[\delta_D, \delta_P, \delta_H] = [17.7, 5.3, 15.9] + t\,[-0.02, -0.12, -0.66]$

The theoretical HSP values of each gelator calculated by the group contribution method using the HSPiP software (Figure 87 b purple and Table 15) also shift to a less polar region of the Hansen space as the length of the alkyl chain increases but presents a smaller slope in the trend line. Each $CH_2$ added to the alkyl chains lead the center of the gelation sphere to move by $\delta_D$ = -0.02; $\delta_P$ = -0.12; $\delta_H$ = -0.17 $MPa^{1/2}$. The vector equations of the trend in the Hansen space is given by (t = number of carbons in each alkyl chain):

Eq 18 : $[\delta_D, \delta_P, \delta_H] = [16.5, 6.9, 6.4] + t\,[-0.02, -0.12, -0.17]$

The discrepancy between measured and calculated HSP is probably due to the small number of S points which makes the determination of the solubility spheres unprecise.
The radius of the gelation sphere decreases regularly from **HSA4** up to **HSA14** and presents a small increase from **HSA14** to **HSA18** (Figure 96 a). The increase in length of the alkyl chain causes the center of the gelation sphere (Figure 96 b green) to a shift to a higher polarity region from **HSA4** to **HSA10**. We then observe a shift to a lower polarity region from **HSA10** to **HSA14** and finally a shift to higher polarity again from **HSA14** to **HSA18**. The centers of the gelation spheres of **HSA8** and **HSA10** on one hand, and **HSA12** and **HSA14** on the other hand, are very close to each other.

*Table 14. Centre of Hansen spheres for HSA based gelators at 2 wt %.*

| | Gelation sphere | | | | Solubility sphere | | | |
|---|---|---|---|---|---|---|---|---|
| **LMWG** | $\delta_D$ ($MPa^{1/2}$) | $\delta_P$ ($MPa^{1/2}$) | $\delta_H$ ($MPa^{1/2}$) | r ($MPa^{1/2}$) | $\delta_D$ ($MPa^{1/2}$) | $\delta_P$ ($MPa^{1/2}$) | $\delta_H$ ($MPa^{1/2}$) | r ($MPa^{1/2}$) |
| **HSA4** | 19.3±2.0 | 6.4±1.0 | 0±0.5 | 11±0.6 | 17.6 | 4.9 | 13.3 | 4.6 |
| **HSA8** | 16.3±0.8 | 9.5±0.4 | 2.0±0.6 | 9.9±0.6 | 17.4 | 2.4 | 10.4 | 2.8 |
| **HSA10** | 15.8±0.8 | 9.9±0.4 | 1.9±0.6 | 9.6±0.5 | 18.5 | 4.3 | 10.5 | 2.3 |
| **HSA12** | 15.9±0.6 | 6.3±1.1 | 0.1±0.1 | 7.6±0.3 | 17.4 | 3.9 | 8.0 | 2.1 |
| **HSA14** | 16.0±0.4 | 6.3±0.9 | 0±0.3 | 6.9±0.6 | | | | |
| **HSA18** | 19.7±0.6 | 17.8±0.5 | 9.1±0.4 | 7.9±0.4 | | | | |

*Table 15. HSP theoretical solubility values of the HSA based gelators*

| **LMWG** | $\delta_D$ ($MPa^{1/2}$) | $\delta_P$ ($MPa^{1/2}$) | $\delta_H$ ($MPa^{1/2}$) |
|---|---|---|---|
| **HSA4** | 16.5 | 6.6 | 5.9 |
| **HSA8** | 16.3 | 5.9 | 5 |
| **HSA10** | 16.3 | 5.7 | 4.7 |
| **HSA12** | 16.3 | 5.4 | 4.3 |
| **HSA14** | 16.2 | 5.2 | 4 |
| **HSA18** | 16,2 | 4.8 | 3.4 |

The standard variation obtained for each parameter ($\delta_D$, $\delta_P$, $\delta_H$) were plotted around the center of the gelation sphere as ellipsoids (figure 97) and given in table 14. Except $\delta_D$ for **HSA4**, all coordinates of the centers of the gelation domains presented a standard deviation inferior to 1 $MPa^{1/2}$ and can be considered as reliable.

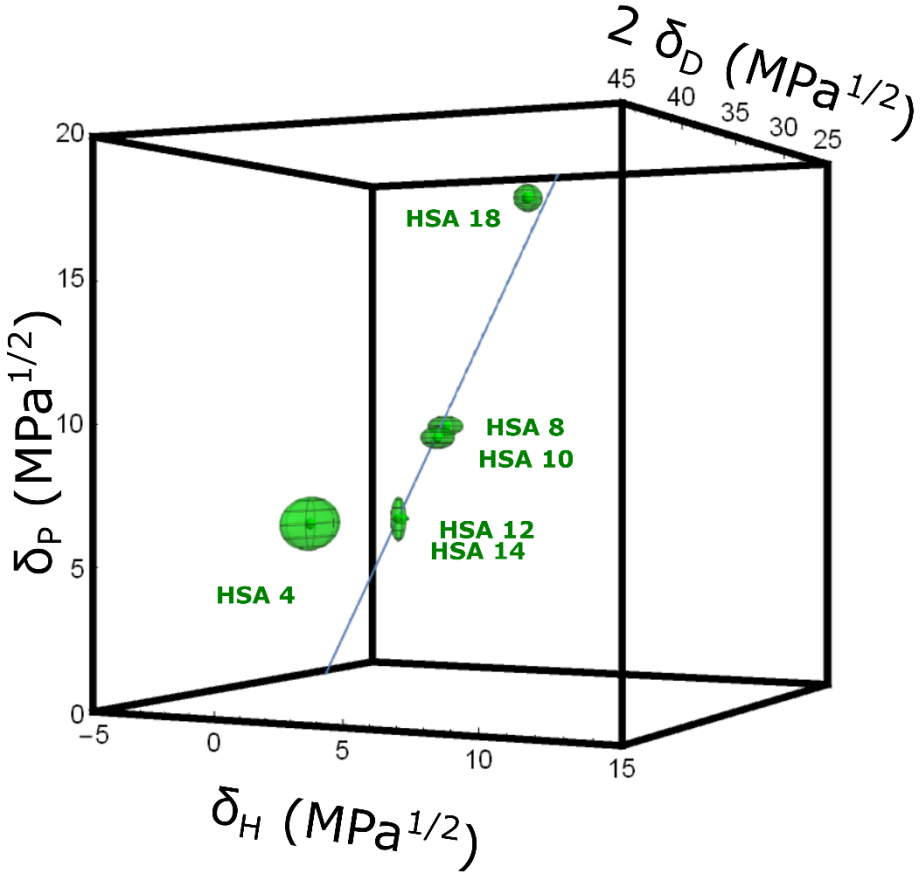


*Figure 97. Center of the gelation spheres (dark green) and the standard deviation (meshed green ellipsoids) represented in Hansen space and hypothetical trend line excluding **HSA4** and **HSA18**.*

With the obtained center of gelation spheres, it was not possible to calculate a regular trend line with all members of this gelator family. Also, the low standard deviation values do not provide arguments to classify any member as an outlier.

A possible alternative to plot a trend line would be to discard the organogelators with the shortest and longest alkyl chain, **HSA4** and **HSA18**. Without these gelators we are able to plot a trend line that crosses all others gelators and has a tendency to shift the center of the gelation spheres to lower polarity regions of the Hansen space with the increase of the alkyl chains. The vector equations of the trend in the Hansen space is given by (t = number of carbons in each alkyl chain):

Eq 19 : $[\delta_D, \delta_p, \delta_H] = [16.8, 13.7, 4.7] + t\ [-0.06, -0.53, -0.34]$

The following part investigates whether all members of the family share the same packing.

## 2.2. Structural analysis of gel fibers

X-ray measurements performed for all HSA based xerogels extracted from toluene yielded just a few and broad diffraction peaks (Figure 98).

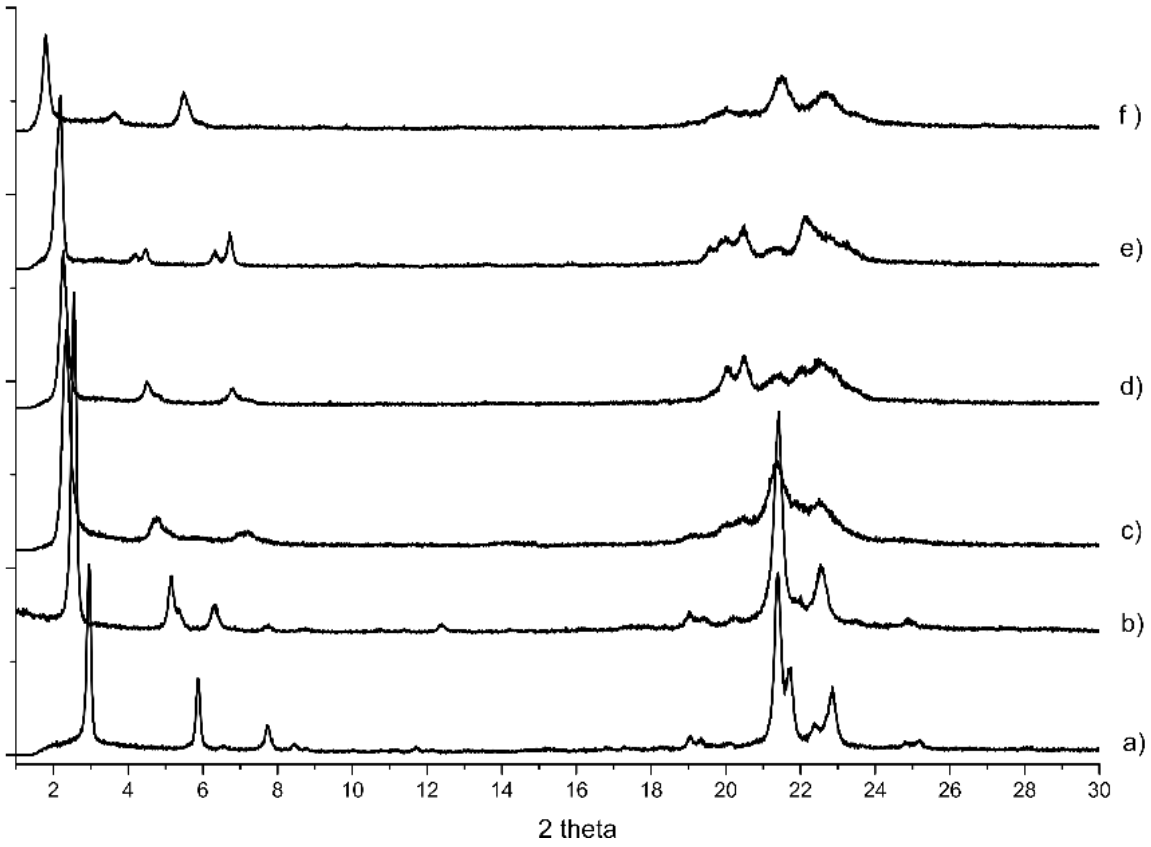


*Figure 98. Comparison of X-ray patterns of the HSA based xerogels extracted from toluene. a)**HSA4**, b)**HSA8**, c)**HSA10**, d)**HSA12**, e)**HSA14** and f)**HSA18**. X-ray wavelength of 1.5406 Å.*

We can observe from the small angle region that the increase in length of the alkyl chain results in a drift of the first observed diffraction peak to lower angle, indicating the periodicity within the gels fibers increases with the elongation of the alkyl chain. We can observe in figure 99 that the distance in real space of the first observed periodicity in the X-ray diffraction patterns increases linearly from **HSA8** to **HSA14**, where **HSA4** and **HSA18** are presented outside of this linear trend.

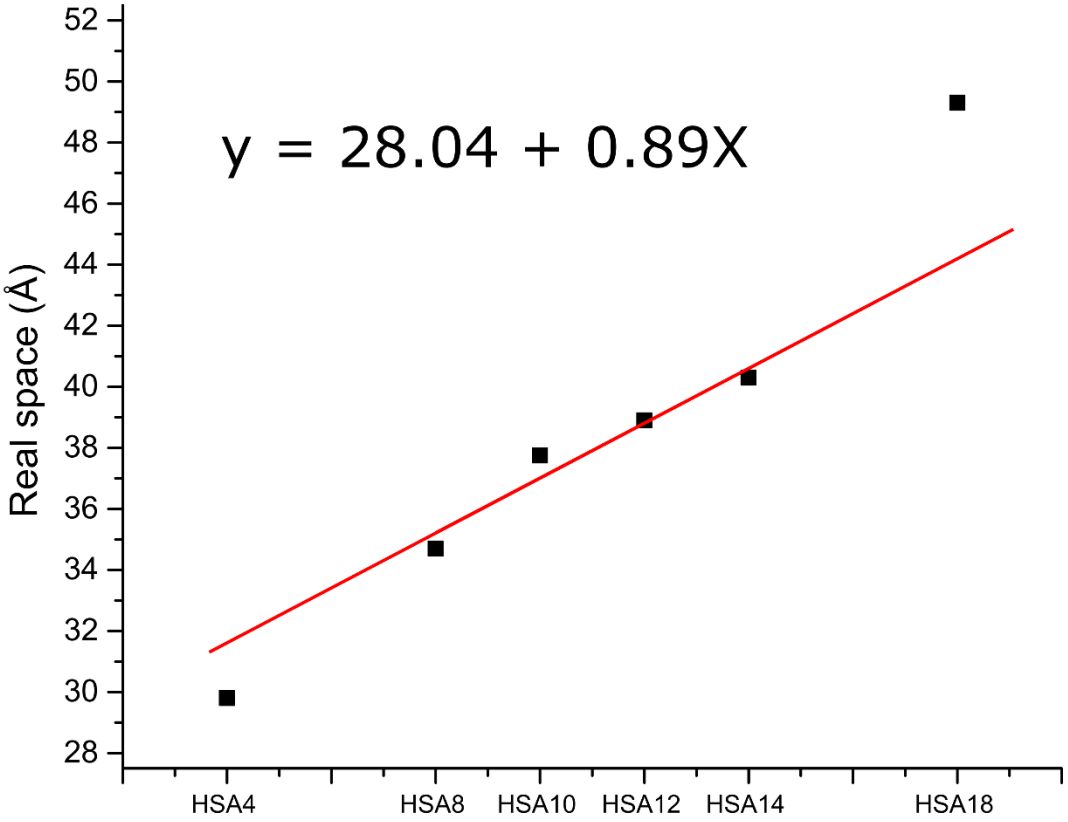


*Figure 99. Real space representation of the first observed diffraction at small angles in figure 98.*

This type of patterns proved to be difficult to analyze with the direct space method used with the previous gelators. Therefore, we performed PDF measurements (Figure 100) with a hope to gain information on the local structure of the gelators. The PDF analysis did not present major differences between the different HSA gelators. This points to a similar local structure, despite the different length in alkyl chains of the gelators.

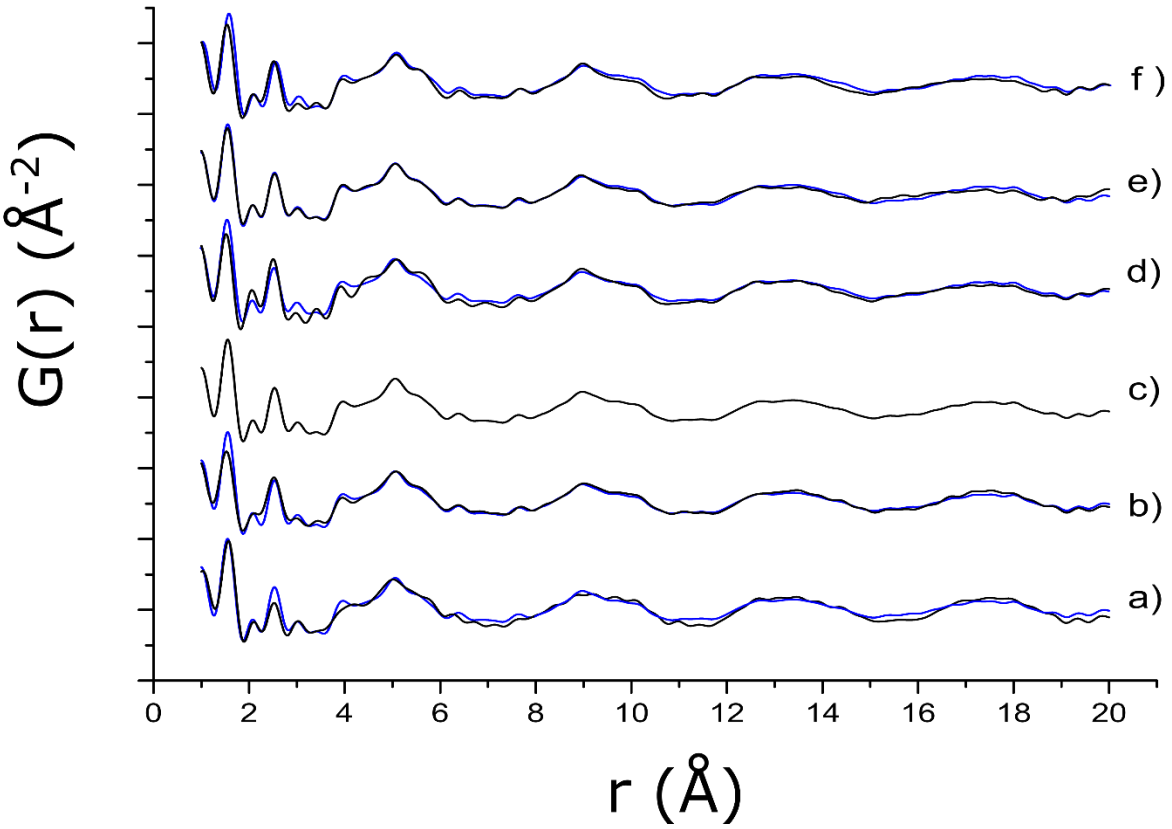


*Figure 100. Comparison of PDF measurements of the HSA based xerogels extracted from toluene. a)**HSA4**, b)**HSA8**, c)**HSA10**, d)**HSA12**, e)**HSA14** and f)**HSA18**. **HSA10** overlapped in blue over all other gelators for comparison.*

Infrared spectroscopy of xerogels extracted from toluene (figure 101) also present a similar spectrum between all gelators, pointing to the same interactions taking place independently of the length of the alkyl chain.

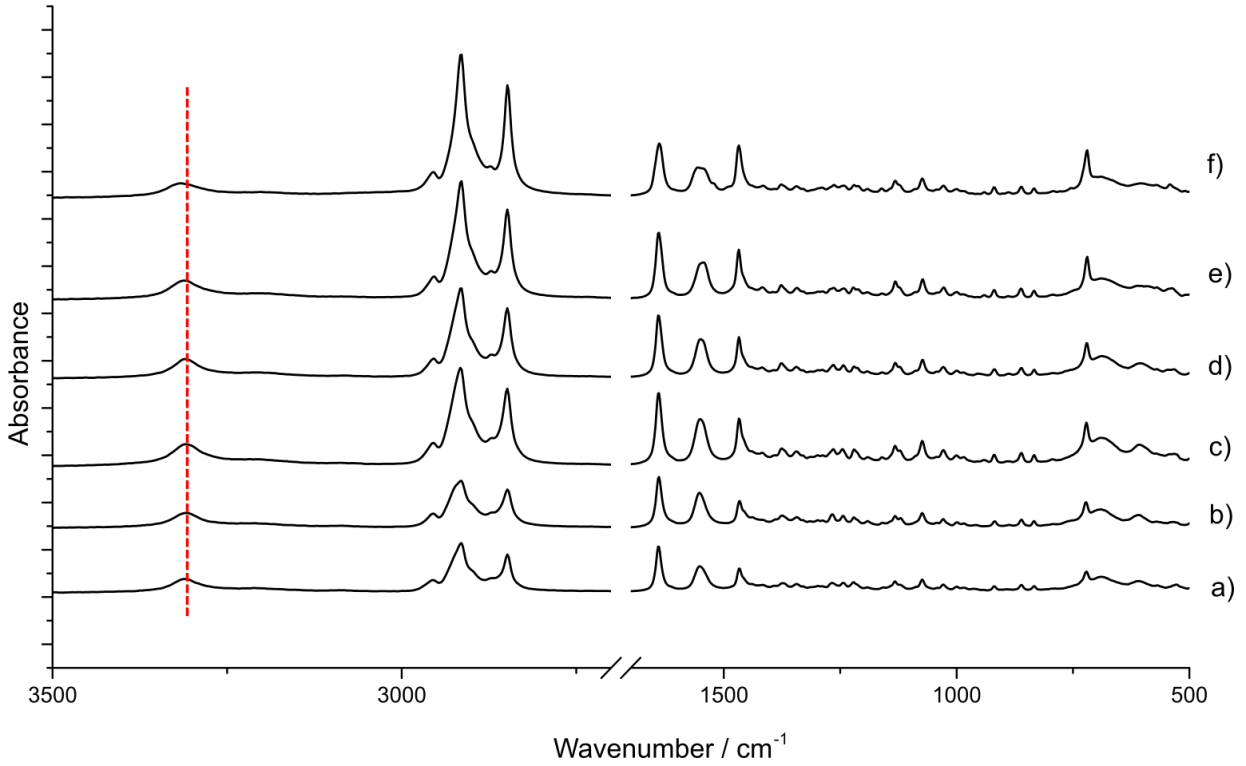


*Figure 101. Infrared absorbance spectrum of HSA based xerogels extracted from toluene. a)**HSA4**, b)**HSA8**, c)**HSA10**, d)**HSA12**, e)**HSA14** and f)**HSA18**.*

From the infrared measurement performed we can observe that all HSA gelators present a broad band at 3300 $cm^{-1}$. This points to the hydroxy and amide NH functions being hydrogen bonded in all gelators.[6] Similarly, the band at 1640 $cm^{-1}$ is characteristic for hydrogen bonded amide C=O functions. However, close inspection of the 3300 $cm^{-1}$ band reveals a slight shift for **HSA18** indicating slightly weaker hydrogen bonds than for the other members of the family.

In addition, we observed that the melting point of xerogels extracted from toluene (Figure 102) increases regularly with the elongation of the alkyl chain (from **HSA8** to **HSA18**). However, the xerogel of **HSA4** (shortest length alkyl chain) presented a melting point higher than **HSA8**, **HSA10**, **HSA12** and **HSA14** which contain longer alkyl chains.

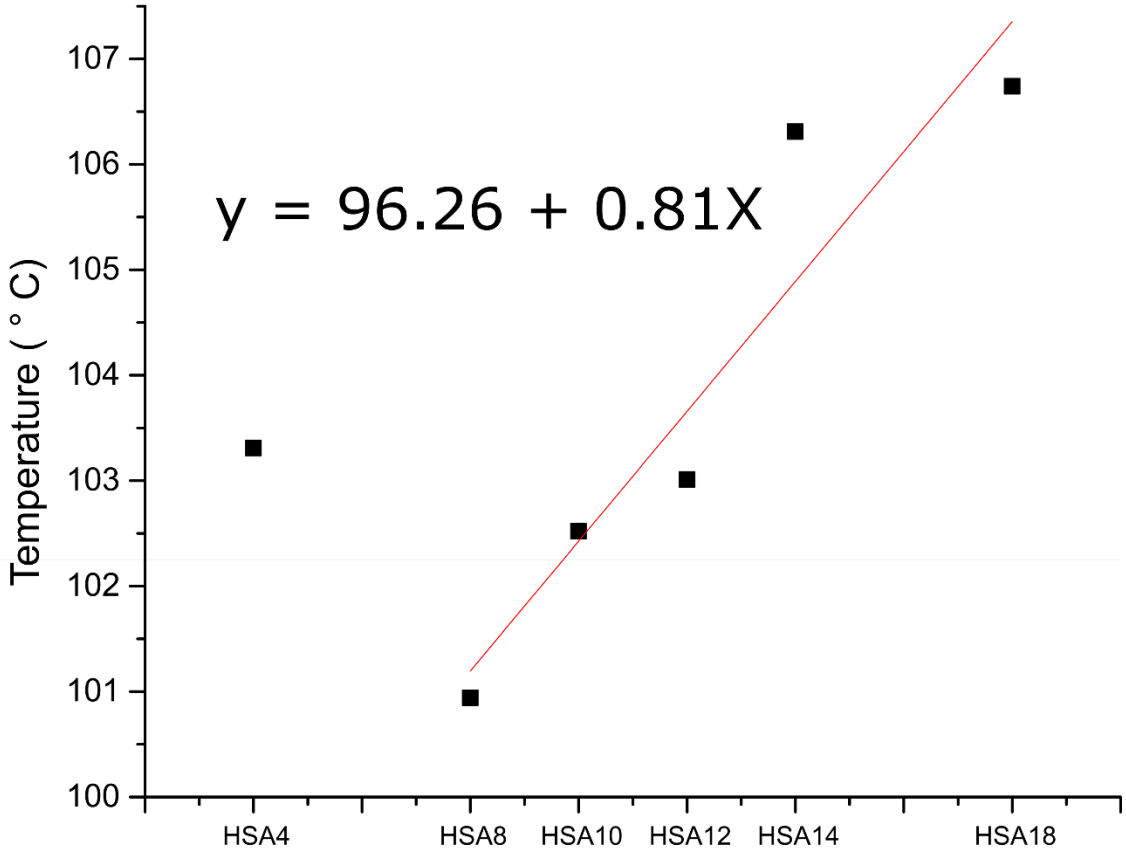


*Figure 102. Melting temperature of HSA xerogels extracted from toluene.*

## 2.3. SEM observation of fibers

To check if the length of the linear alkyl chain could have any impact in the morphology of the gel fibers and thus be correlated with the non-linear trend observed with the center of the gelation spheres, we observed the xerogel of **HSA4, HSA10, HSA14** and **HSA18** by SEM (Figure 103).

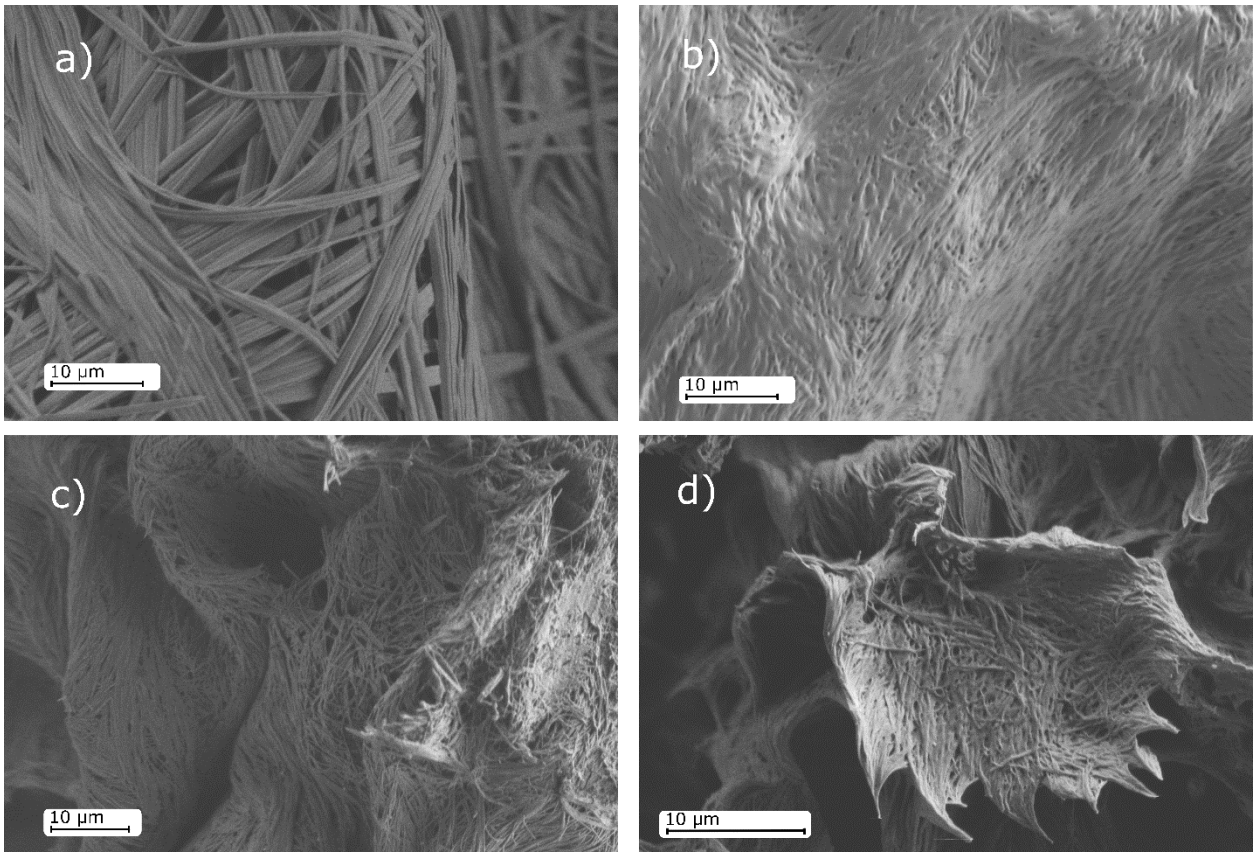


*Figure 103. SEM images of the HSA based xerogels extracted from toluene : a) **HSA4**, b) **HSA10**, c)**HSA14** and d) **HSA18***

All gelators showed similar structures, including cylindrical curved fibers. However, **HSA4** presented fibers with higher diameter and a lower degree of entanglement than **HSA10**, **HSA14** and **HSA18**. Thus, except **HSA4**, the length of the alkyl chains of these organogelators did not present any alterations on the morphology of the gels fibers.

## 2.4. Molecular packing proposal

To predict the local structure of the gelators, the following protocol was applied: indexation using Dicvol on the X-ray patterns, Montecarlo simulation using Expo to obtain the average molecular position and instead of performing Rietveld refinement, the best structures were energetically optimized using Dreiding forcefield. We could not perform Rietveld refinement due to the broadness of the measured X-ray patterns. In an attempt to change as few variables as possible, the forcefield algorithm chosen to optimize energetically the structures was the same as used in the thiazole and bisamide based families of gelators where a combination Rietveld/energetic optimization was performed. The best candidates were chosen by comparing the fit between measured and simulated X-ray pattern and PDF measurement.

After the above-mentioned process, we were only able to obtain two models representing two possible conformations for **HSA8** (figure 104). Both models are packed in similar sized unit-cells and each represents different possibilities for hydrogen bonding within the molecular packing. Model HSA8.1 presents hydrogen bonding between the hydroxy group and the carbonyl oxygen forming dimers and also hydrogen bonding between the amides along the b axis of the unit cell (figure 105). Model HSA8.2 presents hydrogen bonding between two hydroxy groups of different molecules, forming anti-parallel dimers while the amide groups form hydrogen bonding along the b axis of the unit-cell (figure 105). Both models allowed simulate X-ray and PDF patterns in fair agreement with the experiment (table 15 and figures 106 and 107). However, the agreement is not perfect and it is difficult to base further work on these structures. The results for the other members of the family were similar.

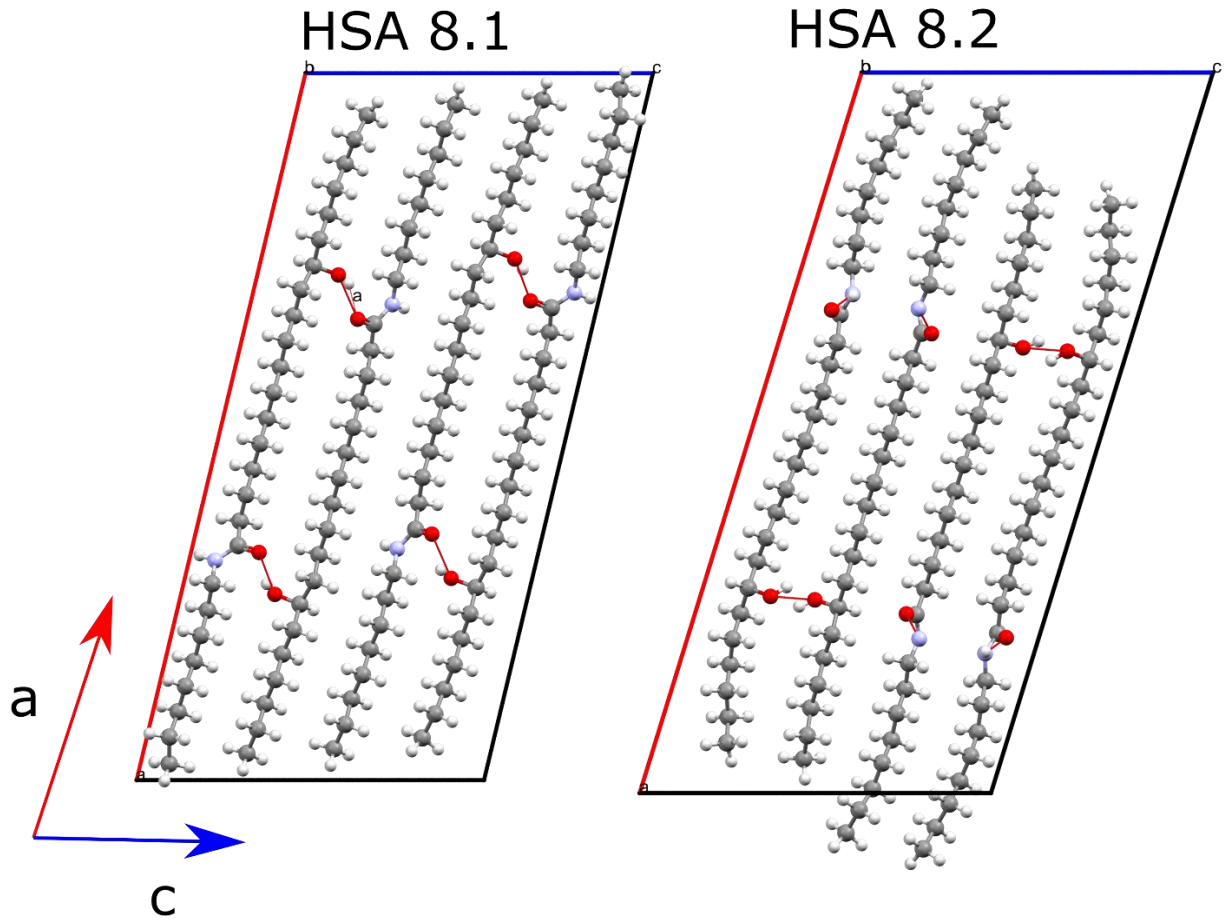


*Figure 104. Proposed models for the molecular packing of HSA based LMWG. Axes color: a (red), b (green) and c (blue)*

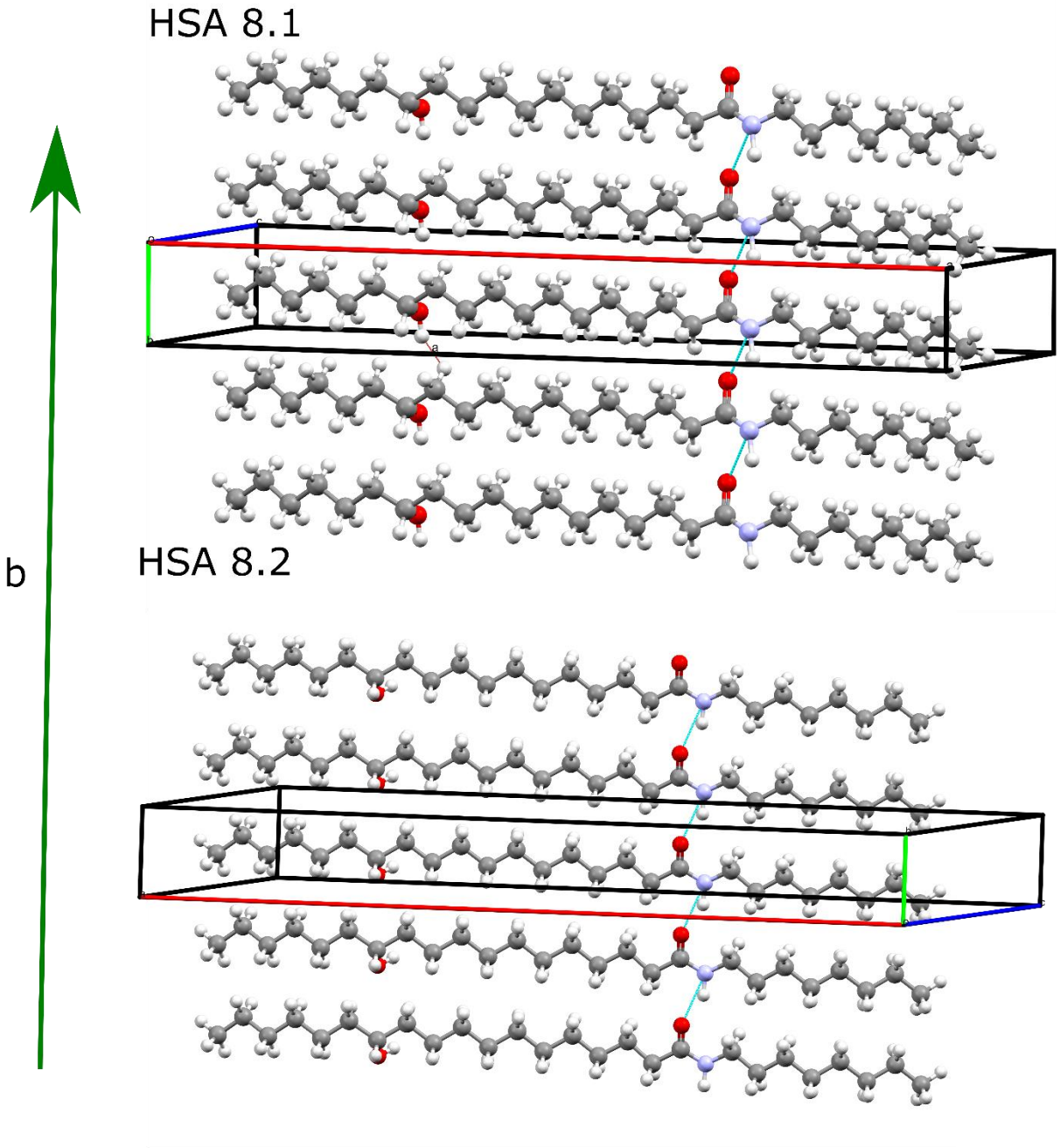


*Figure 105. Side view of the unit cell of both molecular packing proposals for **HSA8**. Axes color: a (red), b (green) and c (blue)*

*Table 15. Proposed unit cell parameters of the HSA8.1 and HSA8.2.*

| compound | | **HSA8.1** | **HSA8.2** |
|---|---|---|---|
| crystal system | | monoclinic | monoclinic |
| space group | | P2 | P21 |
| a(Å) | | 35.10 | 35.22 |
| b(Å) | | 4.06 | 4.16 |
| c(Å) | | 16.82 | 16.45 |
| α(deg) | | 90 | 90 |
| β(deg) | | 102.64 | 107.64 |
| γ(deg) | | 90 | 90 |
| volume ($Å^3$) | | 2377.13 | 2308.91 |
| Z | | 2 | 2 |
| Density $gcm^{-3}$ | | 1.11 | 1.18 |
| formula weight | | $C_{26}H_{53}NO_2$ | $C_{26}H_{53}NO_2$ |
| PDF | $X^2$ | 5.91891 | 5.3920482 |
| | Red. $X^2$ | 0.003116 | 0.0028514 |
| | RW | 0.651481 | 0.6218101 |
| X-ray | Rp | 33.9 | 50.13 |
| | Rwp | 42.815 | 66.021 |

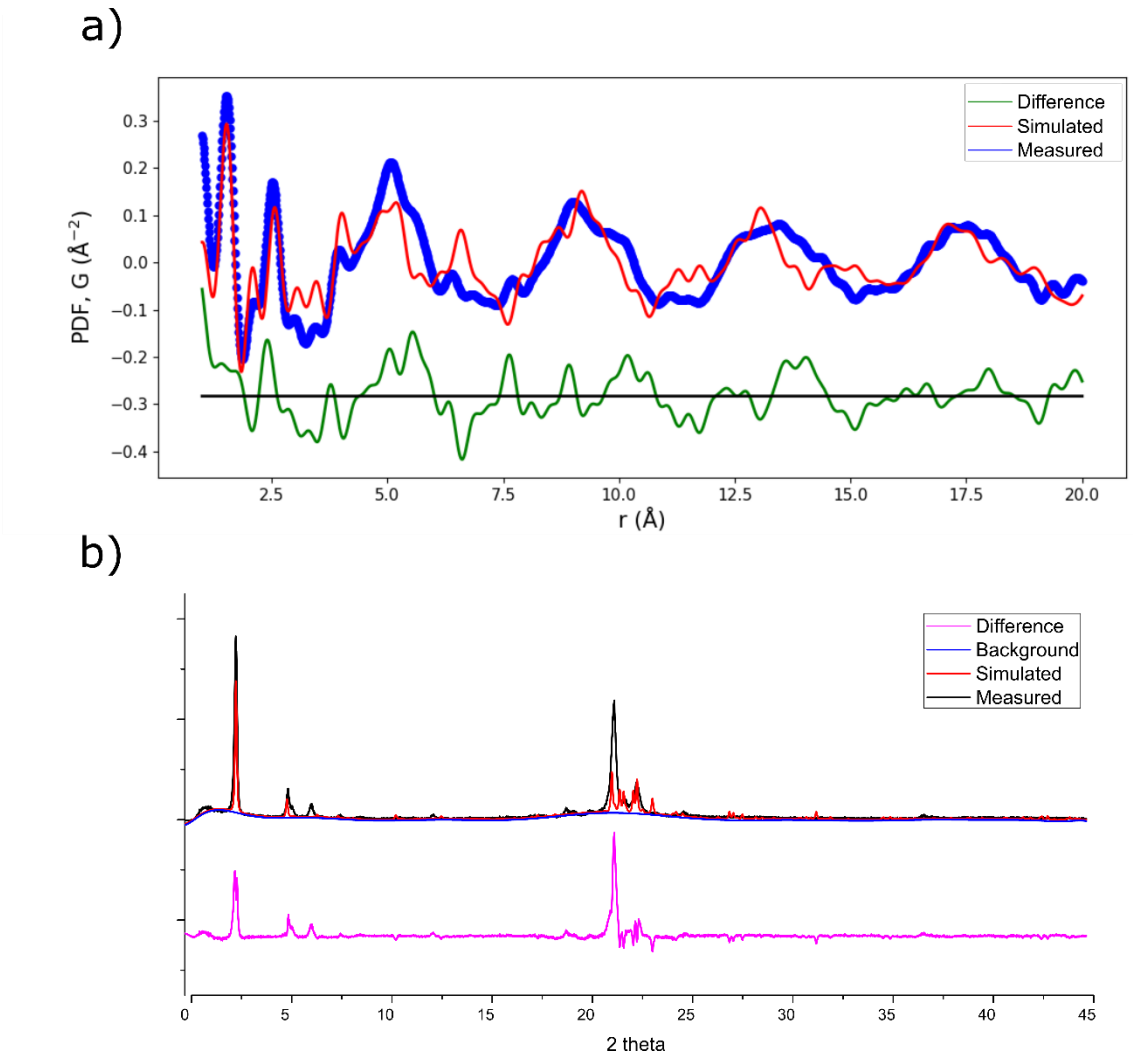


*Figure 107. Comparison between simulation (HSA8.1) and experiment (**HSA8** xerogel extracted from toluene) a) PDF b) X-ray pattern. X-ray wavelength of 1.5406 Å.*

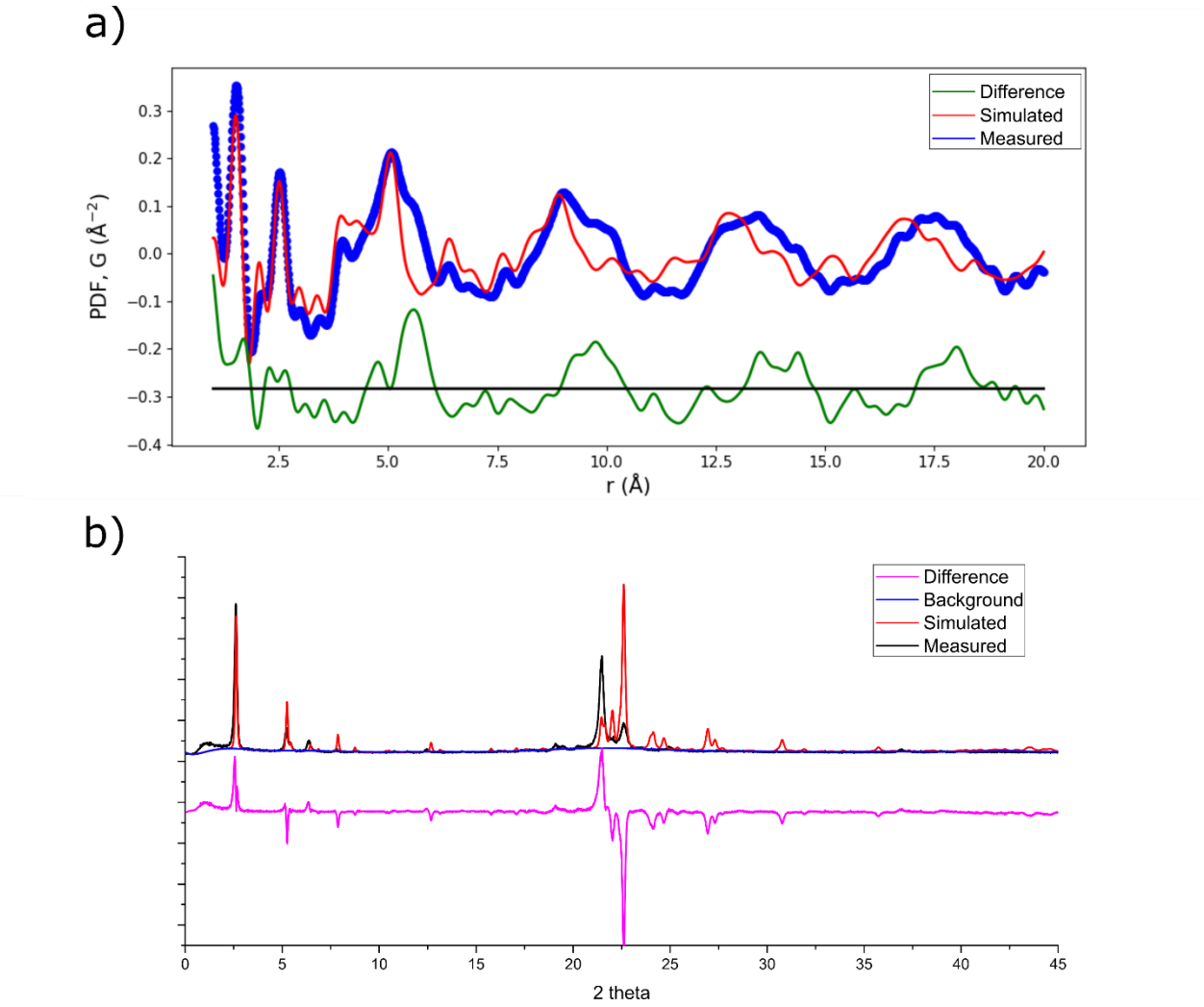


*Figure 108. a) Comparison between simulation (HSA8.2) and experiment (**HSA8** xerogel extracted from toluene) a) PDF b) X-ray pattern. X-ray wavelength of 1.5406 Å.*

## 2.5. Conclusion for HSA based gelators

The HSA based gelators present an apparently erratic movement of the center of the gelation sphere with the increase in length of the alkyl chain. In the original Hansen space characterization studied by Bouteiller et al.[6] it was proposed that **HSA 12** was an outlier, so that the three remaining systems (**HSA4**, **HSA8** and **HSA18**) seemed to present a regular trend. The study of new members of the family (**HSA10** and **HSA14**) clearly allows to rule out this hypothesis.

Structural analysis of the gels fibers was performed in order to understand this complex behavior. PDF analysis shows that all members of the family present a similar local structure. X-ray diffraction shows that the fibers have a poor long-range order so that it is difficult to determine the exact molecular packing. Nevertheless, the first diffraction peak can be used to show that the longest periodicity increases linearly from **HSA8** to **HSA14**, but that **HSA4** and **HSA18** do not follow this linear trend. FTIR spectroscopy also hints at a slightly less strongly hydrogen bonded structure for **HSA18** compared to the other members of the family. At a larger scale, SEM showed that the gel fibers of **HSA4** present a diameter that is significantly larger than for other gelators. **HSA4** gel fibers also present a melting point that is higher than expected based on the trend observed with the remaining organogelator members. Overall, only **HSA8**, **HSA10**, **HSA12** and **HSA14** can be considered to share exactly the same structural features.

Therefore it seems reasonable to exclude **HSA4** and **HSA18** from the gelation data. The analysis of the gelation data of **HSA8**, **HSA10**, **HSA12** and **HSA14** then produces a regular trend: the center of the gelation sphere moves to a region of lower polarity as the length of the alkyl chain is increased.

# 3. Remarks

This chapter presented a class of organogelators whose gelation domains apparently behave in an erratic fashion when subject to the elongation of the alkyl chains.

Concerning the first family (hydrazide based gelators), only one member of the family (**Hydra8**) was found to have a packing slightly different from the other members of the family. Even if **Hydra8** is removed from the study, the gelation data is still very complex. A possible explanation could be the presence of different crystal habits within the family. Even though the molecular packing seems to evolve regularly within the family, we cannot exclude that crystals with different crystallographic faces are formed. If this alteration does not happen in a continuous way, the surface energy of a gel fiber could change abruptly, resulting in an erratic behavior of the center of the gelation spheres.

Concerning the second family (HSA based gelators) it is also possible that a lack of regularity in the crystal habit is responsible for the apparently erratic gelation behavior. This is actually supported for

one member of the family (**HSA4**) by a different melting point and fiber morphology. It is also possible that the slight differences in molecular packing (**HSA18**) that have been detected are responsible for the unregular behavior. If both **HSA4** and **HSA18** are put aside, the remaining data seems to follow the trend detected for the systems described in chapter 3.

# 4. References and notes


1 K. Tomioka, T. Sumiyoshi, S. Narui, Y. Nagaoka, A. Iida, Y. Miwa, T. Taga, M. Nakano and T. Handa, *J. Am. Chem. Soc.*, 2001, **123**, 11817–11818.

2 The simulated pattern of the single crystal structure should show a diffraction peak corresponding to the full length of the c axis, but due to conditions for possible reflections associated to the space group (the molecular packing repeats itself along the c axis) the first diffraction peak observed is in fact the 002 hkl (the symmetry group $I_2/a$ does not contain the 001 hkl).

3 If the alkyl chains were parallel to the c axis, an increase of 3.6 Å would be expected. The value of 2.1 Å corresponds to a tilt of the alkyl chains by an angle of 54° from the c axis.

4 K. Iimura, Y. Nakajima, T. Kato, *Thin Solid Films*, 2000, **379**, 230-239.

5 V. A. Mallia, M. George, D. L. Blair and R. G. Weiss, *Langmuir*, 2009, **25**, 8615–8625.

6 J. Bonnet, G. Suissa, M. Raynal and L. Bouteiller, *Soft Matter*, 2015, **11**, 2308–2312.

7 J. Coates, "Interpretation of infrared spectra, a practical approach." Encyclopedia of analytical chemistry: applications, theory and instrumentation, 2006

# 15. General conclusion

The main objectives of this thesis were to improve the methodology used to rationalize organogelation using the Hansen solubility parameters and to investigate how variations in the structure of an organogelator would affect the gelation proprieties. This last point was studied by observing the effect that changing the length of linear alkyl chains can have on the molecular packing within gel fibers, the fiber morphology and finally on the gelation sphere in the Hansen space.

We chose to use X-ray diffraction techniques to characterize the organogelator systems and obtain a clear idea of how organogelators assemble in the gel state. In order to obtain a model of the gelators molecular packing we first performed X-ray powder diffraction on dried gel fibers. Diffraction had to be performed on dry gels because on native gels, only the diffraction pattern corresponding to the liquid part of the system could be observed. Upon performing X-ray diffraction of several organogelators we observed two different types of diffraction patterns. Some gel networks resulted in diffraction patterns containing several sharp diffraction peaks, while others presented few broad peaks. Sharp diffraction peaks are characteristic of structures that are well organized and present long range order. For gelators that present such diffraction patterns two methods were used to solve the molecular packing structure. The first one is to compare the diffraction pattern of the dried gel fibers with a simulated pattern from a single crystal structure of the same molecule. If the patterns match, the molecular packing structures are the same. In the event when there is no single crystal structure available for a given gelator we need to apply a different method called direct space method. This method based on computational simulation techniques involves the indexation of the powder pattern to uncover the unit cell, Montecarlo simulation to find the average atomic positions and finally a structure position refinement based on Rietveld methodologies. If a gelator presents a pattern with broad peaks, this indicates that these molecules assemble in a poorly organized manner. With these gelators it is only possible to study the local structure, since no long range periodicities are available. To do so we resorted to the PDF method to study the local structure. We performed the same indexation and Montecarlo simulation used in the direct space method without the final Rietveld refinement, since the broad peaks of the diffraction patterns do not provide enough information. The best possible structure was then energetically optimized and compared with the PDF analysis. These two approaches allowed us to study different types of gelators molecular packing to better understand the mechanisms of self-assembly and correlate them with the thermodynamic Hansen solubility parameters.

After compiling different protocols to study the molecular packing of organogelators we focused our attention on the methodology used to rationalize organogelation with the Hansen solubility parameters, particularly the data treatment section that involves the determination of the gelation domains. Rationalizing organogelation with the Hansen solubility parameters is based on determining a gelation domain in resemblance to what is done when studying the solubility of a compound using the Hansen solubility parameters, but this does not mean that both domains need to be determined the same way. The solubility domain in the Hansen space is determined by creating the smallest sphere that includes the majority of liquids that solubilize the target compound and excludes that majority of liquids that do not solubilize the target compound. The first attempt to determine a gelation domain followed the same guidelines, the smallest sphere was created that included the majority of gelated liquids and excluded the majority of liquids that solubilized or precipitated the target gelator. This method was able to describe some of our gelator systems, but not all. Of course, in order to be able to compare various systems together, there was a need for a general methodology to successfully determine the gelation sphere of all organogels. After comparing the various methodologies proposed in the literature, we developed the AO method and validated it against a comprehensive database. This method consists in forming the smallest sphere that includes the majority of gelated liquids and excludes the majority of liquids that precipitate the gelator, with no consideration of the liquids that solubilize the gelator. The biggest advantage of this methodology is that it allows the overlap of the solubility and gelation spheres without forcing it. This method resulted in the same number (or less) of outliers when compared with other methods.

Having compiled these tools to solve molecular packing from powder diffraction and improved the data treatment to determine the gelation domain in the Hansen space, we were ready to investigate the effect that an alteration in a molecule can have on its gelation proprieties. The structural alteration chosen in our case was the variation of the length of a linear alkyl chain. Many LMWG contain in their structures one or more linear alkyl chains, that contribute to the gel formation through van der Waals interactions. Also, the variation of the length of an alkyl chain is easily achievable during the synthesis without any extra steps. Five families of organogelators were chosen, where within the same family the main structure was preserved, and different members were synthesized with alkyl chains of different length. The families of gelators contained from one up to three linear alkyl chains, and the main driving force to trigger fiber formation was provided by hydrogen bonding or π-π stacking. One of the most important information for rationalizing organogelation that we obtained, concerns the polymorphism of organogelators. Four out of the five families of gelators studied presented the same molecular packing independently of the liquid gelated. Only one family presented polymorphism depending on the gelated liquid. Moreover, this family unexpectedly showed that the different polymorphs did not form clusters in Hansen space but were scattered within the gelation

sphere. This means that, at least for this particular family, the formation of polymorphs does not impact the method used to determine the gelation sphere.

Upon characterizing the Hansen space of each family we observed that the variation of the length of the alkyl chain resulted in three different behaviors.

Two families presented a smooth gelation trend by showing a linear increase or decrease of the radius of the gelation sphere and a linear drift of the centers of the gelation sphere to a region of lower polarity in the Hansen space as the length of the linear alkyl chains increased. The movement of the center of the gelation spheres respected a linear trend that makes possible the prediction of the center of the gelation of an untested gelator from the same family. Within these gelators the elongation of the alkyl chains did not result in an alteration of the morphology of gel fibers or molecular packing conformations. The linear move of the center of the gelation sphere was attributed to the increase in exposure of alkyl chains at the fiber/liquid interface as the alkyl chains are elongated, which results in the decrease of the polar nature of the surface of the gels fibers. When the surface of the gel fibers becomes less polar, the center of the gelation spheres moves to a less polar region of the Hansen space.

The second type of behavior observed was only observed in one family of organogelators. In this case, the increase in alkyl chains length did not produce any significant alteration in the radius or center of the gelation spheres. These organogelators self-assemble in a fashion where the alkyl chains are always radiating perpendicularly from the axis of the fibers. If all lateral planes of the local structure are filled by the radiating alkyl chains it is easy to assume that the surface of the gel fibers are also covered by these, probably disordered, alkyl chains. Thus, the elongation of such chains should not alter the thermodynamic stability of surface of the fibers and by consequence the gelation spheres should not be highly affected by the elongation of the alkyl chains.

The last two families of gelators presented an apparently erratic gelation behavior with the variation of the length of the alkyl chains. This behavior consisted in a non-monotonous variation of the radius and center of the gelation spheres when increasing the alkyl chains. Structural characterization studies did not present strong evidence to explain the erratic behavior. Mostly fiber morphology and molecular packing remained similar despite the length of the alkyl chains. The reason for the erratic behavior is still unexplained. Without concrete proof we were only able to theorize that the erratic behavior could be linked to differences in the crystal habit of these molecules.

In conclusion the main contributions of this thesis can be divided in four parts, 1- compilation of tools to solve molecular packing from gel fibers; 2 – improvement of the methodology to rationalize organogel formation in the framework of the Hansen solubility parameters; 3 – discovering that the variation of length of an organogelator alkyl chain can result in various evolutions of the gelation behavior; and 4 – solving the molecular packing of several organogelators, which can be used to

better understand the mechanisms of self-assembly that result in gelation.

Future perspectives of this work require applying computational methods to simulate the Hansen solubility parameters of gelation of a target compound. As already mentioned, a target compound will be miscible with a liquid if both have similar Hansen solubility parameters. We believe that for the phenomenon of organogelation to occur the liquid should allow the gelator to crystalize preferential in one direction, i.e it should make the crystallization much faster in the fiber growth plane than in other directions. It is this rapid crystallization in one direction that favors the formation of a gel fiber instead of a single crystal. Thus, our hypothesis is that organogelation occurs when the Hansen solubility parameters of the growth plane is significantly different from the Hansen solubility parameters of the liquid (promoting aggregation in this direction) and when Hansen solubility parameters of the crystallographic planes containing the fiber axis are similar to the Hansen solubility parameters of the liquid, (decreasing the aggregation of the sides of the fibers). To verify this hypothesis the molecular packing models obtained in this thesis should be used to extract the Hansen solubility parameters from the different faces of the crystal habit and then compare them with the experimental results obtained from the characterization of the Hansen space. The successful realization of this hypothesis would bring to the scientific community a methodology that would predict the gelation Hansen solubility parameters of a LMWG only by studying the molecular packing, thus decreasing greatly the time and cost of laboratory work. Such calculations could also provide some explanation for the erratic behavior of some families of gelators since an in-depth thermodynamic study of the molecular packing models will provide much more information about the crystal habit.

From a different point of view, more work is needed to understand how organogelation can be rationalized with the Hansen solubility parameters. At the present moment this methodology is already able to predict which liquids can be gelated with a given gelator. We also started to understand the effect that the length of a linear alkyl chain has on gelation but, there are many other structural alterations that should be studied. Such alterations include the variation of hydrogen donors and acceptors (hydroxyl groups, amino), the position and nature of an electrodonating or electroaccepting substituent in an aromatic group or just the presence of different halogens in the molecular structure. Despite the huge remaining task, this methodology is already showing promising results in order to one day be able to predict if a molecule will from a gel in a specific liquid without the need of extensive laboratory work.

# 16. Annexes

## I. Procedure to characterize the Hansen space

To correlate the gelation of a LMWG with HSP the first step is to collect a consistent dataset of liquids that interact differently with the LMWG (forming a solution, gelling the liquids or precipitating the gelator).[10] The robustness of the prediction heavily depends on the quality of the Hansen space characterization, and to do so the choice of test liquids is crucial. All gelation tests have to be performed in identical conditions (e.g. concentration, dissolution temperature, cooling rate) and in a range of liquids widely distributed in Hansen space. To choose a proper list if solvents a two-step procedure is used. In the first step, about 20 liquids of known HSPs are selected so that they are homogeneously scattered in Hansen space. Table S1 in the Annexes chapter contains a list of 21 different solvents that illustrate this first step. The second step is then to select solvents that were gelated and perform mixtures with solvents that did not gelate. Solubility tests performed with these mixtures will increase the definition of the characterization of the Hansen space around the cluster of gelated solvents.

***Table S1. List of pure liquids used in solubility tests.***

| **Liquid** | $\delta_D$ ($MPa^{1/2}$) | $\delta_P$ ($MPa^{1/2}$) | $\delta_H$ ($MPa^{1/2}$) |
|---|---|---|---|
| **acetonitrile** | 15.3 | 18 | 6.1 |
| **benzyl alcohol** | 18.4 | 6.3 | 13.7 |
| **1-butanol** | 16 | 5.7 | 15.8 |
| **t-butyl acetate** | 15 | 3.7 | 6 |
| **1-chloropentane** | 16 | 6.9 | 1.9 |
| **chlorobenzene** | 19 | 4.3 | 2 |
| **cyclohexane** | 16.8 | 0 | 0.2 |
| **cyclohexanone** | 17.8 | 8.4 | 5.1 |
| **diacetone alcohol** | 15.8 | 8.2 | 10.8 |
| **dimethylformamide (DMF)** | 17.4 | 13.7 | 11.3 |
| **dimethylsulfoxide (DMSO)** | 18.4 | 16.4 | 10.2 |
| **1,4-dioxane** | 17.5 | 1.8 | 9 |
| **ethanolamine** | 17 | 15.5 | 21 |
| **hexadecane** | 16.3 | 0 | 0 |
| **methanol** | 14.7 | 12.3 | 22.3 |
| **methylethylketone (MEK)** | 16 | 9 | 5.1 |
| **N,N-diethyl acetamide** | 16.4 | 11.3 | 7.5 |
| **propylene carbonate** | 20 | 18 | 4.1 |
| **propylene glycol** | 16.8 | 10.4 | 21.3 |
| **toluene** | 18 | 1.4 | 2 |
| **water** | 15.5 | 16 | 42.3 |
| **N-methylformamide** | 17.4 | 18.8 | 15.9 |

# II. Examples of application of the AO method

## II.1. Comparison between NO method and AO method

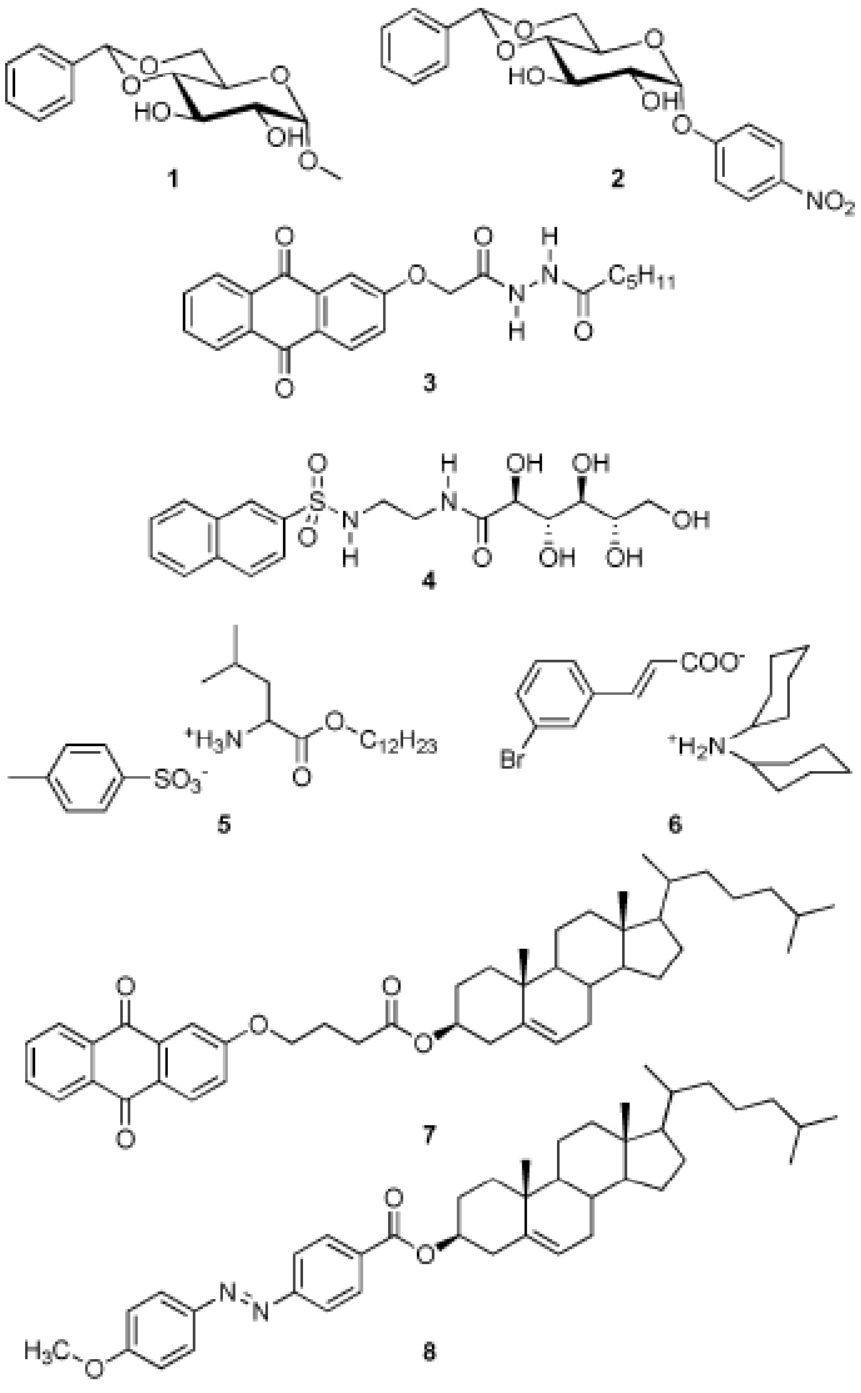


**Scheme 1**

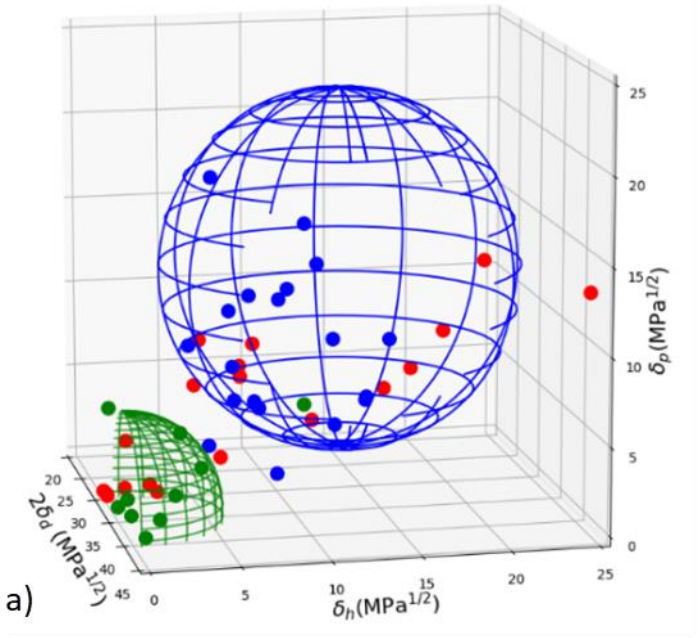


Gelation sphere data

b)

| | NO method | AO method |
|---|---|---|
| $\delta_d$ (MPa$^{1/2}$) | 17.37 | 18.69 |
| $\delta_p$ (MPa$^{1/2}$) | 0 | 0 |
| $\delta_h$ (MPa$^{1/2}$) | 0.88 | 0.91 |
| radius | 5 | 5.4 |
| Wrong in | 3 | 2 |
| Wrong out | 4 | 3 |

**Figure S1. (a)** Solubility data for LMWG **1** (scheme 1) represented in Hansen space (data taken from reference[1] and previously treated with the NO method[2]). Liquids are represented by full circles and calculated domains are represented by meshed spheres. Green: gel; Red: precipitate. Blue: soluble. The solubility sphere was calculated using the HSPiP[3–5] software [$\delta_D$ = 18.85; $\delta_P$ =14.17; $\delta_H$ = 12.05; $R_{Sol}$ = 10.3 MPa$^{1/2}$] and the gelation sphere was calculated with the AO method using the HSPiP[3–5] software. **(b)** Centre, radius and outliers of the gelation sphere from the NO method and the AO method.

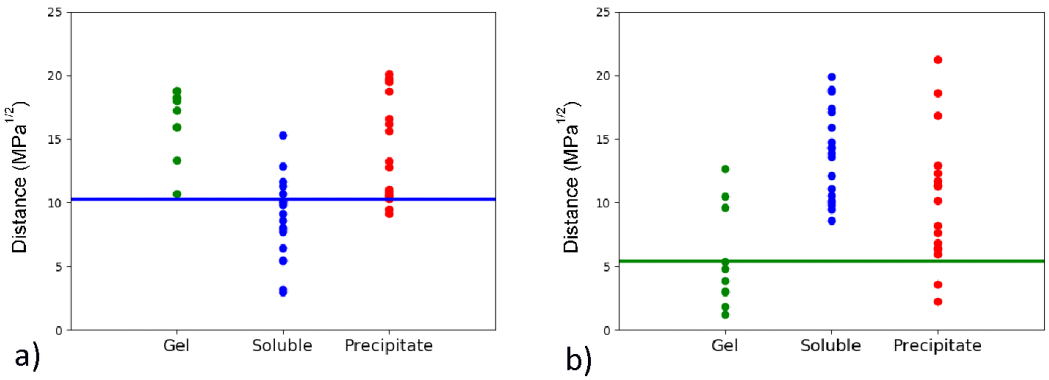


**Figure S2.** Distances in Hansen space to the center of the solubility sphere **(a)** or to the center of the gelation sphere **(b)** for LMWG **1** (AO method). The lines represent the radius of the spheres. Green: gel; Red: precipitate. Blue: soluble.

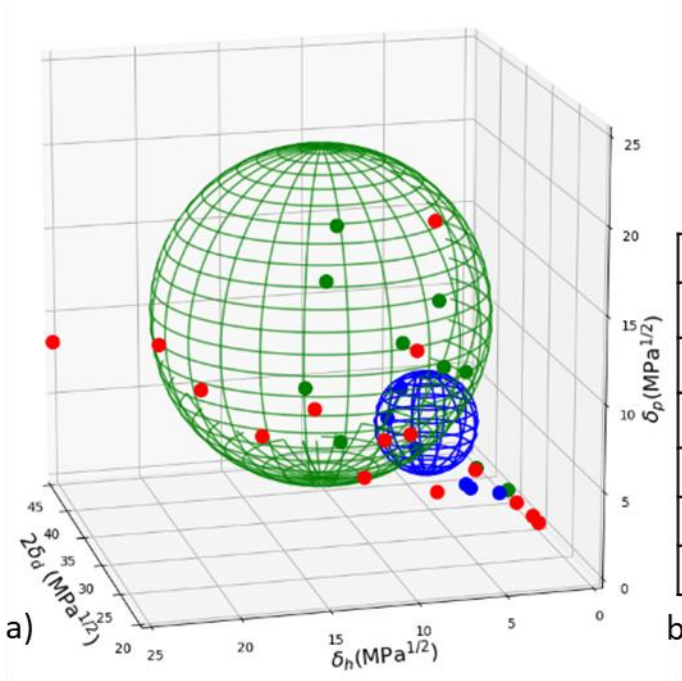


Gelation sphere

b)

| | NO method | AO method |
|---|---|---|
| $\delta_d$ (MPa$^{1/2}$) | 23.83 | 20.27 |
| $\delta_p$ (MPa$^{1/2}$) | 13.96 | 10.09 |
| $\delta_h$ (MPa$^{1/2}$) | 0 | 10.13 |
| radius | 17.2 | 10 |
| Wrong in | 0 | 0 |
| Wrong out | 3 | 2 |

**Figure S3. (a)** Solubility data for LMWG **2** (scheme 1) represented in Hansen space (data taken from reference [6] and previously treated with the NO method[2]). Liquids are represented by full circles and calculated domains are represented by meshed spheres. Green: gel; Red: precipitate. Blue: soluble. The solubility sphere was calculated using the HSPiP[3–5] software [$\delta_D$ = 17.31; $\delta_P$ = 4.9; $\delta_H$ = 5.37; $R_{Sol}$ = 3.0 MPa$^{1/2}$] and the gelation sphere was calculated with the AO method using the HSPiP[3–5] software. **(b)** Centre, radius and outliers of the gelation sphere from the NO method and the AO method.

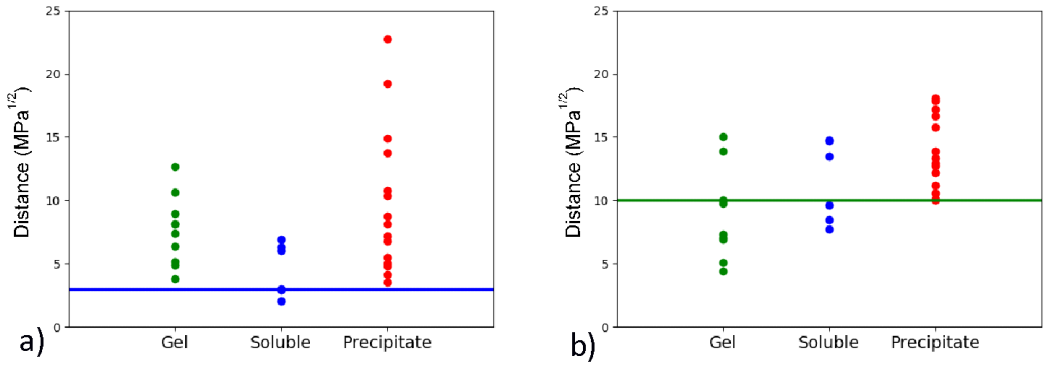


**Figure S4.** Distances in Hansen space to the center of the solubility sphere **(a)** or to the center of the gelation sphere **(b)** for LMWG **2** (AO method). The lines represent the radius of the spheres. Green: gel; Red: precipitate. Blue: soluble.

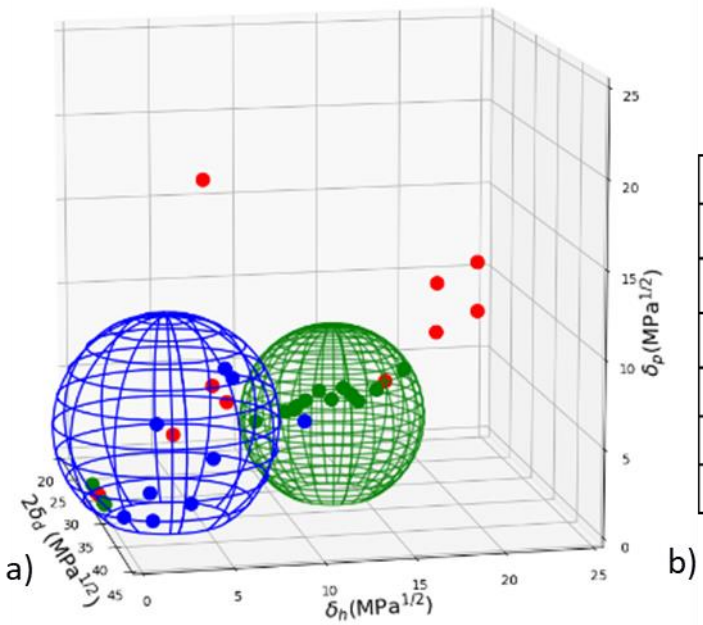


Gelation sphere

b)

| | NO method | AO method |
|---|---|---|
| $\delta_d$ (MPa$^{1/2}$) | 16.16 | 16.62 |
| $\delta_p$ (MPa$^{1/2}$) | 4.48 | 4.65 |
| $\delta_h$ (MPa$^{1/2}$) | 12.55 | 12.99 |
| radius | 5.5 | 5.2 |
| Wrong in | 1 | 1 |
| Wrong out | 3 | 3 |

**Figure S5. (a)** Solubility data for LMWG **3** (scheme 1) represented in Hansen space (data taken from reference[7] and previously treated with the NO method[2]). Liquids are represented by full circles and calculated domains are represented by meshed spheres. Green: gel; Red: precipitate. Blue: soluble. The solubility sphere was calculated using the HSPiP[3–5] software [$\delta_D$ = 18.31; $\delta_P$ = 5.36; $\delta_H$ =2.9; $R_{Sol}$ = 6.3 MPa$^{1/2}$] and the gelation sphere was calculated with the AO method using the HSPiP[3–5] software. **(b)** Centre, radius and outliers of the gelation sphere from the NO method and the AO method.

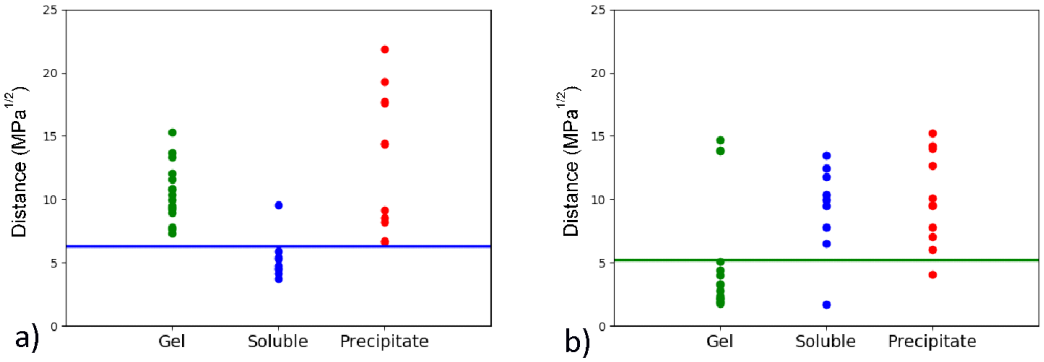


**Figure S6.** Distances in Hansen space to the center of the solubility sphere **(a)** or to the center of the gelation sphere **(b)** for LMWG **3** (AO method). The lines represent the radius of the spheres. Green: gel; Red: precipitate. Blue: soluble.

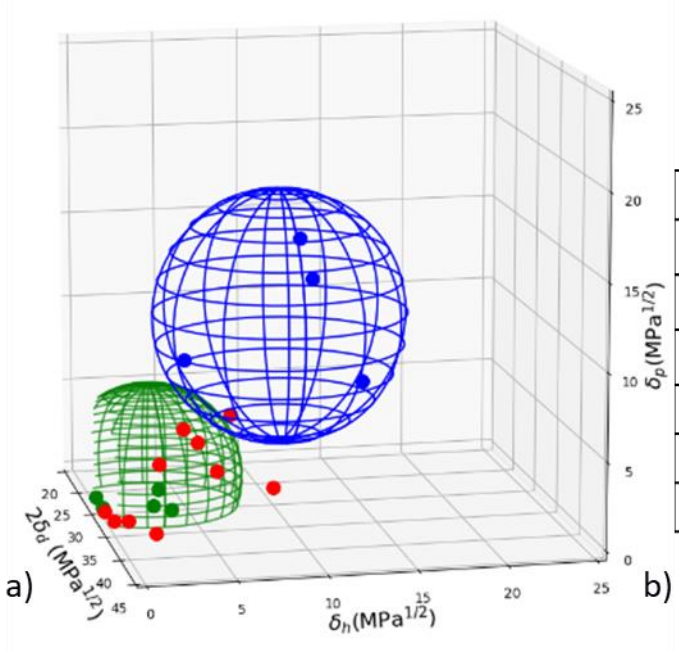


Gelation sphere

| | NO method | AO method |
|---|---|---|
| $\delta_d$ (MPa$^{1/2}$) | 15.87 | 15.42 |
| $\delta_p$ (MPa$^{1/2}$) | 0.08 | 1.83 |
| $\delta_h$ (MPa$^{1/2}$) | 5.44 | 2.66 |
| radius | 5.5 | 5.3 |
| Wrong in | 1 | 2 |
| Wrong out | 3 | 0 |

**Figure S7. (a)** Solubility data for LMWG **4** (scheme 1) represented in Hansen space (data taken from reference[8] and previously treated with the NO method[2]). Liquids are represented by full circles and calculated domains are represented by meshed spheres. Green: gel; Red: precipitate. Blue: soluble. The solubility sphere was calculated using the HSPiP[3–5] software [$\delta_D$ = 18.29; $\delta_P$ = 12.05; $\delta_H$ = 9.11; $R_{Sol}$ = 7.1 MPa$^{1/2}$] and the gelation sphere was calculated with the AO method using the HSPiP[3–5] software. **(b)** Centre, radius and outliers of the gelation sphere from the NO method and the AO method.

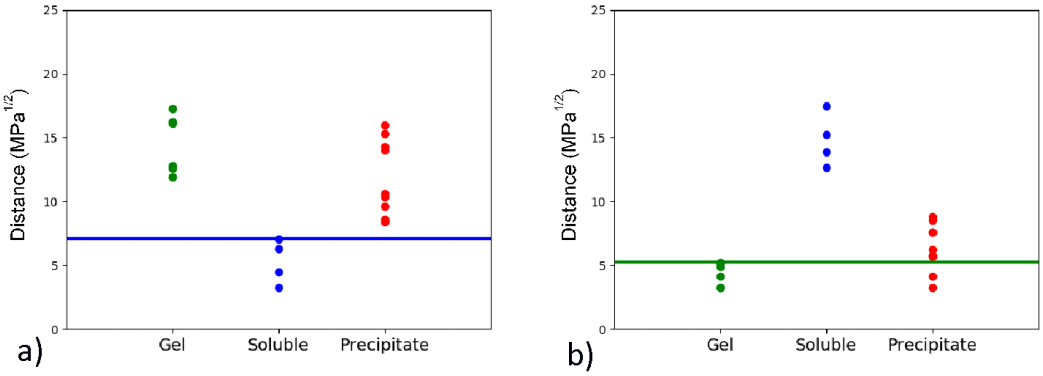


**Figure S8.** Distances in Hansen space to the center of the solubility sphere **(a)** or to the center of the gelation sphere **(b)** for LMWG **4** (AO method). The lines represent the radius of the spheres. Green: gel; Red: precipitate. Blue: soluble.

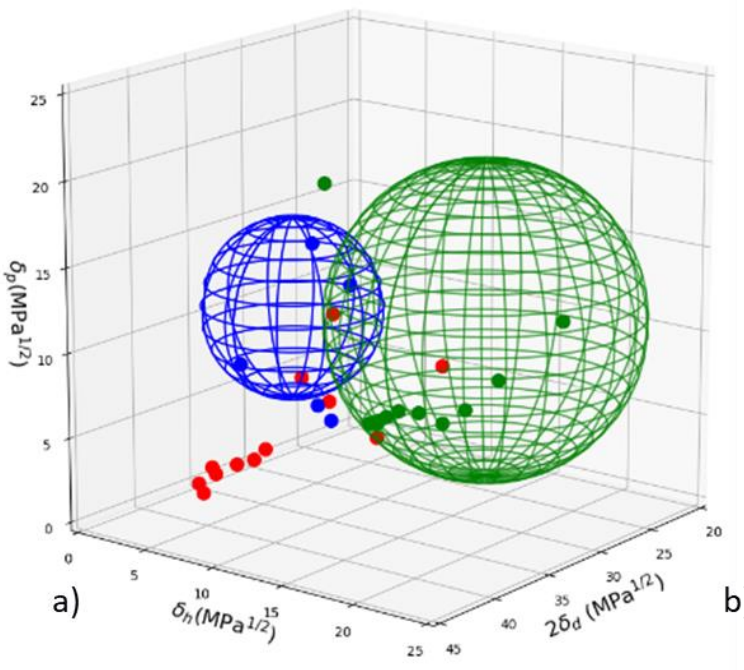


Gelation sphere

| | NO method | AO method |
|---|---|---|
| $\delta_d$ (MPa$^{1/2}$) | 21.09 | 14.24 |
| $\delta_p$ (MPa$^{1/2}$) | 8.16 | 11.06 |
| $\delta_h$ (MPa$^{1/2}$) | 27.95 | 16.21 |
| radius | 20 | 9.3 |
| Wrong in | 2 | 1 |
| Wrong out | 2 | 2 |

**Figure S9. (a)** Solubility data for LMWG **5** (scheme 1) represented in Hansen space (data taken from reference[9] and previously treated with the NO method[2]). Liquids are represented by full circles and calculated domains are represented by meshed spheres. Green: gel; Red: precipitate. Blue: soluble. The solubility sphere was calculated using the HSPiP[3–5] software [$\delta_D$ = 18.65; $\delta_P$ =12.56; $\delta_H$ = 9.18; $R_{Sol}$ = 5.2 MPa$^{1/2}$] and the gelation sphere was calculated with the AO method using the HSPiP[3–5] software. **(b)** Centre, radius and outliers of the gelation sphere from the NO method and the AO method.

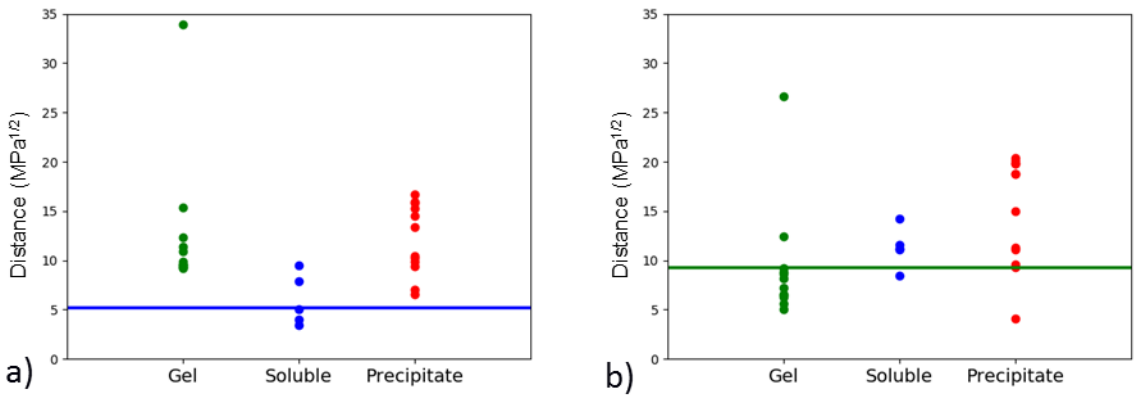


**Figure S10.** Distances in Hansen space to the center of the solubility sphere **(a)** or to the center of the gelation sphere **(b)** for LMWG **5** (AO method). The lines represent the radius of the spheres. Green: gel; Red: precipitate. Blue: soluble.

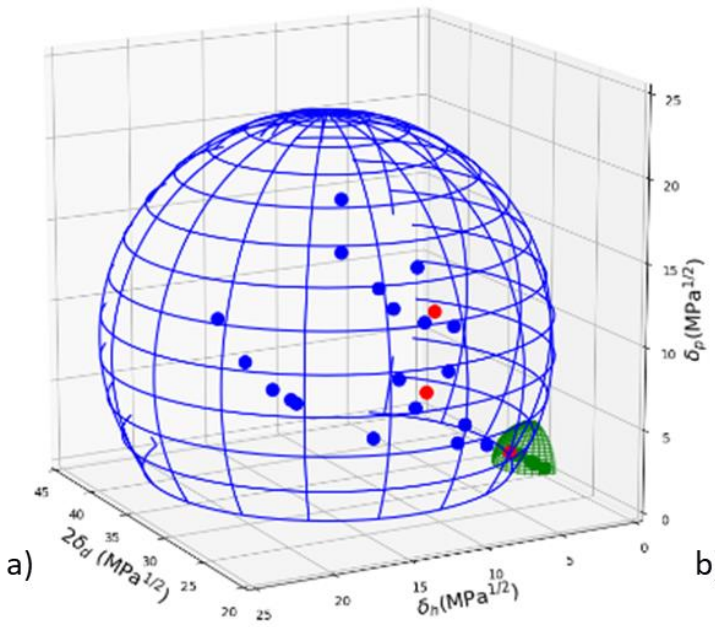


Gelation sphere

b)

| | NO method | AO method |
|---|---|---|
| $\delta_d$ (MPa$^{1/2}$) | 15.5 | 15.42 |
| $\delta_p$ (MPa$^{1/2}$) | 0.0 | 0.0 |
| $\delta_h$ (MPa$^{1/2}$) | 0.0 | 0.0 |
| radius | 2 | 2.6 |
| Wrong in | 0 | 0 |
| Wrong out | 0 | 0 |

**Figure S11. (a)** Solubility data for LMWG **6** (scheme 1) represented in Hansen space (data taken from reference[10] and previously treated with the NO method[2]). Liquids are represented by full circles and calculated domains are represented by meshed spheres. Green: gel; Red: precipitate. Blue: soluble. The solubility sphere was calculated using the HSPiP[3–5] software [$\delta_D$ = 18.09; $\delta_P$ = 8.11; $\delta_H$ = 11.45; $R_{Sol}$ = 13.7 MPa$^{1/2}$] and the gelation sphere was calculated with the AO method using the HSPiP[3–5] software. **(b)** Centre, radius and outliers of the gelation sphere from the NO method and the AO method.

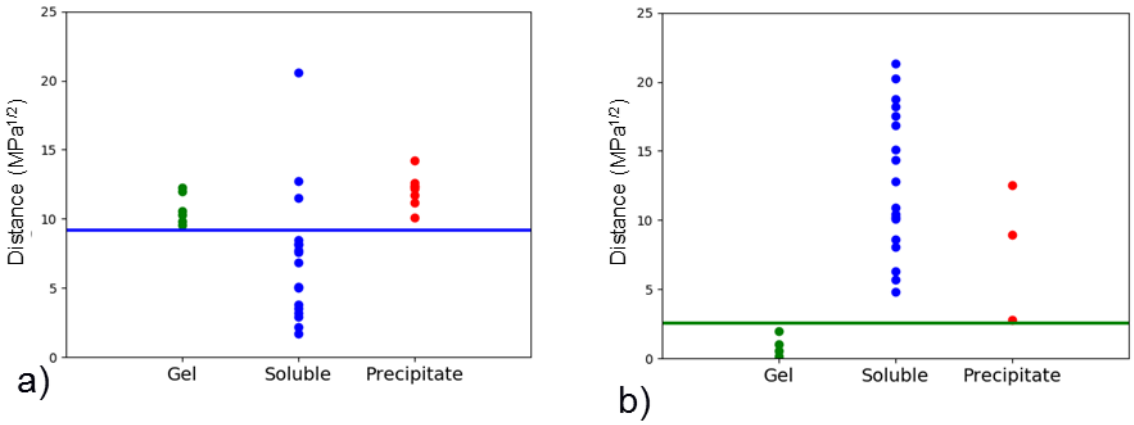


**Figure S12.** Distances in Hansen space to the center of the solubility sphere **(a)** or to the center of the gelation sphere **(b)** for LMWG **6** (AO method). The lines represent the radius of the spheres. Green: gel; Red: precipitate. Blue: soluble.

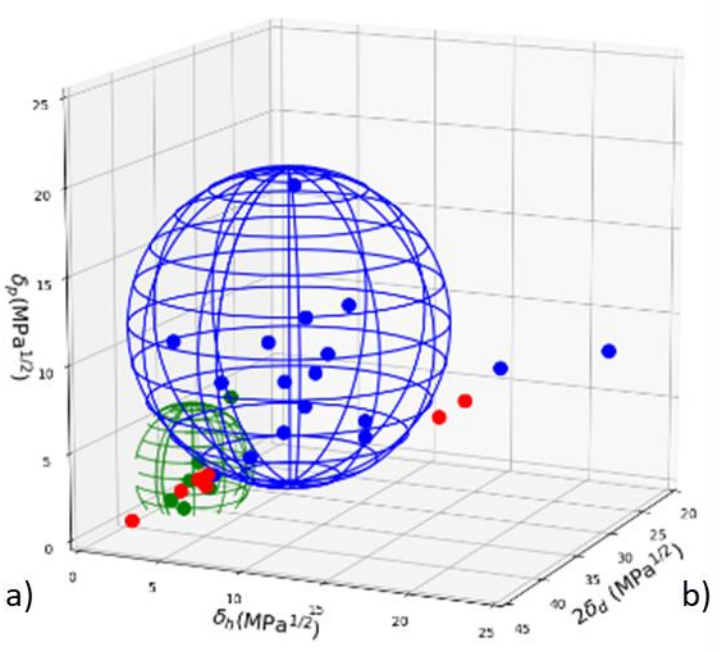


Gelation sphere

| | NO method | AO method |
|---|---|---|
| $\delta_d$ (MPa$^{1/2}$) | 18 | 17.96 |
| $\delta_p$ (MPa$^{1/2}$) | 1.0 | 2.31 |
| $\delta_h$ (MPa$^{1/2}$) | 2.04 | 2.11 |
| radius | 3.18 | 3.6 |
| Wrong in | 0 | 0 |
| Wrong out | 1 | 1 |

**Figure S13. (a)** Solubility data for LMWG **7** (scheme 1) represented in Hansen space (data taken from reference[11] and previously treated with the NO method[2]). Liquids are represented by full circles and calculated domains are represented by meshed spheres. Green: gel; Red: precipitate. Blue: soluble. The solubility sphere was calculated using the HSPiP[3–5] software [$\delta_D$ = 16.34; $\delta_P$ =10.18; $\delta_H$ = 6.78; $R_{Sol}$ = 9.2 MPa$^{1/2}$] and the gelation sphere was calculated with the AO method using the HSPiP[3–5] software. **(b)** Centre, radius and outliers of the gelation sphere from the NO method and the AO method.

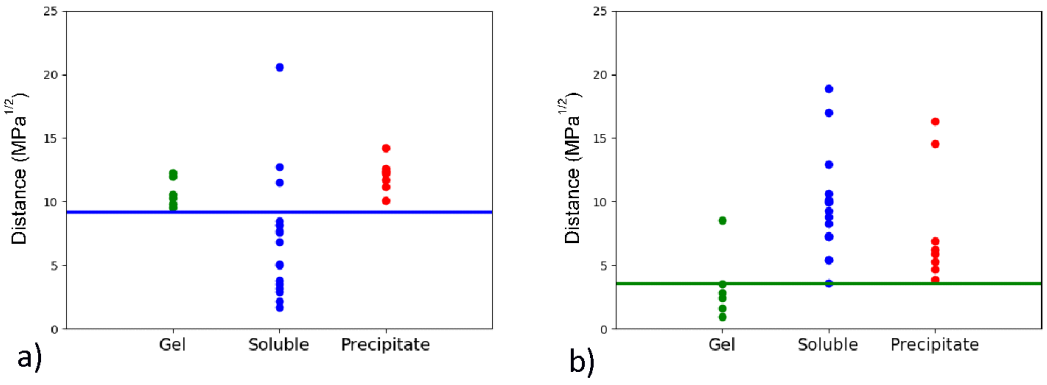


**Figure S14.** Distances in Hansen space to the center of the solubility sphere **(a)** or to the center of the gelation sphere **(b)** for LMWG **7** (AO method). The lines represent the radius of the spheres. Green: gel; Red:

precipitate. Blue: soluble.

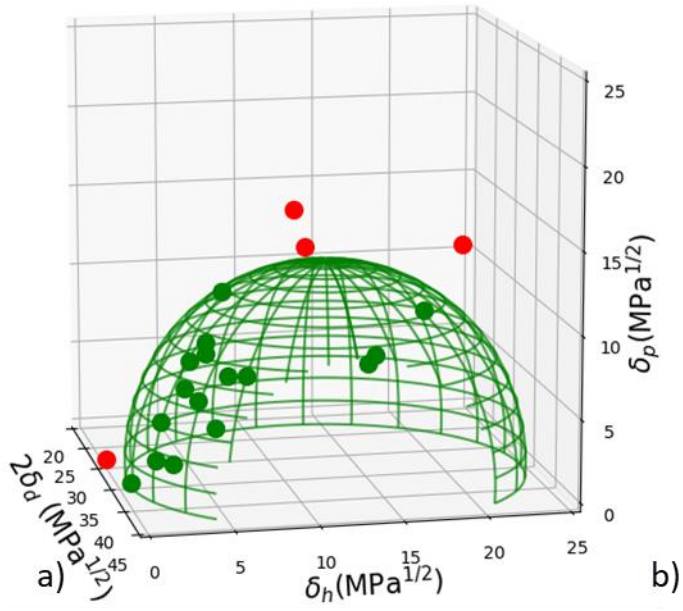


Gelation sphere

| | NO method | AO method |
|---|---|---|
| $\delta_d$ (MPa$^{1/2}$) | 18 | 18 |
| $\delta_p$ (MPa$^{1/2}$) | 1.0 | 1.0 |
| $\delta_h$ (MPa$^{1/2}$) | 12.31 | 12.31 |
| radius | 12 | 12 |
| Wrong in | 0 | 0 |
| Wrong out | 0 | 0 |

**Figure S15. (a)** Solubility data for LMWG **8** (scheme 1) represented in Hansen space (data taken from reference[12] and previously treated with the NO method[2]). Liquids are represented by full circles and calculated domains are represented by meshed spheres. Green: gel; Red: precipitate. **(b)** Centre, radius and outliers of the gelation sphere from the NO method and the AO method. Both methods are identical since no **S** points are present in the data.

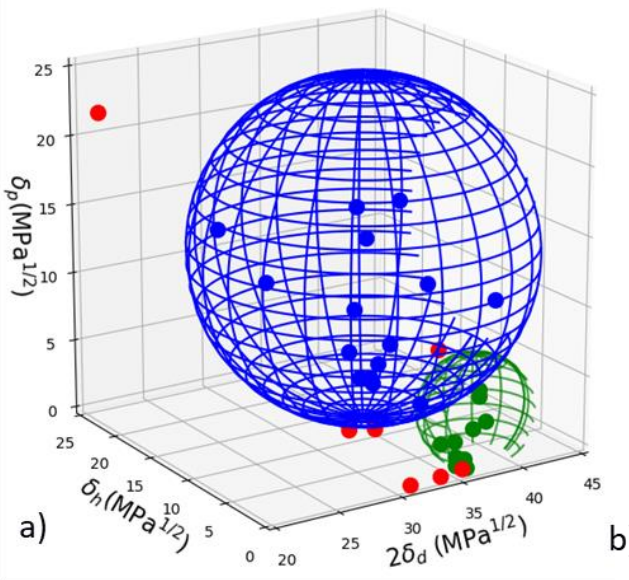


Gelation sphere

| | NO method | AO method |
|---|---|---|
| $\delta_d$ (MPa$^{1/2}$) | 18.80 | 18.87 |
| $\delta_p$ (MPa$^{1/2}$) | 2.86 | 3.29 |
| $\delta_h$ (MPa$^{1/2}$) | 2.20 | 2.02 |
| radius | 3.8 | 4.1 |
| Wrong in | 0 | 0 |
| Wrong out | 0 | 0 |

**Figure S16. (a)** Solubility data for LMWG **a1** reported by Brigitte Jamart-Grégoire et al.[13] (previously treated with the NO method[14]) represented in Hansen space. Liquids are represented by full circles and calculated domains are represented by meshed spheres. Green: gel; Red: precipitate. Blue: soluble. The solubility sphere was calculated using the HSPiP[3–5] software [$\delta_D$ = 17.70; $\delta_P$ = 12.34; $\delta_H$ = 12.50; $R_{Sol}$ = 12.4 MPa$^{1/2}$] and the gelation sphere was calculated with the AO method using the HSPiP[3–5]. **(b)** Centre, radius and outliers of the gelation sphere from the NO method and the AO method.

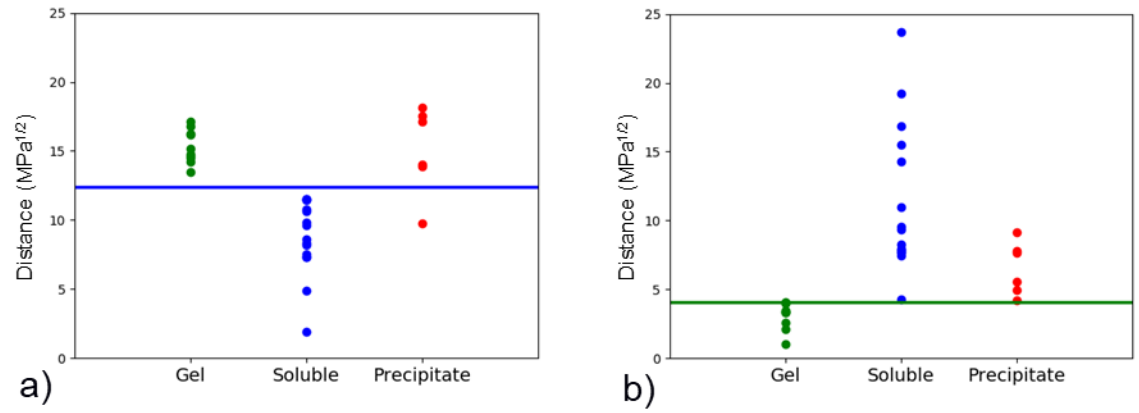


**Figure S17.** Distances in Hansen space to the center of the solubility sphere **(a)** or to the center of the gelation sphere **(b)** for LMWG **a1** (AO method). The lines represent the radius of the spheres. Green: gel; Red: precipitate. Blue: soluble.

# II.2. AO method applied to other studies

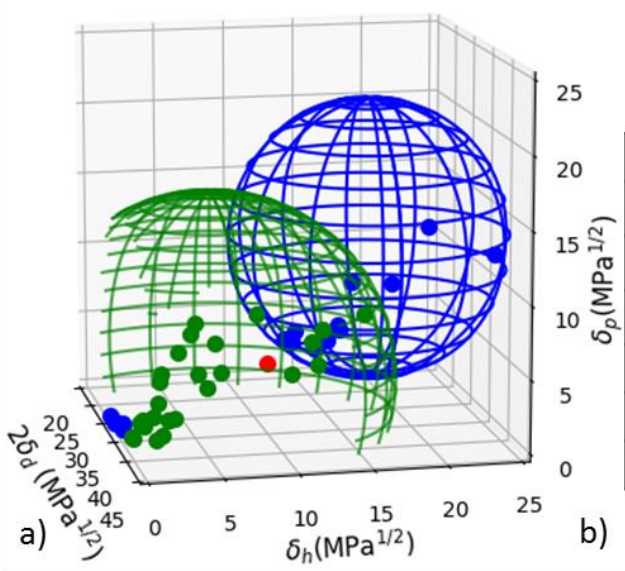


AO method

| | Solubility sphere | Gelation sphere |
|---|---|---|
| $\delta_d$ (MPa$^{1/2}$) | 15.43 | 17.76 |
| $\delta_p$ (MPa$^{1/2}$) | 11.9 | 3.94 |
| $\delta_h$ (MPa$^{1/2}$) | 17.93 | 5.95 |
| radius | 9.7 | 12.5 |
| Wrong in | 3 | 1 |
| Wrong out | 5 | 0 |

**Figure S18. (a)** Solubility data for methyl 4,6-O-(p-chlorobenzylidene)-□-D-glucopyranoside gelator reported by Rongxiu Feng et al[15] represented in Hansen space. Liquids are represented by full circles and calculated domains are represented by meshed spheres. Green: gel; Red: precipitate. Blue: soluble. The solubility sphere was calculated using the HSPiP[3–5] software and the gelation sphere was calculated with the AO method using the HSPiP[3–5]. **(b)** Centre, radius and outliers of the solubility and gelation spheres determined by the AO method.

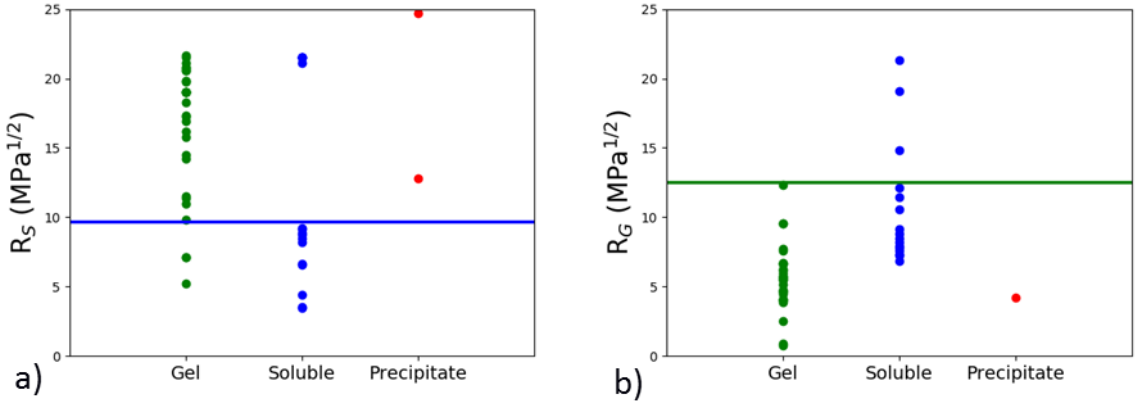


**Figure S19.** Distances in Hansen space to the center of the solubility sphere **(a)** or to the center of the gelation sphere **(b)** for LMWG presented in Figure S18. The lines represent the radius of the spheres. Green: gel; Red: precipitate. Blue: soluble

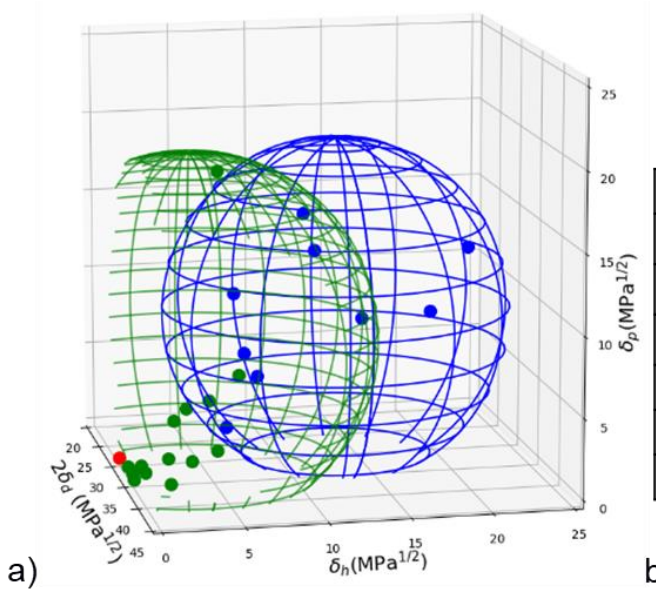


AO method

| | Solubility sphere | Gelation sphere |
|---|---|---|
| $\delta_d$ (MPa$^{1/2}$) | 16.72 | 18.36 |
| $\delta_p$ (MPa$^{1/2}$) | 9.60 | 8.94 |
| $\delta_h$ (MPa$^{1/2}$) | 12.96 | 3.27 |
| radius | 10.7 | 11.4 |
| Wrong in | 1 | 0 |
| Wrong out | 0 | 0 |

b)

**Figure S20. (a)** Solubility data for two-component acid−amine gelation system using G2-Lys and C6 and reported by David K. Smith et al[16] represented in Hansen space. Liquids are represented by full circles and calculated domains are represented by meshed spheres. Green: gel; Red: precipitate. Blue: soluble. The solubility sphere was calculated using the HSPiP[3–5] software and the gelation sphere was calculated with the AO method using the HSPiP[3–5]. **(b)** Centre, radius and outliers of the solubility and gelation spheres determined by the AO method. The reliability of the fit is compromised by the limited number of liquids tested (notably liquids with high $\delta_H$ values).

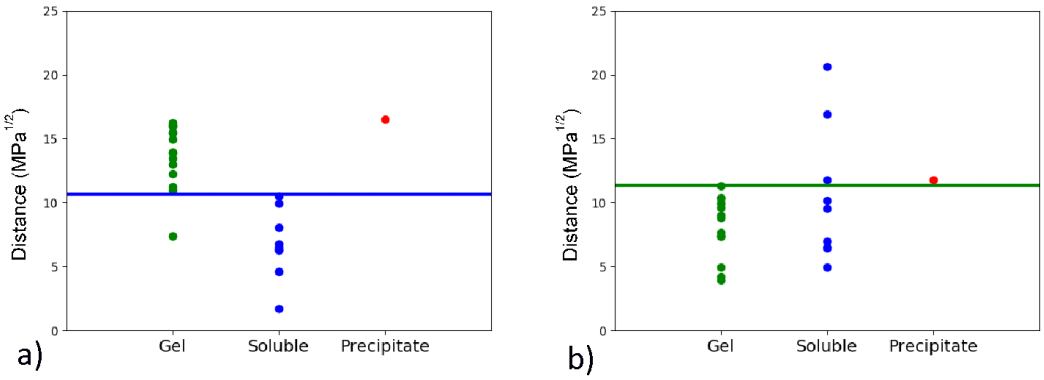


**Figure S21.** Distances in Hansen space to the center of the solubility sphere **(a)** or to the center of the gelation sphere **(b)** for LMWG presented in Figure S20. The lines represent the radius of the spheres. Green: gel; Red: precipitate. Blue: soluble

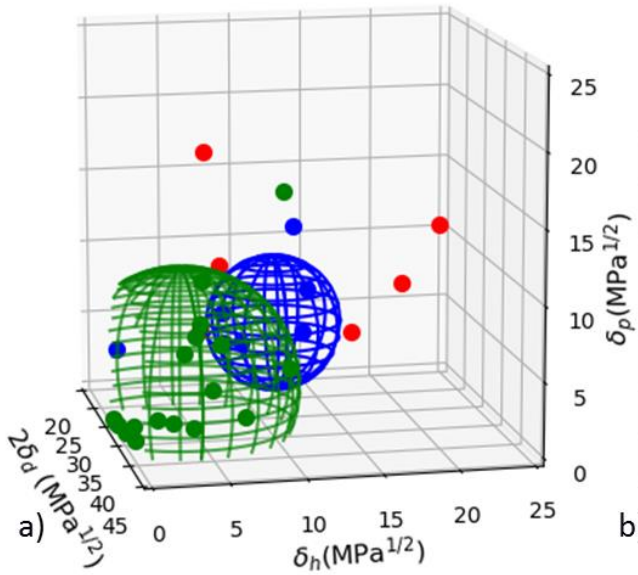


AO method

| | Solubility sphere | Gelation sphere |
|---|---|---|
| $\delta_d$ (MPa$^{1/2}$) | 15.84 | 17.30 |
| $\delta_p$ (MPa$^{1/2}$) | 6.51 | 3.31 |
| $\delta_h$ (MPa$^{1/2}$) | 10.60 | 3.83 |
| radius | 4.5 | 7.8 |
| Wrong in | 0 | 1 |
| Wrong out | 3 | 1 |

**Figure S22. (a)** Solubility data for 2,3-dihydroxycholestane steroids gelator reported by Pablo H. Di Chenna et al[17] represented in Hansen space. Liquids are represented by full circles and calculated domains are represented by meshed spheres. Green: gel; Red: precipitate. Blue: soluble. The solubility sphere was calculated using the HSPiP[3–5] software and the gelation sphere was calculated with the AO method using the HSPiP[3–5]. **(b)** Centre, radius and outliers of the solubility and gelation spheres determined by the AO method.

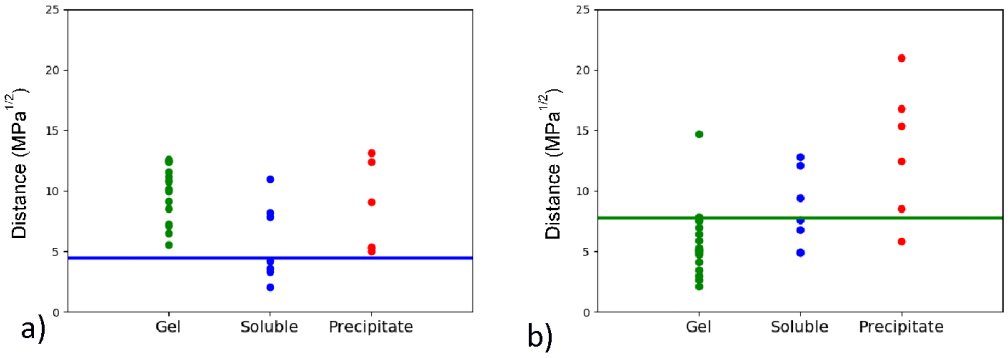


**Figure S23.** Distances in Hansen space to the center of the solubility sphere **(a)** or to the center of the gelation spheres **(b)** for LMWG presented in Figure S22. The lines represent the radius of the spheres. Green: gel; Red: precipitate. Blue: soluble

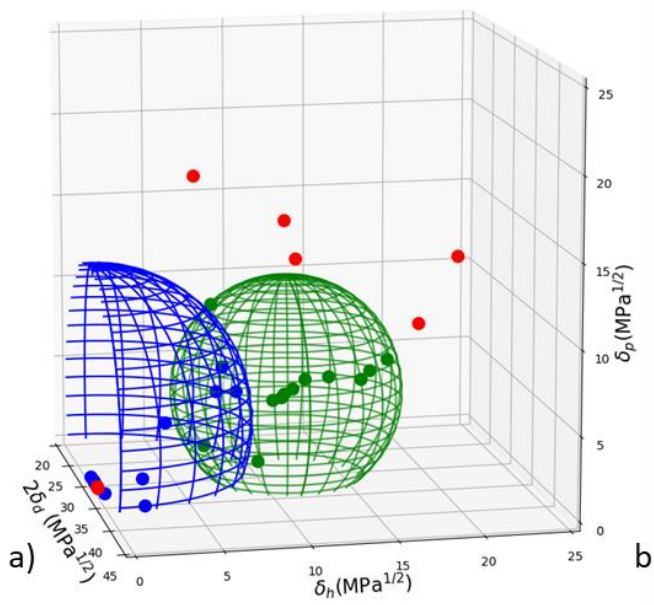


AO method

| | Solubility sphere | Gelation sphere |
|---|---|---|
| $\delta_d$ (MPa$^{1/2}$) | 14.69 | 16.24 |
| $\delta_p$ (MPa$^{1/2}$) | 3.34 | 5.38 |
| $\delta_h$ (MPa$^{1/2}$) | 0.35 | 11.22 |
| radius | 9.3 | 6.8 |
| Wrong in | 3 | 0 |
| Wrong out | 0 | 0 |

**Figure S24. (a)** Solubility data for poly(aryl ether)dendron gelator **2a12** reported by Kazuaki Ito et al[18] represented in Hansen space. Liquids are represented by full circles and calculated domains are represented by meshed spheres. Green: gel; Red: precipitate. Blue: soluble. The solubility sphere was calculated using the HSPiP[3–5] software and the gelation sphere was calculated with the AO method using the HSPiP[3–5]. **(b)** Centre, radius and outliers of the solubility and gelation spheres determined by the AO method.

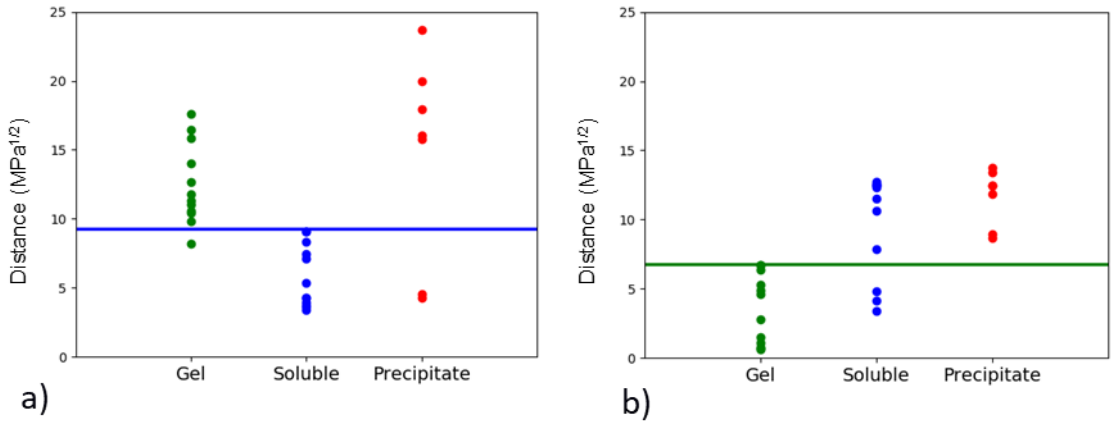


**Figure S25.** Distances in Hansen space to the center of the solubility sphere **(a)** or to the center of the gelation sphere **(b)** for LMWG presented in Figure S24. The lines represent the radius of the spheres. Green: gel; Red: precipitate. Blue: soluble

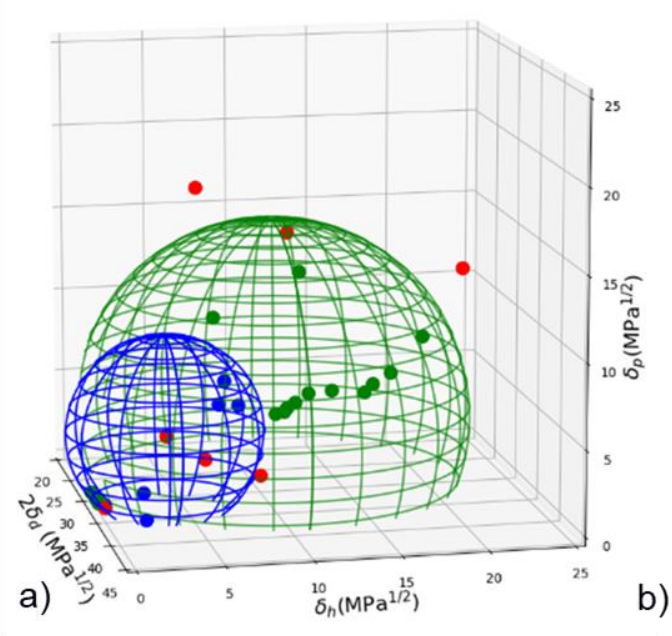


AO method

| | Solubility sphere | Gelation sphere |
|---|---|---|
| $\delta_d$ (MPa$^{1/2}$) | 17.51 | 15.23 |
| $\delta_p$ (MPa$^{1/2}$) | 4.71 | 4.28 |
| $\delta_h$ (MPa$^{1/2}$) | 3.41 | 10.61 |
| radius | 5.7 | 11.6 |
| Wrong in | 1 | 3 |
| Wrong out | 0 | 1 |

b)

**Figure S26. (a)** Solubility data for poly(aryl ether)dendron gelator **2b12** reported by Kazuaki Ito et al[18] represented in Hansen space. Liquids are represented by full circles and calculated domains are represented by meshed spheres. Green: gel; Red: precipitate. Blue: soluble. The solubility sphere was calculated using the HSPiP[3–5] software and the gelation sphere was calculated with the AO method using the HSPiP[3–5]. **(b)** Centre, radius and outliers of the solubility and gelation spheres determined by the AO method. The reliability of the fit is compromised by the limited number of liquids tested.

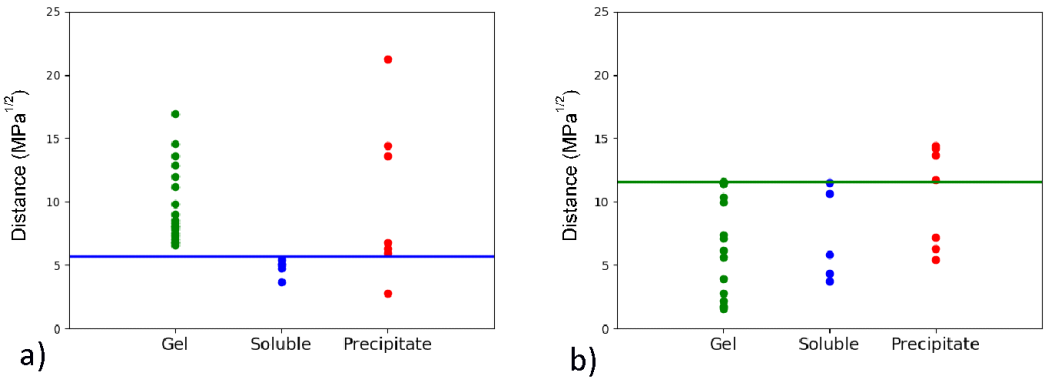


**Figure S27.** Distances in Hansen space to the center of the solubility sphere **(a)** or to the center of the gelation sphere **(b)** for LMWG presented in Figure S26. The lines represent the radius of the spheres. Green: gel; Red: precipitate. Blue: soluble

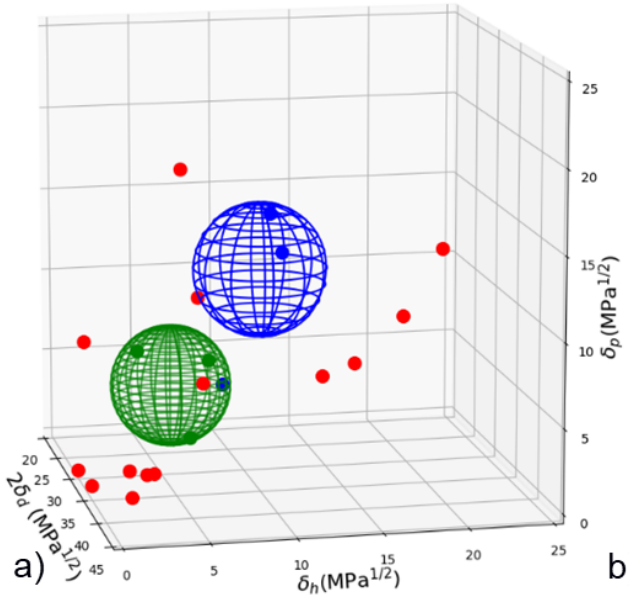


AO method

| | Solubility sphere | Gelation sphere |
|---|---|---|
| $\delta_d$ (MPa$^{1/2}$) | 17.72 | 17.53 |
| $\delta_p$ (MPa$^{1/2}$) | 12.87 | 6.07 |
| $\delta_h$ (MPa$^{1/2}$) | 9.9 | 4.72 |
| radius | 3.9 | 3.5 |
| Wrong in | 0 | 0 |
| Wrong out | 1 | 0 |

**Figure S28. (a)** Solubility data for a adenine–thymine(AT) pyrimido[4,5-d]pyrimidine pyranosyl arabinonucleoside gelation system reported by Yang He et al[19] represented in Hansen space. Liquids are represented by full circles and calculated domains are represented by meshed spheres. Green: gel; Red: precipitate. Blue: soluble. The solubility sphere was calculated using the HSPiP[3–5] software and the gelation sphere was calculated with the AO method using the HSPiP[3–5]. **(b)** Centre, radius and outliers of the solubility and gelation spheres determined by the AO method. The reliability of the fit is compromised by the limited number of liquids tested.

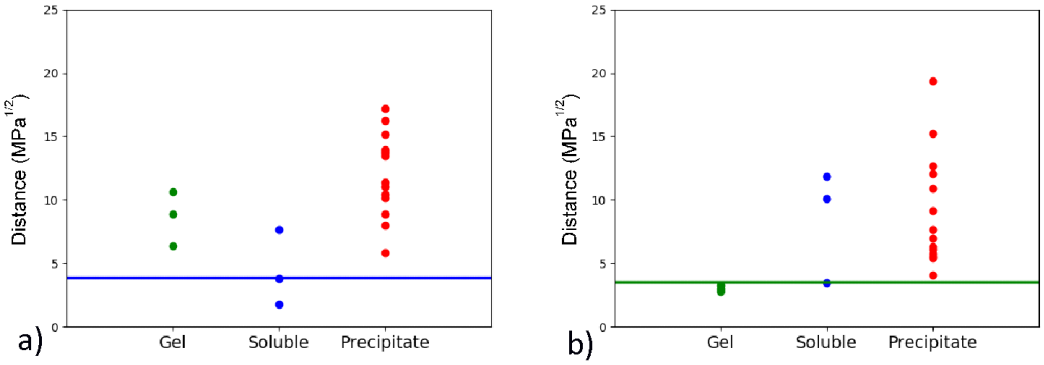


**Figure S29.** Distances in Hansen space to the center of the solubility sphere **(a)** or to the center of the gelation sphere **(b)** for LMWG presented in Figure S28. The lines represent the radius of the spheres. Green: gel; Red: precipitate. Blue: soluble

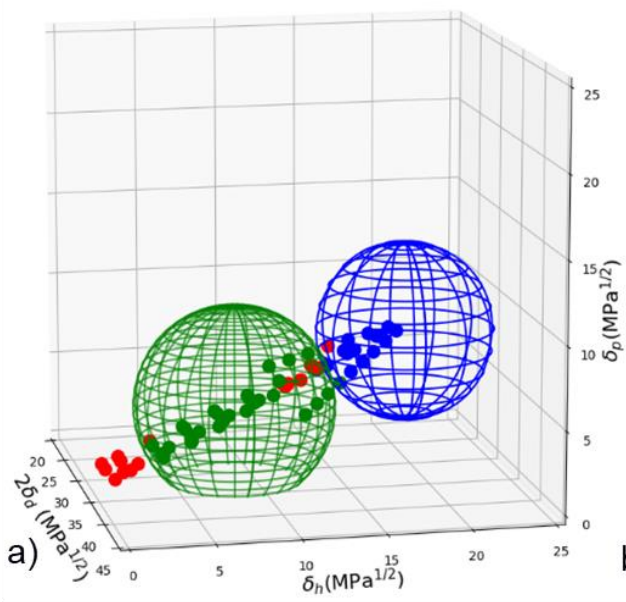


AO method

b)

| | Solubility sphere | Gelation sphere |
|---|---|---|
| $\delta_d$ (MPa$^{1/2}$) | 17.52 | 17.01 |
| $\delta_p$ (MPa$^{1/2}$) | 8.95 | 4.64 |
| $\delta_h$ (MPa$^{1/2}$) | 18.43 | 8.31 |
| radius | 5.3 | 6.0 |
| Wrong in | 0 | 4 |
| Wrong out | 1 | 1 |

**Figure S30. (a)** Solubility data for D-sorbitol-based gelation system reported by Jian Song et al[20] represented in Hansen space. Liquids are represented by full circles and calculated domains are represented by meshed spheres. Green: gel; Red: precipitate. Blue: soluble. The solubility sphere was calculated using the HSPiP[3–5] software and the gelation sphere was calculated with the AO method using the HSPiP[3–5]. **(b)** Centre, radius and outliers of the solubility and gelation spheres determined by the AO method. The reliability of the fit is compromised by the limited number of liquids tested.

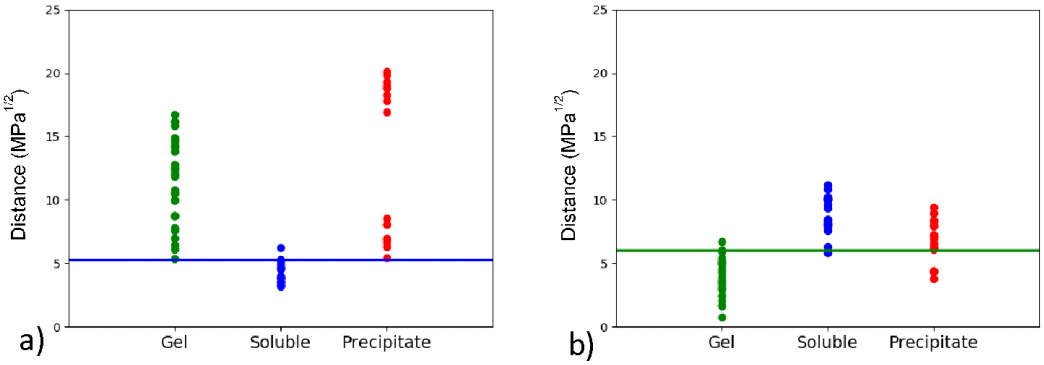


**Figure S31.** Distances in Hansen space to the center of the solubility sphere **(a)** or to the center of the gelation sphere **(b)** for LMWG presented in Figure S30. The lines represent the radius of the spheres. Green: gel; Red: precipitate. Blue: soluble

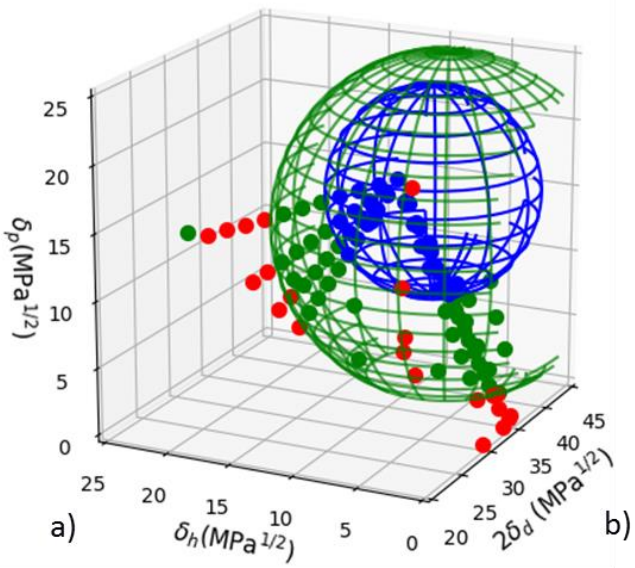


AO method

| | Solubility sphere | Gelation sphere |
|---|---|---|
| $\delta_d$ (MPa$^{1/2}$) | 19.38 | 20.97 |
| $\delta_p$ (MPa$^{1/2}$) | 15.27 | 11.77 |
| $\delta_h$ (MPa$^{1/2}$) | 8.18 | 8.46 |
| radius | 7.9 | 13.1 |
| Wrong in | 0 | 3 |
| Wrong out | 0 | 2 |

**Figure S32. (a)** Solubility data for 1,3:2,4-bis(3,4-dimethylbenzylidene)sorbitol gelator reported by Jian Song et al[21] represented in Hansen space. Liquids are represented by full circles and calculated domains are represented by meshed spheres. Green: gel; Red: precipitate. Blue: soluble. The solubility sphere was calculated using the HSPiP[3–5] software and the gelation sphere was calculated with the AO method using the HSPiP[3–5]. **(b)** Centre, radius and outliers of the solubility and gelation spheres determined by the AO method. The reliability of the fit is compromised by the limited number of liquids surrounding the solubility sphere.

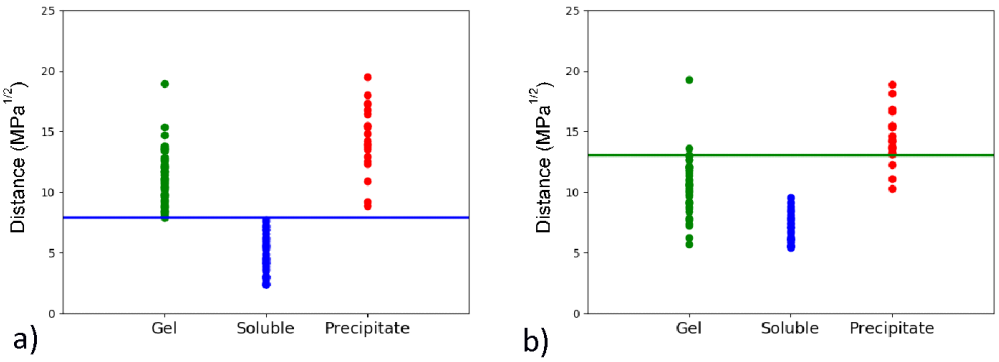


**Figure S33.** Distances in Hansen space to the center of the solubility sphere **(a)** or to the center of the gelation sphere **(b)** for LMWG presented in Figure S32. The lines represent the radius of the spheres. Green: gel; Red: precipitate. Blue: soluble

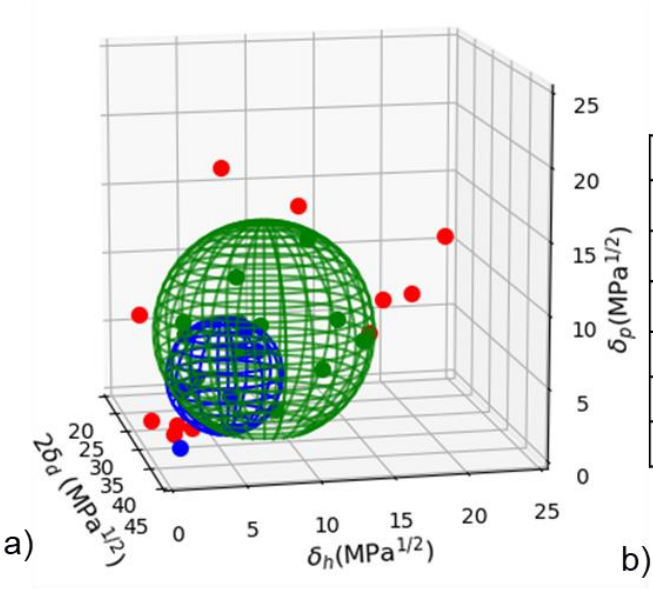


b)

AO method

| | Solubility sphere | Gelation sphere |
|---|---|---|
| $\delta_d$ (MPa$^{1/2}$) | 18.02 | 16.71 |
| $\delta_p$ (MPa$^{1/2}$) | 4.62 | 7.06 |
| $\delta_h$ (MPa$^{1/2}$) | 5.3 | 8.55 |
| radius | 4.0 | 7.6 |
| Wrong in | 0 | 0 |
| Wrong out | 1 | 0 |

**Figure S34. (a)** Solubility data for gelator **6a** reported by Hongmei Qu et al[22] represented in Hansen space. Liquids are represented by full circles and calculated domains are represented by meshed spheres. Green: gel; Red: precipitate. Blue: soluble. The solubility sphere was calculated using the HSPiP[3–5] software and the gelation sphere was calculated with the AO method using the HSPiP[3–5]. **(b)** Centre, radius and outliers of the solubility and gelation spheres determined by the AO method.

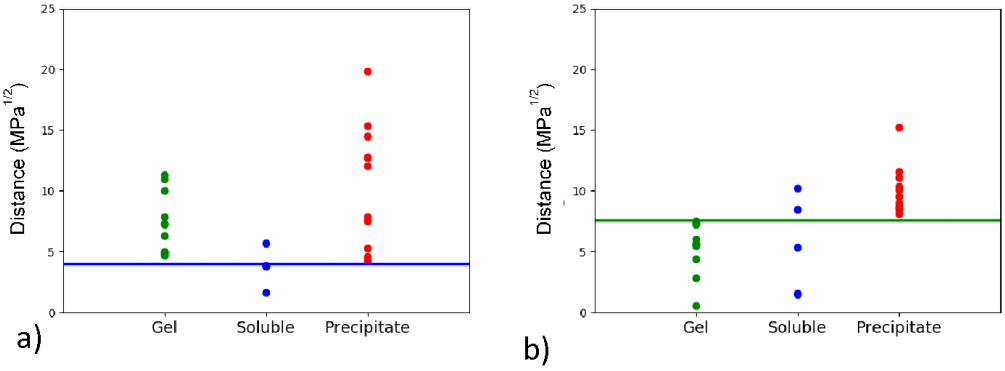


**Figure S35.** Distances in Hansen space to the center of the solubility sphere **(a)** or to the center of the gelation sphere **(b)** for LMWG presented in Figure S34. The lines represent the radius of the spheres. Green: gel; Red: precipitate. Blue: soluble

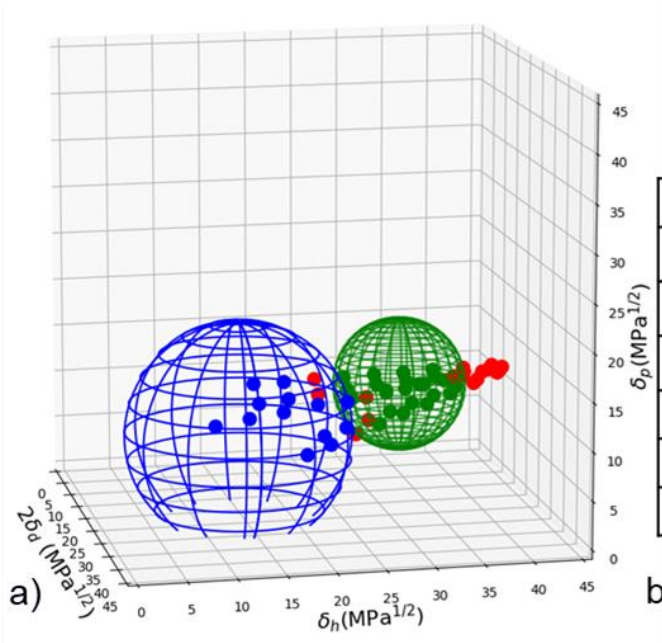


b)

AO method

| | Solubility sphere | Gelation sphere |
|---|---|---|
| $\delta_d$ (MPa$^{1/2}$) | 13.81 | 16.24 |
| $\delta_p$ (MPa$^{1/2}$) | 9.08 | 14.77 |
| $\delta_h$ (MPa$^{1/2}$) | 13.70 | 29.24 |
| radius | 11.7 | 6.7 |
| Wrong in | 1 | 3 |
| Wrong out | 0 | 0 |

**Figure S36. (a)** Solubility data for hydrazine derived gelation system reported by Lijun Guo et al[23] represented in Hansen space. Liquids are represented by full circles and calculated domains are represented by meshed spheres. Green: gel; Red: precipitate. Blue: soluble. The solubility sphere was calculated using the HSPiP[3–5] software and the gelation sphere was calculated with the AO method using the HSPiP[3–5]. **(b)** Centre, radius and outliers of the solubility and gelation spheres determined by the AO method. The reliability of the fit is compromised by the limited number of liquids surrounding the solubility sphere.

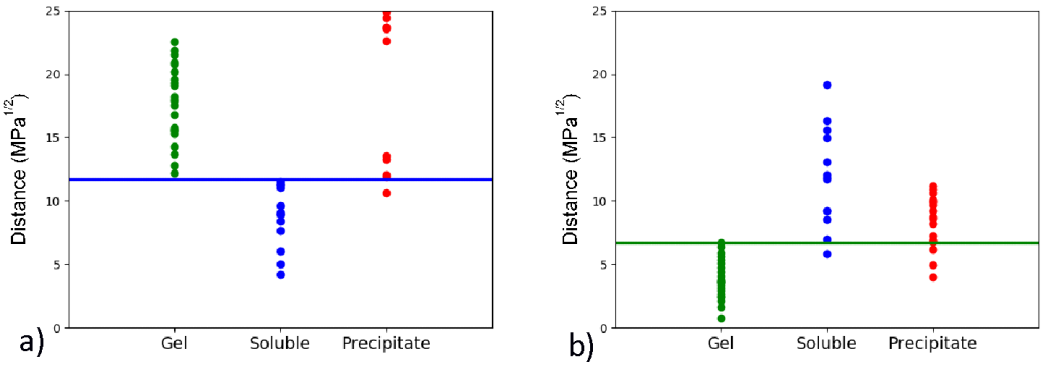


**Figure S37.** Distances in Hansen space to the center of the solubility sphere **(a)** or to the center of the gelation spheres **(b)** for LMWG presented in Figure S36. The lines represent the radius of the spheres. Green: gel; Red: precipitate. Blue: soluble

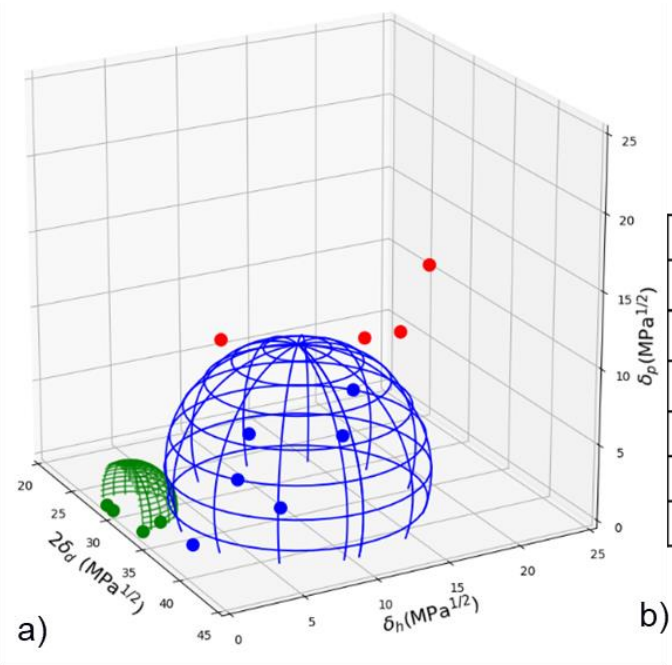


b)

AO method

| | Solubility sphere | Gelation sphere |
|---|---|---|
| $\delta_d$ (MPa$^{1/2}$) | 18.22 | 15.44 |
| $\delta_p$ (MPa$^{1/2}$) | 3.30 | 0.47 |
| $\delta_h$ (MPa$^{1/2}$) | 9.47 | 0.69 |
| radius | 8.2 | 2.9 |
| Wrong in | 0 | 0 |
| Wrong out | 0 | 0 |

**Figure S38. (a)** Solubility data for cholesterol-based gelation system reported by Xiaoli Zhen et al[24] represented in Hansen space. Liquids are represented by full circles and calculated domains are represented by meshed spheres. Green: gel; Red: precipitate. Blue: soluble. The solubility sphere was calculated using the HSPiP[3–5] software and the gelation sphere was calculated with the AO method using the HSPiP[3–5]. **(b)** Centre, radius and outliers of the solubility and gelation spheres determined by the AO method. The reliability of the fit is compromised by the limited number of liquids tested.

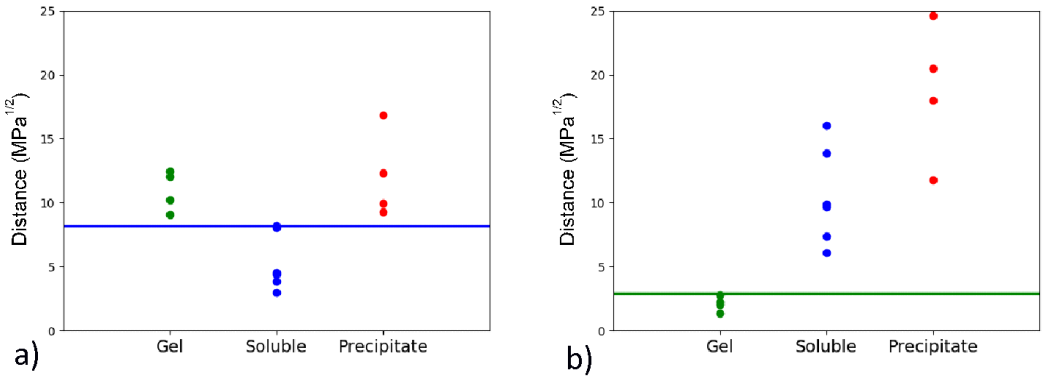


**Figure S39.** Distances in Hansen space to the center of the solubility sphere **(a)** or to the center of the gelation sphere **(b)** for LMWG presented at Figure S38. The lines represent the radius of the spheres. Green: gel; Red: precipitate. Blue: soluble

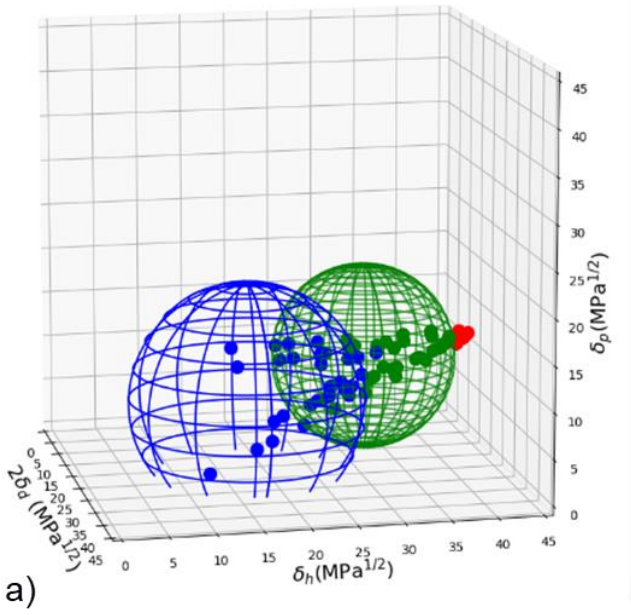


AO method

| | Solubility sphere | Gelation sphere |
|---|---|---|
| $\delta_d$ (MPa$^{1/2}$) | 13.99 | 15.53 |
| $\delta_p$ (MPa$^{1/2}$) | 8.50 | 13.64 |
| $\delta_h$ (MPa$^{1/2}$) | 16.83 | 28.81 |
| radius | 12.8 | 9.8 |
| Wrong in | 2 | 0 |
| Wrong out | 1 | 0 |

b)

**Figure S40. (a)** Solubility data for bis-dipeptide based gelation system reported by Yong Yang et al[25] represented in Hansen space. Liquids are represented by full circles and calculated domains are represented by meshed spheres. Green: gel; Red: precipitate. Blue: soluble. The solubility sphere was calculated using the HSPiP[3–5] software and the gelation sphere was calculated with the AO method using the HSPiP[3–5]. **(b)** Centre, radius and outliers of the solubility and gelation spheres determined by the AO method. The reliability of the fit is compromised by the limited number of liquids surrounding the solubility sphere.

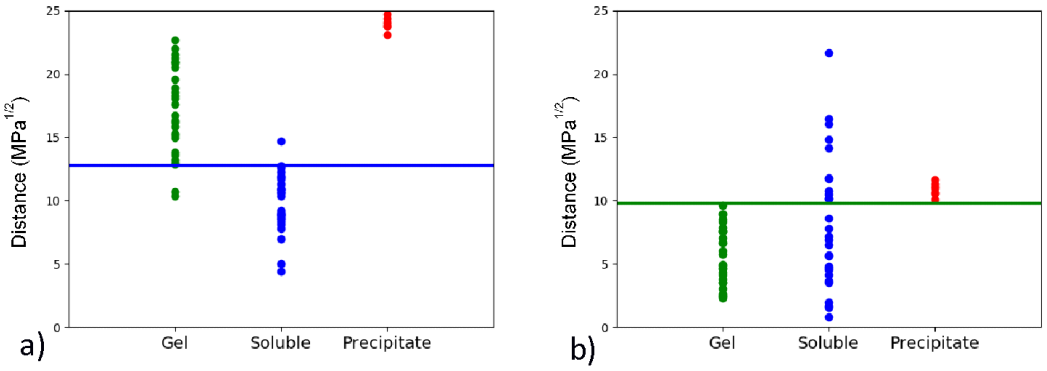


**Figure S41.** Distances in Hansen space to the center of the solubility sphere **(a)** or to the center of the gelation sphere **(b)** for LMWG presented in Figure S40. The lines represent the radius of the spheres. Green: gel; Red: precipitate. Blue: soluble

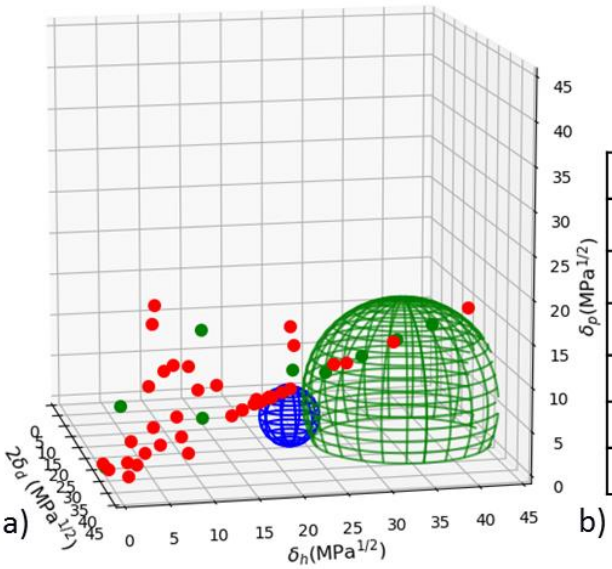


AO method

| | Solubility sphere | Gelation sphere |
|---|---|---|
| $\delta_d$ (MPa$^{1/2}$) | 15.96 | 14.48 |
| $\delta_p$ (MPa$^{1/2}$) | 4.60 | 5.40 |
| $\delta_h$ (MPa$^{1/2}$) | 21.35 | 35.24 |
| radius | 3.4 | 11.5 |
| Wrong in | 1 | 1 |
| Wrong out | 0 | 5 |

**Figure S42. (a)** Solubility data for 1,3:2,5:4,6-tris(3,4-dichlorobenzylidene)-*D*-mannitol gelator reported by Bao Zhang et al[26] represented in Hansen space. Liquids are represented by full circles and calculated domains are represented by meshed spheres. Green: gel; Red: precipitate. Blue: soluble. The solubility sphere was calculated using the HSPiP[3–5] software and the gelation sphere was calculated with the AO method using the HSPiP[3–5]. **(b)** Centre, radius and outliers of the solubility and gelation spheres determined by the AO method. The reliability of the fit is compromised by the limited number of liquids tested.

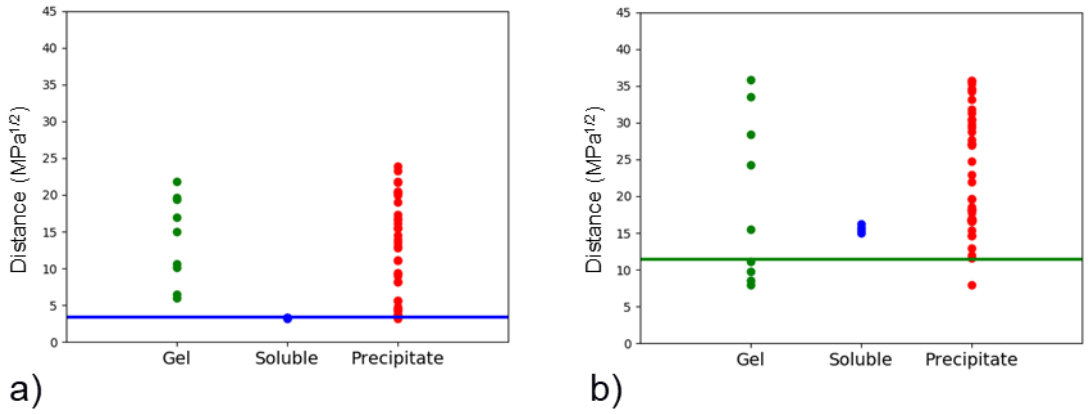


**Figure S43.** Distances in Hansen space to the center of the solubility sphere **(a)** or to the center of the gelation sphere **(b)** for LMWG presented at Figure S42. The lines represent the radius of the spheres. Green: gel; Red: precipitate. Blue: soluble

# III. Solubility data of all gelators

## III.1. Solubility data of Th12 at different concentrations

***Table S2. Gelation tests for LMWG Th12, with pure liquids.*** [a-b]

| **Liquid** | 3% | 2% | 1.50% | 1% | 0.75% |
|---|---|---|---|---|---|
| **acetonitrile** | G | P | P | P | P |
| **benzyl alcohol** | G | S | S | S | S |
| **1-butanol** | G | G | G | S | S |
| **t-butyl acetate** | G | G | G | G | P |
| **1-chloropentane** | G | G | G | P | S |
| **chlorobenzene** | G | S | S | S | S |
| **cyclohexane** | G | P | P | P | P |
| **cyclohexanone** | G | S | S | S | S |
| **diacetone alcohol** | G | G | G | P | P |
| **dimethylformamide (DMF)** | G | G | P | S | S |
| **dimethylsulfoxide (DMSO)** | G | G | P | S | S |
| **1,4-dioxane** | G | P | P | S | S |
| **ethanolamine** | G | G | G | P | P |
| **hexadecane** | G | G | G | G | P |
| **methanol** | G | P | P | P | P |
| **methylethylketone (MEK)** | G | S | S | S | S |
| **N,N-diethyl acetamide** | S | S | S | S | S |
| **propylene carbonate** | G | P | P | P | P |
| **propylene glycol** | G | G | G | P | P |
| **toluene** | G | G | P | P | S |
| **water** | P | P | P | P | P |
| **N-methylformamide** | G | G | G | P | P |

**[a] Gelation is tested by introducing desired amount of gelator and 1 mL of liquid in a screw-cap vial, heating until dissolution and leaving the vial to cool on the bench.**

**[b] G: gel; S: soluble; P: insoluble or formation of a precipitate after cooling.**

**Table S3. Gelation tests for LMWG Th12, with mixtures of liquids.[a-b]**

| **Liquid 1** | Liquid 2 | Composition (%) | 3% | 2% | 1.50% | 1% | 0.75% |
|---|---|---|---|---|---|---|---|
| **propylene glycol** | water | 0/100 | P | P | P | P | P |
| | | 25/75 | P | P | P | P | P |
| | | 50/50 | P | P | P | P | P |
| | | 75/25 | G | P | P | P | P |
| | | 100/0 | G | G | G | P | P |
| **N-methylformamide** | water | 0/100 | P | P | P | P | P |
| | | 25/75 | P | P | P | P | P |
| | | 50/50 | P | P | P | P | P |
| | | 75/25 | G | P | P | P | P |
| | | 100/0 | G | G | G | P | P |
| **chlorobenzene** | dioxane | 0/100 | G | P | P | S | S |
| | | 25/75 | P | S | S | S | S |
| | | 50/50 | P | S | S | S | S |
| | | 75/25 | P | S | S | S | S |
| | | 100/0 | G | S | S | S | S |
| **cyclohexanone** | propylene carbonate | 0/100 | G | P | P | P | P |
| | | 25/75 | G | P | P | P | P |
| | | 50/50 | G | G | G | G | P |
| | | 75/25 | G | P | S | S | P |
| | | 100/0 | G | S | S | S | S |
| **chloropentane** | propylene carbonate | 0/100 | G | P | P | P | P |
| | | 25/75 | P | P | P | P | P |
| | | 50/50 | G | P | P | P | P |
| | | 75/25 | G | G | G | P | P |
| | | 100/0 | G | G | G | P | S |

**[a] Gelation is tested by introducing the desired amount of gelator and 1 mL of liquid in a screw-cap vial,**

**heating until dissolution and leaving the vial to cool on the bench.**

**[b] G: gel; S: soluble; P: insoluble or formation of a precipitate after cooling.**

# III.2. Solubility data of thiazole based gelators at 2 wt%

***Table S4. Gelation tests for thiazole based gelators, with pure liquids.*** [a-b]

| **Liquid** | Th8 | Th12 | Th14 | Th16 | Th18 |
|---|---|---|---|---|---|
| **acetonitrile** | P | P | P | G | G |
| **benzyl alcohol** | S | S | S | G | G |
| **1-butanol** | S | G | G | G | G |
| **t-butyl acetate** | P | G | G | G | G |
| **1-chloropentane** | S | G | G | G | G |
| **chlorobenzene** | S | S | S | G | G |
| **cyclohexane** | P | P | G | G | G |
| **cyclohexanone** | S | S | S | G | G |
| **diacetone alcohol** | S | G | G | G | G |
| **dimethylformamide (DMF)** | S | G | G | G | G |
| **dimethylsulfoxide (DMSO)** | S | G | G | G | G |
| **1,4-dioxane** | S | P | P | G | G |
| **ethanolamine** | P | G | G | G | G |
| **hexadecane** | P | G | G | G | G |
| **methanol** | P | P | G | G | G |
| **methylethylketone (MEK)** | S | S | P | G | G |
| **N,N-diethyl acetamide** | S | S | S | P | P |
| **propylene carbonate** | P | P | G | G | G |
| **propylene glycol** | P | G | G | G | G |
| **toluene** | S | G | G | G | G |
| **water** | P | P | P | P | P |
| **N-methylformamide** | S | G | G | G | G |

***Table S5. Solubility tests for thiazole based gelator, with mixtures of liquids.*** [a-b]

| **Liquid 1** | Liquid 2 | Composition (%) | Th8 | Th12 | Th14 | Th16 | Th18 |
|---|---|---|---|---|---|---|---|
| **propylene glycol** | water | 0/100 | P | P | P | P | P |
| | | 25/75 | P | P | P | P | P |
| | | 50/50 | P | P | P | P | P |
| | | 75/25 | G | P | G | P | P |
| | | 100/0 | P | G | G | G | G |
| **N-methylformamide** | water | 0/100 | P | P | P | P | P |
| | | 25/75 | P | P | P | P | P |
| | | 50/50 | P | P | P | P | P |
| | | 75/25 | G | P | P | P | P |
| | | 100/0 | S | G | G | G | G |
| **chlorobenzene** | dioxane | 0/100 | S | P | P | G | G |
| | | 25/75 | S | S | G | G | G |
| | | 50/50 | S | S | P | G | G |
| | | 75/25 | S | S | P | G | G |
| | | 100/0 | S | S | S | G | G |
| **cyclohexanone** | propylene carbonate | 0/100 | P | P | G | G | G |
| | | 25/75 | P | P | G | P | G |
| | | 50/50 | S | G | G | P | G |
| | | 75/25 | S | P | G | G | G |
| | | 100/0 | S | S | S | G | G |
| **chloropentane** | propylene carbonate | 0/100 | P | P | G | G | G |
| | | 25/75 | S | P | P | G | P |
| | | 50/50 | S | P | P | G | G |
| | | 75/25 | S | G | P | G | G |
| | | 100/0 | S | G | G | G | G |

**[a] Gelation is tested by introducing 20 mg of gelator and 1 mL of liquid in a screw-cap vial, heating until dissolution and leaving the vial to cool on the bench.**

**[b] G: gel; S: soluble; P: insoluble or formation of a precipitate after cooling.**

## III.3. Solubility data of Bis5 at different concentrations

***Table S6. Results of solubility test in pure liquids of Bis5 at different concentration.*** [a-b]

| **Liquid** | 3 wt % | 2 wt % | 1,5 wt % | 1 wt % | 0,75wt % | 0,5 wt % | 0,3 wt % | 0,15 wt % |
|---|---|---|---|---|---|---|---|---|
| **acetonitrile** | G | G | G | G | G | G | S | S |
| **benzyl alcohol** | S | S | S | S | S | S | S | S |
| **1-butanol** | S | S | S | S | S | S | S | S |
| **t-butyl acetate** | G | G | G | G | G | G | S | S |
| **1-chloropentane** | G | G | G | G | G | G | P | S |
| **chlorobenzene** | G | G | G | G | G | G | S | S |
| **cyclohexane** | P | P | P | P | P | P | P | P |
| **cyclohexanone** | G | G | G | G | S | S | S | S |
| **diacetone alcohol** | G | S | S | S | S | S | S | S |
| **dimethylformamide** | G | G | S | S | S | S | S | S |
| **dimethylsulfoxide** | G | G | G | S | S | S | S | S |
| **1,4-dioxane** | G | G | G | G | S | S | S | S |
| **ethanolamine** | G | G | G | G | G | G | S | S |
| **hexadecane** | G | G | G | G | G | P | P | P |
| **methanol** | S | S | S | S | S | S | S | S |
| **methylethylketone** | G | G | G | G | G | S | S | S |
| **N,N-diethyl acetamide** | G | S | S | S | S | S | S | S |
| **propylene carbonate** | G | G | G | G | G | G | G | S |
| **propylene glycol** | G | S | S | S | S | S | S | S |
| **toluene** | G | G | G | G | G | G | G | S |
| **water** | P | P | P | P | P | P | P | P |
| **N-methylformamide** | G | S | S | S | S | S | S | S |

**[a] Gelation is tested by introducing the desired amount of gelator and 1 mL of liquid in a screw-cap vial,**

**heating until dissolution and leaving the vial to cool on the bench.**

**[b] G: gel; S: soluble; P: insoluble or formation of a precipitate after cooling.**

***Table S7. Results of solubility test in mixtures of liquids of Bis5 at different concentrations.*** [a-b]

| **Liquid 1** | Liquid 2 | Composition % | *3 wt %* | *2 wt %* | *1,5 wt %* | *1 wt %* | *0,75 wt %* | *0,5 wt %* | *0.3 wt %* | *0,15 wt %* |
|---|---|---|---|---|---|---|---|---|---|---|

| | | | | | | | | | | |
|---|---|---|---|---|---|---|---|---|---|---|
| **dimethylform amide (DMF)** | methanol | 0/100 | S | S | S | S | S | S | S | S |
| | | 25/75 | S | S | S | S | S | S | S | S |
| | | 50/50 | S | S | S | S | S | S | S | S |
| | | 75/25 | S | S | S | S | S | S | S | S |
| | | 100/0 | G | G | S | S | S | S | S | S |
| **methanol** | water | 0/100 | P | P | P | P | P | P | P | P |
| | | 25/75 | G | G | G | G | G | G | G | S |
| | | 50/50 | G | G | G | G | S | S | S | S |
| | | 75/25 | G | G | S | S | S | S | S | S |
| | | 100/0 | S | S | S | S | S | S | S | S |
| **cyclohexanone** | acetonitrile | 0/100 | G | G | G | G | G | G | S | S |
| | | 25/75 | G | G | G | G | S | S | S | S |
| | | 50/50 | G | G | G | G | S | S | S | S |
| | | 75/25 | G | G | G | S | S | S | S | S |
| | | 100/0 | G | G | G | G | S | S | S | S |
| **diacetone alcohol** | 1,4-dioxane | 0/100 | G | G | G | G | S | S | S | S |
| | | 25/75 | G | G | G | S | S | S | S | S |
| | | 50/50 | G | S | S | S | S | S | S | S |
| | | 75/25 | S | S | S | S | S | S | S | S |
| | | 100/0 | G | S | S | S | S | S | S | S |
| **water** | N-methylform amide | 0/100 | G | S | S | S | S | S | S | S |
| | | 25/75 | G | G | G | S | S | S | S | S |
| | | 50/50 | G | G | G | G | P | S | S | S |
| | | 75/25 | G | G | G | G | G | P | P | S |
| | | 100/0 | P | P | P | P | P | P | P | P |

**[a] Gelation is tested by introducing the desired amount of gelator and 1 mL of liquid in a screw-cap vial,**

**heating until dissolution and leaving the vial to cool on the bench.**

**[b] G: gel; S: soluble; P: insoluble or formation of a precipitate after cooling.**

# III.4. Solubility data of bisamide based gelators at 1 wt%

*Table S8. Results of solubility test in pure liquids of Bisamide based gelators as 1 wt%.* [a-b]

| Liquid | Bis3 | Bis4 | Bis5 | Bis6 | Bis8 | Bis12 | Bis14 | Bis16 | Bis18 |
|---|---|---|---|---|---|---|---|---|---|
| **acetonitrile** | P | G | G | G | G | G | G | G | G |
| **benzyl alcohol** | S | S | S | S | S | S | G | G | G |
| **1-butanol** | S | S | S | S | S | S | P | G | G |
| **t-butyl acetate** | P | G | G | G | G | G | G | G | G |
| **1-chloropentane** | G | G | G | G | G | G | G | G | G |
| **chlorobenzene** | P | G | G | G | G | G | G | G | G |
| **cyclohexane** | G | G | P | G | G | G | G | G | G |
| **cyclohexanone** | S | G | G | S | G | G | G | G | G |
| **diacetone alcohol** | S | S | S | S | S | G | G | G | G |
| **dimethylformamide** | S | S | S | S | G | G | G | G | G |
| **dimethylsulfoxide** | S | S | S | P | G | G | G | G | G |
| **1,4-dioxane** | S | G | G | S | G | G | G | G | G |
| **ethanolamine** | S | P | G | G | G | G | G | G | G |
| **hexadecane** | P | P | G | G | G | G | G | G | G |
| **methanol** | S | S | S | S | S | G | G | G | G |
| **methylethylketone** | S | G | G | G | G | G | G | G | G |
| **N,N-diethyl acetamide** | S | S | S | S | G | G | G | G | G |
| **propylene carbonate** | P | G | G | G | G | G | G | G | G |
| **propylene glycol** | S | S | S | S | G | G | G | G | G |
| **toluene** | P | G | G | G | G | G | G | G | G |
| **water** | S | P | P | P | P | P | P | P | P |
| **N-methylformamide** | S | S | S | S | G | G | G | G | G |

**[a] Gelation is tested by introducing 10 mg of gelator and 1 mL of liquid in a screw-cap vial,**

**heating until dissolution and leaving the vial to cool on the bench.**

**[b] G: gel; S: soluble; P: insoluble or formation of a precipitate after cooling.**

*Table S9. Results of solubility test in mixtures of liquids of Bisamide based gelators at 1 wt%.* [a-b]

| **Liquid 1** | Liquid 2 | Composition % | Bis3 | Bis4 | Bis5 | Bis6 | Bis8 | Bis12 | Bis14 | Bis16 | Bis18 |
|---|---|---|---|---|---|---|---|---|---|---|---|
| **dimethylformamide (DMF)** | methanol | 0/100 | S | S | S | S | S | G | G | G | G |
| | | 25/75 | S | S | S | S | S | G | G | G | G |
| | | 50/50 | S | S | S | S | S | G | G | G | G |
| | | 75/25 | S | S | S | S | S | G | G | G | G |
| | | 100/0 | S | S | S | S | G | G | G | G | G |
| **methanol** | water | 0/100 | S | P | P | P | P | P | P | P | P |
| | | 25/75 | S | P | G | P | P | P | P | P | P |
| | | 50/50 | S | S | G | G | G | P | P | P | P |
| | | 75/25 | S | S | S | G | G | G | G | P | P |
| | | 100/0 | S | S | S | S | S | G | G | G | G |
| **cyclohexanone** | acetonitrile | 0/100 | P | G | G | G | G | G | G | G | G |
| | | 25/75 | S | G | G | G | G | G | G | G | G |
| | | 50/50 | S | G | S | S | G | G | G | G | G |
| | | 75/25 | S | G | S | S | G | G | G | G | G |
| | | 100/0 | S | G | G | S | G | G | G | G | G |
| **diacetone alcohol** | 1,4-dioxane | 0/100 | S | G | G | S | G | G | G | G | G |
| | | 25/75 | S | G | S | S | S | G | G | G | G |
| | | 50/50 | S | S | S | S | S | G | G | G | G |
| | | 75/25 | S | S | S | S | S | G | G | G | G |
| | | 100/0 | S | S | S | S | S | G | G | G | G |
| **water** | N-methylformamide | 0/100 | S | S | S | S | G | G | G | G | G |
| | | 25/75 | S | S | S | G | G | G | G | P | P |
| | | 50/50 | S | S | G | G | G | P | P | P | P |
| | | 75/25 | S | P | G | P | P | P | P | P | P |
| | | 100/0 | S | P | P | P | P | P | P | P | P |

**[a] Gelation is tested by introducing 10 mg of gelator and 1 mL of liquid in a screw-cap vial, heating until dissolution and leaving the vial to cool on the bench.**

**[b] G: gel; S: soluble; P: insoluble or formation of a precipitate after cooling.**

## III.5. Solubility data of trialkyl cis-1,3,5-cyclohexanetri-carboxylamides based gelators at 1 wt%

***Table S10. Results of solubility test in pure liquids of all LMWG as 1 wt%.*** [a-b]

| **Liquid** | Tris12 | Tris14 | Tris16 | Tris18 |
|---|---|---|---|---|
| **acetonitrile** | P | P | P | P |
| **benzyl alcohol** | G | G | P | P |
| **1-butanol** | G | G | G | G |
| **t-butyl acetate** | P | G | G | G |
| **1-chloropentane** | G | G | G | G |
| **chlorobenzene** | G | G | S | S |
| **cyclohexane** | G | G | G | G |
| **cyclohexanone** | G | G | G | G |
| **diacetone alcohol** | G | P | P | P |
| **dimethylformamide (DMF)** | P | P | P | P |
| **dimethylsulfoxide (DMSO)** | P | P | P | P |
| **1,4-dioxane** | P | P | P | P |
| **ethanolamine** | P | P | P | P |
| **hexadecane** | P | G | G | G |
| **methanol** | P | P | P | P |
| **methylethylketone (MEK)** | P | P | G | G |
| **N,N-diethyl acetamide** | G | G | G | G |
| **propylene carbonate** | P | P | P | P |
| **propylene glycol** | P | P | P | P |
| **toluene** | G | G | G | G |
| **water** | P | P | P | P |
| **N-methylformamide** | P | P | P | p |

**[a] Gelation is tested by introducing 10 mg of gelator and 1 mL of liquid in a screw-cap vial,**

**heating until dissolution and leaving the vial to cool on the bench.**

**[b] G: gel; S: soluble; P: insoluble or formation of a precipitate after cooling.**

***Table S11. Results of solubility test in mixtures of liquids of all LMWG as 1 wt%.*** [a-b]

| **Liquid 1** | Liquid 2 | Composition | Tris12 | Tris14 | Tris16 | Tris18 |
|---|---|---|---|---|---|---|
| **DMF** | Ethanolamine | 0/100 | P | P | P | P |
| | | 25/75 | G | P | P | P |

| | | | | | | |
|---|---|---|---|---|---|---|
| | | 50/50 | P | P | P | P |
| | | 75/25 | P | P | P | P |
| | | 100/0 | G | P | P | P |
| **Toluene** | 1,4-Dioxane | 0/100 | P | P | G | G |
| | | 25/75 | G | G | G | G |
| | | 50/50 | G | G | G | G |
| | | 75/25 | G | G | G | G |
| | | 100/0 | G | G | G | G |
| **1-Butanol** | 1,4-Dioxane | 0/100 | P | P | G | G |
| | | 25/75 | G | G | G | G |
| | | 50/50 | G | G | G | G |
| | | 75/25 | G | G | G | G |
| | | 100/0 | G | G | G | G |
| **Toluene** | t-Butyl acetate | 0/100 | P | G | G | G |
| | | 25/75 | G | G | G | G |
| | | 50/50 | G | G | G | G |
| | | 75/25 | G | G | G | G |
| | | 100/0 | G | G | G | G |
| **1-Butanol** | t-Butyl acetate | 0/100 | P | G | G | G |
| | | 25/75 | G | G | G | G |
| | | 50/50 | G | G | G | G |
| | | 75/25 | G | G | G | G |
| | | 100/0 | G | G | G | G |
| **Cyclohexanone** | Propylene carbonate | 0/100 | P | P | P | P |
| | | 25/75 | P | P | P | P |
| | | 50/50 | P | P | P | G |
| | | 75/25 | G | G | G | G |
| | | 100/0 | G | G | G | G |

**[a] Gelation is tested by introducing 10 mg of gelator and 1 mL of liquid in a screw-cap vial, heating until dissolution and leaving the vial to cool on the bench.**

**[b] G: gel; S: soluble; P: insoluble or formation of a precipitate after cooling.**

# III.6. Solubility data of dialkyl hydrazide based gelators at 3 wt%

***Table S12. Results of solubility test in pure liquids of all LMWG as 3 wt%.*** [a-b]

| **Solvent** | Hydra8 | Hydra10 | Hydra12 | Hydra14 | Hydra16 | Hydra18 |
|---|---|---|---|---|---|---|
| **acetonitrile** | P | P | P | P | P | G |
| **benzyl alcohol** | P | P | G | G | G | G |
| **1-butanol** | P | G | G | G | G | G |
| **t-butyl acetate** | P | P | P | P | P | G |
| **1-chloropentane** | P | P | P | P | P | P |
| **chlorobenzene** | P | P | P | P | P | G |
| **cyclohexane** | P | P | P | P | P | G |
| **cyclohexanone** | P | G | G | G | G | G |
| **diacetone alcohol** | P | G | G | G | G | G |
| **dimethylformamide** | P | G | G | G | G | G |
| **dimethylsulfoxide** | P | P | P | G | G | G |
| **1,4-dioxane** | G | G | G | G | G | G |
| **ethanolamine** | P | G | G | G | P | P |
| **hexadecane** | P | P | P | P | P | G |
| **methanol** | P | G | G | P | P | P |
| **methylethylketone** | G | G | G | G | G | G |
| **N,N-diethyl acetamide** | P | G | G | G | G | G |
| **propylene carbonate** | G | G | G | P | P | G |
| **propylene glycol** | P | G | G | G | G | G |
| **toluene** | P | P | P | P | P | G |
| **water** | P | P | P | P | P | P |
| **N-methylformamide** | P | P | P | G | G | G |

**[a] Gelation is tested by introducing 30 mg of gelator and 1 mL of liquid in a screw-cap vial,**

**heating until dissolution and leaving the vial to cool on the bench.**

**[b] G: gel; S: soluble; P: insoluble or formation of a precipitate after cooling.**

***Table S13. Results of solubility test in mixtures of liquids of all LMWG as 3 wt%.***

| **Liquid 1** | Liquid 2 | Composition | Hydra8 | Hydra10 | Hydra12 | Hydra14 | Hydra16 | Hydra18 |
|---|---|---|---|---|---|---|---|---|
| **Propylene carbonate** | DMSO | 100/0 | G | G | G | P | P | G |
| | | 75/25 | G | G | G | P | G | G |
| | | 50/50 | P | G | G | G | G | G |

| | | | | | | | | |
|---|---|---|---|---|---|---|---|---|
| | | 25/75 | P | G | G | G | G | G |
| | | 0/100 | P | P | P | G | G | G |
| **Propylene carbonate** | Acetonitrile | 100/0 | G | G | G | P | P | G |
| | | 75/25 | G | G | G | P | P | G |
| | | 50/50 | G | G | G | P | P | G |
| | | 25/75 | G | G | G | P | P | P |
| | | 0/100 | P | P | P | P | P | G |
| **Propylene carbonate** | Cyclohexanone | 100/0 | G | G | G | P | P | G |
| | | 75/25 | G | G | G | G | P | G |
| | | 50/50 | G | G | G | G | G | G |
| | | 25/75 | G | G | G | G | G | G |
| | | 0/100 | P | G | G | G | G | G |
| **Methanol** | Water | 100/0 | P | G | G | P | P | P |
| | | 75/25 | P | P | P | P | P | P |
| | | 50/50 | P | P | P | P | P | P |
| | | 25/75 | P | P | P | P | P | P |
| | | 0/100 | P | P | P | P | P | P |
| **Chloropentane** | Cyclohexanone | 100/0 | P | P | P | P | P | P |
| | | 75/25 | G | G | G | G | G | G |
| | | 50/50 | G | G | G | G | G | G |
| | | 25/75 | G | G | G | G | G | G |
| | | 0/100 | P | G | G | P | G | G |
| **Chloropentane** | MEK | 100/0 | P | P | P | P | P | P |
| | | 75/25 | G | G | G | G | G | G |
| | | 50/50 | G | G | G | G | P | G |
| | | 25/75 | G | G | G | G | G | G |
| | | 0/100 | G | G | G | G | G | G |
| **DMF** | Methanol | 100/0 | P | G | G | G | G | G |
| | | 75/25 | P | G | G | G | G | G |
| | | 50/50 | P | G | G | G | P | G |
| | | 25/75 | P | G | G | P | P | G |
| | | 0/100 | P | G | G | P | P | P |
| **t-butylacetate** | Methanol | 100/0 | P | P | P | P | P | G |
| | | 75/25 | G | G | G | G | G | G |
| | | 50/50 | P | G | G | G | G | G |
| | | 25/75 | P | G | G | G | G | G |
| | | 0/100 | P | G | G | P | P | P |

# III.7. Solubility data of (R)-12-hydroxystearic acid based gelators at 2 wt%

***Table S14. Results of solubility test in pure liquids of all LMWG as 2 wt%.*** [a-b]

| **Liquid** | HSA4 | HSA8 | HSA10 | HSA12 | HSA14 | HSA18 |
|---|---|---|---|---|---|---|
| **acetonitrile** | G | G | G | I | I | I |
| **benzyl alcohol** | S | I | I | I | I | I |
| **1-butanol** | S | S | I | I | I | I |
| **t-butyl acetate** | G | G | G | G | G | I |
| **1-chloropentane** | G | G | G | G | G | G |
| **chlorobenzene** | G | G | G | G | G | G |
| **cyclohexane** | G | I | G | G | G | I |
| **cyclohexanone** | G | G | G | G | G | I |
| **diacetone alcohol** | G | G | G | I | I | I |
| **dimethylformamide** | I | I | G | I | I | G |
| **dimethylsulfoxide** | I | I | I | I | I | G |
| **1,4-dioxane** | G | G | G | G | G | I |
| **ethanolamine** | I | I | I | I | I | I |
| **hexadecane** | G | G | I | I | G | I |
| **methanol** | S | G | I | I | I | I |
| **methylethylketone** | G | G | G | G | G | I |
| **N,N-diethyl acetamide** | S | I | I | I | I | I |
| **propylene carbonate** | G | I | I | I | I | G |
| **propylene glycol** | S | I | I | I | I | I |
| **toluene** | G | G | G | G | G | G |
| **water** | I | I | I | I | I | I |

**[a] Gelation is tested by introducing 30 mg of gelator and 1 mL of liquid in a screw-cap vial,**

**heating until dissolution and leaving the vial to cool on the bench.**

**[b] G: gel; S: soluble; P: insoluble or formation of a precipitate after cooling.**

***Table S15. Results of solubility test in mixtures of liquids of all LMWG as 2 wt%.*** [a-b]

| **Liquid 1** | Liquid 2 | Composition % | HSA4 | HSA8 | HSA10 | HSA12 | HSA14 | HSA18 |
|---|---|---|---|---|---|---|---|---|
| **Chlorobenzene** | t-butyl acetate | 0/100 | G | G | G | G | G | I |
| | | 20/80 | G | G | G | G | G | I |
| | | 40/60 | G | G | G | G | G | I |

| | | | | | | | | |
|---|---|---|---|---|---|---|---|---|
| | | 60/40 | G | G | G | G | G | I |
| | | 80/20 | G | G | G | G | G | I |
| | | 100/0 | G | G | G | G | G | G |
| **Chloropentane** | DMSO | 0/100 | I | I | I | I | I | G |
| | | 20/80 | I | I | G | I | I | I |
| | | 40/60 | S | I | I | I | I | I |
| | | 60/40 | S | G | S | I | I | I |
| | | 80/20 | S | G | I | I | G | I |
| | | 100/0 | G | G | G | G | G | G |
| **Chloropentane** | t-butyl acetate | 0/100 | G | G | G | G | G | I |
| | | 20/80 | G | G | G | G | G | I |
| | | 40/60 | G | G | G | G | G | I |
| | | 60/40 | G | G | G | G | G | I |
| | | 80/20 | G | G | G | G | G | I |
| | | 100/0 | G | G | G | G | G | G |
| **Cyclohexanone** | Benzyl alcohol | 0/100 | S | I | I | I | I | I |
| | | 20/80 | S | I | I | I | I | I |
| | | 40/60 | S | I | G | I | I | I |
| | | 60/40 | I | I | G | I | I | I |
| | | 80/20 | I | G | G | I | I | I |
| | | 100/0 | G | G | G | G | G | I |
| **Cyclohexanone** | Butanol | 0/100 | S | S | I | I | I | I |
| | | 20/80 | S | S | I | I | I | I |
| | | 40/60 | S | I | I | I | I | I |
| | | 60/40 | S | I | I | I | I | I |
| | | 80/20 | S | G | I | I | I | I |
| | | 100/0 | G | G | G | G | G | I |
| **Cyclohexanone** | Ethanolamine | 0/100 | I | I | I | I | I | I |
| | | 20/80 | I | I | I | I | I | G |
| | | 40/60 | I | I | G | I | I | G |
| | | 60/40 | I | I | G | I | I | I |
| | | 80/20 | I | G | G | I | I | I |
| | | 100/0 | G | G | G | G | G | I |

***Table S16. Results of solubility test in mixtures of liquids of all LMWG as 2 wt%.*** [a-b]

| **Liquid 1** | Liquid 2 | Composition % | HSA4 | HSA8 | HSA10 | HSA12 | HSA14 | HSA18 |
|---|---|---|---|---|---|---|---|---|
| **Chloropentane** | 1,4Dioxane | 0/100 | G | G | G | G | G | I |
| | | 20/80 | G | G | G | G | G | I |
| | | 40/60 | G | G | G | G | G | I |
| | | 60/40 | G | G | G | G | G | I |
| | | 80/20 | G | G | G | G | G | I |

| | | | | | | | | |
|---|---|---|---|---|---|---|---|---|
| | | 100/0 | G | G | G | G | G | G |
| **DMSO** | Ethanolamine | 0/100 | I | I | I | I | I | I |
| | | 20/80 | I | I | I | I | I | I |
| | | 40/60 | I | I | I | I | I | I |
| | | 60/40 | I | I | I | I | I | G |
| | | 80/20 | I | I | I | I | I | G |
| | | 100/0 | I | I | I | I | I | G |
| **DMSO** | progylene glycol | 0/100 | S | I | I | I | I | I |
| | | 20/80 | I | I | I | I | I | G |
| | | 40/60 | I | I | I | I | I | G |
| | | 60/40 | I | G | I | I | I | G |
| | | 80/20 | I | G | I | I | I | G |
| | | 100/0 | I | I | I | I | I | G |
| **MEK** | DMSO | 0/100 | I | I | I | I | I | G |
| | | 20/80 | I | I | G | I | I | G |
| | | 40/60 | I | I | G | I | I | G |
| | | 60/40 | I | I | G | I | I | I |
| | | 80/20 | I | I | I | I | I | I |
| | | 100/0 | G | G | G | G | G | I |
| **MEK** | propylene carbonate | 0/100 | G | I | I | I | I | G |
| | | 20/80 | G | G | G | G | I | G |
| | | 40/60 | G | G | G | G | I | G |
| | | 60/40 | G | G | G | G | G | G |
| | | 80/20 | G | G | G | G | G | I |
| | | 100/0 | G | G | G | G | G | I |
| **propylene carbonate** | t-butyl acetate | 0/100 | G | G | G | G | G | I |
| | | 20/80 | G | G | G | G | G | I |
| | | 40/60 | G | G | G | G | G | I |
| | | 60/40 | G | G | G | G | I | G |
| | | 80/20 | G | G | G | G | I | G |
| | | 100/0 | G | I | I | I | I | G |

***Table S17. Results of solubility test in mixtures of liquids of all LMWG as 2 wt%.*** [a-b]

| **Liquid 1** | Liquid 2 | Composition % | HSA4 | HSA8 | HSA10 | HSA12 | HSA14 | HSA18 |
|---|---|---|---|---|---|---|---|---|
| **propylene carbonate** | DMSO | 0/100 | I | I | I | I | I | G |
| | | 20/80 | I | I | I | I | I | G |
| | | 40/60 | I | I | G | I | I | G |
| | | 60/40 | I | I | G | I | I | G |
| | | 80/20 | I | I | I | I | I | G |

| | | | | | | | | |
|---|---|---|---|---|---|---|---|---|
| | | 100/0 | G | I | I | I | I | G |
| **propylene carbonate** | Toluene | 0/100 | G | G | G | G | G | G |
| | | 20/80 | G | G | G | G | G | I |
| | | 40/60 | G | G | G | G | G | I |
| | | 60/40 | G | G | G | G | G | I |
| | | 80/20 | G | G | G | G | I | G |
| | | 100/0 | G | I | I | I | I | G |
| **Toluene** | Benzyl Alcohol | 0/100 | S | I | I | I | I | I |
| | | 20/80 | S | S | S | I | I | I |
| | | 40/60 | S | S | S | S | I | I |
| | | 60/40 | S | S | S | S | I | I |
| | | 80/20 | S | I | S | I | I | I |
| | | 100/0 | G | G | G | G | G | G |
| **Toluene** | Butanol | 0/100 | S | S | I | I | I | I |
| | | 20/80 | S | G | S | I | I | I |
| | | 40/60 | S | G | S | S | I | I |
| | | 60/40 | S | G | S | S | I | I |
| | | 80/20 | S | G | G | I | I | I |
| | | 100/0 | G | G | G | G | G | G |
| **Toluene** | Diacetone Alcohol | 0/100 | G | G | G | I | I | I |
| | | 20/80 | I | G | G | I | G | I |
| | | 40/60 | I | G | G | I | G | I |
| | | 60/40 | G | G | G | I | G | I |
| | | 80/20 | G | G | G | I | G | G |
| | | 100/0 | G | G | G | G | G | G |

# IV. Synthesis Protocol

## IV.1. Thiazole based gelator (Th) [27,28]

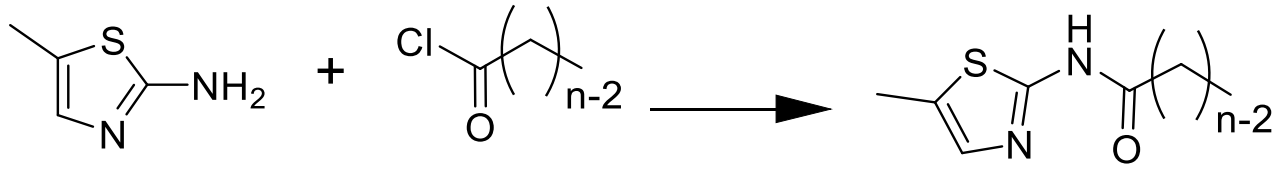


5-methylthiazol-2-amine (8.00 mmol) and triethylamine (9.6 mmol) were added to a solution of acid chloride (8.00 mmol) in dry dichloromethane (100 mL) and the mixture was stirred under a nitrogen atmosphere overnight. The reaction mixture was washed with brine, the organic phase was separated, and the aqueous phase was extracted with chloroform. The organic phases were combined, dried over anhydrous $MgSO_4$ and evaporated under vacuum. The product was purified by repeated recrystallizations from dichloromethane/petroleum ether mixture and dried under vacuum.

***Gelators with characterization matching what is described in the literature*[27,28,29]*:***

Th8

**(N-(5-methylthiazol-2-yl)octanamide**

(60% yield).

$^1$H NMR ($CDCl_3$): δ (ppm) = 11.98 (s, 1H, NH), 7.04 (s, 1H, CH), 2.50 (t, *J* = 7.5 Hz, 2H, $CH_2$), 2.41 (s, 3H, $CH_3$), 1.83 – 1.71 (m, 2H, $CH_2$), 1.43 – 1.23 (m, 8H, $CH_2$), 0.88 (t, 3H, $CH_3$) ppm.

Th12

**(N-(5-methylthiazol-2-yl)dodecanamide**

(60% yield)

$^1$H NMR (400 MHz, $CDCl_3$) δ 11.46 (s, 1H, NH), 7.04 (s, 1H, CH), 2.49(t, 2H, $CH_2$), 2.41(s, 3H, $CH_3$), 1.75 (m, 2H, $CH_2$), 1.25 (m, 16H, $CH_2$), 0.88 (t, 3H, $CH_3$) ppm.

Th14

**(N-(5-methylthiazol-2-yl)tetradecanamide**

(95% yield)

$^1$H NMR (400 MHz, $CDCl_3$) δ 12.13 (s, 1H, NH), 7.10 (s, 1H, CH), 2.57(t, 2H, $CH_2$), 2.43(s, 3H, $CH_3$), 1.76 (m, 2H, $CH_2$), 1.25 (m, 20H, $CH_2$), 0.88 (t, 3H, $CH_3$) ppm.

Th16

**(N-(5-methylthiazol-2-yl)hexadecanamide**

(60% yield)

$^{1}$H NMR (400 MHz, $CDCl_3$) δ 11.76 (s, 1H, NH),), 7.08 (s, 1H, CH), 2.53 (t, 2H, $CH_2$), 2.44 (s, 3H, $CH_3$), 1.78 (m, 2H, $CH_2$), 1.27 (m, 24H, $CH_2$), 0.90 (t, 3H, $CH_3$) ppm.

Th18

**(N-(5-methylthiazol-2-yl)octadecanamide**

(40% yield)

$^{1}$H NMR (300 MHz, $CDCl_3$) δ 11.29 (s, 1H, NH), 7.04 (s, 1H, CH), 2.48(t, 2H, $CH_2$), 2.41 (s, 3H, $CH_3$), 1.75 (m, 2H, $CH_2$), 1.25 (m, 28H, $CH_2$), 0.88 (t, 3H, $CH_3$) ppm.

# IV.2. Bisamide based gelator (Bis) [30]

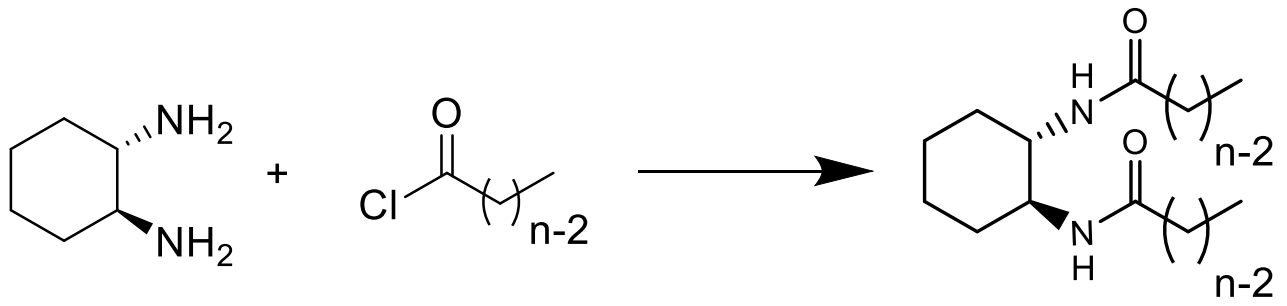


A solution of (0.5 g, 4.3 mmol) (1S,2S)-(−)-1,2-diaminocyclohexane in 20 mL of freshly distilled THF at 0°C was added slowly to a solution of acid chloride (8.6 mmol) in 50 mL of freshly distilled THF and a precipitation was formed immediately. After 10 min (1 g, 10 mmol) triethylamine was added and the solution was stirred for another 30 min at room temperature. Subsequently, the solution was heated at reflux for 2 h. After cooling the solution, THF was evaporated and the solid was washed with water. The precipitate was collected and the solid was washed with CH2Cl2. Compound was dried under vacuum.

***Gelators with characterization matching what is described in the literature[30]:***

Bis3

**N,N'-((1S,2S)-cyclohexane-1,2-diyl)dipropionamide**

(47% yield)

$^1$H NMR (300 MHz, $CDCl_3$) δ 5.87 (s, 2H, NH), 3.66 (m, 2H, CH), 2.17 (q, 4H, $CH_2$), 2.00 (d, 2H, $CH_2$) 1.74 (m, 2H), 1.28 (m, 4H), 1.11 (t, 6H, $CH_3$) ppm.

Bis4

**N,N'-((1S,2S)-cyclohexane-1,2-diyl)dibutylamide**

(80% yield)

$^1$H NMR (400 MHz, $CDCl_3$) δ 5.87(s, 2H, NH), 3.66 (m, 2H, CH), 2.10 (m, 4H, $CH_2$), 2.04 (d, 2H, $CH_2$), 1.57 (m, 4H) , 1.29 (m, 4H), 0.92 (t, 6H, $CH_3$) ppm.

Bis5

**N,N'-((1S,2S)-cyclohexane-1,2-diyl)dipentanamide**

(80% yield)

$^1$H NMR (400 MHz, $CDCl_3$) δ 5.86 (s, 2H, NH), 3.65 (m, 2H, CH), 2.11 (m, 4H, $CH_2$), 2.01 (d, 2H, $CH_2$), 1.73 (m, 2H), 1.59 (m, 4H), 1.31 (m, 8H), 0.90(t, 6H, $CH_3$) ppm.

Bis6

**N,N'-((1S,2S)-cyclohexane-1,2-diyl)dihexanamide**

(77% yield)

$^1$H NMR (400 MHz, $CDCl_3$) δ 5.88(s, 2H, NH), 3.65 (m, 2H, CH), 2.11(m, 4H, $CH_2$), 2.01 (d, 2H, $CH_2$), 1.73 (m, 2H), 1.58 (m, 4H), 1.28 (m, 12H), 0.87 (t, 6H, $CH_3$) ppm.

Bis8

**N,N'-((1S,2S)-cyclohexane-1,2-diyl)dioctanamide**

(71% yield)

$^1$H NMR (400 MHz, $CDCl_3$) δ= 5.94 (s, 2H, NH), 3.64 (m, 2H, CH), 2.15 (m, 4H, $CH_2$), 1.95 (m, 2H, $CH_2$), 1.66 (m, 2H), 1.52 (m, 4H), 1.10-1.25 (m, 20H), 0.87 (t, 6H, $CH_3$) ppm.

Bis12

**N,N'-((1S,2S)-cyclohexane-1,2-diyl)didodecanamide**

(45% yield)

$^1$H NMR (400 MHz, $CDCl_3$) δ 5.90 (s, 2H, NH), 3.65 (m, 2H, CH), 2.11 (m, 4H, $CH_2$), 2.01 (m, 2H, $CH_2$), 1.73 (m, 2H), 1.57 (m, 4H), 1.25 (m, 36H), 0.88 (t, 6H, $CH_3$) ppm.

Bis14

**N,N'-((1S,2S)-cyclohexane-1,2-diyl)ditetradecanamide**

(89% yield)

$^1$H NMR (400 MHz, $CDCl_3$) δ 5.87 (s, 2H, NH), 3.67 (m, 2H, CH), 2.14 (m, 4H, $CH_2$), 2.06 (d, 2H, $CH_2$), 1.76 (m, 2H), 1.60 (m, 4H), 1.28 (m, 44H), 0.89 (t, 6H, $CH_3$) ppm.

Bis16

**N,N'-((1S,2S)-cyclohexane-1,2-diyl)dipalmitamide**

(96% yield)

$^1$H NMR (400 MHz, $CDCl_3$) δ 5.94 (s, 2H, NH), 3.69 (m, 2H, CH), 2.13 (m, 4H, $CH_2$), 2.06 (d, 2H, $CH_2$) 1.78 (m, 2H), 1.59 (m, 4H), 1.27(m, 52H), 0.90 (t, 6H, $CH_3$) ppm.

Bis18

**N,N'-((1S,2S)-cyclohexane-1,2-diyl)distearamide**

(73% yield)

$^{1}$H NMR (300 MHz, $CDCl_3$) δ 5.88 (s, 2H, NH), 3.65 (m, 2H, CH), 2.11 (m, 4H, $CH_2$), 2.01 (d, 2H, $CH_2$), 1.78 (m, 2H), 1.57 (m, 4H), 1.25 (m, 60H), 0.88 (t, 6H, $CH_3$) ppm.

# IV.3. Triamide based gelator (Tris) [31]

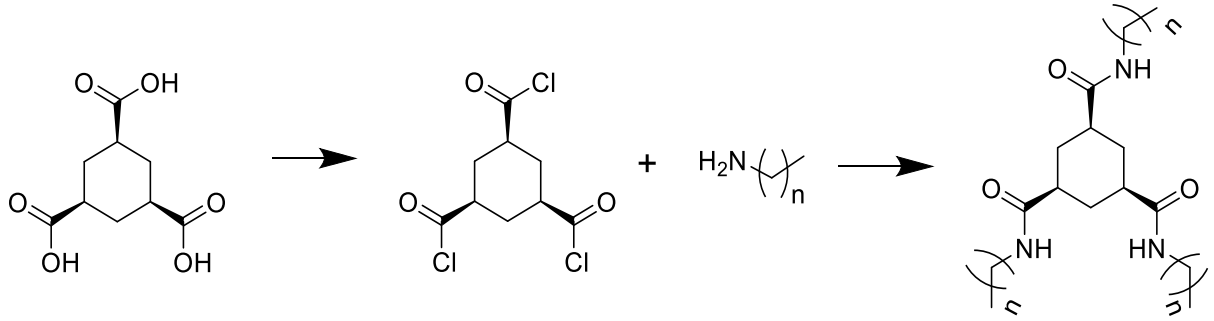

To a suspension of cyclohexane, 1,3,5-tricarboxylic acid (0.300 g, 1.39mmol) in 5 mL of DCM, oxalyl chloride (0,7 mL), and one drop of DMF were added. After stirring under reflux for 3 h, solvents were evaporated from the reaction mixture to give the tri(acid chloride). The product was used in the next reaction without further purification. Cyclohexane tricarboxylic acid trichloride (1.39 mmol) was dissolved into 5 mL of $CHCl_3$ and added to a $CHCl_3$ solution of alkyl amine (4.17 mmol) and triethylamine (2 mL, 14 mmol). As the reaction proceeded, product precipitated from the solution. After stirring under reflux for 2 h, $CHCl_3$ was removed and the crude product was washed with water and recrystallized from $CHCl_3$/ diethyl ether.

***Gelators with characterization matching what is described in the literature*[31]*:***

Tris12

**(1S, 3S, 5S)-N1,N3,N5-tridodecylcyclohexane-1,3,5-tricarboxamide**

(94% yield)

$^1$H NMR (300 MHz, $CDCl_3$) δ 7.62 (m, 3H, NH), 3.43 (m, 6H, $CH_2$), 2.85 (m, 3H, CH), 2.22 (m, 3H, CH, 1.98 (m, 3H, $CH_2$), 1.64 (m, 6H, $CH_2$), 1.33 (m, 54H, $CH_2$), 0.92 (t, 9H, $CH_3$) ppm.

Tris14

**(1S, 3S, 5S)-N1,N3,N5-tritetradecylcyclohexane-1,3,5-tricarboxamide**

(91% yield)

$^1$H NMR (400 MHz, $CDCl_3$) δ 7.80 (m, 3H, NH), 3.44 (m, 6H, $CH_2$), 2.94 (m, 3H, CH), 2.23 (m, 3H, $CH_2$), 1.99 (m, 4H, $CH_2$), 1.90 (m, 3H, $CH_2$), 1.33 (m, 66H, $CH_2$), 0.94 (t, 9H, $CH_3$) ppm.

Tris16

**(1S, 3S, 5S)-N1,N3,N5-trihexadecylcyclohexane-1,3,5-tricarboxamide**

(78% yield)

$^{1}$H NMR (300 MHz, $CDCl_3$) δ 7.57 (m, 3H, NH), 3.40 (m, 6H, $CH_2$), 2.83 (m, 3H, CH), 2.19 (m, 3H, $CH_2$), 1.90 (m, 3H, $CH_2$), 1.62(m, 6H, $CH_2$), 1.32 (m, 78H, $CH_2$), 0.89 (t, 9H, $CH_3$) ppm.

Tris18

**(1S, 3S, 5S)-N1,N3,N5-trioctadecylcyclohexane-1,3,5-tricarboxamide**

(78% yield)

$^{1}$H NMR (300 MHz, $CDCl_3$) δ 7.58(m, 3H, NH), 3.41 (m, 6H, $CH_2$), 2.84 (m, 3H, CH), 2.20 (m, 3H, $CH_2$), 1.95 (m, 3H, $CH_2$), 1.63 (m, 6H, $CH_2$), 1.32 (m, 90H, $CH_2$), 0.92(t, 9H, $CH_3$) ppm.

# IV.4. Dialkyl hydrazine based gelator (Hydra) [32]

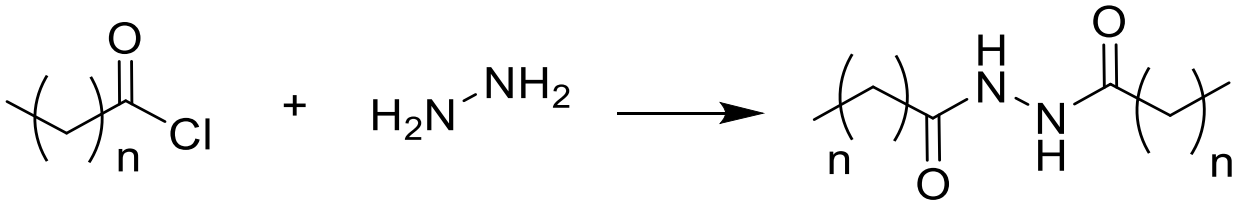

A solution of hydrazine (0.1 mol) in diethyl ether (50 mL) was added dropwise to a solution of acid chloride (0.06 mol) in ether (50 mL). The solution was stirred for 30 min and the precipitated amide was separated by filtration. The crude amides were recrystallized from methanol. Compounds were dried under vacuum.

***Hydra12 with characterization matching what is described in the literature[32]:***

Hydra8

**N,N'-octanoyloctanehydrazide**

(75% yield)

$^1$H NMR (300 MHz, DMSO-$d_6$) δ 9.38 (s, 2H, NH), 2.11 (t, 4H, $CH_2$), 1.50 (m, 4H, $CH_2$), 1.26 (m, 16H, $CH_2$), 0.88 (t, 6H, $CH_3$) ppm. Calculated for $C_{16}H_{32}N_2O_2$, [M+ $Na^+$]+:307.23 , found: 307.23. Melting temperature: 159.3$^o$ C.

Hydra10

**N,N'-decanoyldecanehydrazide**

(64% yield)

$^1$H NMR (300 MHz, DMSO-$d_6$) δ 9.6 (s, 2H, NH), 2.08 (t, 4H, $CH_2$), 1.49 (m, 4H, $CH_2$), 1.24 (m, 24H, $CH_2$), 0.86 (t, 6H, $CH_3$) ppm. Calculated for $C_{20}H_{40}N_2O_2$, [M+ $Na^+$]+:363.29, found: 363.29. Melting temperature: 154.0$^o$ C.

Hydra12

**N,N'-dodecanoyldodecanehydrazide**

(65% yield)

$^1$H NMR (300 MHz, DMSO-$d_6$) δ 9.59 (s, 2H, NH), 2.05 (t, 4H, $CH_2$), 1.50 (m, 4H, $CH_2$), 1.25 (m, 32H, $CH_2$), 0.86 (t, 6H, $CH_3$) ppm. Calculated for $C_{24}H_{48}N_2O_2$, [M+ $Na^+$]+:419.36, found: 419.36. Melting temperature: 151.4$^o$ C.

Hydra14

**N,N'-tetradecanoyltetradecanehydrazide**

(61% yield)

$^{1}$H NMR (300 MHz, DMSO-$d_6$) δ 9.32 (s, 2H, NH), 2.08 (t, 4H, $CH_2$), 1.54(m, 4H, $CH_2$), 1.30 (m, 40H, $CH_2$), 0.90 (t, 6H, $CH_3$) ppm. Calculated for $C_{28}H_{56}N_2O_2$, [M+ $Na^+$]+:475.42, found: 475.42. Melting temperature: 149.4º C.

Hydra16

**N,N'-palmitoylpalmitohydrazide**

(59% yield)

$^{1}$H NMR (300 MHz, DMSO-$d_6$) δ 9.30 (s, 2H, NH), 2.12 (t, 4H, $CH_2$), 1.52 (m, 4H, $CH_2$), 1.30 (m, 48H, $CH_2$), 0.88 (t, 6H, $CH_3$) ppm. Melting temperature: 148.1º C.

Hydra18

**N,N'-stearoylstearohydrazide**

(75% yield)

$^{1}$H NMR (300 MHz, DMSO-$d_6$) δ 9.32 (s, 2H, NH), 2.00 (t, 4H, $CH_2$), 1.47 (m, 4H, $CH_2$), 1.24 (m, 56H, $CH_2$), 0.86 (t, 6H, $CH_3$) ppm. Melting temperature: 145.9º C.

# IV.5. (R)-12-hydroxystearic acid based gelators (HSA)[33,34]

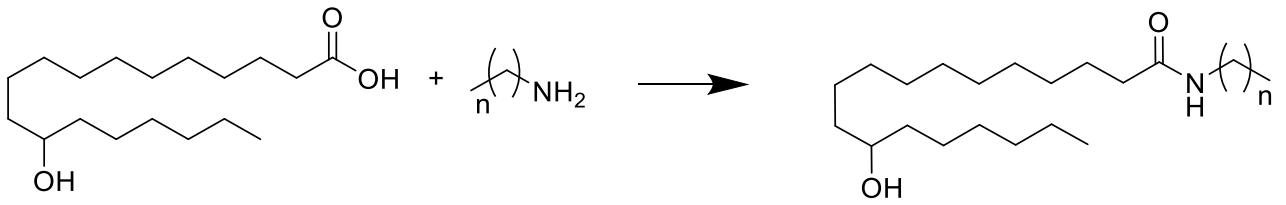


Amides were prepared from (R)-12-hydroxystearic acid (12-HSA) and the corresponding amine according to the following procedure. 12-HSA was recrystallized (mp 78.6 C).[40] To a cooled (at 5 °C) and stirred solution of ethyl chloroformate in dry THF (50 mL) was added slowly a solution of 12-HSA and triethylamine in dry THF (50 mL) while maintaining the temperature at 5 °C. The mixture was stirred for an additional 40 min at room temperature. The amine (24 mmol) in 50 mL dry THF was added to the vigorously stirred solution at 5 °C, and the reaction mixture was kept at room temperature for 24 h. The solvent was removed under reduced pressure and the residue was washed successively with ethyl acetate (200 mL), 3 N HCl (150 mL), aqueous 1M $Na_2CO_3$ (200 mL), water (250 mL) and diethyl ether (200 mL) and finally dried under vacuum.

***Gelators with characterization matching what is described in the literature[33,34]:***

HSA4

**N-butyl-12-hydroxyoctadecanamide**

(35% yield)

$^1$H NMR (300 MHz, $CDCl_3$) δ 5.39 (m, 1H, CH), 3.62 (1H, OH), 3.26 (m, 2H, $CH_2$), 2.14 (m, 2H, $CH_2$), 1.30 (m, 32H, $CH_2$), 0.95 (t, 6H, $CH_3$) ppm.

HSA8

**N-octyl-12-hydroxyoctadecanamide**

(32% yield)

$^1$H NMR (300 MHz, $CDCl_3$) δ 5.38 (m, 1H, CH), 3.62 (1H, OH), 3.27 (m, 2H, $CH_2$), 2.17 (m, 2H, $CH_2$), 1.30 (m, 40H, $CH_2$), 0.90(t, 6H, $CH_3$) ppm.

HSA10

**N-decyl-12-hydroxyoctadecanamide**

(51% yield)

$^1$H NMR (400 MHz, $CDCl_3$) δ 5.39 (m, 1H, CH), 3.62 (1H, OH), 3.25 (m, 2H, $CH_2$), 2.17 (m, 2H,

$CH_2$), 1.31 (m, 44H, $CH_2$), 0.91 (t, 6H, $CH_3$) ppm.

HSA12

**N-dodecyl-12-hydroxyoctadecanamide**

(47% yield)

$^1$H NMR (300 MHz, $CDCl_3$) δ 5.38 (m, 1H, CH), 3.62 (1H, OH), 3.27 (m, 2H, $CH_2$), 2.17 (m, 2H, $CH_2$), 1.28 (m, 48H, $CH_2$), 0.91(t, 6H, $CH_3$) ppm.

HSA14

**N-tetradecyl-12-hydroxyoctadecanamide**

(47% yield)

$^1$H NMR (400 MHz, $CDCl_3$) δ 5.60 (m, 1H, CH), 3.59 (1H, OH), 3.25 (m, 2H, $CH_2$), 2.18 (m, 2H, $CH_2$), 1.28 (m, 52H, $CH_2$), 0.90 (t, 6H, $CH_3$) ppm.

HSA18

**N-octadecyl-12-hydroxyoctadecanamide**

(91.76% yield)

$^1$H NMR (300 MHz, $CDCl_3$) δ 5.36 (m, 1H, CH), 3.59 (1H, OH), 3.24 (m, 2H, $CH_2$), 2.14 (m, 2H, $CH_2$), 1.25 (m, 60H, $CH_2$), 0.88(t, 6H, $CH_3$) ppm.

# V. Purity study of trisamide-based gelators

In X-ray diffraction measurements, diffraction peaks with different widths usually indicate that the measured sample contains more than one phase. To confirm this hypothesis, we performed temperature dependent X-ray diffraction (Figure S44) to evaluate if the fine peaks could originate from some mesomorphic phase.

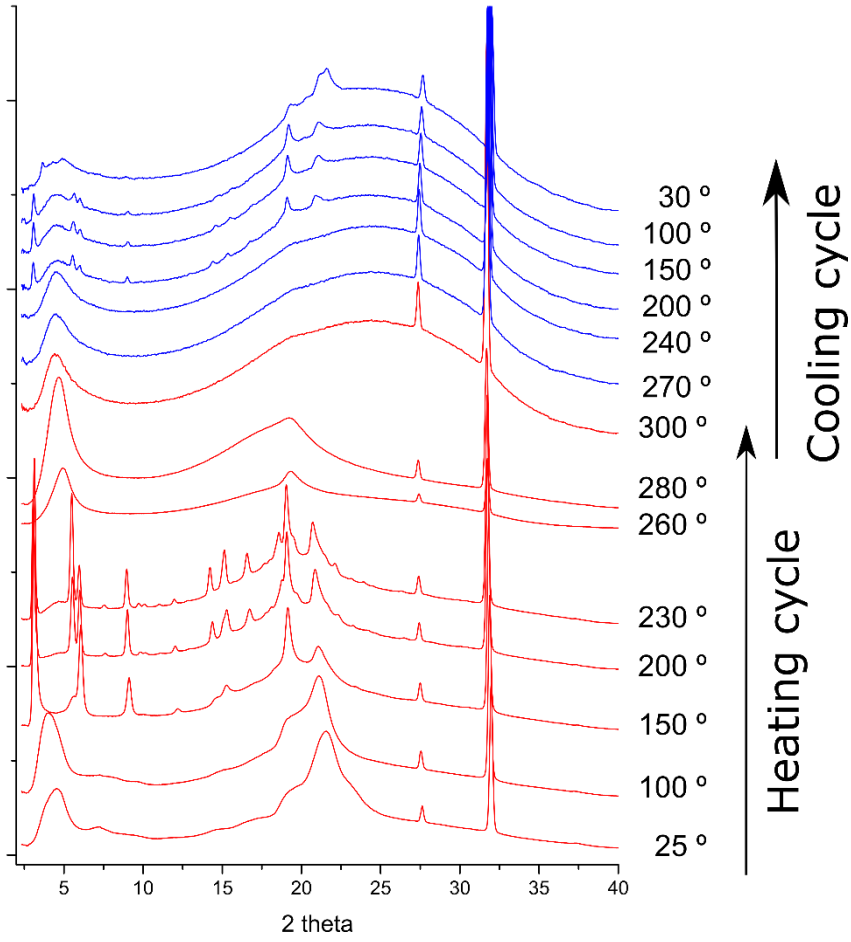


*Figure S44. Temperature dependent X-ray diffraction of* ***Tris12*** *xerogel extracted form toluene. X-ray wavelength of 1.5406 Å.*

The xerogel of **Tris12** extracted from toluene was heated until broadening of the diffraction peaks at 25 2θ was observed (300ºC) and then cooled down to room temperature. Even above 300ºC the fine peaks between 24º and 33º were still observable while the remaining powder patterns only presented broad peaks, indicating that they belong to an impurity. A second point is the aspect of the diffraction circles associated to the peaks, as observed on the 2D diffraction pattern (*Figure S45*). They appear punctuated that means they originate from a restricted number of crystallites.

Figure S44 also shows a structural transition already characterized by Sijbesma et al.[2] and Schmidt et al.[3]. Up to 200 °C the X-ray patterns are characteristic of amorphous/poorly organized structures and from 200 °C up to 260 ºC the sharpening of diffraction peaks indicates a higher order organization of the gelator. Above 260 ºC the final broadening of the diffraction peaks indicates that the gelator melts. The transition observed at 200 °C represents the transition between amorphous and a columnar nematic phase.

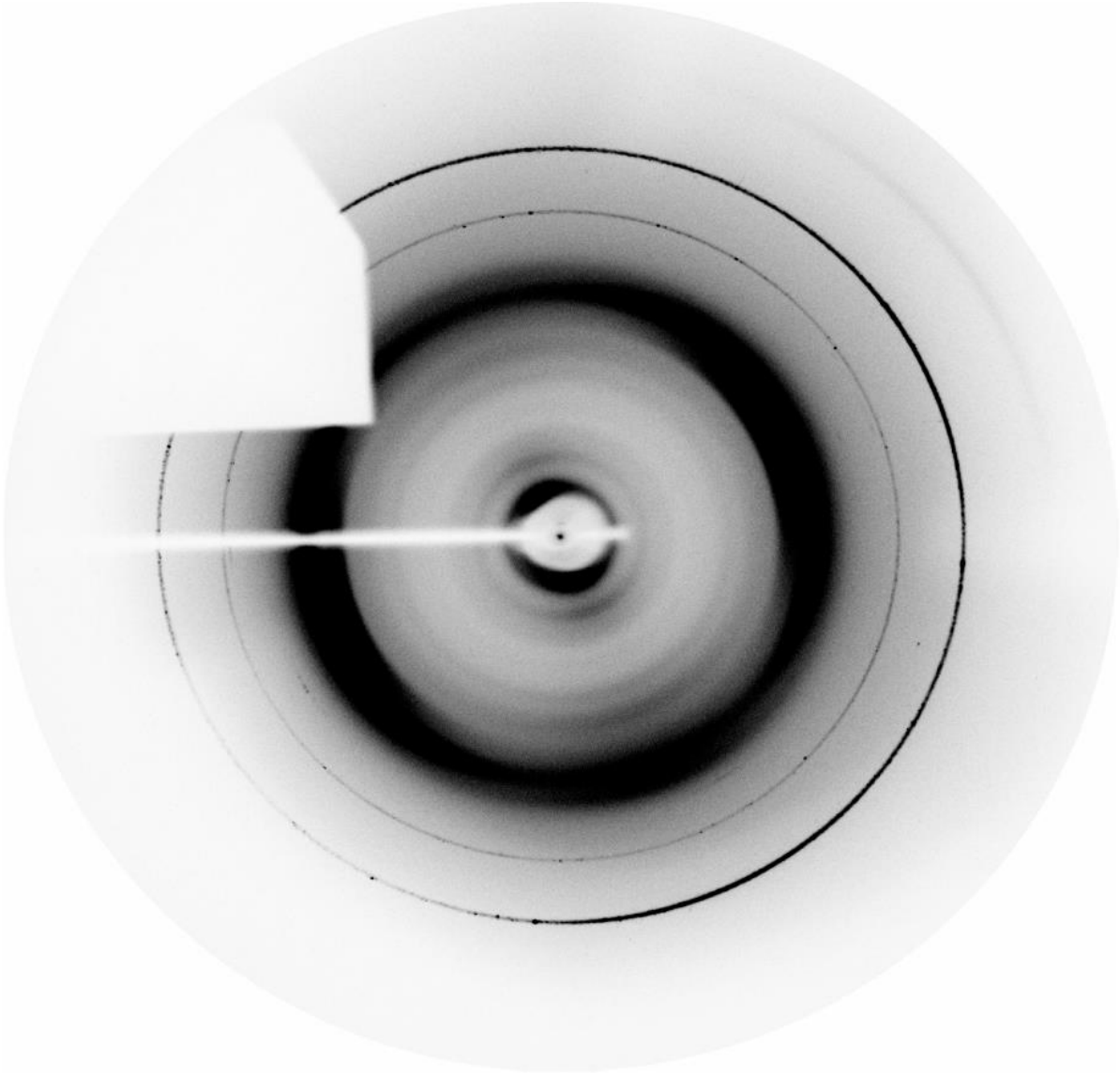

*Figure S45. 2D diffraction patterns of* ***Tris12*** *xerogel extracted form toluene (25ºC). X-ray wavelength of 1.5406 Å.*

In an attempt to identify the inorganic impurity, we compared the sharp peaks presented in the diffraction patterns with the most common form of MgSO4 and SiO2 (common inorganic compound found as impurities in organic synthesis). Unfortunately, none of the tested inorganic compounds matched the sharp peaks present in the diffraction pattern of **Tris12** (Figure S46).

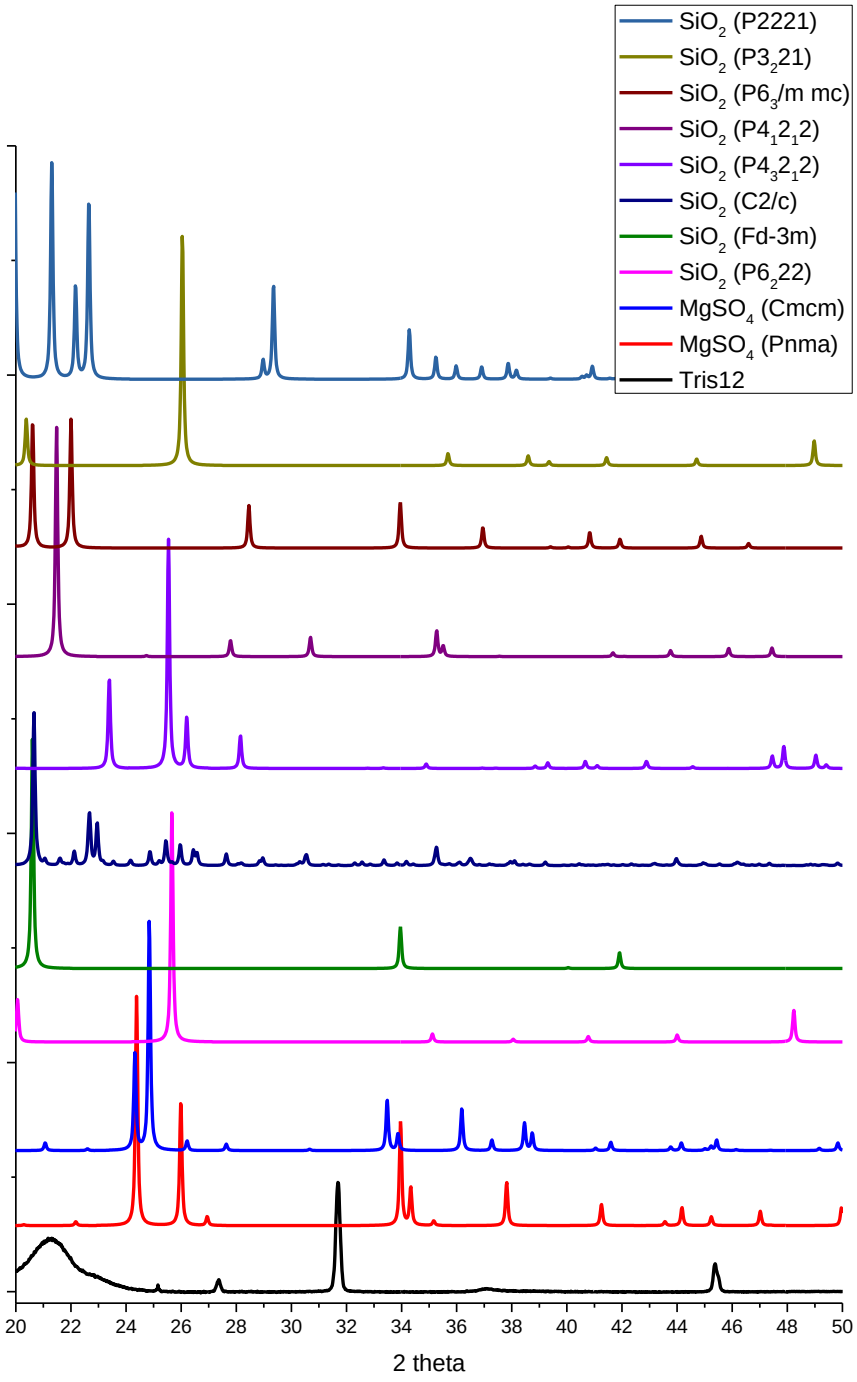


*Figure S46. Comparison of Tris12 xerogel extracted form toluene and most common forms of $MgSO_4$ and $SiO_2$.*

$^{1}H$ and $^{13}C$ NMR spectroscopy does not allow to detect any impurity (Figures S46 and S47). Finally, elemental analysis performed on the bulk solid gelators for the elements of carbon, oxygen, hydrogen and nitrogen presented a total sum of 85% to 90% of the measured elements (Table S18). When normalized, the values fitted the expected amount of each element. This means that the bulk gelators contain *ca.* 10 wt% of an inorganic impurity, whose origin could not be identified.

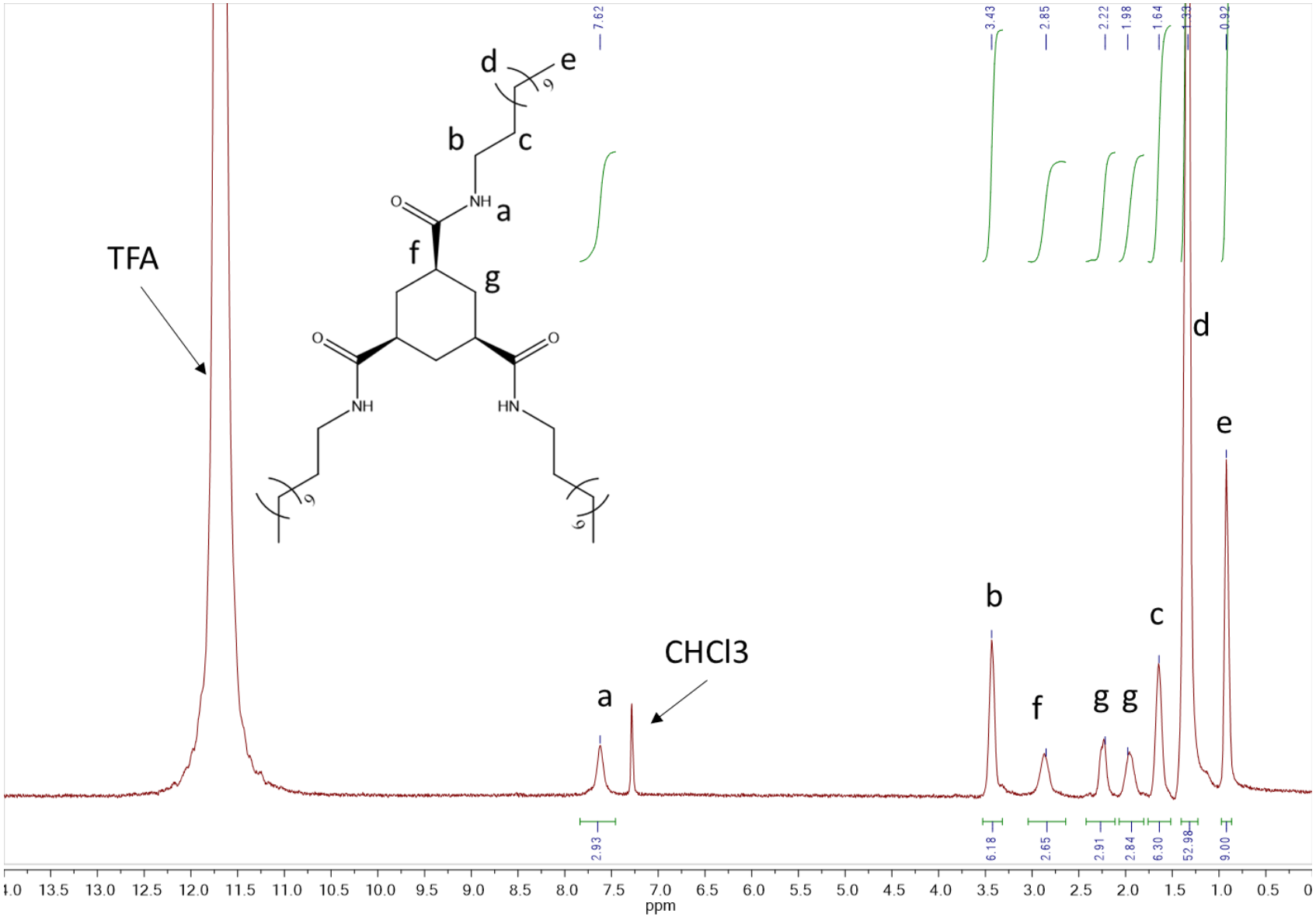


Figure S47. 1H NMR (300 MHz, CDCl3/TFA) of Tris12.

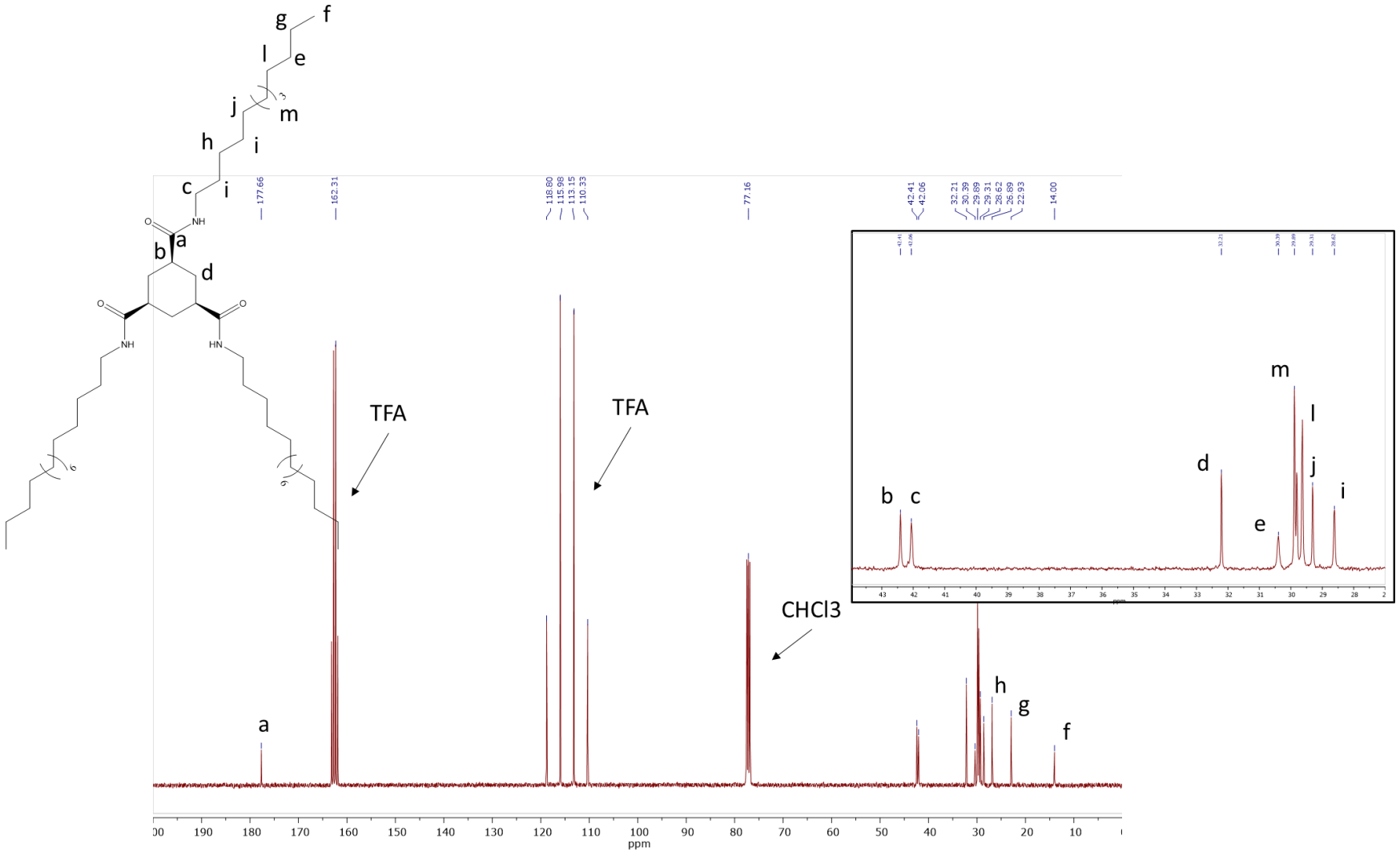


Figure S48. 13C NMR (300 MHz, CDCl3/TFA) of Tris12.

***Table S18. Elemental analyses of trisamide-based gelators.***

| | | | |
|---|---|---|---|
| | | ***Tris12*** | |
| | *experimental* | *normalized experimental value (sum = 100%)* | *expected* |
| ***C*** | *66.31 %* | *74.90 %* | *75.26 %* |
| ***H*** | *11.04 %* | *12.47 %* | *12.21 %* |
| ***N*** | *4.99 %* | *5.63 %* | *5.85 %* |
| ***O*** | *6.19 %* | *6.99 %* | *6.68 %* |
| ***Sum*** | 88.53% | 100.00% | 100.00% |
| | | ***Tris14*** | |
| ***C*** | *70.76 %* | *76.92 %* | *76.34 %* |
| ***H*** | *11.5 %* | *12.50 %* | *12.44 %* |
| ***N*** | *4.59 %* | *4.99 %* | *5.24 %* |
| ***O*** | *5.14 %* | *5.59 %* | *5.98 %* |
| ***Sum*** | 91.99% | 100.00% | 100.00% |
| | | ***Tris16*** | |
| ***C*** | *64.89 %* | *76.62 %* | *77.23 %* |
| ***H*** | *10.87 %* | *12.83 %* | *12.62 %* |
| ***N*** | *3.95 %* | *4.66 %* | *4.74 %* |
| ***O*** | *4.98 %* | *5.88 %* | *5.41 %* |
| ***Sum*** | 84.69% | 100.00% | 100.00% |
| | | ***Tris18*** | |
| ***C*** | *67.89 %* | *77.26* | *77.95 %* |
| ***H*** | *11.55 %* | *13.14* | *12.77 %* |
| ***N*** | *3.61 %* | *4.11* | *4.33 %* |
| ***O*** | *4.82 %* | *5.48* | *4.94 %* |
| ***Sum*** | 87.87% | 100.00% | 100.00% |

# VI.References


1 N. Amanokura, K. Yoza, H. Shinmori, S. Shinkai and D. N. Reinhoudt, *J. Chem. Soc. Perkin Trans. 2*, 1998, **0**, 2585–2592.

2 M. Raynal and L. Bouteiller, *Chem. Commun.*, 2011, **47**, 8271.

3 C. M. Hansen, *Hansen solubility parameters A User ' s Handbook Second Edition*, 2007.

4 S. Abbott and C. M. Hansen, *Hansen Solubility Parameters in Practice*, 2008.

5 M. J. Louwerse, A. Maldonado, S. Rousseau, C. Moreau-Masselon, B. Roux and G. Rothenberg, *ChemPhysChem*, 2017, **18**, 2999–3006.

6 K. Murata, M. Aoki, T. Suzuki, T. Harada, H. Kawabata, T. Komori, F. Ofaseto, K. Ueda and S. Shinkai, *J. Am. Chem. Soc.*, 1994, **116**, 6664–6676.

7 R. Mukkamala and R. G. Weiss, *Langmuir*, 1996, **12**, 1474–1482.

8 D. R. Trivedi, A. Ballabh, P. Dastidar and B. Ganguly, *Chem. - A Eur. J.*, 2004, **10**, 5311–5322.

9 M. Fang, J. Long, W. Zhao, L. Wang and G. Chen, *Langmuir*, 2010, **26**, 16771–16774.

10 K. Hanabusa, H. Kobayashi, M. Suzuki, M. Kimura and H. Shirai, *Colloid Polym. Sci.*, 1998, **276**, 252–259.

11 O. Gronwald and S. Shinkai, *Chem. - A Eur. J.*, 2001, **7**, 4328–4334.

12 J. W. Liu, J. T. Ma and C. F. Chen, *Tetrahedron*, 2011, **67**, 85–91.

13 P. Curcio, F. Allix, G. Pickaert and B. Jamart-Grégoire, *Chem. - A Eur. J.*, 2011, **17**, 13603–13612.

14 J. Bonnet, G. Suissa, M. Raynal and L. Bouteiller, *Soft Matter*, 2014, **10**, 3154.

15 H. Xu, J. Song, T. Tian and R. Feng, *Soft Matter*, 2012, **8**, 3478.

16 W. Edwards and D. K. Smith, *J. Am. Chem. Soc.*, 2013, **135**, 5911–5920.

17 V. C. Edelsztein, A. S. Mac Cormack, M. Ciarlantini and P. H. Di Chenna, *Beilstein J. Org. Chem.*, 2013, **9**, 1826–1836.

18 T. Ando and K. Ito, *J. Incl. Phenom. Macrocycl. Chem.*, 2014, **80**, 285–294.

19 S. He, H. Zhao, X. Guo, X. Xu, X. Zhou, J. Liu, Z. Xing, L. Ye, L. Jiang, Q. Chen and Y. He, *Chem. - A Eur. J.*, 2014, **20**, 15473–15481.

20 C. Tong, K. Fan, L. Niu, J. Li, X. Guan, N. Tao, H. Shen and J. Song, *Soft Matter*, 2014, **10**, 767–772.

21 H. Shen, L. Niu, K. Fan, J. Li, X. Guan and J. Song, *Langmuir*, 2014, **30**, 9176–9182.

22 Y. Huang, Y. Yuan, W. Tu, Y. Zhang, M. Zhang and H. Qu, *Tetrahedron*, 2015, **71**, 3221–3230.

23 Y. Li, X. Ran, Q. Li, Q. Gao and L. Guo, *Chem. - An Asian J.*, 2016, **11**, 2157–2166.

24 T. Wang, X. Yu, Y. Li, J. Ren and X. Zhen, *ACS Appl. Mater. Interfaces*, 2017, **9**, 13666–13675.

25 T. Xiao, X. Zhang, J. Wu, J. Yang and Y. Yang, *Chempluschem*, 2017, **82**, 879–887.

26 P. Lin, N. X. Zhang, J. J. Li, J. Zhang, J. H. Liu, B. Zhang and J. Song, *Chinese Chem. Lett.*, 2017, **28**, 771–776.

27 P. Yadav, D. Kour, V. K. Gupta, Rajnikant and A. Ballabh, *RSC Adv.*, 2013, **3**, 8417–8421.

28 P. Yadav and A. Ballabh, *New J. Chem.*, 2015, **39**, 721–730.

29 D. Rosa Nunes, M. Reche-Tamayo, E. Ressouche, M. Raynal, B. Isare, P. Foury-Leylekian, P.-A. Albouy, P. Brocorens, R. Lazzaroni and L. Bouteiller, Langmuir, 2019, 35, 7970–7977.

30 N. Zweep, A. Hopkinson, A. Meetsma, W. R. Browne, B. L. Feringa and J. H. Van Esch, *Langmuir*, 2009, **25**, 8802–8809.

31 K. Hanabusa, A. Kawakami, M. Kimura and H. Shirai, *Chem. Lett.*, 1997, **26**, 191–192.

32 K. Tomioka, T. Sumiyoshi, S. Narui, Y. Nagaoka, A. Iida, Y. Miwa, T. Taga, M. Nakano and T. Handa, *J. Am. Chem. Soc.*, 2001, **123**, 11817–11818.

33 J. Bonnet, G. Suissa, M. Raynal and L. Bouteiller, *Soft Matter*, 2015, **11**, 2308–2312.

34 V. A. Mallia, M. George, D. L. Blair

35 I. Tomatsu, C. F. C. Fitié, D. Byelov, W. H. De Jeu and P. C. M. M. Magusin, *Mol. Phys.*, 2009, 1–5.

36 A. Timme, R. Kress, R. Q. Albuquerque and H. W. Schmidt, *Chem. - A Eur. J.*, 2012, **18**, 8329–8339.

université PARIS-SACLAY
ÉCOLE DOCTORALE
Physique en île-de-France (EDPIF)

**Titre :** Synthèse et caractérisation d'organogels par des techniques de rayons X

**Mots clés :** organogels , matière molle, rayons X

**Résumé :** Les organogels sont un type particulier de gels formés dans des liquides organiques par un réseau de polymères supramoléculaires. Ces matériaux diffèrent principalement des autres classes de gels en raison de la nature de leur réseau. Les gélifiants de faible poids moléculaire (LMWG) ont tendance à s'auto-agréger dans une direction préférentielle. Cela conduit à la formation de structures allongées, principalement des fibres, qui, par une évolution continue du processus d'assemblage, forment un réseau fibrillaire auto-assemblé enchevêtré (SAFIN). Ce mécanisme d'auto-assemblage est dirigé par des interactions non covalentes telles que la liaison hydrogène, l'empilement π – π, les interactions donneur – accepteur, la coordination des métaux et les interactions de van der Waals. La formation d'un réseau basé uniquement sur des interactions faibles affecte considérablement l'intégrité structurelle, rendant les organogels métastables et thermoréversibles.
Il existe une grande variété structurelle d'organogélifiants, ce qui en fait un type de matériau intéressant, permettant une large gamme de propriétés et d'applications. Le principal défi des organogels est de prédire quel gélifiant est capable de gélifier quel liquide. Ainsi, il devient nécessaire de développer une méthodologie capable de réduire le temps et les dépenses nécessaires à la recherche de nouveaux organogélateurs ou du réglage de leurs propriétés. Cette thèse contient deux approches expérimentales principales. La première porte sur la détermination de l'empilement moléculaire d'organogélateurs dans les fibres par des techniques de diffusion de rayons X. La deuxième approche consiste à optimiser une méthodologie basée sur les paramètres de solubilité de Hansen, qui peut être utilisée pour rationaliser la formation d'organogel. La combinaison de ces deux outils a permis d'étudier l'effet qu'une altération structurelle du gélifiant a sur l'organogélation. Cinq familles d'organogélateurs ont été synthétisées avec des chaînes alkyles linéaires de différentes longueurs. À partir de ces cinq familles, nous avons pu déterminer l'assemblage cristallin de trois d'entre elles. Ces familles montrent une évolution régulière de la sphère de gélification qui est cohérente avec l'empilement cristallin. Ainsi, pour cette famille, la prédiction des sphères de gélification est possible. Les deux familles restantes d'organogélateurs ont présenté une évolution irrégulière de la gélification et il n'a pas été possible de déterminer avec précision l'empilement cristallin. Ce comportement est probablement dû à de petites différences du mode de cristallisation des membres de la famille.

**Title :** Synthesis of organogels and characterization by X-ray techniques

**Keywords :** organogels, X-ray diffraction, soft matter

**Abstract:** Organogels are a particular type of gels formed in organic liquids by a supramolecular polymer network. These materials mainly differ from other classes of gels due to the nature of their network. Low molecular weight gelators (LMWG) tend to self-aggregate in a preferential direction. This leads to the formation of elongated structures, mainly fibers, that by continuous evolution of the assembly process form an entangled Self-Assembled Fibrillar Network (SAFIN). This mechanism of self-assembly is led by non-covalent interactions like hydrogen-bonding, π–π stacking, donor–acceptor interactions, metal coordination and van der Waals interactions. Forming a network only based on weak interactions highly affects the structural integrity, making organogels metastable and thermoreversible.
There is a wide structural variety of organogelators that makes them such an interesting type of materials, allowing a wide range of properties and applications. The main challenge with organogels is predicting which gelator is capable of gelating which liquid. Therefore, the discovery of new organogelators is still mainly the result of serendipity and their gelation abilities are usually probed by exhaustive trial and error processes. Thus, arises a need to develop a methodology capable to decrease time and expenses when researching new organogelators or tuning their proprieties.
This thesis contains two main experimental approaches. The first focuses on the determination of the molecular packing of organogelators within the fibers by scattering techniques. The second approach consists in the optimization of a methodology based on Hansen solubility parameters, that can be used to rationalize organogel formation. The combination of these two tools has allowed to study the effect that a structural alteration of the gelator has on organogelation. Five families of organogelators were synthesized with linear alkyl chains at different lengths. From these five families we could determine the crystal packing for three of them. These families show a regular evolution of the gelation sphere that is coherent with the crystal packing. Thus, for these families the prediction of the gelation spheres is possible. The remaining two families of organogelators presented and erratic evolution of gelation and it was not possible to accurately determinate the crystal packing. This behavior is probably due to small differences in the crystal habit between all members of the family.

**Université Paris-Saclay**
Espace Technologique / Immeuble Discovery
Route de l'Orme aux Merisiers RD 128 / 91190 Saint-Aubin, France